# The Effects of Tetrahydrobiopterin and Hyperglycaemia on Macrophage Metabolism in Cardiovascular Inflammation

Faseeha Ayaz

Department of Cardiovascular Medicine

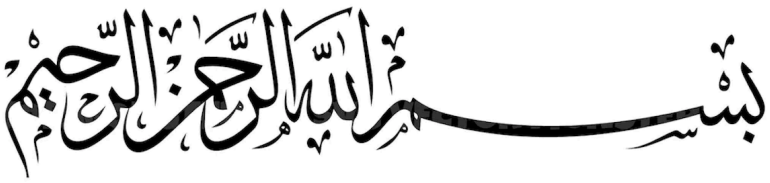
Corpus Christi College




A thesis submitted for the degree of Doctor of Philosophy in Cardiovascular Science

University of Oxford

Hilary Term 2023



# Abstract

## The Effects of Tetrahydrobiopterin and Hyperglycaemia on Macrophage Metabolism in Cardiovascular Inflammation



**Faseeha Ayaz**

Corpus Christi College, University of Oxford

Submitted for the degree of DPhil in Cardiovascular Science

Hilary Term 2023



Macrophages are highly heterogeneous, plastic immune cells that perform a diverse spectrum of functions. Defined by their metabolic signature, macrophages stimulated by LPS/IFN-γ ($M^{LPS/IFN-\gamma}$) display reduced oxidative phosphorylation, due to breaks in the TCA cycle, switching instead to glycolysis to meet their energy requirements. Through targeted modulation of this glycolytic switch, and modulating macrophage metabolism generally, there is potential to alter macrophage function and impact their role in the development of cardiovascular diseases.

Previously, our group has shown that tetrahydrobiopterin (BH4) alters mitochondrial respiration in $M^{LPS/IFN-\gamma}$ macrophages. A newly generated model of BH4 deficiency revealed that BH4 is required for the TCA cycle breaks to completely occur resulting in downregulation of glycolysis, and increased reliance on OXPHOS, due to glutaminolysis supplementation in BH4-deficient $M^{LPS/IFN-\gamma}$ macrophages. These BH4-deficient $M^{LPS/IFN-\gamma}$ macrophages exhibited a less inflammatory phenotype due to decreased levels of pro-inflammatory metabolites such as eicosanoids, and increased levels of anti-inflammatory metabolites, such as itaconate, which was also discovered to be secreted from macrophages in large quantities. Itaconate was used as a marker of inflammation throughout the study. *ACOD1*, encoding CAD enzyme which produces itaconate, minor allele rs17470171 was associated with altered redox state and improved vascular function in patients with cardiovascular disease. Following on, itaconate treatment caused loss of constriction in mouse aortas via endothelial independent mechanisms. This study proposes a non-immune related role for itaconate, adding to the evidence for a therapeutic role for itaconate.

In addition, the study investigated the impact of hyperglycaemia as an inflammatory and metabolic stimulus in $M^{LPS/IFN-\gamma}$. In vitro high glucose treatment did not yield alterations in the inflammatory or metabolic profile of macrophages but in vivo hyperglycaemia primed $M^{LPS/IFN-\gamma}$ to have altered proinflammatory cytokine release. Metabolomics analysis revealed increased levels of glycolytic metabolites and sphingomyelins following secondary stimulus in diabetic $M^{LPS/IFN-\gamma}$ macrophages. The majority of other metabolic pathways and inflammatory metabolites remained unchanged, including itaconate. Further studies are required to determine if these metabolic changes translate into functional outcomes.

Overall, the study demonstrates altering cell bioenergetics, via BH4 loss or hyperglycaemia, can be a viable approach to modifying macrophage phenotype. Additionally, itaconate has potential non-immune related roles that need to be further explored but are promising treatments for cardiovascular or inflammatory diseases.

## Acknowledgements

All the work presented in this thesis would not be possible without funding from the British Heart Foundation 4-year doctoral training programme. I would first like to thank Dr Mark Christie for always challenging me and pushing me to reach higher. Without his encouragement, I may not have even applied to Oxford. Next, I would like to thank the DCC and the Brain lab for giving me the scientific foundation needed to apply and Prof David Greaves, Prof Kim Dora and Prof Nicola Smart for accepting me onto the programme.

For taking me under their wings, I would like to thank Dr Mark Crabtree and Prof Keith Channon. I would also like to thank Prof Robin Choudhury. For the rest of the group, I always wanted to be in the lab because of the people, and you as people are wonderful. To Sandy who helped me choose this lab, and to Tom who first showed me the ropes. To Marina who took over them, and to Sally who saved me on actual ropes. To Katie who is a joy, and to Gareth who will make it. To Gillian and her cat, and to Surawee and his fads. To Channon lab meetings and lab refurbishments. It has been the best of times.

Much of my personal growth came from Corpus, the opportunities provided and the encounters had there. To Alma, Nik, Olek and Rita who I first lived with. To Robert, Llewelyn, Christos and the many other friendships. To Sinan, who gave me so much. To Hannah, Hira, Komal and Tayyaba for providing a refuge for roots alien to Oxford. To the other BHF girls: Laura, Lucy, Yasemin, ours is a lovely group. To Cheryl for her warmth, to Daan for his constant support, to Mona for her unwavering strength. To My-Nhan and Line who left too early. To Hui, Fulye and Mila who are the Queens from Kings. To Christos, Kar Lai and KC and any others I may have missed. And to Tom and Aleena who are wonderful treasure finds.

To my brilliant family, who have always supported me, this is your achievement as much as mine. I am a different person now to when I began my DPhil. The journey is complete.

# Table of Contents


ABSTRACT ..... 3
ACKNOWLEDGEMENTS ..... 4
TABLE OF CONTENTS ..... 5
LIST OF FIGURES ..... 10
LIST OF TABLES ..... 13
LIST OF ABBREVIATIONS ..... 14

CHAPTER 1: INTRODUCTION ..... 19

1.1 MACROPHAGE OVERVIEW ..... 19
1.1.1 Cardiovascular disease overview ..... 19
1.1.2 Inflammation and macrophages in cardiovascular disease ..... 19
1.1.3 Targeting inflammation as a therapy in cardiovascular disease ..... 20
1.1.4 Bone marrow derived macrophages ..... 22
1.1.5 TLR4 signalling ..... 23
1.2 MACROPHAGE METABOLISM ..... 24
1.2.1 Arginine and NO metabolism ..... 24
1.2.2 Glycolysis ..... 24
1.2.3 Pentose phosphate pathway ..... 27
1.2.4 TCA cycle and Oxidative Phosphorylation ..... 27
1.2.5 Fatty acid metabolism ..... 31
1.2.6 Glutaminolysis ..... 32
1.3 INNATE IMMUNE CELL MEMORY ..... 32
1.3.1 Background ..... 32
1.3.2 Metabolism and immune cell memory ..... 33
1.3.3 Epigenetic reprogramming ..... 35
1.3.4 Hyperglycaemic memory ..... 36
1.4 ITACONATE ..... 37
1.4.1 Itaconate origins ..... 37
1.4.2 Itaconate derivatives ..... 37
1.4.3 Itaconate as an anti-oxidant ..... 40
1.4.4 Itaconate in metabolism ..... 41
1.4.5 Itaconate in cardiovascular disease ..... 42
1.5 VASCULAR HOMEOSTASIS ..... 44
1.5.1 Endothelium dependent mechanisms of contraction ..... 44
1.5.2 Endothelium independent mechanisms of vasocontraction ..... 45
1.5.3 Nitric oxide in vessels and macrophages ..... 45
1.5.4 NOS catalysis ..... 46
1.5.5 Tetrahydrobiopterin synthesis ..... 47
1.6 HYPOTHESIS AND AIMS ..... 50
1.6.1 Hypothesis ..... 50
1.6.2 Aims ..... 50

CHAPTER 2: MATERIALS AND METHODS ..... 52

2.1 ANIMALS ..... 52
2.1.1 R26 CreER$^{T2}$ Gch$^{fl/fl}$ mouse ..... 52
2.1.2 Gch$^{fl/fl}$ Tie2Cre mouse ..... 53
2.1.3 βV59M (Kir6.2-V59M) mouse ..... 53
2.2 CELL CULTURE ..... 54
2.2.1 Bone Marrow Derived Macrophages ..... 54
2.2.2 Human Embryonic Kidney cells ..... 57
2.2.3 Cell viability ..... 57
2.3 GENOTYPING PCR ..... 57
2.3.1 Excision PCR - R26 CreER$^{T2}$ Gch$^{fl/fl}$ ..... 57
2.3.2 βV59M BMDM ..... 60

2.4 FLOW CYTOMETRY ..... 60
2.5 QUANTITATIVE REAL-TIME QPCR ..... 60
2.5.1 RNA extraction and quantification ..... 61
2.5.2 Generation of cDNA by RT-qPCR ..... 61
2.5.3 RT-qPCR primers ..... 62
2.5.4 Quantitative real-time RT-PCR ..... 62
2.6 WESTERN BLOT ..... 63
2.6.1 Preparation of protein lysates ..... 63
2.6.2 Measuring protein content ..... 64
2.6.3 Western blotting ..... 64
2.7 CYTOKINE MEASUREMENTS BY ELISA ..... 66
2.8 MEASUREMENT OF NITRITE ACCUMULATION USING GRIESS ASSAY ..... 67
2.9 SEAHORSE XFE96 EXTRACELLULAR FLUX ASSAYS ..... 68
2.9.1 Preparation for Seahorse extracellular flux assays ..... 68
2.9.2 Seahorse MitoStress Test to analyse mitochondrial respiration in BMDMs ..... 69
2.9.3 Seahorse MitoStress Test calculations ..... 71
2.9.4 Glycolytic rate assay ..... 72
2.9.5 Seahorse ATP rate assay in BMDMs ..... 73
2.9.6 Seahorse Glutamine dependency assay in BMDMs ..... 74
2.9.7 Seahorse Fatty Acid oxidation assay in BMDMs ..... 75
2.9.8 Calcein Live/Dead cell assay ..... 76
2.10 MEASUREMENT OF BH4 BY HPLC ..... 76
2.11 METHOD DEVELOPMENT AND VALIDATION FOR THE DETECTION OF ITACONIC ACID BY HIGH PERFORMANCE LIQUID CHROMATOGRAPHY ..... 78
2.11.1 INTRODUCTION ..... 78
2.11.2 METHOD ..... 79
2.11.2.1 Instrumentation ..... 79
2.11.2.2 Chemicals and Reagents ..... 79
2.11.2.3 Chromatographic conditions ..... 80
2.11.2.4 Preparation of standard solutions ..... 80
2.11.2.5 Preparation of sample solutions ..... 80
2.11.2.6 Method validation ..... 81
2.11.2.7 Specificity ..... 81
2.11.2.8 Linearity and range ..... 81
2.11.2.9 Sensitivity ..... 82
2.11.2.10 Accuracy and Precision ..... 82
2.11.2.11 Stability ..... 82
2.11.2.12 Data Processing ..... 83
2.11.3 RESULTS AND DISCUSSION ..... 84
2.11.3.1 SAMPLE PREPARATION – PROTEIN PRECIPITATION ..... 84
2.11.3.2 METHOD VALIDATION ..... 86
2.11.3.2.1 Specificity ..... 86
2.11.3.2.2 Linearity and range ..... 90
2.11.3.2.3 Limit of Detection and Limit of Quantification ..... 92
2.11.3.2.4 Accuracy and Precision ..... 92
2.11.3.2.5 Stability ..... 93
2.11.4 CONCLUSION ..... 94
CHAPTER 3: THE ROLE OF TETRAHYDROBIOPTERIN IN MACROPHAGE METABOLISM ..... 96
3.1 INTRODUCTION ..... 96
3.2 HYPOTHESIS AND AIMS ..... 99
3.2.1 Hypothesis ..... 99
3.2.2 Aims ..... 99
3.3 METHODS ..... 100
3.3.1 R26-CreER$^{T2}$Gch$^{fl/fl}$ and GchTie2Cre BMDM culture ..... 100
3.4 RESULTS ..... 101
3.4.1 Gch1 is excised from R26-CreER$^{T2}$Gch$^{fl/fl}$ bone marrow derived macrophages ..... 101

3.4.2 R26-CreER$^{T2}$Gch$^{fl/fl}$ BMDMs have diminished BH4 and nitrite levels ..... 103
3.4.3 Characterisation of Gch-KO unstimulated and M$^{LPS/IFN\gamma}$ ..... 105
3.4.4 BH4-deficient M$^{LPS/IFN-\gamma}$ have increased IL1β cytokine release ..... 107
3.4.5 BH4-deficient M$^{LPS/IFN\gamma}$ macrophages have increased mitochondrial respiration ..... 109
3.4.6 BH4-deficient M$^{LPS/IFN-\gamma}$ have increased glycolytic capacity ..... 113
3.4.7 Abundance of glycolytic metabolites are decreased and Pentose Phosphate Pathway unchanged in BH4 deficient M$^{LPS/IFN\gamma}$ ..... 115
3.4.8 BH4-deficient M$^{LPS/IFN-\gamma}$ have decreased expression of certain enzymes in the glycolytic pathway 117
3.4.9 ATP generation via Glycolysis or OXPHOS in Gch$^{fl/fl}$ and BH4-deficient macrophages ..... 119
3.4.10 BH4-deficient M$^{LPS/IFN-\gamma}$ do not use fatty acid oxidation for ATP production ..... 121
3.4.11 Most fatty acid metabolism metabolites remain unchanged in BH4-deficient M$^{LPS/IFN-\gamma}$ .. 122
3.4.12 BH4-deficient M$^{LPS/IFN-\gamma}$ have decreased eicosanoid levels ..... 124
3.4.13 BH4-deficient M$^{LPS/IFN-\gamma}$ are more dependent on the Glutamine oxidation pathway ..... 126
3.4.14 Glutamine levels are unchanged in BH4-deficient M$^{LPS/IFN-\gamma}$ macrophages ..... 127
3.5 DISCUSSION ..... 129
3.5.1 Overview ..... 129
3.5.2 A novel mouse model of BH4 and NO deficiency ..... 129
3.5.3 Loss of BH4 alters TCA substrate metabolism ..... 130
3.5.4 Metabolism drives Inflammation? ..... 131
3.5.5 Itaconate – the anti-inflammatory metabolite in a pro-inflammatory macrophage ..... 133
3.5.6 Future work ..... 134

CHAPTER 4: EFFECTS OF HYPERGLYCAEMIA ON WT AND BH4 DEFICIENT MACROPHAGES 136

4.1 INTRODUCTION ..... 136
4.2 HYPOTHESIS AND AIMS ..... 138
4.2.1 Hypothesis ..... 138
4.2.2 Aims ..... 138
4.3 METHODS ..... 139
4.3.1 Cell culture ..... 139
4.4 RESULTS ..... 140
4.4.1 Glycolytic gene expression is unaltered in HG-treated Gch$^{fl/fl}$ and GCH-KO macrophages . 140
4.4.2 IL1β and IL6 levels are unaltered with HG in Gch$^{fl/fl}$ and Gch-KO BMDMs ..... 142
4.4.3 NO production is unaltered with HG in Gch$^{fl/fl}$ and Gch-KO BMDMs ..... 144
4.4.4 Irg1 expression and itaconate levels are unaltered HG in Gch$^{fl/fl}$ and Gch-KO BMDMs ..... 146
4.4.5 Literature on hyperglycaemic macrophages reveal inconsistent results ..... 148
4.5 DISCUSSION ..... 150
4.5.1 Overview ..... 150
4.5.2 HG as an inflammatory stimulus yields inconsistent results ..... 150
4.5.3 Studies of HG as a metabolic stimulus report heterogenous results ..... 152
4.5.4 In vitro vs in vivo hyperglycaemia – differences in models and methodology ..... 152
4.5.5 Future work ..... 154

CHAPTER 5: HYPERGLYCAEMIA-INDUCED CHANGES IN MACROPHAGE METABOLISM .. 156

5.1 INTRODUCTION ..... 156
5.2 HYPOTHESIS AND AIMS ..... 158
5.2.1 Hypothesis ..... 158
5.2.2 Aims ..... 158
5.3 METHODS ..... 159
5.3.1 Cell culture ..... 159
5.3.2 Metabolomics sample preparation ..... 159
5.3.3 Metabolomics analysis ..... 160
5.4 RESULTS ..... 161
5.4.1 βV59M-diabetic mouse model ..... 161
5.4.2 βV59M-diabetic mice have altered inflammatory profile ..... 163
5.4.3 Itaconate levels are unaltered in βV59M-diabetic mice ..... 165

5.4.4 Metabolomics analysis of Control and βV59M-diabetic macrophages ..... 167
5.4.5 Hierarchical clustering analysis (HCA) of Control and βV59M-diabetic mice ..... 169
5.4.6 Significantly altered metabolites in Control and βV59M-diabetic macrophages due to LPS/IFNγ and hyperglycaemia ..... 170
5.4.7 Enrichment and pathway analysis ..... 172
5.4.8 Glycolysis ..... 174
5.4.9 TCA cycle ..... 177
5.4.10 Fatty acid metabolism ..... 179
5.4.11 Eicosanoids ..... 182
5.4.12 Glutamine metabolism ..... 183
5.4.13 Arginine metabolism ..... 186
5.4.14 Aspartate metabolism ..... 189
5.4.15 Sphingomyelin metabolism ..... 191
5.5 DISCUSSION ..... 194
5.5.1 Overview ..... 194
5.5.2 Hyperglycaemia alters macrophage inflammatory profile ..... 194
5.5.3 Hyperglycaemia alters macrophage response to stimulation ..... 195
5.5.4 Hyperglycaemia induces priming in macrophages ..... 196
5.5.5 Experimental Design ..... 197
5.5.6 Is hyperglycaemia alone sufficient to induce long term metabolic changes? ..... 197
5.5.7 Future work ..... 198
CHAPTER 6: THE ROLE OF EXOGENOUS ITACONATE ON VASCULAR FUNCTION ..... 200
6.1 INTRODUCTION ..... 200
6.2 HYPOTHESIS AND AIMS ..... 204
6.2.1 Hypothesis ..... 204
6.2.2 Aims ..... 204
6.3 METHODS ..... 205
6.3.1 The Oxford Heart, Vessels & Fat cohort ..... 205
6.3.2 The AdipoRedox study ..... 207
6.3.3 Sample collection and superoxide ..... 208
6.3.4 Measurement of superoxide production ..... 208
6.3.5 oxHVF cohort Genome wide SNP array ..... 208
6.3.6 Wire myography in mouse aorta ..... 209
6.3.6.1 Animals ..... 209
6.3.6.2 Isometric Tension Vasomotor Studies ..... 209
6.4 RESULTS ..... 211
6.4.1 Demographics of study participants ..... 211
6.4.2 Study design and analysis workflow of oxHVF cohort to identify ACOD1 SNP ..... 213
6.4.3 ACOD1 Rs17470171 is associated with increased superoxide production ..... 216
6.4.4 ACOD1 Rs17470171 is associated with improved vasorelaxation ..... 218
6.4.5 4-octyl itaconate treatment blunts preconstriction in mouse aorta ..... 220
6.4.6 4-octyl itaconate prevents reconstruction via endothelium independent mechanisms in mouse aorta 222
6.4.7 Octanol prevents preconstriction to a lesser extent to 4-octyl itaconate in mouse aortas and independent of the endothelium ..... 224
6.4.8 Itaconate prevents preconstriction less potently than 4-octyl itaconate and independent of endothelium ..... 226
6.4.9 Itaconate and Octanol mediated loss of constriction have additive effect ..... 228
6.5 DISCUSSION ..... 230
6.5.1 Overview ..... 230
6.5.2 ACOD1 in cardiovascular disease ..... 230
6.5.3 Is itaconate a vasodilator? ..... 231
6.5.4 Itaconate or itaconate derivatives ..... 233
6.5.5 Itaconate as a potential therapeutic ..... 234
6.5.6 Future work ..... 235
CHAPTER 7: FINAL DISCUSSION ..... 238

7.1 Original hypotheses and aims ..... 238
7.2 Key findings ..... 238
7.3 Perspectives and future directions ..... 239
REFERENCES ..... 243
APPENDICES ..... 261
TIMING AND VENUE OF RESEARCH ..... 263
RESEARCH FUNDING ..... 263
PUBLICATIONS ..... 263
PRESENTATIONS ..... 263

# List of Figures

Figure 1. 1 Glycolysis overview ..... 26
Figure 1. 2 TCA cycle in resting macrophages ..... 29
Figure 1. 3 TCA cycle rewiring in inflammatory macrophages ..... 30
Figure 1. 4 Chemical structures of itaconate, itaconate derivatives and structurally similar metabolites ..... 39
Figure 1. 5 Cellular signalling pathways by which itaconate regulates the inflammatory response ..... **Error! Bookmark not defined.**

Figure 2. 1 Murine bone marrow isolation procedure ..... 55
Figure 2. 2 Schematic of BMDM culture protocol timeline ..... 56
Figure 2. 3 Genotyping R26-CreER$^{T2}$Gch$^{fl/fl}$ BMDMs ..... 59
Figure 2. 4 Representative Griess assay 96 well plate ..... 68
Figure 2. 5 Schematic MitoStress test profile with calculated parameters and representative MitoStress test trace ..... 70
Figure 2. 6. High Performance Liquid Chromatography (HPLC) setup with key components: UV-Vis detector, degasser, pump and autosampler labelled. ..... 79
Figure 2. 7 Protein precipitation sample preparation optimisation ..... 85
Figure 2. 8 Chromatograms of itaconic acid on HPLC ..... 88
Figure 2. 9 Standards of structurally similar metabolites to itaconate **Error! Bookmark not defined.**
Figure 2. 10 Linearity and range for itaconic acid. ..... 91

Figure 3. 1 Mitochondrial respiration in Gch$^{fl/fl}$Tie2cre model of BH4 deficiency ..... 98
Figure 3. 2 Schematic of Gch-KO BMDM culture protocol ..... 100
Figure 3. 3 *Gch1* is excised from R26-CreER$^{T2}$ Gch$^{fl/fl}$ bone marrow derived macrophages ..... 102
Figure 3. 4 R26 CreER$^{T2}$Gch$^{fl/fl}$ BMDMs have diminished BH4 and nitrite levels ..... 104
Figure 3. 5 Characterisation of R26-CreER$^{T2}$Gch$^{fl/fl}$ unstimulated and M$^{LPS/IFN-\gamma}$ ..... 106
Figure 3. 6 BH4-deficient M$^{LPS/IFN-\gamma}$ have increased inflammatory cytokine expression . 108
Figure 3. 7 BH4-deficient M$^{LPS/IFN-\gamma}$ have increased mitochondrial respiration ..... 110
Figure 3. 8 TCA cycle anti-inflammatory metabolite, itaconate, production is increased in BH4-deficient M$^{LPS/IFN-\gamma}$ ..... 112
Figure 3. 9 BH4-deficient M$^{LPS/IFN-\gamma}$ have increased glycolytic capacity ..... 114
Figure 3. 10 BH4-deficient M$^{LPS/IFN-\gamma}$ have decreased glycolytic and unchanged Pentose Phosphate Pathway metabolites ..... 116
Figure 3. 11 BH4-deficient M$^{LPS/IFN-\gamma}$ have decreased expression of certain enzymes in the glycolytic pathway ..... 118
Figure 3. 12 Ratio of ATP generated via Glycolysis or OXPHOS in Gch$^{fl/fl}$ and BH4-deficient macrophages ..... 120

Figure 3. 13BH4-deficient $M^{LPS/IFN-\gamma}$ macrophages do not have increased mitochondrial respiration due to Fatty Acid Oxidation ..... 121
Figure 3. 14 Metabolites involved in Fatty acid synthesis and metabolism in BH4-deficient macrophages ..... 123
Figure 3. 15 Metabolites involved in eicosanoid production ..... 125
Figure 3. 16 BH4-deficient $M^{LPS/IFN-\gamma}$ are more dependent on the glutaminolysis pathway ..... 126
Figure 3. 17 BH4-deficient $M^{LPS/IFN-\gamma}$ do not have increased glutamine levels..... 128

Figure 4. 1 $Gch^{fl/fl}$ and R26Cre-$ER^{T2}Gch^{fl/fl}$ culture protocol..... 139
Figure 4. 2 *Slc2a1* and *Hk2* expression is unaltered with HG in $Gch^{fl/fl}$ and Gch-KO BMDMs ..... 140
Figure 4. 3 IL1β and IL6 levels are unaltered with HG in $Gch^{fl/fl}$ and Gch-KO BMDMs 142
Figure 4. 4 NO production is unaltered with HG in $Gch^{fl/fl}$ and Gch-KO BMDMs..... 144
Figure 4. 5 Irg1 expression and itaconate levels are unaltered with HG in $Gch^{fl/fl}$ and Gch-KO BMDMs ..... 146

Figure 5. 1 Schematic of βV5M-diabetic BMDM culture protocol ..... 159
Figure 5. 2 Overview of diabetic mouse model..... 162
Figure 5. 3 IL1β and TNF-α levels are increased in control and diabetic macrophages ± LPS/IFN-γ and ± HG ..... 163
Figure 5. 4 Itaconate levels are unchanged in control and diabetic macrophages ± LPS/IFN-γ and ± HG ..... 166
Figure 5. 5 Metabolomics analysis workflow ..... 168
Figure 5. 6 Hierarchical Clustering Analysis (HCA) of Control and βV59M-Diabetic macrophages samples based on stimulation, glucose treatment, and mouse genotype..... 169
Figure 5. 7 Enrichment analysis and pathway analysis ..... 173
Figure 5. 8 Glycolysis in control and diabetic macrophages ± LPS/IFN-γ and ± HG ..... 175
Figure 5. 9 TCA cycle overview of control and diabetic macrophages ± LPS/IFN-γ and ± HG ..... 177
Figure 5. 10 Fatty acid metabolism in control and diabetic macrophages ± LPS/IFN-γ and ± HG ..... 180
Figure 5. 11 Eicosanoids in control and diabetic macrophages ± LPS/IFN-γ and ± HG .. 183
Figure 5. 12 Glutamine metabolism in Control and Diabetic macrophages ± LPS/IFN-γ and ± HG ..... 184
Figure 5. 13 Arginine metabolism in control and diabetic macrophages ± LPS/IFN-γ and ± HG ..... 187
Figure 5. 14 Aspartate metabolism in control and diabetic macrophages ± LPS/IFN-γ and ± HG ..... 189
Figure 5. 15 Sphingomyelins of control and diabetic macrophages ± LPS/IFN-γ and ± HG ..... 191

Figure 6. 1 The structure of itaconate itaconate derivatives: 4-octyl itaconate (4-OI) and dimethyl itaconate (DI) ..... 200
Figure 6. 2 The Oxford Heart Vessels and Fat (OxHVF) cohort work flow ..... 206
Figure 6. 3 ACOD1 SNPs identification workflow ..... 214
Figure 6. 4 ACOD1 rs17470171 is associated with increased superoxide production in IMA of patients ..... 217
Figure 6. 5 ACOD1 rs17470171 is associated with improved vasorelaxation in IMA of patients ..... 219
Figure 6. 6 4-OI treatment prevents preconstriction in mouse aorta ..... 221
Figure 6. 7 4-OI prevents preconstriction via endothelium independent mechanisms in mouse aorta ..... 223
Figure 6. 8 Octanol prevents preconstriction to a lesser extent to 4-OI in mouse aortas and independent of the endothelium ..... 225
Figure 6. 9 Itaconate causes loss of vasoconstriction less potently than 4OI and independent of endothelium ..... 227
Figure 6. 10 Loss of vasoconstriction by itaconate and octanol have an additive effect ..... 229

Appendix A – Other parameters measured in oxHVF cohort participants ..... 262

## List of Tables

Table 2. 1 Thermocycler settings for Gch1 genotyping PCR ..... 58
Table 2. 2 Details of TaqMan assays used in RT-qPCR reactions ..... 62
Table 2. 3 Thermocycler setting for RT-qPCR ..... 63
Table 2. 4 Table of antibodies used for western blot analyses ..... 66
Table 2. 5 Functions of drugs on inner mitochondrial membrane ..... 70
Table 2. 6 Settings used to carry out Seahorse XF96 MitoStress test ..... 70
Table 2. 7 Calculations to determine respiratory function ..... 71
Table 2. 8 Glycolytic rate assay calculations to determine respiratory function ..... 72
Table 2. 9 ATP rate assay calculations to determine respiratory function ..... 73
Table 2. 10 Glutamine Dependency assay calculations to determine respiratory function ..... 74
Table 2. 11 Fatty Acid Oxidation assay calculations to determine respiratory function ..... 75
Table 2. 12 High performance liquid chromatographic condition ..... 80
Table 2. 13 LOD and LOQ for cell lysates (PBS) and supernatants (media) ..... 92
Table 2. 14 Results of precision and accuracy ..... 93
Table 2. 15 Results of stability and repeatability ..... 94

Table 4. 1 Summary of selected studies on the effects of hyperglycaemia in macrophages ..... 149

Table 5. 1 Samples sent for metabolomics analysis ..... 167
Table 5. 2 Significantly altered metabolites due to LPS/IFN-ɣ stimulation in Control and βV59M-diabetic macrophages ..... 171
Table 5. 3 Significantly altered metabolites due in Control and βV59M-diabetic macrophages ..... 171
Table 5. 4 Significantly altered metabolites due to HG-treatment in Control and βV59M-diabetic macrophages ..... 171

Table 6. 1 Therapeutic evidence of itaconate and its derivatives in various models of disease ..... 203
Table 6. 2 Summary of population inclusion and exclusion criteria ..... 207
Table 6. 3 Demographics of study participants ..... 212
Table 6. 4 Position, function and associations found for 7 identified ACOD1 SNPs ..... 215

## List of Abbreviations

| | |
|---|---|
| **AAA** | Abdominal Aortic Aneurysm |
| **ACC** | Acetyl-CoA carboxylase |
| **ACLY** | ATP-citrate lyase |
| **ACOD1** | Aconitate decarboxylase 1 |
| **AGE** | Advanced glycation end products |
| **ALDOA** | Aldolase A |
| **Arg-1** | Arginase 1 |
| **ASCVD** | Atherosclerotic cardiovascular disease |
| **Asl** | Arginosuccinate lyase |
| **Ass1** | Arginosuccinate synthetase |
| **ATF3** | Activating transcription factor |
| **ATM** | Adipose tissue macrophages |
| **BCA** | Bicinchoninic acid |
| **BCG** | Bacillus Calmette-Guerin |
| **BH4** | 5,6,7,-tetrahydrobiopterin |
| **BHF** | British Heart Foundation |
| **BMDM** | Bone marrow derived macrophages |
| **CABG** | Coronary artery bypass graft |
| **CANTOS** | Canakinumab Anti-inflammatory Thrombosis Outcome Study |
| **CARKL** | Carbohydrate kinase-like protein |
| **cDNA** | complementary DNA |
| **cGMP** | Cyclic guanosine monophosphate |
| **coA** | Coenzyme A |
| **CRP** | C-reactive protein |
| **Ct** | Cycle threshold |
| **CVD** | Cardiovascular disease |
| **DAG** | Diacylglycerol |
| **DHAP** | Dihydroxyacetone phosphate |
| **DHFR** | Dihydrofolate reductase |
| **DI** | Dimethyl itaconate |
| **ECAR** | Extracellular acidification rate |
| **EDCF** | Endothelium constricting factors |
| **EDH** | Endothelium-dependent hyperpolarization |
| **EDRF** | Endothelium derived relaxing factors |
| **EDTA** | Etheylenediaminetetraacetic acid |
| **eIF2a** | Eukaryotic initiation factor 2 |
| **ELISA** | Enzyme-linked immunosorbent assay |
| **eNOS** | Endothelial NOS |
| **ESI** | Electron spray ionisation |
| **ETC** | Electron transport chain |
| **FAD** | Flavin, adenine dinucleotide |
| **FAM** | 6-carboxyfluorescien |

| | |
|---|---|
| **FAO** | Fatty acid oxidation |
| **FAS** | Fatty acid synthesis |
| **FGF** | Functional Genetics Facility |
| **FMN** | Flavin mononucleotide |
| **G6PD** | Glucose-6-phosphate dehydrogenase |
| **GAPDH** | Glyceraldehyde-3-phosphate dehydrogenase |
| **GLUT1** | Glucose transporter 1 |
| **GMCSF** | Granulocyte-macrophage colony-stimulating factor |
| **GOI** | Gene of interest |
| **GPCR** | G-protein coupled receptors |
| **GSDMD** | Gasdermin-D |
| **GSH** | Glutathione |
| **GTP** | Guanine triphosphate |
| **GTPCH** | GTP cyclohydrolase |
| **HCA** | Hierarchical clustering analysis |
| **HEK** | Human embryonic kidney |
| **HG** | High glucose |
| **HPLC** | High-performance liquid chromatography |
| **ICAM1** | Intercellular adhesion molecule 1 |
| **IDH1** | Isocitrate dehydrogenase |
| **IFN-γ** | Interferon-gamma |
| **IL-6** | Interleukin-6 |
| **IL1β** | Interleukin-1 beta |
| **iNOS** | Inducible nitric oxide synthase |
| **IP3** | Inositol 1,4,5-triphosphate |
| **IRAK** | Interleukin-1-receptor-associated-kinase |
| **JAK1** | Janus kinase 1 |
| **KEGG** | Kyoto encyclopaedia of genes and genomes |
| **KHB** | Krebs henseleit buffer |
| **LDHA** | Lactate dehydrogenase |
| **LOD** | Limit of detection |
| **LOQ** | Limit of quantification |
| **LPS** | Lipopolysaccharide |
| **M** | Mannitol |
| **MCSF** | Macrophage colony stimulating factor |
| **MD2** | Myeloid differentiation protein 2 |
| **MLCK** | Myosin light chain kinase |
| **MSEA** | Metabolite set enrichment analysis |
| **MUT** | Methylmalonyl-CoA mutase |
| **m/z** | Mass to charge ratio |
| **NADPH** | Nicotinamide adenine-dinucleotide phosphate |
| **NG** | Normoglycaemia |
| **NH2-triP** | 7-8 dihydroneopterin triphosphate |

| | |
|---|---|
| **NLRP3** | NLR family pyrin domain containing 3 |
| **NO** | Nitric oxide |
| **Nrf2** | Nuclear factor erythroid 2-related factor 2 |
| **NTC** | Non-template control |
| **OCR** | Oxygen consumption rate |
| **ODQ** | 1H-(1,2,4)oxadiazolo[4,3-a]quinoxalin-1-one |
| **OX-HVF** | Oxford Heart, Vessels & Fat |
| **oxLDL** | Oxidized low-density lipoproteins |
| **OXPHOS** | Oxidative phosphorylation |
| **PBS** | Phosphate buffered saline |
| **PCR** | Polymerase chain reaction |
| **PE** | Phenylephrine |
| **PGF2a** | Prostaglandin F2α |
| **PIP2** | Phosphatidylinositol 4,5-biphosphate |
| **PKA** | Protein kinase A |
| **PKG** | Protein kinase G |
| **PL** | Protein leak |
| **PPP** | Pentose phosphate pathway |
| **PTPS** | 6-pyruvoly tetrahydropterin synthase |
| **RI** | Retention time/index |
| **RNS** | Reactive nitrogen species |
| **ROS** | Reactive oxygen species |
| **Rot/AA** | Rotenone/antimycin A |
| **RT-qPCR** | Reverse transcriptase quantitative PCR |
| **SDH** | Succinate dehydrogenase |
| **sGC** | Soluble guanylyl cyclase |
| **SM** | Sphingomyelin |
| **SMC** | Smooth muscle cell |
| **SMS** | Sphingomyelin synthases |
| **SNP** | Single nucleotide polymorphism |
| **SR** | Sepiapterin reductase |
| **STZ** | Streptozotocin |
| **SUNCR1** | Succinate receptor 1 |
| **SV** | Saphenous vein |
| **TAK1** | Transforming growth factor-β (TGF-β)-activated kinase 1 |
| **TCA** | Tricarboxylic acid |
| **TET** | Ten-eleven translocation |
| **TGF-beta** | Transforming growth factor-beta |
| **TIR** | Toll-interleukin 1 receptor |
| **TIRAP** | Toll-interleukin 1 receptor domain containing adapter protein |
| **TLR4** | Toll like receptor 4 |
| **TNF-α** | Tumour necrosis factor alpha |
| **TRAF6** | Tumour necrosis factor receptor associated factor 6 |

| | |
|---|---|
| **TRAM** | TRIF-related adaptor molecule |
| **TRIF** | TIR-domain-containing adapter-inducing interferon-β |
| **UPLC** | Ultra-performance liquid chromatography |
| **VCAM1** | Vascular cell adhesion molecule 1 |
| **4-EI** | 4-ethyl itaconate |
| **4-OHT** | 4-hydroxytamoxifen |
| **4-OI** | 4-octyl itaconate |

# Chapter 1

# Introduction

# Chapter 1: Introduction

## 1.1 Macrophage overview

### 1.1.1 Cardiovascular disease overview

Cardiovascular diseases (CVD) are the leading cause of mortality globally (Roth et al., 2020; WHO, 2021). In the UK alone, 7.6 million people live with cardiovascular diseases, with related healthcare costs estimated at £9 billion per year (BHF, 2023). Many risk factors contribute to cardiovascular disease development including hypertension, diabetes, chronic kidney function, obesity, air pollution and smoking. Of these, hypertension affects approximately 28% of adults in the UK and is linked to half of heart attacks and stroke. Furthermore, diabetic patients are 2-3 times more likely to develop and twice as likely to die from cardiovascular diseases (BHF, 2023). Better understanding of this complex set of diseases will lead to discovery of new targets and development of novel therapies to ultimately improve prognosis, quality of life and survival rates.

### 1.1.2 Inflammation and macrophages in cardiovascular disease

It was over 200 years ago that pathologists Rudolph Virchow and Carl von Rokitansky debated whether inflammatory changes within atherosclerotic vessel walls played a primary or secondary role in atherogenesis (Virchow, 1989; von Rokitansky, 1854). The critical role of inflammatory macrophages in the development and progression of atherosclerosis is now well established (Moore et al., 2013; Willerson & Ridker, 2004). During atherogenesis, lipid deposition in the artery intima activates endothelial cells resulting in increased expression of adhesion molecules (i.e., Vascular Cell Adhesion Molecule 1 (VCAM1), Intercellular Adhesion Molecule 1 (ICAM1)) on the cell's surface (Gimbrone & García-Cardeña, 2016). This leads to the recruitment and differentiation of monocytes to macrophages which take up oxidized low-density lipoproteins (oxLDLs) and become foam cells (Goldstein et al.,

1979). Macrophages also release pro-inflammatory cytokines and chemokines, which attract more immune cells to the site of injury and promote the further accumulation of foam cells. Moreover, macrophages located in the plaques secrete proteolytic enzymes that can break down the extracellular matrix of the plaque. This reduces the stability of the plaque, which increases the chances of rupture, potentially resulting in a stroke or myocardial infarction (Bentzon et al., 2014; Libby, 2013).

Chronic low-grade inflammation can cause the production of pro-inflammatory cytokines, such as TNF-alpha and interleukin-6 (IL-6), which interfere with insulin signalling and contribute to insulin resistance. Studies have shown that adipose tissue macrophages (ATMs) accumulate in the adipose tissue of obese individuals, and release pro-inflammatory cytokines and chemokines that contribute to insulin resistance (Guria et al., 2023). Adipose tissue macrophage polarization from anti-inflammatory M2 to pro-inflammatory M1 phenotype exacerbates inflammation and insulin resistance (Fujisaka, 2021). In fact, ablation of CD11c+ macrophages normalised insulin sensitivity in obese insulin resistant animals (Patsouris et al., 2008). Hyperglycaemia can also contribute to activation of the transcription factor NFkB which again can lead to the production of IL1β, IL6 and TNF-α from macrophages and endothelial cells (Patel & Santani, 2009). Furthermore, hyperglycaemia can lead to the production of advanced glycation end products (AGEs) which form when glucose bind to proteins or lipids in a non-enzymatic process and accumulate in tissues. These AGEs can stimulate immune cells to produce pro-inflammatory cytokines (Singh et al., 2014).

### 1.1.3 Targeting inflammation as a therapy in cardiovascular disease

Although inflammation has long been recognized as a contributing factor, it was not until the proof-of-concept Canakinumab Anti-Inflammatory Thrombosis Outcomes Study

(CANTOS) trial that targeting inflammation was established as a therapeutic target (Ridker et al., 2017). IL1β is a potent inducer of the innate immune response and has been implicated in the development of atherosclerosis through decades of extensive experimental research (Dewberry et al., 2000; Dinarello, 2011).

In the trial, over 10,000 patients with a history of myocardial infarction and with CRP levels above 2 mg/L were treated with canakinumab, an anti-IL1β monoclonal antibody. In the CANTOS trial, after a median treatment period of 3.7 years, canakinumab treatment resulted in a reduction in IL6 and C-reactive protein (CRP) levels by up to 40-60%, as well as a reduction in major cardiovascular events by 15% overall and 25% in patients who achieved on treatment CRP level below 2 mg/L. However, overall mortality was not reduced. The CANTOS trial was followed by other studies including the Colchicine Cardiovascular Outcomes Trial (COLCOT) in 2019 which investigated the effects of colchicine in 2366 patients recruited within 30 days of having an acute MI. With a median follow-up of 28.6 months, daily treatment with colchicine resulted in a 31% lower relative risk of cardiovascular disease endpoints compared to placebo. In addition, colchicine reduced the risk of atherosclerotic cardiovascular disease by 23% compared to placebo in patients with coronary artery disease, although CRP levels were not measured in this trial (Tardif et al., 2019). Both colchicine and canakinumab are believed to inactivate the NLR Family Pyrin Domain Containing 3 (NLRP3) inflammasome, which, when activated, can lead to caspase 1-dependent release of IL1β. Other anti-inflammatory drugs are currently being investigated for the treatment of cardiovascular diseases; some trials include ASSAIL-MI which assesses anti-IL6 therapy, LILACS which assesses anti-IL2 therapy, CIRT which assesses methotrexate therapy, and CLEAR-synergy, CONVINCE and LoDoCo which all evaluate colchicine therapy for cardiovascular outcomes (Soehnlein & Libby, 2021). Although there are promising results from clinical trials, anti-inflammatory therapy has not yet been

approved for the treatment of any cardiovascular diseases. Therefore, it remains an area of active research and development (Ma & Chen, 2020).

### 1.1.4 Bone marrow derived macrophages

Macrophages are integral to the innate immune system and are arguably the most plastic cells in the haemopoietic system (Mosser & Edwards, 2008; Wynn et al., 2013). First described in 1883 by Metchnikoff, these ancient professional phagocytic cells display great functional diversity making them difficult to classify (Gordon, 2008). Tissue resident macrophages are sentinel cells involved in tissue homeostasis, responding to physiological changes as well as outside challenges. In contrast, in times of challenge, monocytes can be recruited from reservoirs located in the blood, spleen and bone marrow (Honold & Nahrendorf, 2018; Yona et al., 2013). This thesis focuses exclusively on bone marrow derived macrophages (BMDM) as a model to study macrophage differentiation and biology. Monocytes are differentiated to macrophages following exposure to macrophage colony stimulating factor (MCSF) and granulocyte-macrophage colony-stimulating factor (GMCSF). The subsequent differentiated macrophages were categorised into resting ($M^{Resting}$, also known as M0, or unstimulated macrophages), inflammatory ($M^{LPS/IFN\text{-}\gamma,}$ also known as M1 or classically activated macrophages) and reparative macrophages ($M^{IL4}$, also known as M2, or alternatively activated macrophages) but the validity of this M1/M2 paradigm has been seriously questioned (Murray et al., 2014; Nahrendorf & Swirski, 2016). Macrophages in fact respond with a mixture of traditionally thought pro-inflammatory and anti-inflammatory responses depending on the stimuli presented. Hence in this thesis we have referred to macrophages according to the stimulus encountered.

$M^{Resting}$ macrophages are the baseline state of macrophages, are characterised by low levels of cytokine production, and can be stimulated towards a phenotype. $M^{LPS/IFN\text{-}\gamma}$ macrophages, are induced by microbial production (such as LPS) and Th1 cytokines (such as interferon-

gamma (IFNγ)) (Pace et al., 1983). The phenotype of the macrophage is dependent on the specific stimuli used. $M^{LPS/IFN\text{-}\gamma}$ produce high levels of pro-inflammatory cytokines such as interleukin-1 beta (IL1β), tumour necrosis factor (TNF-α), interleukin-6 (IL6). In addition, they produce reactive oxygen species (ROS) and reactive nitrogen species (RNS) which aid removal of pathogens (Mosser & Edwards, 2008). On the other hand, $M^{IL4}$ macrophages, are induced by Th2 cytokines such as interleukin-4 and interleukin-13 (Doyle et al., 1994; Stein et al., 1992). These macrophages produce high levels of anti-inflammatory cytokines such as interleukin-10 and transforming growth factor-beta (TGF-beta) (Mantovani et al., 2013; Orecchioni et al., 2019).

This thesis focuses primarily on $M^{Resting}$ and $M^{LPS/IFN\text{-}\gamma}$ macrophages.

### 1.1.5 TLR4 signalling

Toll like receptor 4 (TLR4) is a cell surface receptor that plays a key role in innate immune response, specifically recognising gram negative bacteria derived lipopolysaccharide (LPS). Binding of LPS to the TLR4/Myeloid differentiation protein 2 (MD2) receptor complex activates the TLR4 signalling pathway (Park et al., 2009). In macrophages, TLR4 can also be activated by interferon-gamma (IFNγ) which induces TLR4 expression and enhances LPS sensitivity (Kang et al., 2019). Upon activation, the Toll-interleukin 1 receptor (TIR) domain of TLR can be bound by TIR domain containing adaptor protein (TIRAP) or TIR domain containing adaptor inducing interferon-β (TRIF), and the recruitment of which determines subsequent signalling (Horng et al., 2002). In the plasma membrane, MyD99 adaptor protein is recruited via TIRAP and recruits interleukin-1-receptor-associated-kinase (IRAK) to the TLR4/MD2 complex, followed by recruiting of E3 ubiquitin ligase TNF receptor-associated factor 6 (TRAF6) and serine/threonine kinase Transforming grown factor-β-activated kinase 1 (TAK1) (Fitzgerald & Kagan, 2020). This leads to activation of NFκB and the subsequent transcription of pro-inflammatory cytokines, chemokines and other immune-related genes.

In the endosome, TLR4 binds to TRIF/TRAM, then Receptor-interacting serine/threonine-protein kinase 1 (RIP1) and TRAF6 before activating TAK1 to re-join the MyD88-dependant pathway (Fitzgerald & Kagan, 2020; Fitzgerald et al., 2003).

## 1.2 Macrophage metabolism

### 1.2.1 Arginine and NO metabolism

Macrophage polarisation states are also defined by their metabolic signature. In the simplest sense, $M^{LPS/IFN\text{-}\gamma}$ and $M^{IL4}$ have different arginine metabolism characteristics. $M^{LPS/IFN\text{-}\gamma}$ metabolise L-arginine into NO and L-citrulline via inducible nitric oxide synthase (iNOS), a classic marker of $M^{LPS/IFN\text{-}\gamma}$ macrophages, whereas $M^{IL4}$macrophages hydrolyse arginine to ornithine and urea by Arginase-1 (Arg-1) (Corraliza et al., 1995; Munder et al., 1998). Citrulline can react with aspartate to form arginosuccinate, a reaction catalysed by arginosuccinate synthetase (Ass1), and arginosuccinate can be further catalysed to arginine and fumarate via arginosuccinate lyase (Asl). In the early stages of NO production, macrophages reply mainly on extracellular arginine to synthesise NO. Once exogenous arginine is depleted, cells depend on citrulline to synthesise arginine in order to retain NO production (Qualls et al., 2012). Collectively, NO can dampen mitochondrial function and the local concentration of NO is critical in determining the pro-inflammatory or anti-inflammatory response in M1 macrophages to maintain the balance between host defence and tissue damage.

### 1.2.2 Glycolysis

Glycolysis is a 16-step fundamental metabolic pathway involving the breakdown of glucose to pyruvate for the production of ATP, the primary energy source for cellular activities. An overview of the glycolytic pathway is shown in Figure 1.1.

In macrophages, glycolysis can be induced by various stimuli such as inflammatory cytokines, microbial products, and hypoxia. This shift towards glycolysis is known as the

Warburg effect, and it enables macrophages to rapidly produce energy and biosynthetic intermediates needed for immune responses (Krawczyk et al., 2010; Warburg et al., 1927). Furthermore, the Warburg effect is associated with the polarization of macrophages towards the pro-inflammatory M1 phenotype, which promotes the production of pro-inflammatory cytokines and reactive oxygen species required for host defence against infections (Kelly & O'Neill, 2015; Krawczyk et al., 2010). Indeed, LPS stimulation has been shown to increase glucose transporter 1 (Glut1) expression resulting in increased glucose influx (Freemerman et al., 2014; Fukuzumi et al., 1996). Furthermore, Glut1 overexpression in RAW cells were shown to lead to increased glycolysis and be linked to a proinflammatory phenotype. Pentose phosphate pathway metabolism too was increased with GLUT1 overexpression whilst oxygen consumption rate (OCR) was significantly reduced (Freemerman et al., 2014). A similar pattern can be observed in endothelial cells too, which are basally more glycolytic. These cells saw increased glycolysis when activated by HIF-1α, which increased VCAM1 as well as other inflammatory cytokines (Soto-Heredero et al., 2020). Overall, the above studies provide evidence that increased glycolysis is a marker for the inflammatory state of macrophages.

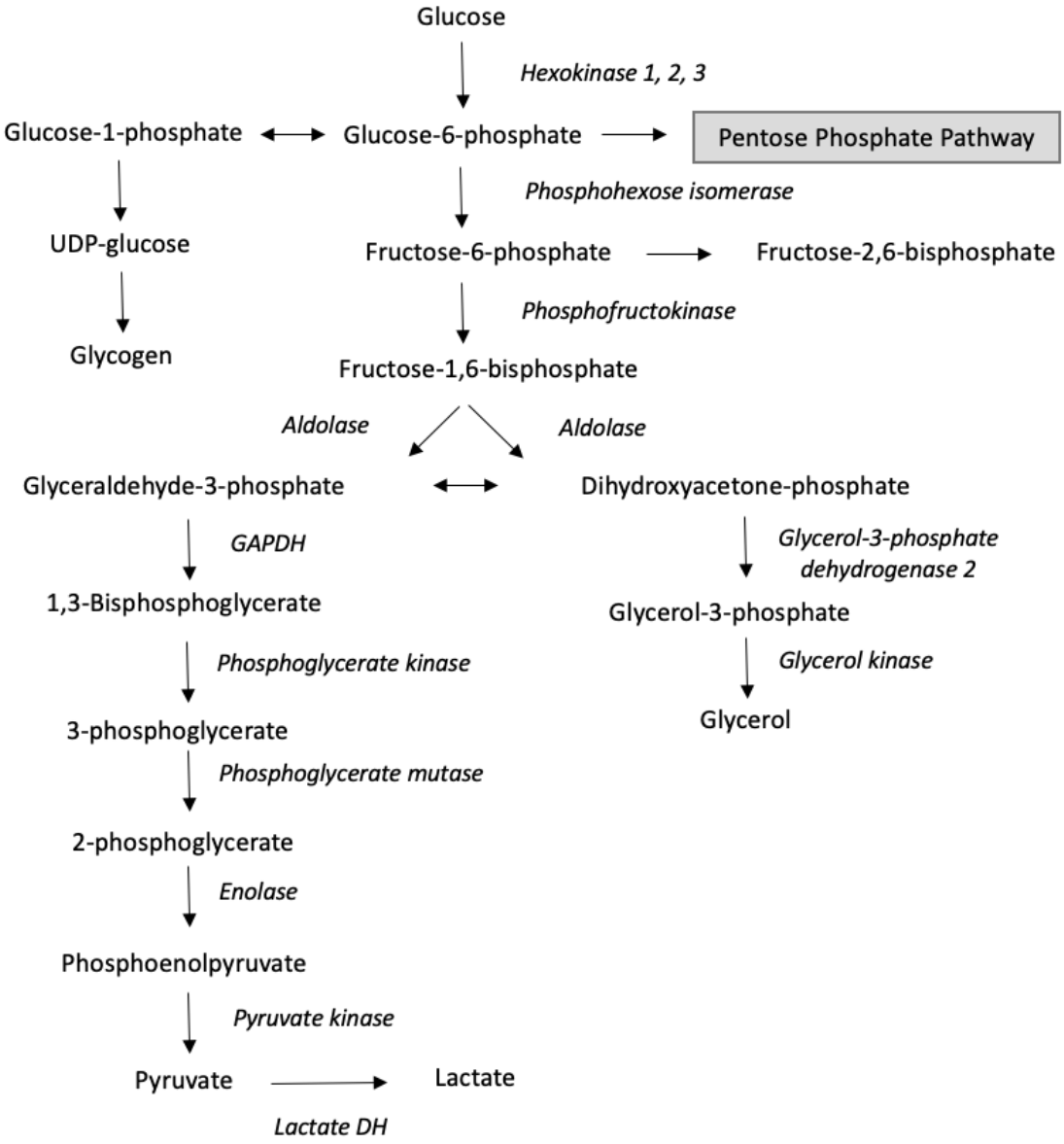



**Figure 1. 1 Glycolysis overview**

Glycolysis can be divided into the preparatory phase and the payoff phase. In the preparatory phase, glucose is phosphorylated by hexokinase or glucokinase to generate glucose-6-phosphate. The glucose-6-phosphate is then isomerized into fructose-6-phosphate by phosphohexose isomerase, followed by phosphorylation by phosphofructokinase to produce fructose-1,6-bisphosphate. This step is considered the committed step in glycolysis since it is irreversible and determines the rate of the pathway. In the payoff phase, fructose-1,6-bisphosphate is cleaved by aldolase to generate two 3-carbon molecules of glyceraldehyde-3-phosphate (G3P). Each G3P molecule is oxidized by glyceraldehyde-3-phosphate dehydrogenase to produce 1,3-bisphosphoglycerate (1,3-BPG), which is then converted into 3-phosphoglycerate by phosphoglycerate kinase, resulting in the generation of two ATP molecules. The 3-phosphoglycerate is then converted into pyruvate by the consecutive action of phosphoglycerate mutase and enolase. This conversion produces two more ATP molecules, as well as NADH, which can be used by the cell in various metabolic processes. The end product of glycolysis is lactate.

### 1.2.3 Pentose phosphate pathway

In inflammatory macrophages, the pentose phosphate pathway (PPP) is upregulated to support the biosynthesis of nucleotides, amino acids, and lipids required for cell growth and proliferation (Haschemi et al., 2012; Jha et al., 2015; Patra & Hay, 2014). This is driven by increased glucose flux through the PPP, with the upregulation of key enzymes such as glucose-6-phosphate dehydrogenase (G6PD), which catalyses the first and rate-limiting step of the oxidative PPP (Alving et al., 1956; Horecker, 2002).

Studies have shown that the increased production of reactive oxygen species (ROS) in inflammatory macrophages can activate the PPP, providing reducing equivalents in the form of NADPH for the antioxidant defence system (Patra & Hay, 2014). Jha et al found that macrophages deficient in G6PD exhibit decreased NADPH production and are less efficient at clearing bacterial infections (Jha et al., 2015). In another study, carbohydrate kinase-like protein (CARKL), which catalyses an orphan reaction in PPP was required for M1 and M2 polarisation (Haschemi et al., 2012). Furthermore, PPP inhibition has been shown to deactivate the inflammatory macrophage response in hypercholesterolemia (Baardman et al., 2018).

### 1.2.4 TCA cycle and Oxidative Phosphorylation

The tricarboxylic acid (TCA) cycle (also known as the Krebs cycle or the citric acid cycle) is a central metabolic pathway, which takes place in the mitochondria of eukaryotic cells, that generates energy through the oxidation of acetyl-CoA derived from different sources, including glucose, fatty acids, and amino acids. In macrophages, the primary fuel for the TCA cycle is glucose, which is transported into the mitochondria by glucose transporter 1 (GLUT1) (Martínez-Reyes & Chandel, 2020). The TCA cycle in resting macrophages is summarised in Figure 1.2.

In response to stimuli such as LPS/IFN-γ, macrophages undergo a dramatic switch in metabolic state. M1 macrophages shut down oxidative phosphorylation, instead to use the faster glycolytic and pentose phosphate pathways for primary ATP production. Glycolysis generates 2 units of ATP per molecule of glucose whereas oxidative phosphorylation (OXPHOS) generates 36. Despite this difference, M1 cells are able to generate the required levels of ATP in their activated state (Everts et al., 2012; Robin et al., 1984). M1 cessation of oxidative phosphorylation stems from a dual break in the TCA cycle, hypothesised initially to be at isocitrate dehydrogenase and followed by succinate dehydrogenase. The first break reroutes aconitate conversion to itaconate which, due to its structural similarity to succinate, inhibits succinate dehydrogenase, forming the second TCA cycle break. The resulting high levels of succinate are oxidised to fumarate and are associated with increased ROS generation, activation of HIF-1α and subsequent increased IL1β production (Mills et al., 2018; Puchalska et al., 2018; Tannahill et al., 2013). In contrast, the metabolic profile of M2 macrophages demonstrate decreased glycolytic flux, an intact TCA cycle and enhanced fatty acid oxidation. This method of energy generation is more sustainable, hence lending itself to M2 macrophage repair function. Blocking oxidative phosphorylation blocks the M2 phenotype, shifting the macrophage towards M1 state; forcing oxidative phosphorylation in M1 macrophages potentiates the M2 phenotype (S. C. Huang et al., 2014; Vats et al., 2006).

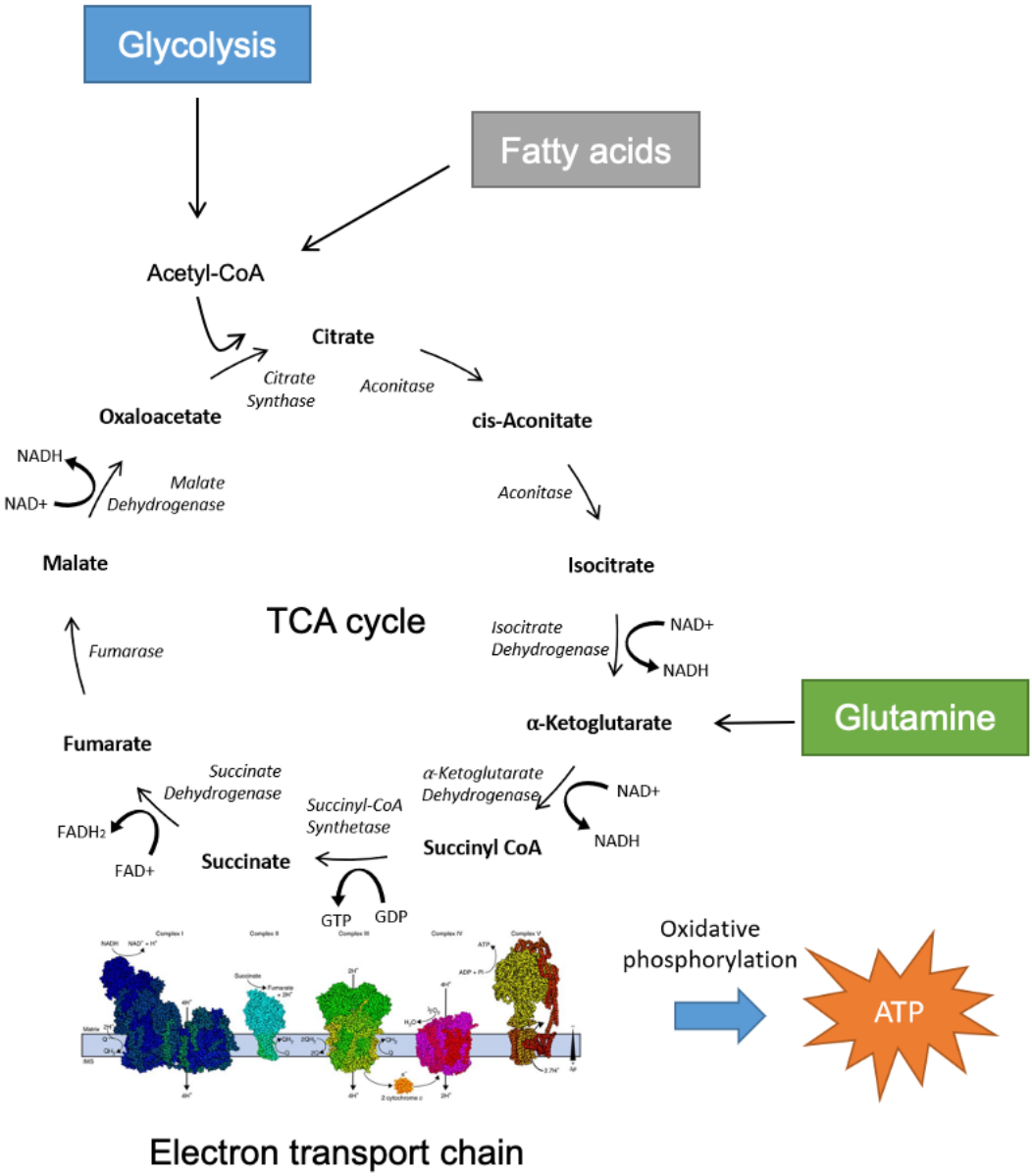



**Figure 1. 2 TCA cycle in resting macrophages**

In the TCA cycle, acetyl-CoA is produced from the breakdown of glucose or fatty acids, which is then combined with oxaloacetate to form citrate. Citrate is then converted to isocitrate via aconitase. Isocitrate is then oxidized to α-ketoglutarate, which generates NADH and $CO_2$, and this step is catalyzed by the enzyme isocitrate dehydrogenase. α-ketoglutarate is further oxidized to succinyl-CoA, which generates NADH and $CO_2$, and this step is catalyzed by the enzyme α-ketoglutarate dehydrogenase. Succinyl-CoA is then converted into succinate by the enzyme succinyl-CoA synthetase, which generates GTP. Succinate is further oxidized to fumarate by the enzyme succinate dehydrogenase, which generates $FADH_2$, and fumarate is then converted into malate by the enzyme fumarase. Finally, malate is oxidized to oxaloacetate by the enzyme malate dehydrogenase, which generates NADH. The TCA cycle generates reducing equivalents in the form of NADH and $FADH_2$, which are then used in the ETC to generate ATP via oxidative phosphorylation.

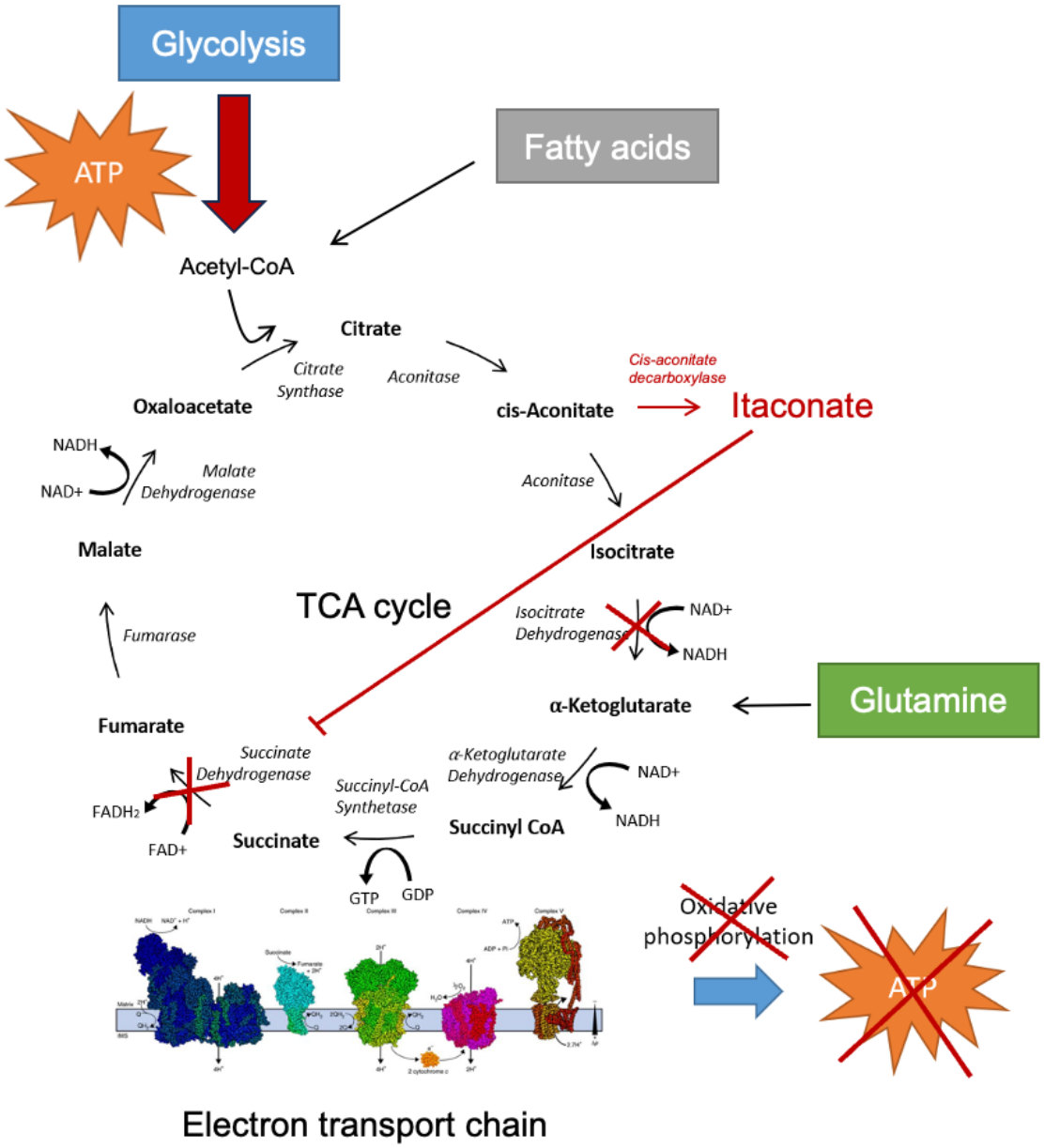



**Figure 1. 3 TCA cycle rewiring in inflammatory macrophages**

Inflammatory macrophages are proposed to have breaks in the TCA cycle at isocitrate dehydrogenase, which leads to the accumulation of itaconate. Itaconate inhibits succinate dehydrogenase to create the second break. This results in increased glycolysis as the cell is no longer able to generate ATP via oxidative phosphorylation. For more details, see section 1.2.4.

### 1.2.5 Fatty acid metabolism

The fatty acid synthesis (FAS) pathway is a crucial cellular process that plays a vital role in membrane biosynthesis and energy storage. Typically, citrate produced from the TCA cycle is exported from the mitochondria to the cytosol and then converted into acetyl-CoA and oxaloacetate via ATP-citrate lyase (ACLY). Acetyl-CoA is subsequently transformed into malonyl CoA by acetyl-CoA carboxylase (ACC). The FA synthase then elongates the nascent fatty acid chain, leading to the production of palmitate, which is the first product of FAs. Normally, circulating lipids are engulfed by macrophages where they are esterified and stored in lipid droplets. Upon changing energy requirements, these lipids are catabolized to generate fatty acids or cholesterol. Fatty acids are transported to the mitochondria via carnitines where they are broken down to acetyl-coA, which feeds into the TCA cycle via citrate. This process is known as fatty acid oxidation (FAO) or beta-oxidation.

Upon LPS activation, in the majority of instances, macrophages upregulate fatty acid synthesis, storage and production of intermediaries which support increased expression of pro-inflammatory metabolites. In fact, removal of fatty acid synthase diminished production of pro-inflammatory cytokines in diabetes, indicating FA synthesis regulates macrophage polarisation state; changes in cell membrane mediates this effect (Wei et al., 2016).

In contrast, reparative macrophages are defined by their increased OXPHOS due to increased use of FAO and breakdown of fatty acids to produce ATP for anti-inflammatory purposes (Kolliniati et al., 2022). This increased lipolysis, FAO and OXPHOS is observed in both murine and human IL4 stimulated macrophages. It is necessary for reparative macrophage function since inhibiting it decreases classical reparative functions and characteristics such as CD206, CD301 surface markers as well as parasitic removal (S. C. Huang et al., 2014).

### 1.2.6 Glutaminolysis

Glutaminase (GLS) converts glutamine in cells to glutamate, which is subsequently converted to α-ketoglutarate to replenish the TCA cycle. Additionally, glutamine plays a role in producing glutathione and serves as a precursor for nucleotides and lipid synthesis through reductive carboxylation (Yoo et al., 2020). The role of glutamine is still being understood in $M^{LPS/IFN\text{-}\gamma}$ and $M^{IL4}$ macrophages. Pharmacological inhibition of glutamine synthase, which synthesises glutamine from glutamate, skewed M2 macrophages towards M1 state as shown by decreased glutamine, increased succinate and increased glycolysis (Palmieri et al., 2017).

In inflammatory macrophages, the first break in the TCA cycle in activated macrophages is supposedly at isocitrate dehydrogenase (IDH1), which converts isocitrate to α-ketoglutarate (Jha et al., 2015). Carbon flux studies indicated the aspartate-arginosuccinate shunt could compensate for this break. Additionally, the study showed that a lack of glutamine affecting $M^{IL4}$ polarisation but not inflammatory state metabolism (Jha et al., 2015). Furthermore α-ketoglutarate production via glutaminolysis was shown to be required for alternative activation of macrophages (P. S. Liu et al., 2017)

## 1.3 Innate immune cell memory

### 1.3.1 Background

Traditionally, the innate immune system has been considered to be non-specific and lacking in memory in contrast to acquired immune responses. In the past decade this paradigm has been challenged. All major myeloid cell populations, including monocyte, macrophages, neutrophils and dendritic cells have demonstrated innate immune memory, or trained immunity. Innate immune cell memory is the long-term functional adaptation of innate immune cells that results in heightened anti-microbial functions, increased cytokine productions and improved pathogen clearance following a secondary pathogen encounter

(Netea et al., 2020). The trained phenotype has been shown to last at least 3 months to a year (Nankabirwa et al., 2015).

Trained immunity is distinct from tolerance and priming. Tolerance results in unresponsiveness to a particular stimulus following repeated exposure to an antigen. Primed macrophages characterized by increased expression of surface receptors and effector molecules, and enhanced responsiveness to subsequent challenges (Divangahi et al., 2021). Mechanistically, trained immunity is induced by long-lasting epigenetic reprogramming through chromatin accessibility and DNA methylation which results in increased gene transcription upon a second stimulation (van der Heijden et al., 2018). In addition, cells undergo metabolic reprogramming, including increased glycolysis, alterations in OXPHOS, and repurposing of glutaminolysis and the TCA cycle. These changes result in accumulation of metabolites, such as succinate and fumarate, which can modulate epigenetic enzymes involved in trained immunity (Fanucchi et al., 2021; van der Heijden et al., 2018).

### 1.3.2 Metabolism and immune cell memory

Metabolic reprogramming of macrophages refers to alterations in the cellular metabolism of these immune cells, particularly the shift from oxidative phosphorylation to aerobic glycolysis, in response to environmental stimuli such as microbial products or cytokines. As described above, there are six primary metabolic pathways critical for activating innate immune cells: glycolysis, TCA cycle, PPP, FAO, FAS and amino acid metabolism. These are key for meeting the increased energetic and biosynthetic demands required for their activation and effector functions, including phagocytosis, cytokine production, and antigen presentation (O'Neill et al., 2016). Different stimuli induce different pathways which can sway the balance between either pro-inflammatory or anti-inflammatory responses (Bahrar et al., 2023; Riksen & Netea, 2021).

Increased glycolysis is not only a feature of M1 macrophages but is also required for trained immunity as it is activated the akt-mTOR-HIF1a pathway (Cheng et al., 2014). Stimulation by several stimuli (BCG, β-glucan, oxLDL) increased glucose uptake and glycolytic enzymes (Keating, Groh, Thiem, et al., 2020). Glycolysis also promotes NAD+ to NADH conversion which is needed by many enzymes to function. The glycolysis intermediary metabolite glucose-6-phosphate fuels the PPP which also produces NADPH. Lactate can bind to histones to modify the epigenetic landscape of inflammatory macrophages (Zhang, Tang, et al., 2019). Furthermore, inhibition of glycolysis reduces cytokine production which is a characteristic of trained immunity (Caslin et al., 2018).

Trained macrophages exhibit elevated oxygen consumption which indicates increased OXPHOS. Furthermore, macrophages trained by initial exposure to β-glucan, bacilli Calmete-Guerin (BCG) and oxLDL displayed heightened basal and maximal OCR after 6 days from initial exposure. Inhibition of OXPHOS via the complex IV inhibitor oligomycin prevented oxLDL and beta-glucan induced trained immunity (R. J. W. Arts et al., 2016; Keating, Groh, Thiem, et al., 2020; van der Heijden et al., 2018). Increased OXPHOS observed with β-glucan is linked to epigenetic activation of enzymes including succinate dehydrogenase through upregulation of methyltransferase.

Glutamine replenishment of the tricarboxylic acid (TCA) cycle is essential for the development of trained immunity. In monocytes stimulated with β-glucan or BCG, upregulation of glutaminolysis leads to an accumulation of fumarate, succinate, and malate. Preventing the conversion of glutamine to glutamate can impede trained immunity (R. J. Arts et al., 2016). Fumarate, in isolation, can induce training in human primary monocytes, while malate and succinate cannot promote training. Additionally, fumarate inhibits lysine demethylase 5 (KDM5), a histone 3 lysine demethylase, promoting the persistence of histone trimethylation at the promoter regions of pro-inflammatory genes (R. J. Arts et al., 2016).

Acetyl-CoA holds a central position at the intersection of several metabolic pathways that are crucial for inducing trained immunity and is a major substrate for histone acetyltransferases. Moreover, acetyl-CoA can be utilized for fatty acid synthesis (FAS) (O'Neill et al., 2016). β-glucan trained macrophages exhibit an increase in the FAS pathway, although inhibition of this pathway during the 24-hour exposure to β-glucan did not hinder trained immunity (R. J. Arts et al., 2016). However, upregulation of the FAS pathway through the mineralocorticoid receptor is crucial for the elevated production of IL-6 and TNF-α in training with the endogenous adrenal hormone aldosterone (van der Heijden et al., 2020).

### 1.3.3 Epigenetic reprogramming

In addition to metabolic changes, trained immunity is also regulated by epigenetic reprogramming. Epigenetic modifications include DNA methylation, histone modifications, and non-coding RNA expression can control gene expression by altering chromatin structure and accessibility, which can have long-lasting effects on cellular function following stimulation of immune cells (Saeed et al., 2014). In trained immunity, these histone modifications are only partially removed resulting in enrichment of promotors of cytokines with H3K4me3 and enhancers with H3K4me1. Few epigenetic enzymes have been characterised for their role in trained immunity. H3K4 is demethylated by KDM5 family of histone demethylases, which were decreased in BCG-induced training of monocytes (R. J. W. Arts et al., 2016). Furthermore, Set7 methyltransferase, which writes H3K4me1 marks, was shown to regulate plasticity in OXPHOS needed for β-glucan induced training (Keating, Groh, van der Heijden, et al., 2020).

### 1.3.4 Hyperglycaemic memory

Studies have identified both acute and long-term effects of glucose on innate immune cells, which persist even after plasma glucose levels are lowered (van Diepen et al., 2016). It was observed in diabetic patients that even after glucose levels are normalized, this metabolic memory contributes to long lasting changes in macrophage function, including altered gene expression, increased inflammatory cytokine expression and an increased risk for the development of atherosclerotic cardiovascular disease (ASCVD) (Holman et al., 2008; van Diepen et al., 2016). This phenomenon has been termed "hyperglycaemic memory" and thought to be due to trained immunity via epigenetic modifications (Edgar et al., 2021; Holman et al., 2008; Reddy et al., 2015).

Hyperglycaemic memory was first observed in endothelial cells, which are often the first sensors of harmful endogenous stimuli (El-Osta et al., 2008). More recently the effects of hyperglycaemia have been studied on myeloid progenitor cells in the bone marrow. Streptozotocin (STZ)-induced diabetic mice had increased circulating neutrophils and Ly6-C(hi) monocytes due to increased myelopoiesis in the bone marrow (Nagareddy et al., 2013). Furthermore, high glucose was found to sensitise macrophages to have increased pro-inflammatory cytokine production (Ayala et al., 2019; Pavlou et al., 2018). Macrophages from diabetic mice were found to also have increased pro-inflammatory and pro-atherogenic phenotypes through glycolysis dependent mechanisms even after exposure to normoglycaemia, suggesting training. Bone marrow transplantation from diabetic mice to normoglycemic $Ldlr^{-/-}$ mice increased aortic root atherosclerosis, which was reversed by Runx1 inhibition (Edgar et al., 2021)

## 1.4 Itaconate

### 1.4.1 Itaconate origins

Itaconate, also known as itaconic acid and methylenesuccinic acid, is a dicarboxylic acid ($C_5H_6O_4$) containing a double bond and two carboxyl groups (Robert & Friebel, 2016). It was first synthesised by Samuel Baup in 1836 through thermal decomposition of citric acid (Baup, 1836). Four years later, Gustav Crasso synthesised the same compound by decarboxylation of *cis*-aconitate naming it itaconate (Crasso, 1840). Since then, itaconate has been widely used for decades by the polymer industry with 40,000 tons of it currently produced per year (Cordes et al., 2015). The first suggestions of itaconate's role in immunity only came a decade ago when groups described the production of itaconic acid in LPS-activated RAW264.7 macrophages and the VM-M3 macrophage-like cell line (Cordes et al., 2015; Shin et al., 2011; Sugimoto et al., 2012). Importantly, in 2013, Michelucci et al. demonstrated that the IRG1 gene, which is almost exclusively expressed in immune cells, was responsible for itaconate production in LPS-activated or inflammatory macrophages (Michelucci et al., 2013). Since this discovery, research into itaconate's function has been fervently expanded.

### 1.4.2 Itaconate derivatives

Itaconate's high polarity and hydrophilicity limits its ability to cross cellular membranes. To increase cell permeability, esterified derivates of negatively charged polar metabolites are commonly used. Dimethyl itaconate (DI) was first synthesised as a cell permeable derivative of itaconate and was shown to increase Nuclear factor erythroid 2-related factor 2 (Nrf2) protein levels as well as downstream targets haemoxygenase 1 and glutathione (Lampropoulou et al., 2016; Mills et al., 2018). However, it was found to be a far more potent activator of Nrf2 compared to itaconate and was degraded rapidly intracellularly

without releasing itaconate in both RAW 264 cells and mouse BMDMs (ElAzzouny et al., 2017).

Mills et al, synthesised the derivative 4-octyl itaconate (4-OI) as a cell permeable alternative to DI. 4-OI has lower thiol reactivity compared DI making it a less potent Nrf2 activator. 4-OI was also shown to increase intracellular itaconate levels in a concentration dependent manner in mouse myoblast C2C12 cells and LPS-activated macrophages (Mills et al., 2018). Here, 4-OI was also shown to increase anti-oxidant glutathione (GSH) levels and Nrf2 activation by hydrogen peroxide. Other octyl esters 4-octyl 2 methylsuccinate and octyl succinate, did not alter Nrf2 activity, confirming 4-OI effects are due to itaconate (Mills et al., 2018). The chemical structure of itaconate, its commonly used derivatives and structurally similar metabolites can be seen in Figure 1.4.

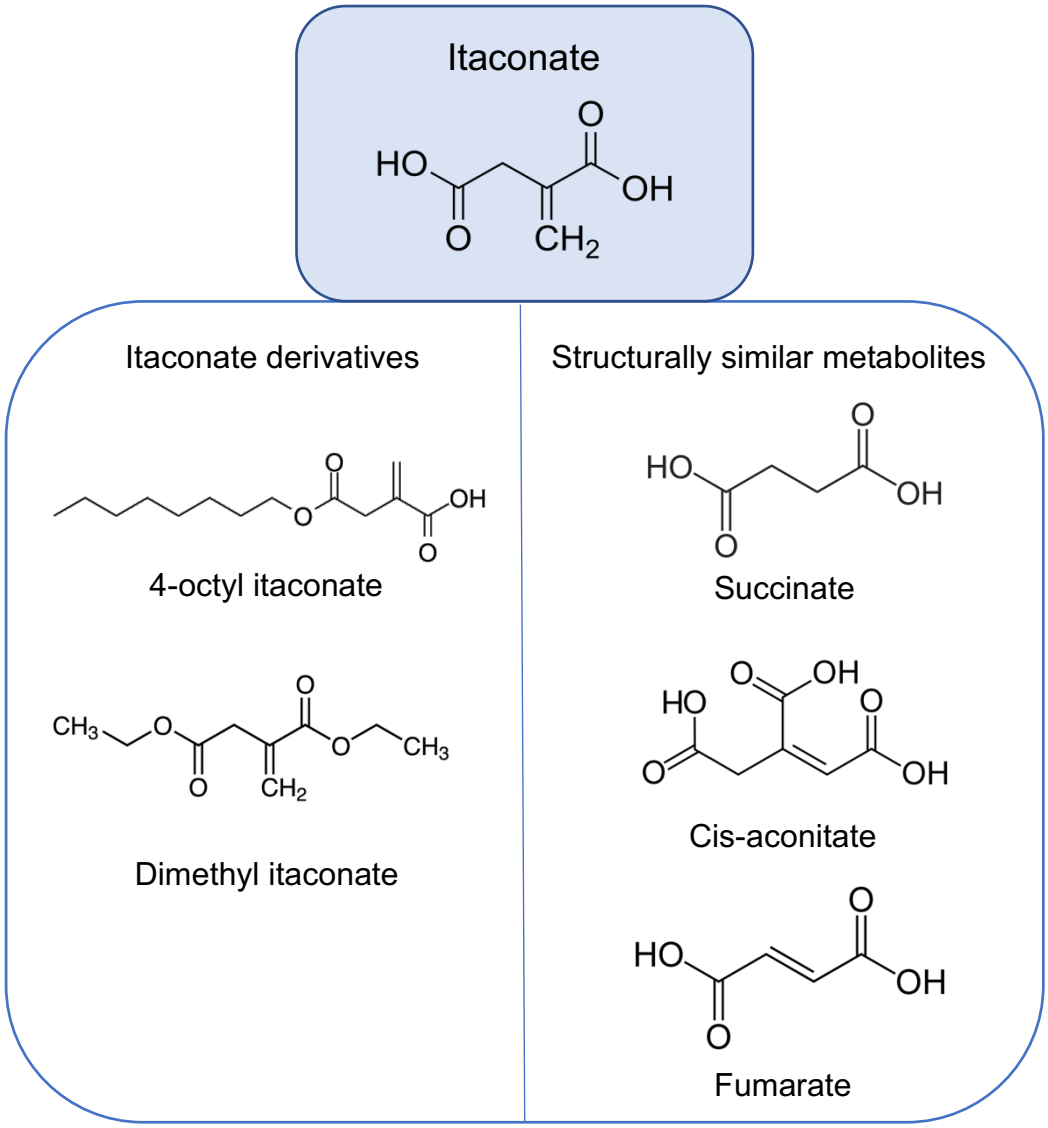



**Figure 1. 4 Chemical structures of itaconate, itaconate derivatives and structurally similar metabolites**

### 1.4.3 Itaconate as an anti-oxidant

Recently, it has become evident that endogenous itaconate can directly modulate inflammation, in addition to its indirect effects on glycolysis, succinate dehydrogenase (SDH) inhibition, and KEAP1/NRF2 action. Itaconate induces the production of activating transcription factor (ATF3) protein, which inhibits IκBζ, a regulator of inflammation that interacts with the NF-κB family (Bambouskova et al., 2018). This explains why pro-inflammatory cytokines such as IL6 and IL12 are reduced by itaconate, but not TNF-α, which is primarily transcribed.

Moreover, itaconate plays a role in activating signal 2 of the inflammasome, NLRP3, was demonstrated recently (Hooftman et al., 2020). This leads to a decrease in IL1β, independent of SDH inhibition, NRF2, and ATF3 signalling pathways. Itaconate modifies Cys77 to C192 of gasdermin-D (GSDMD), which plays a role in oligomerization and pore formation with Caspase-1 to induce pyroptosis, an important cell death occurring in highly inflamed cells, and to which IL1β secretion relies (Hooftman et al., 2020; Qin et al., 2020). The decrease in IL1β during late inflammasome activation was shown to be dependent on the presence of both inducible nitric oxide synthase (iNOS) and IRG1 (Hooftman et al., 2020).

The interplay between iNOS and IRG1 has been recently revealed suggested by the observation that the depletion of NO production causes a significant increase in itaconate levels following LPS/IFNγ stimulation (Bailey et al., 2019; Palmieri, Gonzalez-Cotto, et al., 2020; Price et al., 2019). These results point to a complementary co-regulation between NO and itaconate to orchestrate the response to damage and infection, which could play an essential role in the treatment of cardiovascular diseases where both oxidative stress and inflammation can lead to further vascular damage. Nitrite therapy has been reported to improve left ventricular function in ischemia-induced heart failure through Nrf2-dependent signalling and increased antioxidant proteins (Donnarumma et al., 2016). On the other hand,

inflamed resident macrophages in vessels can also produce large quantities of NO through iNOS. Recent studies have measured the release of large quantities of itaconate by activated macrophages, which could also play a role in resolution and repair of vessels by modulating NO or vice versa (Cordes & Metallo, 2021).

### 1.4.4 Itaconate in metabolism

The strong correlation between itaconate and succinate was noted by Cordes et al in both primary macrophages and RAW264.7 cells. Using LPS-stimulated BMDMs from Irg1$^{-/-}$ mice, a significant decrease in succinate levels was detected, due to the structural similarity and co-localization of succinate and itaconate within the mitochondrial matrix. Lampropoulou et al. also demonstrated the post-transcriptional inhibitory role of itaconate towards SDH using dimethyl itaconate to treat LPS-stimulated BMDMs from IRG1−/− mice, which led to succinate accumulation and decreased pro-inflammatory cytokines and oxidative response markers (Lampropoulou et al., 2016). Although TNF-α was not affected, itaconate decreased the induction of IL1β expression via HIF-1α stabilization, which contributes to ROS production. This suggests that itaconate acts as an immunomodulatory metabolite and a potential therapeutic target for ischemia-reperfusion injury. Cordes et al. demonstrated that itaconate inhibits SDH in a dose-response manner, allowing succinate accumulation and preventing further oxidation by SDH, which shields against ROS damage (Cordes & Metallo, 2021).

Itaconate has also been shown to inhibit glycolysis via alkylation of several glycolytic enzymes including aldolase A (ALDOA), glyceraldehyde-3-phosphate dehydrogenase (GAPDH) and lactate dehydrogenase (LDHA) (Mills et al., 2018). Irg1-/- mice had increased ALDOA activity and itaconate inhibited ALDOA activity and glucose consumption (Qin et al., 2019). Itaconate inhibited GAPDH activity through alkylation of its Cys22 residue resulting in decreased extracellular acidification rate (ECAR), lactate

production and decreased levels of IL1β and iNOS (Liao et al., 2019; Peace & O'Neill, 2022).

### 1.4.5 Itaconate in cardiovascular disease

Due to its anti-inflammatory and antioxidative properties, itaconate may be a promising candidate in the treatment of cardiovascular inflammation. Studies have reported on the use of itaconate and its derivatives in preventing cardiac damage and promoting repair after brain and heart ischemia-reperfusion injury (Zhang, Lu, et al., 2019). Although there are differences in the molecular mechanisms of itaconate and its derivatives because of their electrophilic nature, they all have a beneficial effect on oxidative damage and inflammation (Ryan & O'Neill, 2020). One study reported dimethyl itaconate (DI) reduced myocardial infarct size in mice treated intravenously, compared to mice treated with saline solution. DI also protected hypoxic rat neonatal cardiomyocytes from hypoxia-induced cell death in vitro (Lampropoulou et al., 2016). In cerebral ischemia-reperfusion injury, DI significantly reduced the neurologic deficit score and inhibited microglia toxic conversion in mice (Cordes & Metallo, 2021). Mechanistic insights have been provided by studies using 4-OI in mouse models of cerebral reperfusion injury, ischemia, or traumatic brain injury. The studies demonstrated that itaconate-succinate dehydrogenase inhibition led to a reduction in reactive species and an increase in glutathione, which aided in brain tissue recovery (Lampropoulou et al., 2016). Similarly, exogenous addition of 4-OI inhibited the formation of angiotensin II-induced abdominal aortic aneurysm (AAA) and led to the up-regulation of Nrf2 and a subsequent decrease in pro-inflammatory cytokines. Although not exclusive, both itaconate and Nrf2 were essential in reducing AAA formation (Song et al., 2020).

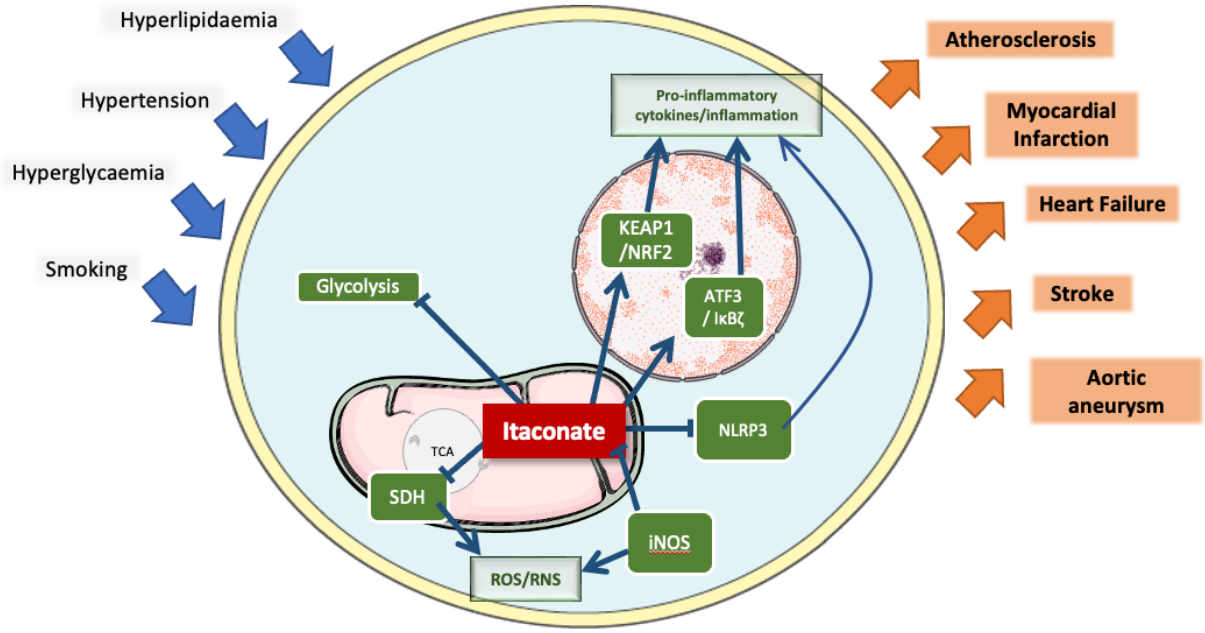



**Figure 1. 5 Cellular signalling pathways by which itaconate regulates the inflammatory response**

The classical signalling pathways by which itaconate regulates the inflammatory response and oxidative stress include:

1. Itaconate inhibits succinate dehydrogenase (SDH) and hence the TCA cycle.
2. Itaconate alkylates cysteine 22 residues on GAPDH which inhibits glycolysis. Alkylation of ALDOA by itaconate also inhibits glycolysis
3. Itaconate alkylates Keap1 cysteine residues resulting in disassociation of Keap1-Nrf2 complex whereby Nrf2 translocates to the nucleus and transcribes anti-inflammatory and anti-oxidant genes.
4. Itaconate increases ATF3 protein levels which inhibit eukaryotic initiation factor 2 (eIF2a) to inhibit IκBξ, a nuclear protein which regulates the DNA binding activity of the transcription factor NFκB.
5. Itaconate abolishes NLRP3-NEK7 complex through dicarboxypropylation on C548 of NLRP3 resulting in prevention of NLRP3-dependent IL1β release.
6. Itaconate levels are regulated by iNOS with loss of iNOS or NO resulting in increased itaconate production.

These pathways have also been implicated in cardiovascular diseases. They can be altered by cardiovascular risk factors to have adverse cardiovascular disease outcomes. The use of itaconate as a potential therapy for cardiovascular diseases, with its anti-inflammatory and anti-oxidant properties, is an expanding area of research.

## 1.5 Vascular homeostasis

### 1.5.1 Endothelium dependent mechanisms of contraction

The vascular endothelium lines the internal surface of blood vessels and is an important regulator of vascular tone, vascular inflammation, cellular adhesion, coagulation and thrombosis (Rajendran et al., 2013). More than a passive barrier, endothelial cells produce a variety of vasoactive substances including:

Endothelium derived relaxing factors (EDRF) which include NO, prostracyclin and endothelium-dependent hyperpolarization (EDH) (Moncada et al., 1976). Endothelium constricting factors (EDCF) such as thromboxane A2 and endothelin-1 (Yanagisawa et al., 1988). Endothelium derived hyperpolarising factors (EDHF) which include hydrogen peroxide and potassium (Edwards et al., 1998; Matoba et al., 2002). It is the balance between EDRFs, EDCFs and EDHFs which regulates vascular tone and blood pressure and their imbalance leads to endothelial dysfunction which is characteristic of many cardiovascular diseases.

Endothelium derived NO activates soluble guanylate cyclase (sGC) in smooth muscle cells to dilate blood vessels (Ignarro et al., 1986). This leads to increased conversion rate of cyclic guanosine monophosphate (cGMP) from guanosine triphosphate (GTP) and the activation of protein kinase G (PKG), which decreases intracellular calcium levels and results in smooth muscle cell (SMC) relaxation (Collins et al., 1986; Jones et al., 1999). NO can also activate $K_{ATP}$ channels to cause smooth muscle cell hyperpolarisation and SMC relaxation. Endothelium derived prostacyclin activates prostacyclin receptor on SMC to activate adenylyl cyclase and lead to increased intracellular cAMP levels, which activates protein kinase A (PKA) which decreases intracellular calcium levels, inhibiting myosin light chain kinase (MLCK) to result in SMC relaxation (Moncada et al., 1976; Stitham et al., 2011).

### 1.5.2 Endothelium independent mechanisms of vasocontraction

The contraction and dilation of smooth muscle cells in blood vessels can also be regulated by endothelium-independent mechanisms (Tesfamariam & Halpern, 1988). This can be via the activation of specific receptors on the smooth muscle cells in vessel walls by substances such as noradrenaline. Activation of G-protein coupled receptors (GPCRs) leads to the activation of phospholipase C, which cleaves phosphatidylinositol 4,5-biphosphate (PIP2) to form inositol 1,4,5-triphosphate (IP3) and diacylglycerol (DAG). Upon formation, IP3 binds to its receptor on the endoplasmic reticulum, causing release of calcium ions into the cytosol. Increased calcium activates MLCK which phosphorylates myosin light chain so it can bind to actin and leads to SMC contraction (Allen & Walsh, 1994). Activation of voltage gated calcium channels, such as by angiotensin II, leads to influx of extracellular calcium ions into smooth muscle cells which leads to contraction as described (Matsuda et al., 1997). Mechanical stretch of blood vessel walls, can also activate stretch receptors to lead to increased calcium influx and vasoconstriction (Touyz et al., 2018).

### 1.5.3 Nitric oxide in vessels and macrophages

Nitric oxide plays a variety of roles, in both physiology and pathophysiology, and in a variety of cells owing to its flexibility/promiscuity. There are three nitric oxide synthase enzymes, all of which use L-arginine as a substrate as well as oxygen and require the cofactors 5,6,7,-tetrahydrobiopterin (BH4), nicotinamide adenine-dinucleotide phosphate (NADPH), flavin, adenine dinucleotide (FAD) and flavin mononucleotide (FMN). All of the NOSs bind calmodulin and contain a haem group. The N-terminal oxygenase and the C terminal reductase domains are linked by the calmodulin binding site. Neuronal NOS (Nos1, chromosome 12) which is constitutively expressed in the central and peripheral nervous system as well as some other cell types (Prast & Philippu, 2001). Inducible NOS, (NOS2, chromosome 17) is not expressed basally but induced as response to inflammatory stimuli;

iNOS produces large amounts of NO which exert anti-microbial and anti-parasitic effects. Endothelial NOS (NOS3, chromosome 7), is primarily expressed in endothelial cells and regulates blood pressure (Lamas et al., 1992; Michel & Feron, 1997). Furthermore, it has many other vasoprotective and anti-atherosclerotic roles as well as uncoupling of eNOS leads to oxidative stress and endothelial dysfunction are indicators, or the beginnings of many cardiovascular diseases including diabetes, hypertension and atherosclerosis. Targeting vascular oxidative stress and restoring coupled eNOS function limits CVD. Genes encoding the NOS enzymes are located on different chromosomes, encoded by separate genes and share 60% homology. Their differences in genes, modulation, function, tissue specificity, localisation defines their different isoforms.

Nitric oxide plays significantly different roles in the endothelium and in macrophages. In macrophages, NO has been shown to affect the electron transport chain and prevent M1 polarisation to the reparative phenotype (Van den Bossche et al., 2016). Another study showed NO in murine BMDMs alters TCA cycle metabolites with glucose C13 tracing showing NO mediated suppression of aconitase (Palmieri, Gonzalez-Cotto, et al., 2020). Bailey et al, also showed the same NO mediated alterations in TCA cycle, impaired the electron transport chain and regulates itaconate levels (Bailey et al., 2019). Other studies have shown that NO plays a dual role in RAW 264.7 cells, a macrophage cell line, stimulated with LPS. Low NO locally results in increased iNOS expression. High NO concentration decreases the expression of iNOS and cyclooxygenase 2 (COX2) and hence indicates decrease of the pro-inflammatory response. Also, citrulline is catalysed by Ass1 and Asl to recover arginine and leads to the production of NO.

### 1.5.4 NOS catalysis

NOS enzymes are responsible for catalysing the production of NO from L-arginine and oxygen, resulting in the production of L-citrulline. These enzymes work as homodimers,

with electrons flowing from the reductase domain of one monomer to the oxygenase catalytic site of the other. In the reductase domain, electrons are donated by NADPH molecules and transported through FAD and FMN flavins before being transferred to the haem in the oxygenase domain, triggered by calcium-induced calmodulin binding (Abu-Soud & Stuehr, 1993). In the oxygenase domain, L-arginine is converted into N-hydroxy-L-arginine, followed by the production of L-citrulline and NO, which requires electron donations to the ferrous-dioxygen complex in haem from BH4, as well as the flavins in the reductase domain (Abu-Soud et al., 1997; Berka et al., 2004). During the reaction, BH4 forms a protonated trihydrobiopterin cation radical (BH3.H+) but is eventually regenerated as BH4 (Wei et al., 2003).

### 1.5.5 Tetrahydrobiopterin synthesis

There are two major routes for the availability of BH4, de novo synthesis of BH4, and the salvage pathway. De novo synthesis of BH4 is a 3-step reaction beginning with guanine triphosphate (GTP). GTP is sequentially catalysed by GTP cyclohydrolase (GTPCH), 6-pyruvoly tetrahydropterin synthase (PTPS) and sepiapterin reductase (SR). GTPCH is encoded by the *Gch1* gene located on chromosome 14 in humans and mice. GCH1 catalyses GTP to 7-8 dihydroneopterin triphosphate (NH2-triP) which is converted by PTPS to 6-pyruvorltetrahydrobiopterin (6-PTP). 6-PTP forms BH4 following SR managed 3-fold successive reductions . The first step catalysed by GTPCH is the rate limiting step in the reaction and is highly complex and regulated at the transcriptional, translational and post-translational levels (Ignarro, 2000). *Gch1* transcription is induced upon exposure to inflammatory stimuli such as LPS in many cell types, as well as in response to hydrogen peroxide in endothelial cells. In the final step of BH4 de novo synthesis, BH2 is converted to BH4 by dihydrofolate reductase (DHFR) (Crabtree, Tatham, Al-Wakeel, et al., 2009; Crabtree, Tatham, Hale, et al., 2009). Importantly, this also occurs when the final reduction

of 6-PTP does not happen resulting in the formation of 1-oxo-2-hydroxypropyl-BH4. Sepiapterin is formed from this compound which can be converted to BH2 by SR and reduced to DHFR to form BH4 (Figure 1.5) (Thöny et al., 2000).

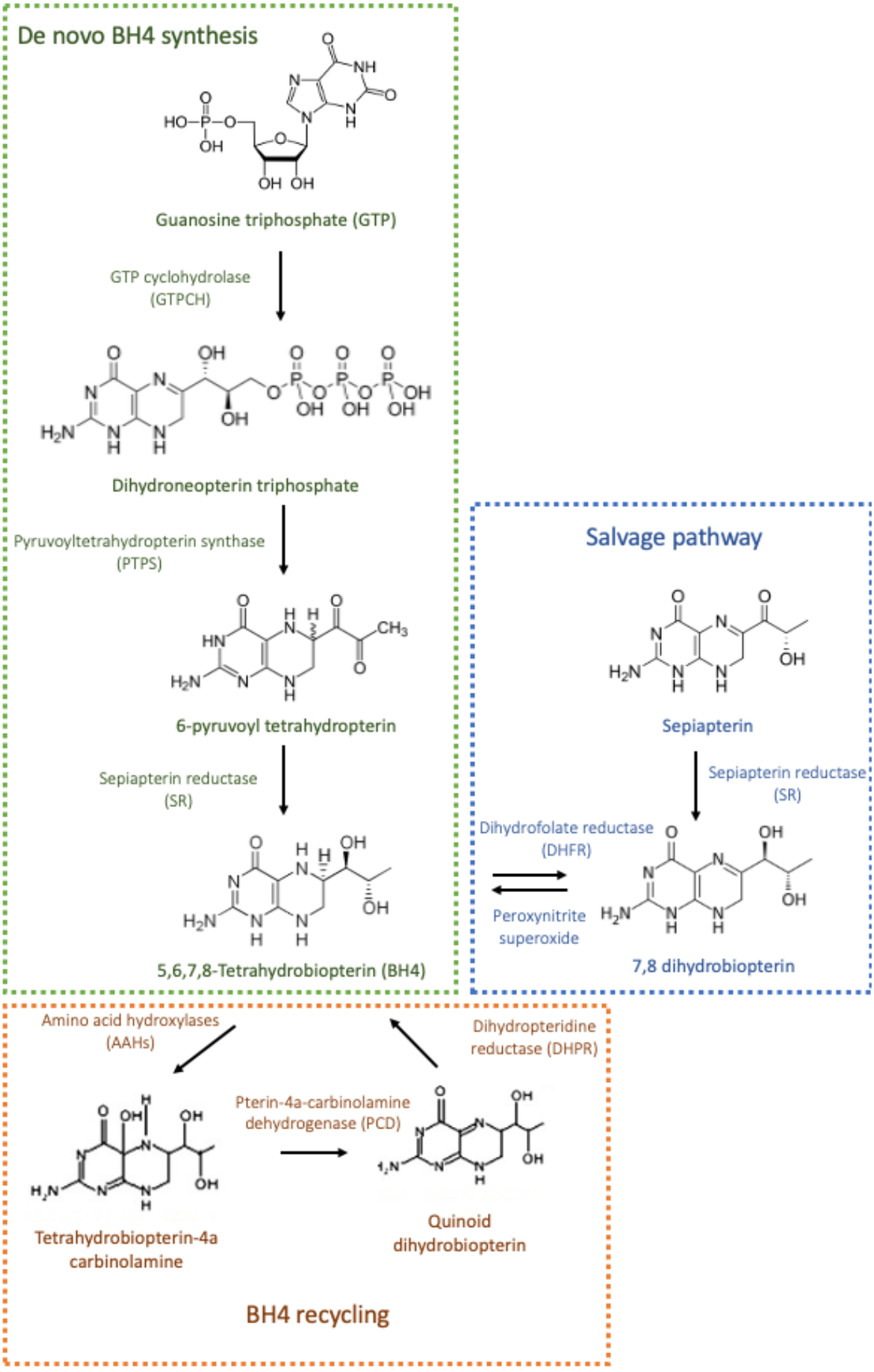



**Figure 1.5 Tetrahydrobiopterin synthesis, recycling and salvage pathways**

Cells synthesize tetrahydrobiopterin (BH4) de novo from GTP through a three-step process. Additionally, BH4 can be produced from sepiapterin via the salvage pathway and recycled from tetrahydrobiopterin-4a-carbinolamine through AAH catalysis.

## 1.6 Hypothesis and aims

### 1.6.1 Hypothesis

The work in this thesis tested the hypothesis that changes in macrophage function due BH4 deficiency or hyperglycaemia are underpinned by alterations in metabolic pathways and substrate use (glucose, fatty acids, glutamine) in inflammatory macrophages. As the study progressed, specific hypotheses were refined in each chapter. The discovery that itaconate is secreted from cells led to further hypotheses that itaconate has paracrine functions, and effects not limited to immune cells. Similarly, after an in-depth review on the topic, a large metabolomics study on the effects of hyperglycaemia on macrophage metabolism was undertaken.

### 1.6.2 Aims

This study aimed to understand different substrate use and metabolic pathways in BH4-deficient and hyperglycaemic macrophages, correlating these findings to the inflammatory profile of the cells. The overall aims were:

1. To explore how substrate use is altered by BH4 in inflammatory macrophages
2. To investigate if hyperglycaemia alters the inflammatory or metabolic profile of macrophages
3. To explore the role of itaconate as a therapeutic target in cardiovascular disease

# Chapter 2

# Materials and Methods

# Chapter 2: Materials and Methods

## 2.1 Animals

### 2.1.1 R26 CreER$^{T2}$ Gch$^{fl/fl}$ mouse

All animals were maintained in accordance with the UK Home Office Animals (Scientific Procedures) Act 1986 under Project License 30/3080 and culled via Schedule 1 methods. Mice were housed in groups of 2-5, in individually ventilated cages at the Functional Genetics Facility (FGF), a specific pathogen free environment, at the Wellcome Centre for Human Genetics, Oxford. Temperatures were maintained at 20-22 °C with 12-hour light/dark cycles and mice were given access to standard chow diet (19.67% protein, 4.13% oil and 3.22% fibre) and sterile water *ad libitum*.

A novel mouse model of BH4 deficiency was generated by conditional and tamoxifen-inducible deletion of *Gch1*, the gene encoding GTP cyclohydrolase I, the rate limiting enzyme in BH4 biosynthesis. As BH4 is a cofactor for nitric oxide synthase (NOS) enzymes, without *Gch1*, there is no BH4 synthesis and the NOS enzymes cannot produce nitric oxide (NO). Global deletion of *Gch1* is embryonically lethal, mice containing a *Gch1* conditional KO (floxed) allele was generated using the Cre/LoxP strategy. To do this, exons 2 and 3 of *Gch1*, encoding the active site of GTPCH protein were flanked by LoxP sites in a targeting construct that was used to produce Gch$^{fl/fl}$ mice, following homologous recombination with embryonic stem cells.

These Gch$^{fl/fl}$ mice were backcrossed for >8 generations to a C57BL/6J background and then crossed with R26 ER$^{T2}$-Cre transgenic mice to produce R26-CreER$^{T2}$Gch$^{fl/fl}$ mice. Tamoxifen administration results in conformational change in ER$^{T2}$-Cre allowing Cre recombinase enzyme to translocate to the nucleus where it can splice the flanked *Gch1* gene. R26-CreER$^{T2}$ is expressed globally. Specificity was achieved by administering

tamoxifen (1 μM 4-hydroxytamoxifen (4-OHT)) to bone marrow cells, after bone marrow isolation, and during cell culture. Bone marrow was isolated from 12-16 week old adult male and female $Gch^{fl/fl}$ mice and R26-$CreER^{T2}Gch^{fl/fl}$ mice. Animals genotypes were confirmed by PCR (see section 2.3).

### 2.1.2 $Gch^{fl/fl}$ Tie2Cre mouse

$Gch^{fl/fl}$ animals were bred with Tie2cre transgenic mice to produce $Gch^{fl/fl}$Tie2Cre where *Gch1* is deleted in endothelial and bone marrow derived cells, resulting in BH4 deficiency (Chuaiphichai et al., 2014). As the transgene is active only in the female germline, male mice were exclusively used to establish breeding pairs for maintaining conditional expression. Experiments were conducted using bone marrow from both male and female mice (Chuaiphichai et al., 2014).

### 2.1.3 βV59M (Kir6.2-V59M) mouse

Legs from the βV59M (Kir6.2-V59M) mouse (Brereton et al., 2014) were donated by the Ashcroft group in the Department of Physiology Anatomy and Genetics (University of Oxford) for the generation of bone marrow derived macrophages at the Wellcome Centre for Human Genetics, Oxford. All animal studies were conducted in accordance with the UK Animals (Scientific Procedures) Act (1986) and approved by the local Department of Physiology Anatomy and Genetics (University of Oxford) ethical review committee. They were maintained on a 12 h light–dark cycle at 21 °C. Mice had unrestricted access to water and a regular chow diet (63% carbohydrate, 23% protein, 4% fat; Special Diet Services, RM3).

Mice hemizygously expressing Kir6.2-V59M in pancreatic β-cells (βV59M mice) were generated using a Cre-lox approach but using an inducible rat insulin promoter II (RIPII-Cre-ER mice) (Brereton et al., 2014). Kir6.2-V59M expression was induced in 12-week-

old mice by a single subcutaneous injection of tamoxifen in corn oil (10µl/g body weight of 20 mg $ml^{-1}$ , Sigma). Mice were culled two weeks later. The background strain of mice was C57BL/6 (Jackson Labs, USA) and experiments were conducted using bone marrow from both male and female mice. Tamoxifen injected wild-type mice, RIPII-Cre-ER mice and mice expressing only the Kir6.2-V59M$^{fl/fl}$ littermates (pooled) were used as controls. Body weight and blood glucose levels were monitored routinely. Blood glucose levels were measured from the tail vein using the Freestyle Lite device and Freestyle Lite test strips (both Abbott).

## 2.2 Cell culture

### 2.2.1 Bone Marrow Derived Macrophages

For bone marrow isolation, bone marrow was flushed from murine femurs and tibias with 10 mL phosphate buffered saline (PBS, Gibco). These bone marrow extracts were passed through a 70 µm filter (BD Falcon, UK) to remove any remaining bone fragments or other debris, and to create a single cell suspension. Cell suspensions were centrifuged at 500 *g* for 5 minutes. Following this, the supernatant was decanted and the remaining pellet resuspended in 2ml of freezing suspension (BioWest FBS + 5% DMSO). This final suspension then aliquoted into cryovials, containing approximately 10 million cells per vial, and stored in a Mr Frosty at -80 °C for 3 days before being transferred into liquid nitrogen (Figure 2.1) (Bailey et al., 2020).

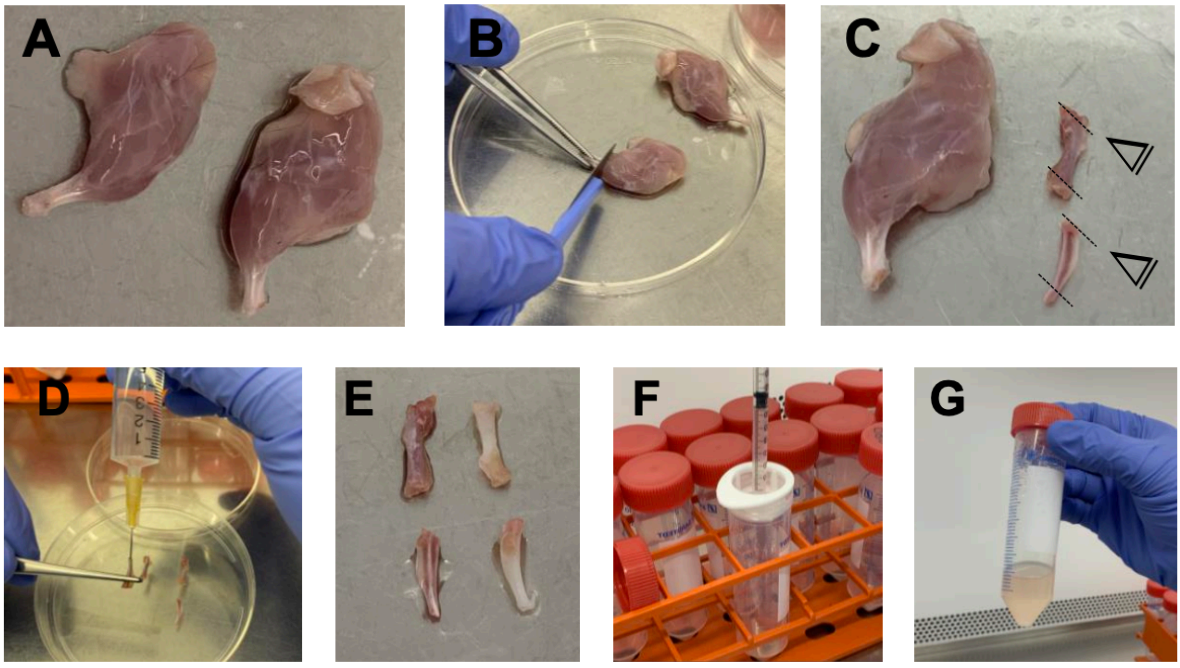



**Figure 2. 1 Murine bone marrow isolation procedure**

A) Under sterile conditions, dissected legs are placed in a clean bacteriological petri dish after being washed in 70% ethanol. B) Muscles are carefully removed using forceps and scalpel scraping along the bones. C) The extremities of the bones are then cut off to expose the bone marrow. D) The bone marrow is flushed from the bones using a 10 ml syringe filled with 10 ml of PBS by inserting the needle into the lumen of the bone. E) The needle is run up and down through the bone to ensure all bone marrow is dislodged. The bone should appear white and clear at that stage with the dislodged bone marrow collected in the petri dish. F-G) Repeat for all bones, collecting the disaggregated bone marrow in the 1ml syringe, and pass it through a 70 µm cell strainer into a clean 50 ml centrifuge tube. Spin down and resuspend cells in freezing media for later use (Diotallevi et al., 2021).

For BMDM culture, cryovials containing bone marrow cells were defrosted quickly in 37 °C water bath and transferred into 5 ml of warm DMEM:F12 (Gibco) supplemented with 5% FBS, 1% Penicillin/Streptomycin. After centrifugation at *500g*, and the supernatant removed, the cell pellet was resuspended in supplemented DMEM:F12 containing 25ng/ml monocyte colony stimulating factor (MCSF, Peprotech). Cells were plated into non-TC treated petri dishes containing 10 ml media and incubated at 37 °C and 5% $CO_2$. On Day 4, cultures were treated with an additional 50% supplemented DMEM:F12 containing 50 ng/ml MCSF, and two days later with 10µg/ml granular macrophage colony

stimulating factor (GMCSF, Peprotech). By Day 7, differentiated macrophages had attached to the petri dish. To collect them, media was removed and the macrophages were scraped and replated into 6 well, 12 well or 96 well non-TC treated plates as required, in DMEM:F12 (2% FBS) containing 25 ng/ml MCSF and 50 ng/ml GMCSF. To polarise cells to $M^{LPS/IFN\gamma}$, cells were stimulated for 16-18 hours with 100 ng/ml LPS (Peprotech) and 10 ng/ml IFN-γ (Peprotech). The next day, cells were harvested by scraping in cold PBS and pelleted by centrifugation at *250g* for 5 minutes at 4 °C. Pellets were stored at -80 °C until required (Figure 2.2).

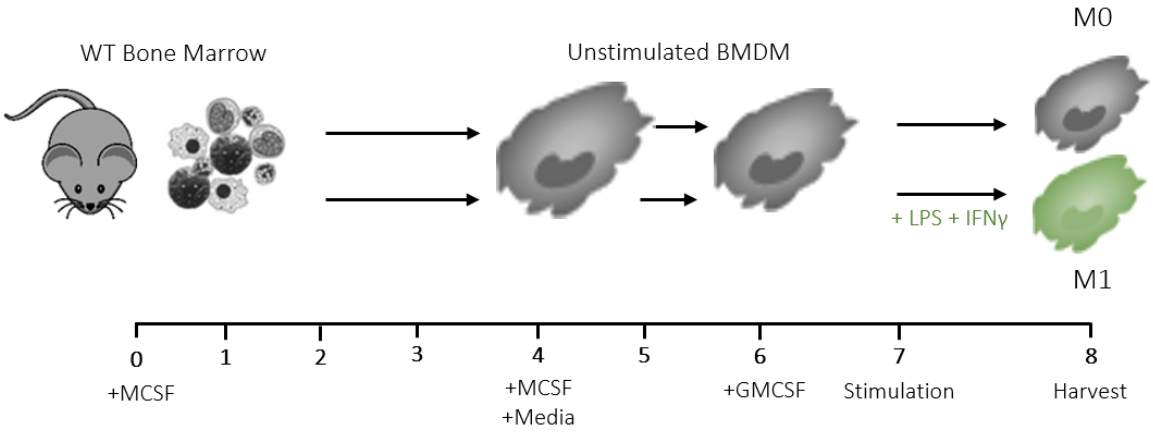



**Figure 2. 2 Schematic of BMDM culture protocol timeline**

Bone marrow cells are isolated and cultured in supplemented DMEM:F12 containing 25 ng/ml MCSF in non-TC treated petri dishes for 8 days. On Day 4, cells are given an additional 50% supplemented DMEM:F12 containing 50 ng/ml MCSF. On Day 6, cells are treated with 10 µg/ml GMCSF. On Day 7, cells are replated into the required non-TC treated plate, supplemented with DMEM:F12 containing 2% FBS. After attaching, cells are stimulated with 100 ng/ml LPS and 10 ng/ml IFN-γ for 16-18 hours before being harvested on Day 8.

### 2.2.2 Human Embryonic Kidney cells

Human Embryonic Kidney (HEK 293T, ECACC/Merck) cells were cultured in 25 mM glucose Dulbecco's Modified Eagle Medium (DMEM) with 10 % FBS (Sigma), 2 % penicillin/streptomycin (Sigma) and 2 mM glutamine (Sigma) in T175 flasks. At 90% confluency, culture medium was removed, cells were washed with warm PBS (Gibco) and incubated in warm 5 ml trypsin (Sigma) for 5 minutes at 37°C. Following detachment of cells from flask, 10 ml culture medium was added to neutralise trypsin and create a cell suspension. Cells were pelleted at 500 xg for 5 minutes and resuspended in 1 ml media. After resuspending cells in media, one fifth of the cells were transferred to new T175 flasks containing growth media to maintain their culture. Alternatively, cells were counted using a Cellometer Auto 2000 (Nexcelom Bioscience), and seeded at required density for subsequent assays in flasks or 6 well plates.

### 2.2.3 Cell viability

Trypan blue exclusion assay was conducted by mixing 10 µL of trypan blue with an equal volume of cell suspension. This mixture is transferred to a cell counting chamber (Nexcelom Bioscience) and into a Cellometer Auto 2000 (Nexcelom Bioscience), to give readings of live (unstained) and dead (stained blue) cells.

## 2.3 Genotyping PCR

### 2.3.1 Excision PCR - R26 CreER$^{T2}$ Gch$^{fl/fl}$

For DNA extraction, ear notches were incubated in alkaline lysis buffer (Sodium hydroxide (25 mM) and EDTA (0.2 mM)) at 95°C for 30 minutes. Samples were cooled to 4 °C briefly, then an equal volume of neutralisation buffer (Tris-HCl (40 mM)) was added and DNA was used for polymerase chain reaction (PCR) reactions. Mice were

genotyped using PCR. Genotyping was carried out by Dr Tom Nicol and representative gels are shown in Figure 2.3.

The primers used for the *Gch1* excision PCR were:

Gx5128 (Forward): 5'- GTCCTTGGTCTCAGTAAACTTGCCAGG -3'

Gch New (Reverse): 5'- GCCCAGCCAAGGATAGATGCA -3'

Pri5 (Forward): 5'- GCTCATCCCCCACACTTGTCT -3'

Primer stocks were made up at 100 ng/µL. The PCR reaction mix (25 µl) consisted of 2 µL crude DNA stock, 9.5 µL water, 12.5 µL (2x) Biomix Red (Bioline), 0.25 µL Gx5128 primer, 0.5 µL Gch new primer and 0.25 µL Pri5 primer. The PCR reaction was run on a Thermocycler following the protocol outlined in Table 2.1. The expected PCR product sizes were: Floxed *Gch1* 1030 base pairs (bp), Excised *Gch1* 1392 bp, Wild type *Gch1* 906 bp (Figure 2.3).

| | Step | Temperature (°C) | Time (mm:ss) |
|---|---|---|---|
| | 1 | 94 | 07:00 |
| 40 cycles | 2 | 94 | 00:30 |
| | 3 | 65 | 01:00 |
| | 4 | 68 | 01:00 |
| | 5 | 68 | 05:00 |
| | 6 | 7 | 01:00 |

Table 2. 1 Thermocycler settings for Gch1 genotyping PCR

For gel electrophoresis, PCR products were run on 2% agarose gels made in TAE buffer (Tris acetate (2 M) and Na2EDTA (100 mM)) with addition of ethidium bromide (0.004%). Gels were run at 120 V for 60 minutes in TAE running buffer and DNA was visualised using UV illumination. An outer lane running the Bioline

hyperladder I (Bioline) was used to determine the size of PCR products. Genotyping for R26 CreER$^{T2}$ Gch$^{fl/fl}$ was performed by Dr Tom Nicol in the Channon group.

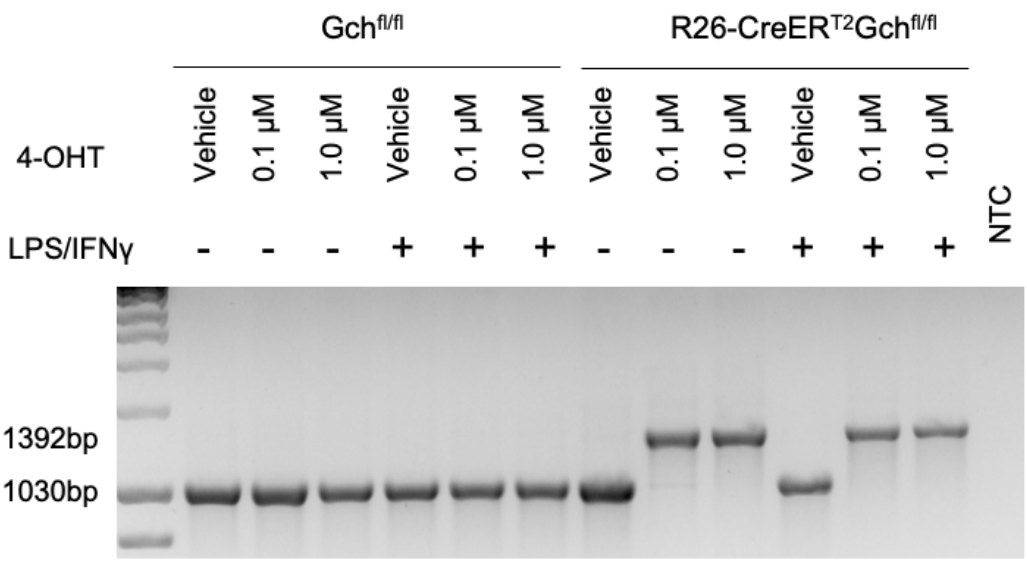



**Figure 2. 3 Genotyping R26-CreER$^{T2}$Gch$^{fl/fl}$ BMDMs**

Representative genotyping gels. PCR products from Gch1 and R26-CreER$^{T2}$Gch$^{fl/fl}$ reactions were separated by electrophoresis. Gch$^{fl/fl}$ products (1030bp) were observed in non-excised samples whereas excised Gch1 products (1392bp) were observed in 4-hydroxytamoxifen (4-OHT) R26-CreER$^{T2}$Gch$^{fl/fl}$ samples. Vehicle controls as well as non-template control (NTC) was used in all genotyping gels.

### 2.3.2 βV59M BMDM

Genotyping of this mouse model was performed by Dr Elizabeth Haythorne in the Ashcroft group, in the Department of Physiology Anatomy and Genetics, University of Oxford.

## 2.4 Flow Cytometry

For flow cytometry, cells grown in 6 well plates were harvested in 1ml FACs buffer (5mM EDTA, 0.05 % BSA) by scraping and transferred into 5ml FACs tubes before centrifugation at 300g for 5 minutes at 4°C. Control samples were prepared using spare cells for one unstained control, three single stain controls for each antibody, two fluorescence minus one controls with all except the antibody of interest (MHC II). After centrifugation, supernatant was removed, and pellet was resuspended in 100 µL FACs buffer with 1 µL anti-CD16/32 (1:100 dilution) and stored at 4°C for 15 minutes. Antibodies (F4/80, CD11b, MHCII (BioLegend)) were added to experimental and control samples at 1:200 dilution of each antibody per sample (1 µL in 100µL), before being mixed and stored at 4°C for 30 minutes. Antibodies were diluted out with 3 mL FACs buffer, centrifuged at 300g for 5 minutes at 4°C. Next sample and control cells were resuspended and incubated for 10 minutes in 100 µL 4% PFA (methanol free) in PBS at room temperature. After centrifugation at 300g for 5 minutes at 4°C, and resuspended with 200 µL FACs buffer for sample acquisition. Data were acquired using LSRFortessa cytometer and data analysed using FlowJo (version 10.8.1).

## 2.5 Quantitative real-time qPCR

All RNA techniques were carried out using filter tips, molecular biology grade DNase and RNase free water on a bench cleaned with RNase*Zap* RNase Decontamination

Solution (Thermo Fisher Scientific) and DNA*Zap* PCR DNA Degradation Solutions (Thermo Fisher Scientific) to avoid contamination with nucleic acid or RNase.

### 2.5.1 RNA extraction and quantification

To harvest cells grown in 6 well plates, 1 mL of TRIzol Reagent (Thermo Fisher Scientific) was added and cells were collected by scraping. The collected cells were transferred to Eppendorf tubes and stored at -80°C until RNA extraction. RNA extraction was performed by adding 200 µL chloroform to the defrosted TRIzol samples and incubating for 5-10 minutes at room temperature, followed by vortexing and centrifugation at 12,000 x g for 15 minutes at 4°C. The transparent upper phase was transferred to a new tube and an equal volume of 70% ethanol was added, vortexed, and RNA was extracted using RNeasy Mini Kits (Qiagen) according to the manufacturer's protocol. After transfer to RNeasy Mini spin columns, RNA was eluted from the column with RNase-free water and kept on ice. RNA levels were quantified by measuring the absorbance at 260 nm using a NanoDrop, with a 260 nm to 280 nm absorbance ratio of approximately 2 to ensure RNA purity.

### 2.5.2 Generation of cDNA by RT-qPCR

RNA was converted into complementary DNA (cDNA) using a QuantiTect Reverse Transcription Kit (Qiagen) through reverse transcriptase quantitative PCR (RT-qPCR). To remove genomic DNA contamination, RNA samples were first mixed with gDNA Wipeout Buffer (1000 ng template RNA and 2 µL gDNA Wipeout Buffer with RNase-free water to make up 14 µL) and incubated at 42°C in the thermocycler for 2 minutes. Next, samples were mixed with a mastermix consisting of reverse transcriptase and primers (1 µL Quantiscript Reverse Transcriptase, 1 µL RT Primer Mix and 4 µL Quantiscript RT Buffer). The thermocycler protocol was continued at 42°C for 30 minutes to generate cDNA and 95°C for 3 minutes to inactivate the reverse transcriptase. Negative control samples were included, replacing Quantiscript Reverse Transcriptase with RNase-free water (-RT), to

identify possible genomic DNA contamination. The resulting cDNA was at 30 ng/µL and stored at -20°C until quantitative real time RT-PCR (qRT-PCR) was performed.

### 2.5.3 RT-qPCR primers

To perform RT-qPCR, Applied Biosystems TaqMan gene expression assays (Table 2.2) were utilized. These assays contained primers and probes designed to bind to exon-exon junctions and match the target cDNA sequence. Probes were labelled with a 5' 6-carboxyfluorescien (FAM) reporter fluorophore, and they annealed to a target DNA sequence between the forward and reverse primers. Initially, the fluorophore was quenched by close proximity of a 3' quencher until primer extension took place, causing cleavage by the 5' exonuclease activity of Taq polymerase. Consequently, fluorescence from the fluorophore was no longer quenched, and its intensity was directly proportional to the amount of cDNA present.

| Assay | Assay ID |
|---|---|
| TaqMan murine *Hif1a* | Mm00468869_m1 |
| TaqMan murine *Hk2* | Mm00443385_m1 |
| TaqMan murine *Il6* | Mm00446190_m1 |
| TaqMan murine *Il1b* | Mm00434228_m1 |
| TaqMan murine *Irg1* | Mm01224532_m1 |
| TaqMan murine *Nos2* | Mm00440502_m1 |
| TaqMan murine *Slc2a1* | Mm00441480_m1 |
| TaqMan murine *ActB* | 4352341E |
| TaqMan murine *Gapdh* | 4325792 |
| TaqMan eukaryote 18s | 4352655 |

Table 2. 2 Details of TaqMan assays used in RT-qPCR reactions

### 2.5.4 Quantitative real-time RT-PCR

cDNA was diluted from 30 ng/µL to 10 ng/µL in RNase-free water. 1 µL of cDNA (10ng) was added to each well of a 384 well qPCR plate in triplicate, along with negative controls (-RT and water samples) for each gene expression assay to detect contamination in the RT-

PCR and qRT-PCR reactions, respectively. Gene expression assays were prepared by mixing 5 µl of 2x TaqMan Universal Master Mix and 0.5 µL of 20x TaqMan gene expression assay, followed by the addition of RNAse-free water to reach a final volume of 10 µL per well. After running a housekeeping gene panel consisting of GAPDH, ACTB, and 18S, the *ActB* gene expression assay was selected as the housekeeping gene to control for sample variability. The plates were covered with an adhesive strip, briefly centrifuged, and the cDNA was amplified on an Agilent Applied Biosystems Real-time detection system (BioRad Laboratories Ltd) using the protocol specified in Table 2.3.

The qRT-PCR reaction produced an exponential increase in product, leading to an increase in fluorescence until the reaction components reached their limit, resulting in a plateau. The software from Applied BioSciences then determined the threshold cycle (Ct) value during the linear phase of amplification, which was set above the background fluorescence level. To determine the relative gene expression, the Ct values of all samples were normalized to the Ct values of the ActB gene. This was done using the following calculation: $2^{-\Delta Ct(\text{Gene of interest (GOI)} - \text{ActB})}$.

| | Temperature (°C) | Time (min:second) | Step |
|---|---|---|---|
| | 50 | 2:00 | Taq polymerase activation |
| | 95 | 0:20 | Denaturation |
| 35 cycles | 95 | 0:03 | Annealing |
| | 60 | 0:30 | Extension |

Table 2. 3 Thermocycler setting for RT-qPCR

## 2.6 Western Blot

### 2.6.1 Preparation of protein lysates

Sample pellets were resuspended in lysis buffer, consisting of 10 ml CelLytic M buffer (Sigma), 1x Complete Mini EDTA-free Protease Inhibitor Cocktail tablet (Sigma) and (if

required) 1x PhosSTOP Phosphatase Inhibitor Cocktail tablet (Sigma). After one freeze thaw cycle on dry ice, samples were centrifuged at 17,000 x g and 4°C for 10 minutes. Supernatant lysates were transferred to fresh tubes and protein levels quantified using a BCA protein assay as described in Section 2.6.2.

### 2.6.2 Measuring protein content

The Pierce bicinchoninic acid (BCA) Protein Assay kit (Thermo Fisher Scientific) was used to quantify the total protein content in each lysate. Sample buffer was used to prepare a blank sample and BSA standards were serially diluted from 4 to 0.0625 mg/ml. A 12 µl sample or standard was mixed with 12 µL of iodoacetamide (20 mg/mL in 0.4% sodium hydroxide) and incubated at 37°C for 15 minutes to prevent reaction of BCA reagents with thiols, thus improving the accuracy of the assay (Hill and Straka, 1988). BCA reagents were prepared according to the manufacturer's instructions (1:50 Solution A: Solution B) and 480 µl of this solution was added to each sample and standard. They were then incubated in a 37°C water bath for 30 minutes. Duplicates of each sample and standard (200 µL) were transferred to clear 96 well microtiter plates and read at 590 nm. The protein concentration of each sample was calculated by using the BSA standard curve with blank correction and taking the mean of the duplicate wells.

### 2.6.3 Western blotting

To prepare the samples, lysates with known protein concentrations (as described in Section 2.6.2) were diluted with water, and then x10 NuPAGE Sample Reducing Agent 69 and x4 NuPAGE LDS Sample Buffer (both from Thermo Fisher Scientific) were added to achieve the desired final concentration (usually 5 µg/mL, unless otherwise specified). The samples were then denatured by incubation at 90°C for 5 minutes before loading onto a gel. At this point, the samples were usually stored at -20°C, although -80°C was used for the detection

of phosphorylated proteins. SDS-PAGE was employed to separate proteins based on their denatured molecular weights. Samples were heated at 90°C for 5 minutes and loaded onto NuPAGE Novex 4-12% gradient Bis-Tris 1 mm pre-cast polyacrylamide gels (Thermo Fisher Scientific), together with 50 mL of 20x NuPAGE MOPS SDS Running Buffer per litre (also Thermo Fisher Scientific), and subjected to a constant voltage of 200 V until the sample dye reached the bottom, typically around 60 minutes. An outer lane containing 6 µL of Amersham ECL Full Range Recombinant Molecular Weight Rainbow Marker (from GE Healthcare Life Sciences) was included to estimate the mass of target proteins. The proteins were transferred from the gel to a polyvinylidene membrane using a wet transfer in a buffer consisting of Tris-base (3.03 g/L), glycine (15 g/l), and methanol (20%) for 90 minutes with a constant current of 300 mA. The membranes were then blocked with 5% milk in PBST (0.1% Tween in PBS) for at least 1 hour at room temperature or overnight at 4°C on a rocker. Primary antibodies (see Table 2.4) against the proteins of interest were incubated with the membranes overnight at 4°C on a rocker. The next day, the membranes were washed briefly three times in PBST, followed by three 5-minute washes on a rocker. Membranes were incubated with secondary antibodies for 1 hour at room temperature on a rocker and protected from light (Table 2.5). The membranes were again washed three times briefly in PBST, followed by three 5-minute washes on a rocker, before development using LI-COR Odyssey.

| Antibody | Dilution | Specificity | Species | Product information |
|---|---|---|---|---|
| Anti-iNOS | 1:1000 | Mouse | Mouse | Abcam (ab49999) |
| Anti- GTPCH | 1:5000 | Mouse | Rabbit | Prof S. Gross, Cornell University |
| Anti-hexokinase 2 | 1:1000 | Mouse | Rabbit | Cell Signalling (2867S) |
| Anti-IRG1 | 1:1000 | Mouse, Human | Rabbit | Abcam (ab2221411) |
| Anti-β-tubulin | 1:20,000 | Mouse | Rabbit | Abcam (ab6046) |
| Anti-GAPDH | 1:20,000 | Mouse | Mouse | Millipore (MAB374) |
| Anti-mouse IgG | 1:50,000 | Mouse | Rabbit | IRDye 800CW |
| Anti-mouse IgG | 1:50,000 | Mouse | Donkey | IRDye 680CW |

Table 2. 4 Table of antibodies used for western blot analyses

## 2.7 Cytokine measurements by ELISA

DuoSet enzyme-linked immunosorbent assays (ELISAs) (R&D Systems) were used to measure TNF-α, IL-6, and IL-1β in condition media supernatants collected from macrophages re-plated at $1x10^6$ cells per well of a 6 well plate on day 7 of culture and stimulated with LPS/IFN-γ for 16 hours. To measure cytokines neat supernatants were used for IL-1β, and supernatants were diluted 1:100 and 1:400 for TNFα and IL-6 respectively to allow comparison with standard curves. The day before the assay Nuncimmuno 96 well plates (ThermoFisher Scientific) were pre-coated overnight at room temperature with Capture antibodies (DuoSet R&D Systems) resuspended in PBS according to the manufacturer's instructions. On the day of the assay, plates were washed in Wash Buffer (0.05% Tween20 in PBS) and blocked in Reagent Diluent (1% fatty acid free BSA (Sigma) in PBS) for 1 hour. After further washing, samples and standards were

added in duplicate (made up in Reagent Diluent/media as appropriate), and incubated for 2 hours before additional wash steps. Detection antibodies (DuoSet R&D Systems) were added to wells and incubated for 2 hours before additional wash steps. Wells were incubated with Streptavidin-HRP (DuoSet) for 20 minutes protected from light, and then washed again. Substrate Solution (Substrate 184 Reagent Pack, R&D Systems) was added, comprised of 1:1 mixture of Colour Reagent A and B, for 20 minutes protected from light. Stop Solution was added (0.67 N $H_2SO_4$) and plates were read on a BMG microplate reader at 450 and 540 nm. For data analysis, 540 nm readings were subtracted from 450 nm values to correct for optical imperfections in the plates, duplicate readings were averaged and blank optical densities subtracted from standards and samples. Sample concentrations were calculated against standard curves generated using a four-parameter logistic curve-fit, and multiplied by dilution factors if appropriate.

### 2.8 Measurement of nitrite accumulation using Griess assay

Culture media was centrifuged at 500 x g for 10 minutes at 4 °C to pellet cell debris, after which 100 µl of supernatant was carefully transferred in duplicate into clear 96 well microtiter plates. Subsequently, 100 µl of Griess assay reagent was added (made up of a 1:1 mixture of Griess solution 1 (0.1% w/v N-(1-Naphthyl)ethylenediamine dihydrochloride (Sigma) in water stored at 4 °C wrapped in foil) and Griess solution 2 (1% w/v sulphanilamide (Sigma) in 5% orthophosphoric acid stored at 4 °C wrapped in foil)). The plate was then incubated at room temperature for 15 minutes before reading at 550 nm absorbance. Nitrite accumulation was determined against a standard curve prepared from a 500 mM sodium nitrite stock, serially diluted from 100 to 3.15 µM in sample media and a blank media sample for background correction (Figure 2.4).

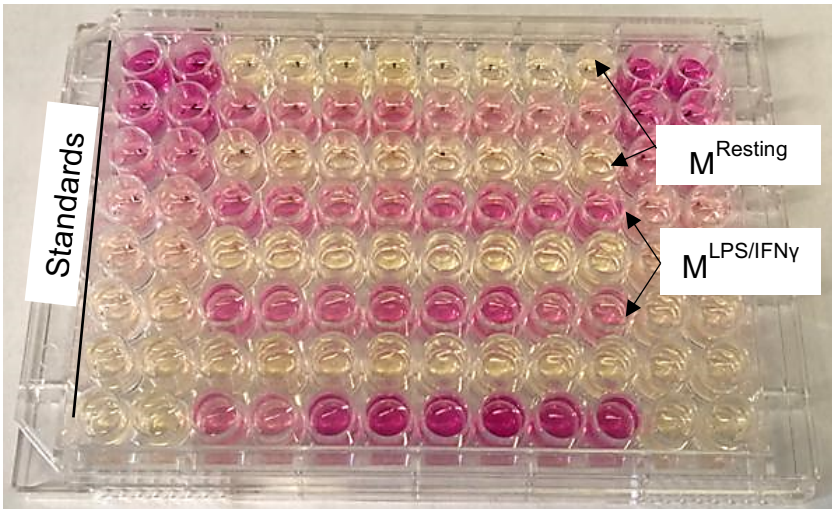



**Figure 2. 4 Representative Griess assay 96 well plate**

Plate shows highest standard to blank in columns 1 and 2 (and 11 and 12). Nitrite levels in WT $M^{Resting}$ and $M^{LPS/IFN\text{-}\gamma}$ in the rows indicated.

## 2.9 Seahorse XFe96 Extracellular flux assays

The Seahorse XFe96 Bioanalyzer (Agilent Technologies) was used to conduct extracellular flux assays. To do this, a monolayer of live cells was seeded into Seahorse XFe96 microplates and the media surrounding them was analysed for oxygen consumption rate (OCR) and extracellular acidification rate (ECAR) using Seahorse XFe96 FluxPacks. The FluxPacks consisted of 96 sensors that were lowered to 200 µm above the cells, creating a transient microchamber. Fluorophores sensitive to oxygen and pH changes were used to measure OCR and ECAR, respectively. The injection of compounds that modulate metabolism allowed the calculation of metabolic parameters. All reagents used for these assays were purchased from Agilent Technologies unless specified otherwise.

### 2.9.1 Preparation for Seahorse extracellular flux assays

The day before conducting Seahorse extracellular flux assays, cells were plated into Seahorse XFe96 microplates using cell-specific growth media. Seeding densities were optimized for each cell type to achieve a monolayer of cells on the day of the assay. Basal OCR readings were maintained between 100-200 pmol O2/min/well to ensure sufficient

oxygen levels for response to compound injections. Hydration of Seahorse XFe96 FluxPacks was also carried out the day prior to the assay. Each FluxPack was hydrated with 200 µL of Seahorse XF Calibrant per well, wrapped in Parafilm, and incubated at atmospheric $CO_2$ levels in a 37°C incubator overnight.

### 2.9.2 Seahorse MitoStress Test to analyse mitochondrial respiration in BMDMs

On day 7 of culture, macrophages were plated at a density of 75,000 cells per well into XFe96 microplates following optimization of seeding density. Cells were left to attach for 1 hour at room temperature to minimise an "edge effect" and placed in the incubator at 37°C and 5% $CO_2$ for at least 2 hours before stimulation with LPS/IFN-γ or IL-4 if required, for 16-18 hours. Cells were placed in the Seahorse XFe Bioanalyzer and extracellular flux analysis was then performed. Serial injections of the following compounds from the XF Cell Mito Stress Test Kit (Agilent): oligomycin (2 µmol/L, injection port A), FCCP (2 µmol/L, injection port B), and combined antimycin A (0.5 µmol/L), and rotenone (0.5 µmol/L, injection port C) was added to each well (Table 2.5, 2.6). Oxygen consumption rate and extracellular acidification rate of cells were measured in at least 4 replicate wells (Figure 2.5). All Seahorse data was normalised using the live/dead cell assay described in 2.9.8.

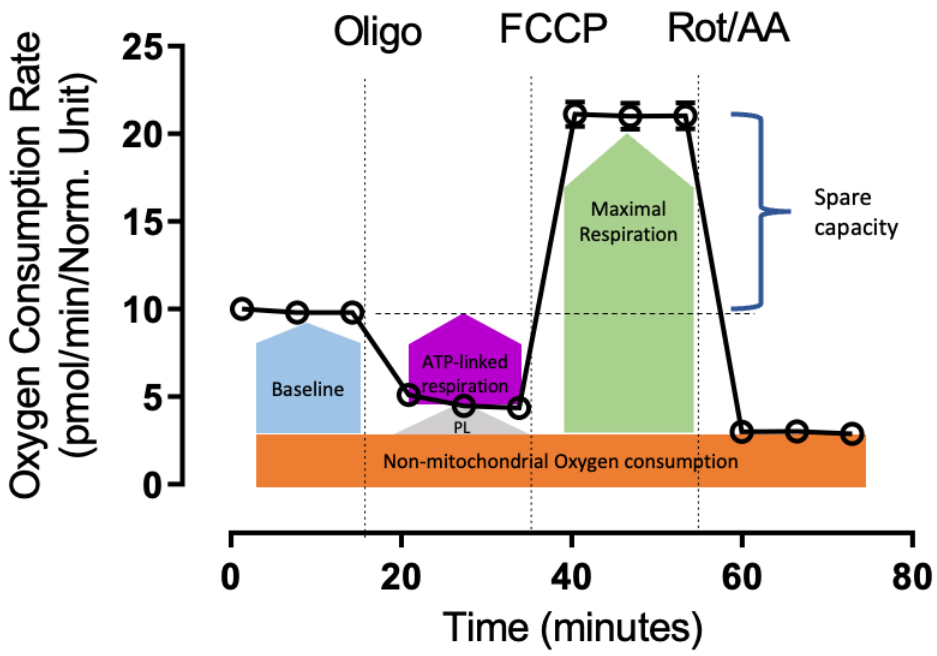



**Figure 2. 5 Schematic MitoStress test profile with calculated parameters and representative MitoStress test trace**

Representative oxygen consumption rate (OCR) trace measured by a Seahorse XFe96 Bioanalyzer during a MitoStress test assay to determine mitochondrial respiratory function. Baseline readings and readings taken following sequential injection of oligomycin, FCCP and combined rotenone/antimycin A (Rot/AA) to allow determination of basal, ATP-linked, maximal, spare-respiratory capacity, proton leak (PL) and non-mitochondrial OCR.

| Compound | Function |
|---|---|
| Oligomycin | Inhibition of Complex 5 of the electron transport chain |
| FCCP | Permeabilization of mitochondrial membrane |
| Rot/Antimycin A | Inhibition of Complexes 1 and 3 of the electron transport chain |

Table 2. 5 Functions of drugs on inner mitochondrial membrane

| Settings (min:sec) | Basal (3 cycles) | Oligomycin (3 cycles) | FCCP (3 cycles) | Rot/Antimycin A (3 cycles) |
|---|---|---|---|---|
| Mix | 3:00 | 3:00 | 3:00 | 3:00 |
| Wait | 0:00 | 0:00 | 0:00 | 0:00 |
| Measure | 3:00 | 3:00 | 3:00 | 3:00 |
| Total Duration | 18:00 | 18:00 | 18:00 | 18:00 |

Table 2. 6 Settings used to carry out Seahorse XFe96 MitoStress test

### 2.9.3 Seahorse MitoStress Test calculations

Oxygen consumption rate (OCR) readings were used to determine mitochondrial respiratory function. Baseline OCR measurements included oxygen consumption by the electron transport chain (ETC) during oxidative phosphorylation and by other oxidase enzymes. To calculate ATP-linked OCR, oligomycin was used to inhibit ATP synthase in the first injection. FCCP, in the second injection, uncoupled ATP synthesis from the ETC by dissipating the proton gradient across the mitochondrial inner membrane and allowed maximum mitochondrial OCR to be achieved by transferring electrons uninhibited. The third and fourth injections included rotenone and antimycin A, respectively, which inhibited Complex I and Complex III of the ETC, shutting down mitochondrial oxygen consumption. These injections allowed the proportion of baseline OCR attributed to mitochondrial respiration to be calculated. For a full list of the calculations, please refer to Table 2.7.

| Respiratory function parameter | Calculation |
|---|---|
| Basal OCR | Average all baseline replicates |
| ATP-linked OCR | Basal OCR – Oligomycin |
| Maximal OCR | Average FCCP technical replicates |
| Spare respiratory capacity OCR | FCCP – Basal OCR |
| Proton Leak OCR | Oligomycin – Rot/AA |
| Non-mitochondrial OCR | Rot/AA |

Table 2. 7 Calculations to determine respiratory function

### 2.9.4 Glycolytic rate assay

Glycolytic activity was determined using the simultaneous ECAR readings generated during the above XF Cell Mito Stress Test, and included the subsequent addition of 2-deoxyglucose (100 mM, Sigma) injected through port D. The third ECAR measurement following the 2-deoxyglucose injection was subtracted from the third base-line ECAR reading to calculate 'basal glycolysis'.

The Seahorse XF Glycolytic Rate Assay protocol was used to generate a measurement of glycolysis that takes into account acidification by $CO_2$ generated through the TCA cycle (Mookerjee et al., 2015). Cells were plated, stimulated and culture medium replaced as for the XF Cell Mito Stress Test (Section 2.9.1). Immediately prior to the assay this media was again replaced. Three baseline OCR and ECAR measurements were taken followed by 3 measurements after injection of combined antimycin A (0.5 μM), and rotenone (0.5 μM) (injection port A, Mito Stress Test Kit), and 5 measurements after injection of 2-deoxyglucose (50 mM, Sigma). Glycolytic function was calculated as seen in Table 2.8.

| Respiratory function parameter | Calculation |
|---|---|
| Basal ECAR | Average baseline replicates |
| Compensatory glycolysis | Average post Rot/AA replicates |
| Glycolytic reserve | (Compensatory glycolysis - Basal ECAR)*100 |
| Post 2-DG acidification | Average post 2-DG replicates |

Table 2. 8 Glycolytic rate assay calculations to determine respiratory function

### 2.9.5 Seahorse ATP rate assay in BMDMs

Cells were plated, stimulated and culture medium replaced as above for the XF Glycolytic Rate assay. Three baseline OCR and ECAR measurements were taken followed by 3 measurements after injection of oligomycin (2 μmol/L, injection port A) followed by combined antimycin A (0.5 μmol/L), and rotenone (0.5 μmol/L) (injection port A, Mito Stress Test Kit) at basal respiration. ATP production rate from glycolysis and mitochondrial respiration was calculated as seen in Table 2.9.

| Respiratory function parameter | Calculation |
|---|---|
| Basal ECAR | Average baseline replicates |
| GlycoATP production rate | pmol of H+ produced per minute |
| MitoATP production rate | $OCR_{ATP}$ (pmol $O_2$/min) = OCR (pmol $O_2$/min) - $OCR_{Oligo}$ (pmol $O_2$/min)<br><br>mitoATP Production Rate (pmol ATP/min) = $OCR_{ATP}$ (pmol $O_2$/min) * 2 (pmol O/pmol $O_2$) * P/O (pmol ATP/pmol O)<br><br>P/O value = 2.75 (number of molecules of ATP synthesised per atom of oxygen (O) reduced by an electron pair flowing through the mitochondrial electron transport chain, as determined by Agilent) |
| Total ATP production rate | GlycoATP + mitoATP production rates |
| % ATP production | % Glycolysis = GlycoATP/Total ATP *100<br>% OXPHOS = MitoATP/Total ATP *100 |

Table 2. 9 ATP rate assay calculations to determine respiratory function

### 2.9.6 Seahorse Glutamine dependency assay in BMDMs

Cells were plated, stimulated and culture medium replaced as above for the XF Glycolytic Rate assay. Three base-line OCR and ECAR measurements were taken followed by 3 measurements after injection of BPTES (3 μM, injection port A), a glutaminase inhibitor, followed by combined Etomoxir (4 μM), carnitine palmitoyltransferase-1 inhibitor, and UK5099 (2 μM) (injection port A, Mito Stress Test Kit), mitochondrial pyruvate carrier inhibitor, at basal respiration. Dependency of cells on glutamine for ATP production was calculated as seen in Table 2.10.

| Respiratory function parameter | Calculation |
|---|---|
| Basal OCR | Average baseline replicates |
| Glutamine dependency | $\frac{\text{Basal OCR - BPTES OCR average}}{\text{Basal OCR - UK5099/Etomoxir OCR}}$ |

Table 2. 10 Glutamine Dependency assay calculations to determine respiratory function

### 2.9.7 Seahorse Fatty Acid oxidation assay in BMDMs

Cells were plated, stimulated and culture medium replaced as above for the XF Glycolytic Rate assay. Three base-line OCR and ECAR measurements were taken followed by 3 measurements after injection of Etomoxir (4 μmol/L, injection port A) followed by combined UK5099 (2 μM), and BPTES (3 μM) (injection port A, Mito Stress Test Kit) at basal respiration. Dependency of cells on fatty acid oxidation was calculated as seen in Table 2.11.

| Respiratory function parameter | Calculation |
|---|---|
| Basal ECAR | Average baseline replicates |
| FAO dependency | $\frac{\text{Basal OCR - Etomoxir OCR average}}{\text{Basal OCR - UK5099/BPTES OCR}}$ |

Table 2. 11 Fatty Acid Oxidation assay calculations to determine respiratory function

### 2.9.8 Calcein Live/Dead cell assay

Once Seahorse run was complete the XFe96 sensor cartridge was ejected and the culture medium removed from the XFe cell culture plate. A master mix was prepared consisting of: 7.5 ml PBS, 15µL ethidium (Invitrogen, Thermo Fisher Scientific) 3.75 µL Calcein (Invitrogen, Thermo Fisher Scientific). Cells were washed gently with 200 µL PBS before 70 µL of the prepared master mix was added to each well and then immediately wrapped in foil for protection from light. After 30 minutes incubation on a rocker at room temperature, before reading at 645 nm and 530 nm fluorescence.

## 2.10 Measurement of BH4 by HPLC

Biopterins were quantified using a high-performance liquid chromatography (HPLC) system equipped with an electrochemical detector for BH4 and a fluorescent detector for BH2 and biopterin. To prevent biopterin oxidation, samples were collected and immediately stored at -80 °C and prepared for HPLC analysis on ice. Sample pellets were lysed in ice-cold Resuspension buffer containing phosphate-buffered saline (50 mM) with dithioerythritol (1 mM) and EDTA (100 µM), and centrifuged to transfer the supernatants to fresh tubes. To precipitate the proteins, Precipitation buffer, which is a x10 solution of phosphoric acid (1 M), trichloroacetic acid (2 M), and dithioerythritol (1 mM) in PBS (50 mM) at pH 7.4, was added to the samples. The mixture was vortexed, centrifuged again, and the supernatants were injected onto an HPLC system for analysis. An isocratic HPLC system was used to separate the samples using a 250 mm, ACE C-18 column and a mobile phase consisting of sodium acetate (50 mM), citric acid (5 mM), EDTA (48 µM), and dithioerythritol (160 µM) at pH 5.2 and a flow rate of 1.3 ml/min. BH4 was detected on electrochemical cells E1 and E2 using background currents of +500 µA and -50 µA, respectively. BH2 and biopterin were detected using a Jasco FP2020 fluorescence detector. Quantification of BH4, BH2, and

biopterin was performed by comparing peak areas with authentic external standards. All data were normalized to sample protein content using the BCA assay.

## 2.11 Method development and validation for the detection of Itaconic acid by high performance liquid chromatography

### 2.11.1 Introduction

Upon activation, macrophages undergo significant metabolic reprogramming, displaying striking changes in abundance of glycolysis and TCA cycle metabolites (Y. Liu et al., 2021). Notably, itaconate, derived from the decarboxylation of cis-aconitate by IRG1 in the mitochondria, was one of the most highly upregulated metabolites in inflammatory macrophages (Strelko et al., 2011). This discovery has led to a surge of research into the small molecule from its mechanisms of immunomodulation to its potential as a therapeutic target in a variety of diseases (Diotallevi et al., 2021). Our group too developed interest in itaconate, having observed >4-fold increases in itaconate levels on a metabolomics analysis of NO-deficient LPS/IFN-γ macrophages (Bailey et al., 2019). To follow up on these observations, we aimed to develop and validate an in-house method for the detection of itaconate in primary macrophages.

The most commonly used methods for the detection of itaconate rely on mass spectrometry, which can be expensive and difficult to access. Mass spectrometers are typically used in tandem with gas or liquid chromatography. We found several published HPLC methods optimised for itaconate detection in bacteria using a variety of instruments, and chromatographic conditions (Bafana et al., 2017; Fan et al., 2021; X. Huang et al., 2014; Kanamasa et al., 2008). To set up initial chromatographic conditions, we noted all groups used 210nm wavelength regardless of sample type. Mobile phase composition was adapted by Dr Marina Diotallevi from Kanamasa et al, as they had optimised itaconate detection on a HPLC instrument most similar to ours (Kanamasa et al., 2008). Standard flow rate of 1 ml/min was employed. Following this, we set out to optimise sample preparation, and the method itself, before validating its fitness for purpose. We sought to measure intracellular,

in cell lysate, as well as extracellular levels of itaconate, in cell supernatant, to assess potential roles of the metabolite in autocrine or paracrine signalling.

### 2.11.2 Method

#### 2.11.2.1 Instrumentation

A Jasco X-LC HPLC system equipped with a PU-2080 Plus HPLC pump, AS-2057 autosampler, DG-2080-53 3-Line degasser and 3075UV UV-VIS detector was used (Figure 2.6). Data were collected with Azur v5 data acquisition software.

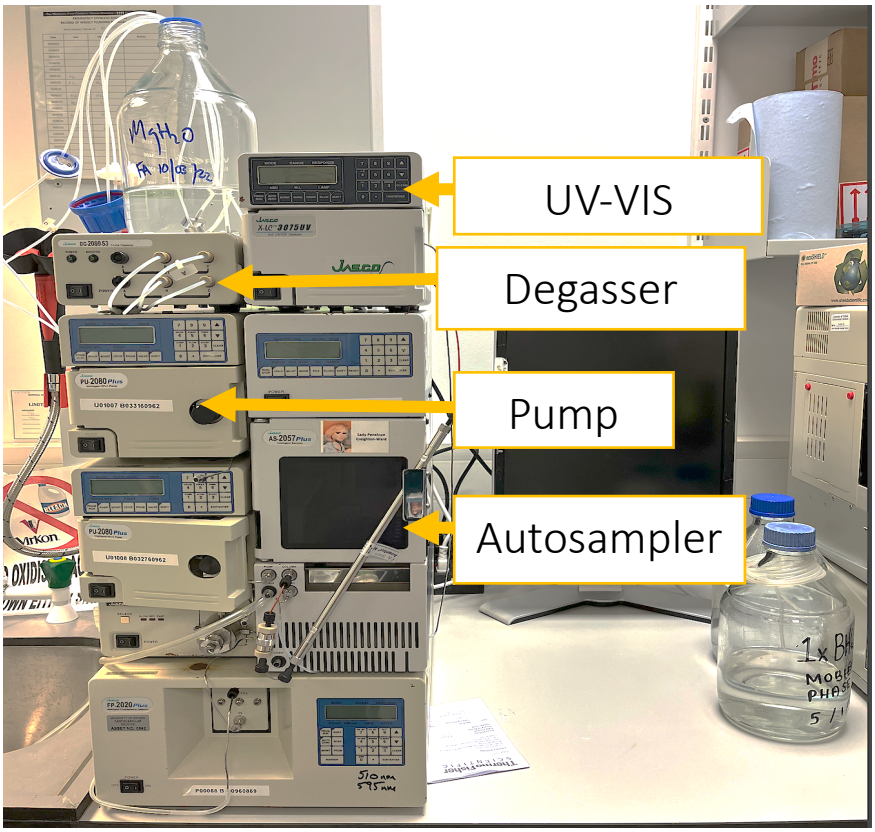



**Figure 2. 6. High Performance Liquid Chromatography (HPLC) setup with key components: UV-Vis detector, degasser, pump and autosampler labelled.**

#### 2.11.2.2 Chemicals and Reagents

Compounds were purchased from Sigma Aldrich: itaconic acid (Sigma, 129204), succinate (Sigma, 398055), cis-aconitate (Sigma, A3412), Fumarate (Sigma, 47910). Mobile phase

was composed of HPLC grade acetonitrile (Fischer 34851) and Orthophosphoric acid (Fischer O/0515/PB08) and water. Water was deionised and purified using Milli-Q Reagent Grade water system (Millipore Corp, USA).

#### 2.11.2.3 Chromatographic conditions

Isocratic reverse-phase HPLC chromatography with Ace 5 C18-PFP column (ACE-1210-2546) was used. The mobile phase was composed of 2.5% Acetonitrile and 0.01% Orthophosphoric acid. Chromatographic conditions are outlined in Table 2.12.

| HPLC chromatographic conditions | |
|---|---|
| Flow rate | 1.0 mL/min |
| Wavelength (λ) | 210 nm |
| Temperature | 20 ℃ |
| Injection volume | 100 µL |

Table 2. 12 High performance liquid chromatographic condition

#### 2.11.2.4 Preparation of standard solutions

Stocks of 100mM itaconic acid, cis-aconitate, succinate and fumarate were prepared in PBS (Gibco 10010023) and stored at room temperature. From this stock, working solutions of 500 µM were prepared in PBS or media as required and serially diluted to the intended concentrations (range 62.5-0.22µM).

#### 2.11.2.5 Preparation of sample solutions

To prepare cell lysate samples for the measurement of intracellular itaconate, PBS (148µL) was added to each pellet and lysed by 3 freeze/thaw cycles in dry ice and 37°C water bath. Next, to remove cellular debris, the cell lysates were centrifuged at 17,000g for 10mins at 4°C and the supernatant transferred into a new Eppendorf tube. For data normalisation, 12µl of the supernatant was removed for protein assay while 2M perchloric acid (15µL or 10%

of total volume) was added for protein precipitation (protein precipitation optimisation shown in Fig 2.3). Samples were centrifuged again at 17,000g for 10mins at 4°C and the supernatants transferred into chromovials for analysis by HPLC.

To prepare supernatants from cells for the measurement of extracellular itaconate, supernatants were defrosted on ice and 148µL transferred to new tubes. Similarly to cell lysates, perchloric acid (15µL) was added to each tube for protein precipitation. Samples were centrifuged again at 17,000g for 10mins at 4°C and the supernatants transferred into chromovials for analysis by HPLC. The data acquired was normalised to intracellular protein levels obtained by BCA protein assay (see section 2.6.2).

#### 2.11.2.6 Method validation

The HPLC method for itaconate measurement was validated in terms of specificity, linearity and range, limit of detection (LOD) and quantification (LOQ), accuracy, precision, stability, reproducibility and robustness.

#### 2.11.2.7 Specificity

Specificity is the ability of the analytical method to distinguish between the analyte and other components in the sample matrix. For the HPLC method, it is assessed by complete separation of the analyte peak from other peaks in the sample matrix. Specificity was evaluated by injecting separately 100 µL solutions of standard, sample and blank into the chromatographic system.

#### 2.11.2.8 Linearity and range

To evaluate linearity of the method, standard solutions of itaconic acid were prepared by diluting stock standards in PBS to obtain exact concentrations of itaconic acid (62.5 µM, 31.25 µM, 15.625 µM, 7.813 µM, 3.907 µM, 1.953 µM, 0.977 µM, 0.488µM, 0.244 µM, 0

μM), with target intracellular and extracellular concentrations estimated around 3.907 μM and 7.812 μM respectively. Linear regression analysis was used to evaluate the linearity of the calibration curve by using the least square linear regression method, with >0.995 deemed acceptable.

#### 2.11.2.9 Sensitivity

The Limit of Detection (LOD) is the lowest amount of analyte in a sample that can be detected and not necessarily quantitated. The Limit of Quantification (LOQ) is the lowest amount of analyte that can be determined quantitively with adequate precision. The LOD here was determined as a minimum signal-to-noise ratio of 3:1 and the LOD as 10:1 signal-to-noise ratio.

#### 2.11.2.10 Accuracy and Precision

The accuracy of the method was determined by recovery studies for itaconic acid from cell lysate matrix. HEK cell pellets were lysed with cell lysates and spiked with the target concentration of itaconic acid (7.8μM) as well as 20% (6.24μM) lower and 20% higher (9.36μM) than the target concentration. At each concentration level, three samples were lysed and spiked. Spiked samples were then processed via the sample preparation method and compared against the standard curve to assess the recovery rate for each replicate sample.

#### 2.11.2.11 Stability

The stability of the analytical solutions was determined by analysing placebo (HEK) cell lysate spiked at the target concentration (7.8 μM) stored at room temperature, 4 °C, -20 °C, -80 °C. Furthermore, freeze/thaw study was conduction on these spiked samples as well as on supernatants from LPS-stimulated BMDMs and percentage loss of analyte determined from peak area.

#### 2.11.2.12 Data Processing

Chromatographic peaks were acquired on Azur software. GraphPad Prism (version 9.0) was used for statistical analysis of analytical results.

### 2.11.3 Results and Discussion

#### 2.11.3.1 Sample Preparation – protein precipitation

Protein precipitation is an important step of sample preparation. Optimised protein precipitation can increase the detection window of the analyte as well as the longevity of the HPLC column. We tested several acids: orthophosphoric acid, sulfuric acid, hydrochloric acid and perchloric acid at different concentrations (1-2M) and volumes (10-20% of the final volume) to identify which most proficiently reduced protein levels in our cell lysate as measured by BCA protein assay. Protein precipitation in cell supernatants was assessed visually by the size of protein pellets since BCA protein assay cannot be performed on media. We found that 2M perchloric acid was most suitable for protein precipitation in cell pellets and media, and 10% of the final volume minimally diluted the analyte concentration (Figure 2.7).

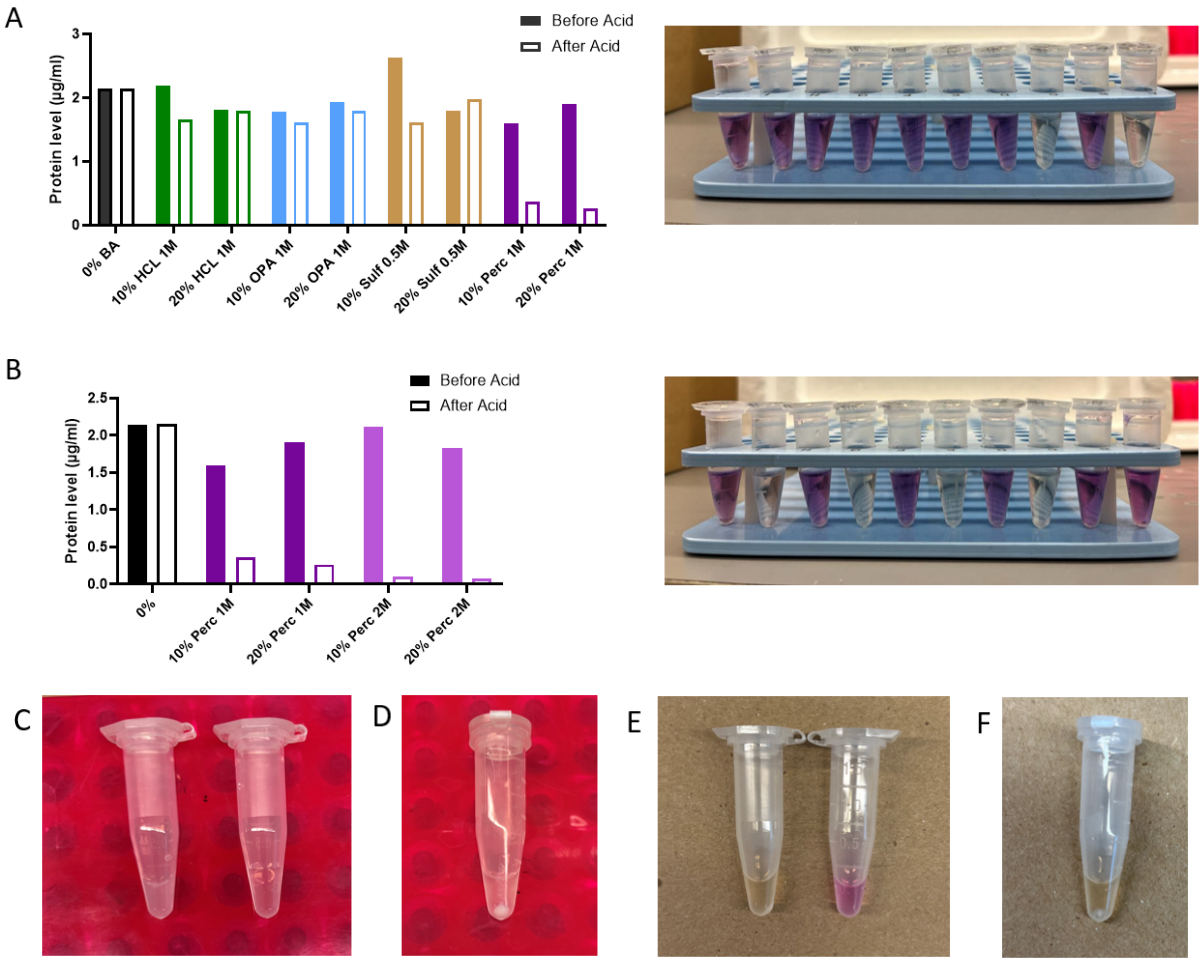



**Figure 2. 7 Optimising Protein precipitation**

The effects of several acids (hydrochloric acid, orthophosphoric acid, sulfuric acid, perchloric acid) on protein precipitation in BMDM cell pellets were determined by A) measurement of protein levels in HEK cell lysate before and after treatment with several acids, and seen visually (high purple indicates higher protein content) B) protein levels in HEK cell lysate before and after treatment with 1M-2M perchloric acid at 10-20% volume, and seen visually (high purple indicates higher protein content). C) cell lysate following addition of selected 10% 2M perchloric acid and D) the protein precipitation pellet formed following centrifugation. This is similarly demonstrated in E) the cell supernatant and F) the pellet formed following centrifugation.

### 2.11.3.2 Method validation

#### 2.11.3.2.1 Specificity

Specificity is the ability of the developed analytical method to distinguish between the analyte and other components in the sample matrix; it is achieved with complete separation of the analyte peak from any other peaks detected in the sample. To evaluate specificity, chromatograms of a blank, standard at target concentration (7.8μM), a test sample and structurally similar compounds (succinate, cis-aconitate, fumarate) were compared.

No peak was observed at 13-14 minutes (itaconic acid retention time) in the blank (Figure 2.8A-B). A peak was observed at 13.82 minutes with 7.8 μM itaconic acid standard in PBS (Figure 2.8C) as well as in a Wildtype BMDM $M^{LPS/IFN\gamma}$ cell pellet (Figure 2.8D). Similarly, peaks of a similar size and retention time were observed with 7.8 μM itaconic acid standard in media (Figure 2.8E) and WT BMDM $M^{LPS/IFN\gamma}$ supernatant (Figure 2.8F). Some day-to-day variability is expected in retention times and peak sizes. There was no co-eluting peak at the retention time of itaconic acid in pellets or in supernatants although cell lysate chromatograms have fewer non-specific peaks (or noise) compared to supernatants. This is understandable as supernatants contain media constituents as well as secreted compounds from the cell.

Succinate and cis-aconitate were detectable by this method in PBS whilst fumarate was not (Figure 2.9A, 2.9C). However, succinate and cis-aconitate elute at approximately 6 minutes and 9 minutes respectively, with no interfering peak observed 13-14 minutes. Furthermore, the HPLC method was more than 100 times and 10 times less sensitive for the detection of succinate and cis-aconitate, respectively, in comparison to itaconic acid in PBS (Figure 2.9A, 2.9C). In media, both succinate and cis-aconitate were not reliably detectable; although peaks were observed at similar retention times as their counterparts in PBS, the standard concentration to peak area ratio were not consistent (Figure 2.9B, 2.9D). Fumarate and

malate were not detectable at the concentrations tested (125μM-0.22μM). This result indicates the peak of the analyte itaconate is pure, and confirmed the specificity of the method.

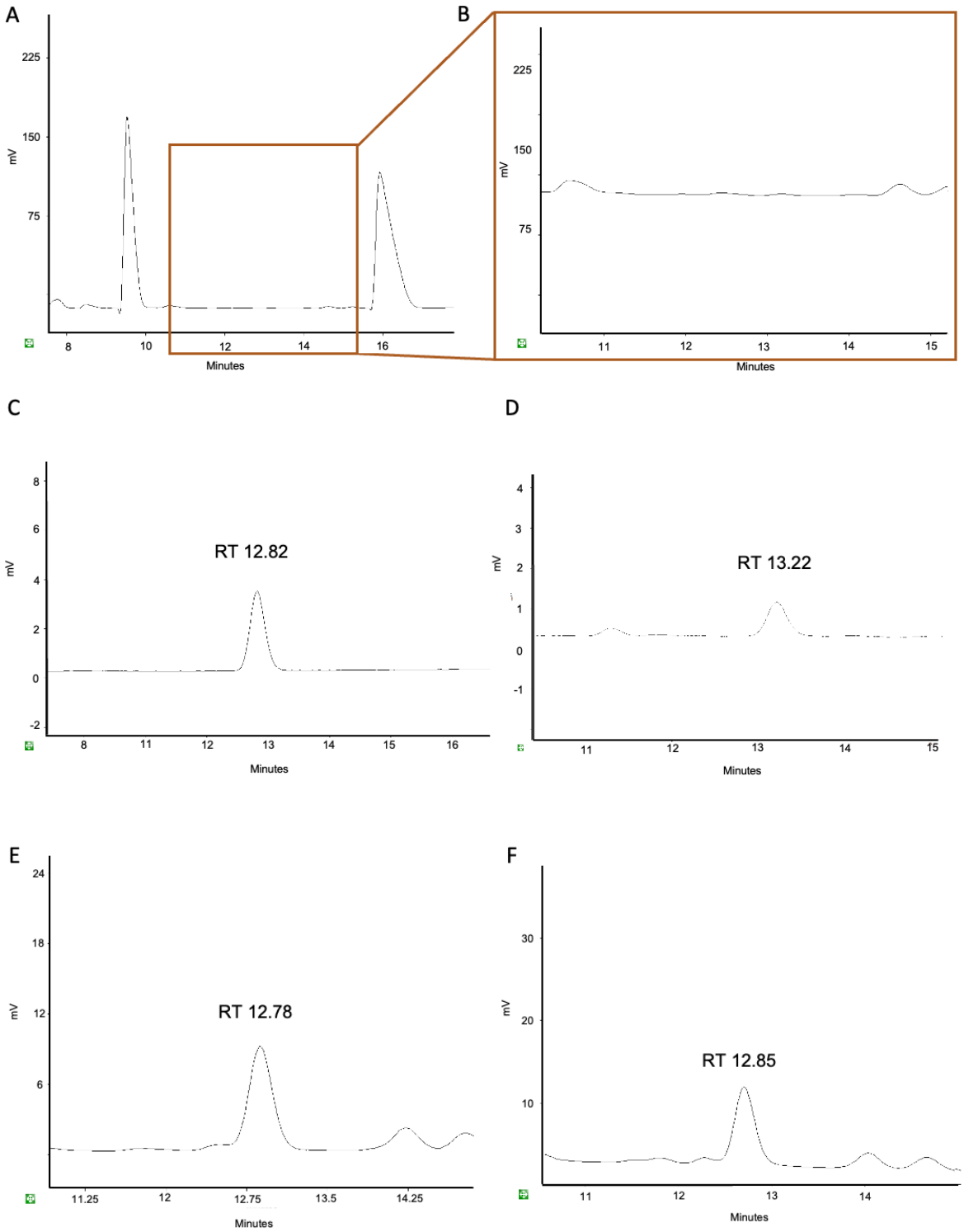
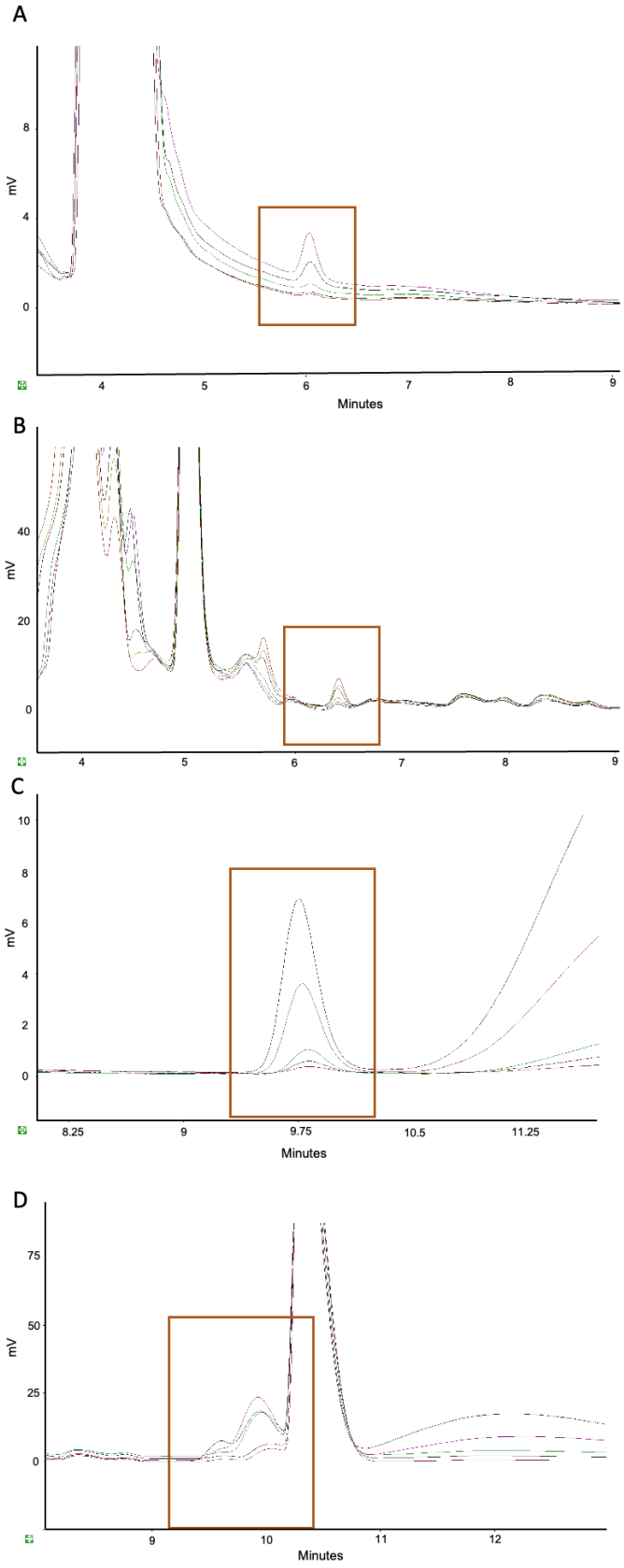



**Figure 2. 8 Chromatograms of itaconic acid on HPLC**

A) Full chromatogram of blank samples (media) and B) zoomed in chromatogram of blank media sample to confirm no peak is detected. C) Chromatogram of 7.8µM itaconic acid standard (PBS) and D) chromatogram of intracellular itaconic acid level in WT BMDM $M^{LPS/IFN\gamma}$ macrophages. E) chromatogram of 7.8µM itaconic acid standard (media) and F) chromatogram of extracellular itaconic acid level in WT BMDM $M^{LPS/IFN\gamma}$ macrophages.




| Succinate standard (PBS) | RT (min) | Peak Area |
|---|---|---|
| 125µM | 6.03 | 19.48 |
| 62.5µM | 6.03 | 9.63 |
| 15µM | 6.03 | 2.21 |
| 7.8µM | 6.03 | 1.22 |
| 3.9µM | 6.02 | 0.96 |

| Succinate standard (media) | RT (min) | Peak Area |
|---|---|---|
| 125µM | 6.03 | 18.79 |
| 62.5µM | 6.03 | 10.18 |
| 15µM | 6.03 | 1.73 |
| 7.8µM | 6.03 | 0 |
| 3.9µM | 6.02 | 0 |

| Cis-aconitate standard (PBS) | RT (min) | Peak Area |
|---|---|---|
| 125µM | 9.75 | 109.97 |
| 62.5µM | 9.78 | 56.65 |
| 15µM | 9.82 | 14.9 |
| 7.8µM | 9.82 | 7.68 |
| 3.9µM | 9.85 | 3.7 |

| Cis-aconitate standard (media) | RT (min) | Peak Area |
|---|---|---|
| 125µM | 9.75 | 142.37 |
| 62.5µM | 9.78 | 226.05 |
| 15µM | 9.82 | 136.59 |
| 7.8µM | 9.82 | 23.52 |
| 3.9µM | 9.85 | 18.16 |

**Figure 2. 9 Standards of structurally similar metabolites to itaconate**

Succinate standard A) in PBS (125-3.9µM) and B) in media (125-3.9µM). Cis-aconitate standard C) in PBS D) in media.

#### 2.11.3.2.2 Linearity and range

To ensure method linearity, the ability of the method to obtain test results that are directly proportional to the analyte concentration was assessed. The peak area was obtained from the HPLC Azur software v5.0 and plotted against corresponding concentrations to obtain the calibration graph. The results of the linearity study are shown in Figure 2.10 and show a linear relationship over the concentration range of 62.5-0μM. For the regression analysis, the linear equation obtained was y=1.89x-0.08571 for itaconic acid in PBS and y=1.8766x-5.343 for itaconic acid in media. Furthermore, the coefficient of determination $R^2$ was 1.000 in PBS and 0.998 in media, indicating a linear relationship between the concentration of analyte and peak area.

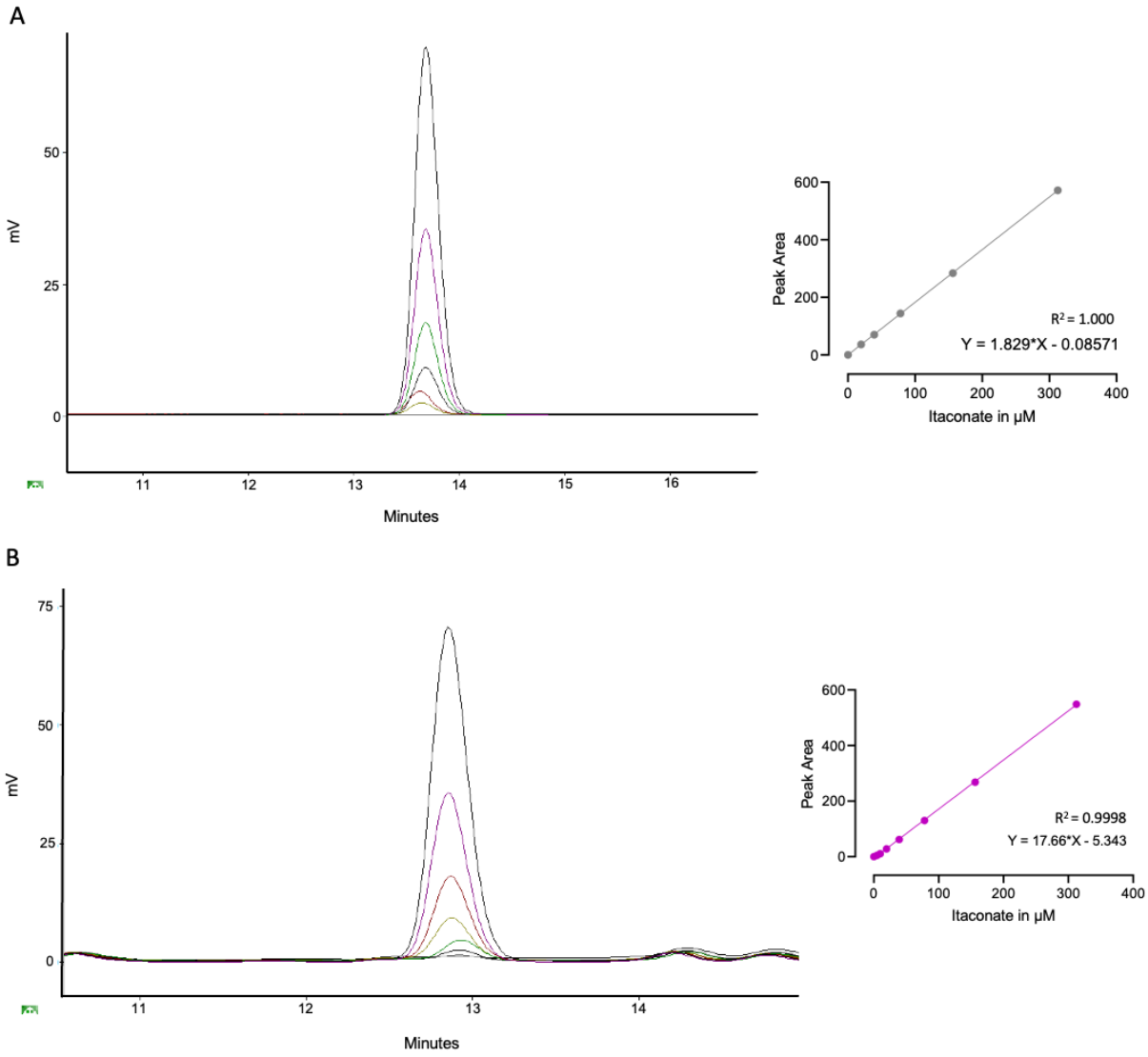



**Figure 2. 10 Linearity and range for itaconic acid.**

Overlaid chromatograms and linear regression analysis of standard curves for itaconic acid ranging 62.5-0.22µM A) in PBS and B) in media

#### 2.11.3.2.3 Limit of Detection and Limit of Quantification

The limit of detection (LOD) is the lowest amount of analyte in a sample that can be detected, but not necessarily quantitated, while the limit of quantification (LOQ) is the lowest amount of analyte in a sample that can be quantitatively determined with suitable precision. For itaconate, LODs and LOQs for cell lysates in PBS and cell supernatants in media are shown in Table 2.13 The higher LOD and LOQ in supernatants is due to the higher noise in chromatogram traces from cell media.

| | **Limit of Detection (LOD)** | **Limit of Quantification (LOQ)** |
|---|---|---|
| Cell lysates (in PBS) | 0.24 μM | 0.98 μM |
| Supernatants (media) | 0.98 μM | 1.95 μM |

Table 2. 13 LOD and LOQ for cell lysates (PBS) and supernatants (media)

#### 2.11.3.2.4 Accuracy and Precision

The accuracy of the method is a determination of the closeness of the results obtained by the method to the true value. To assess this, HEK cell pellets were lysed and spiked with the target concentration of itaconic acid (7.8 μM) as well as 20% (6.24 μM) lower and 20% higher (9.36 μM) than the target concentration to account for biological variation in primary cells. The spiked samples were then processed via the sample preparation method, injected into the HPLC, and assessed for percentage loss of analyte (or recovery rate) in comparison to the standard curve. As shown in Table 2.14, the results have a 78-82% recovery rate suggesting medium loss of analyte due to extraction process and <2% recovery standard deviation (RSD) indicating high repeatability and precision of the method.

| Spiked level | Spiked amount | Replicate | Peak Area | Post Extraction (μM) | % Recovery, RSD |
|---|---|---|---|---|---|
| 80% | 6.24μM | 1 | 87.03 | 4.611 | 73.9 |
| | | 2 | 90.85 | 4.827 | 77 |
| | | 3 | 111.54 | 5.998 | 95 |
| | | mean | 96.47 | 5.15 | 81.97, 0.75 |
| 100% | 7.8μM | 1 | 112.28 | 6.040 | 77 |
| | | 2 | 109.87 | 5.903 | 75 |
| | | 3 | 121.70 | 6.573 | 84 |
| | | mean | 114.62 | 6.172 | 78.6, 0.35 |
| 120% | 9.36μM | 1 | 136.84 | 7.43 | 79 |
| | | 2 | 136.42 | 7.406 | 79.1 |
| | | 3 | 135.13 | 7.333 | 78.3 |
| | | mean | 136.13 | 7.39 | 78.8, 0.05 |

Table 2. 14 Results of precision and accuracy

**2.11.3.2.5 Stability**

Since the recovery rates were within an acceptable range, this indicated good stability of the sample and standards. To assess stability of the analyte further, we tested its durability under different storage conditions. Since cell pellets are always stored at -80 degrees and only undergo one freeze/thaw cycle we focussed on cell supernatants. Furthermore, we know itaconic to be stable at room temperature for several months in PBS due to our stocks. Therefore, we tested to see if several freeze/thaw cycles at different time points resulted in analyte degradation in cell supernatants (Table 2.15). In spiked media samples, we observed that storage at -20 °C or -80 °C made minimal difference to itaconic acid measurements after one FT cycle and loss of analyte was low (2-4%) even after the two FT cycles. Surprisingly, itaconic acid levels after storage at 4 °C and 25 °C were comparable to storage at -20 °C or -80 °C. Greater loss of analyte was observed after 3 days at 25 °C but remained minimal after 3 days at 4 °C.

In supernatants from WT $M^{LPS/IFN\gamma}$ BMDMs, always stored at -80 °C, significant biological variation was observed in itaconate levels between samples, with WT1 $M^{LPS/IFN\gamma}$ measuring least 40% less itaconate than WT2 $M^{LPS/IFN\gamma}$ and WT3 $M^{LPS/IFN\gamma}$. Furthermore, loss of analyte is <3% after two freeze/thaw cycles but increases to approximately 10% after three freeze-thaw cycles. This indicates supernatants used for the measurement of itaconic acid should not undergo more than two freeze/thaw cycles. Overall the data demonstrates high stability of itaconic acid from 25 °C to -80 °C for at least 3 days or two freeze/cycles.

| | Storage | FT cycle 1 (Day 1) | FT cycle 2 (Day 3) | % change from Day 1 | FT cycle 3 Day 5 | % change from Day 1 |
|---|---|---|---|---|---|---|
| Spiked media sample (7.8µM) | 25 ℃ | 7.63 µM | 7.19 µM | 5.8 | 6.78 µM | 12.8 |
| | 4 ℃ | 7.56 µM | 7.46 µM | 1.3 | 7.22 µM | 4.4 |
| | -20 ℃ | 7.58 µM | 7.31 µM | 3.5 | 7.01 µM | 7.5 |
| | -80 ℃ | 7.45 µM | 7.28 µM | 2.2 | 7.08 µM | 4.9 |
| WT1 $M^{LPS/IFN\gamma}$ | -80 ℃ | 3.7 µM | 3.81 µM | +2.9 | 3.49 µM | 8.4 |
| WT2 $M^{LPS/IFN\gamma}$ | -80 ℃ | 6.82 µM | 6.99 µM | +2.5 | 6.17 µM | 11.7 |
| WT3 $M^{LPS/IFN\gamma}$ | -80 ℃ | 7.15 µM | 7.25 µM | +1.3 | 6.42 µM | 11.4 |

Table 2. 15 Results of stability and repeatability

### 2.11.4 Conclusion

To conclude, a simple, accurate, precise and robust HPLC method has been developed for the detection of itaconate in biological samples, with a particular focus on murine BMDM cell pellets and supernatant. The method has been validated and is suitable for its intended application, providing accurate and precise quantitative results for the measurement of itaconate in cell pellets and media.

# Chapter 3

## The Role of Tetrahydrobiopterin in Macrophage Metabolism

# Chapter 3: The role of tetrahydrobiopterin in macrophage metabolism

## 3.1 Introduction

Macrophages are highly heterogeneous, plastic immune cells that perform a variety of functions. Integral to the immune response, these phagocytic cells adopt a spectrum of polarisation states by altering their metabolic profile depending on their surrounding microenvironment (Viola et al., 2019). Inflammatory macrophages, stimulated by LPS and IFN-γ ($M^{LPS/IFN-\gamma}$), produce high levels of pro-inflammatory cytokines (IL1β, IL6, TNF-α), reactive oxygen species (ROS) and nitric oxide (NO). Together, these play a critical role in further production of inflammatory mediators, microbial killing, clearance of cellular debris and immune regulation (Thapa & Lee, 2019). To support this activated state, $M^{LPS/IFN-\gamma}$ undergo a metabolic switch which includes upregulation of glycolysis, remodelling of the TCA cycle and the overall inhibition of mitochondrial respiration.

A key part of polarisation to the inflammatory state is the induction of iNOS, which requires tetrahydrobiopterin (BH4) as a cofactor to produce large quantities of NO. This small pleiotropic molecule has both inflammatory and metabolic roles. NO generation inhibits OXPHOS through nitrosylation of complex I and reversible inhibition of complex IV of the electron transport chain (Cleeter et al., 1994; Moncada & Erusalimsky, 2002). However, the effects of BH4 and NOS-derived NO on the wider metabolome of the cell are only beginning to be explored.

BH4 deficiency in endothelial cells and macrophages has been studied by our group using a murine model with conditional deletion of *Gch1* ($Gch^{fl/fl}$Tie2cre) (Bailey et al., 2019; Chuaiphichai et al., 2017; McNeill et al., 2015; McNeill et al., 2018). In the $Gch^{fl/fl}$Tie2cre model, *Gch1* deletion results in a lack of GTPCH protein, the rate limiting enzyme in biopterin synthesis, and loss of BH4 reduces the ability for NOS-derived NO production (McNeill et al., 2015). A limitation of this model was that a subset of $Gch^{fl/fl}$Tie2cre mice

had incomplete *Gch1* deletion in myeloid cells. These mice were identified via routine genotyping and not used. Over time an accumulation of unusable mice has rendered this model uneconomical and its breeding unjustifiable. To address this, and to build on previous findings in the group on BH4 deficient macrophages, the first aim of this chapter was to create a new model of induced *Gch1* knockout and BH4 deficiency.

To study the role of BH4 in macrophage metabolism, metabolomics analysis of $Gch^{fl/fl}$Tie2cre macrophages was previously performed (Bailey et al, 2019). This dataset revealed significant alterations in mitochondrial respiration and perturbations in the TCA cycle. Although early TCA cycle metabolites (citrate, aconitate) were decreased with BH4 deficiency, succinate and itaconate were increased (Figure 3.1) (Bailey et al., 2019). Much of the focus in previous work was placed on NO-modulation of the TCA cycle via accumulation of itaconate (Bailey et al., 2019). We compared these findings with the R26-$CreER^{T2}Gch^{fl/fl}$ (Gch-KO) mouse to validate this new model of BH4 deficiency. Going further, we interrogated the effects of BH4-deficiency in other pathways relevant to the TCA cycle: glycolysis, fatty acid oxidation and glutaminolysis. Both the $Gch^{fl/fl}$Tie2cre and Gch-KO have the same *Gch1* deletion resulting in undetectable BH4 levels. Furthermore, it was established that mitochondrial respiration, indicative of the metabolic profile of both the $Gch^{fl/fl}$Tie2cre and Gch-KO models, were comparable before investigating the wider metabolome of Gch-KO BMDMs .

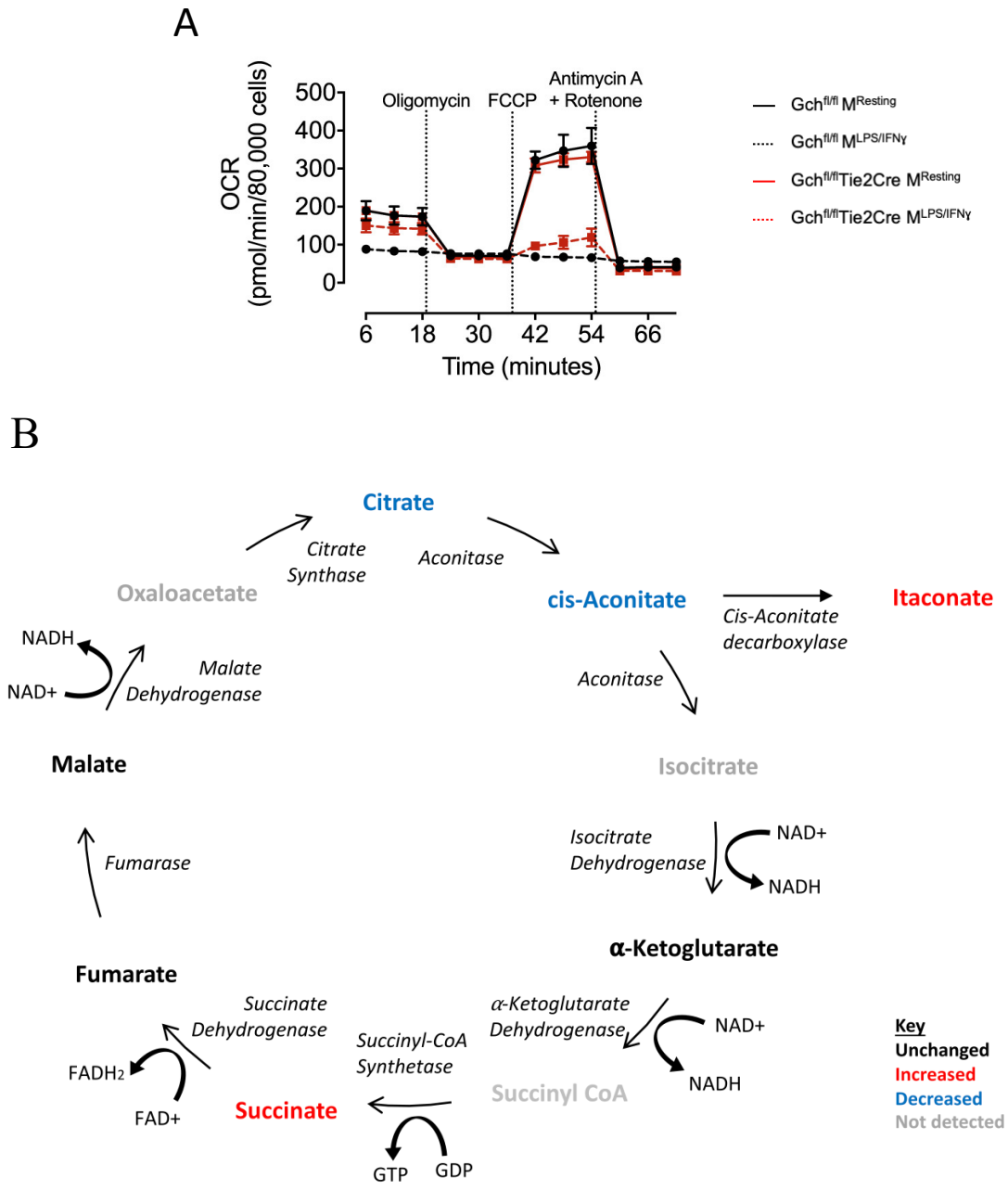



**Figure 3. 1 Mitochondrial respiration in Gch$^{fl/fl}$Tie2cre model of BH4 deficiency**

(A) Oxygen consumption rate (OCR) measured using XFe Seahorse analyser with sequential injection of Oligomycin, FCCP, combined Rotenone and Antimycin A (Rot/AA) in Gch$^{fl/fl}$Tie2cre. (B) TCA cycle pathway showing changes (>20%) in abundance of enzymes and metabolites in LPS/IFNγ stimulated Gch$^{fl/fl}$Tie2cre versus Gch$^{fl/fl}$ macrophages as published in Bailey et al, 2019. Data are mean ± SEM. *P* values calculated using 2-way ANOVA with Tukey's post-test.

## 3.2 Hypothesis and Aims

### 3.2.1 Hypothesis

It was hypothesised that the Gch-KO mouse model would have undetectable BH4 levels and have a comparable mitochondrial function compared to the GchTie2Cre model. Next, it was hypothesised that TCA cycle substrates (glucose, fatty acids, glutamine) may be altered alongside TCA cycle perturbations in BH4-deficient $M^{LPS/IFN\text{-}\gamma}$.

### 3.2.2 Aims

Aim 1: To establish a novel murine model of BH4 deficiency

Aim 2: To understand how inducible loss of BH4 synthesis affects inflammatory profile of bone marrow derived macrophages

Aim 3: To understand how inducible loss of BH4 synthesis affects TCA cycle substrate use in bone marrow derived macrophages

## 3.3 Methods

### 3.3.1 R26-CreER$^{T2}$Gch$^{fl/fl}$ and GchTie2Cre BMDM culture

BMDM culture was performed as described in Section 2.2.1. In addition to the steps outlined before, to induce deletion of *Gch1* gene, all cells were cultured in 1 μM 4-hydroxytamoxifen, administered on Day 1 and Day 3 of culture (Figure 3.2). GchTie2Cre BMDM were cultured as described previously (Bailey et al., 2019; Bailey et al., 2020).

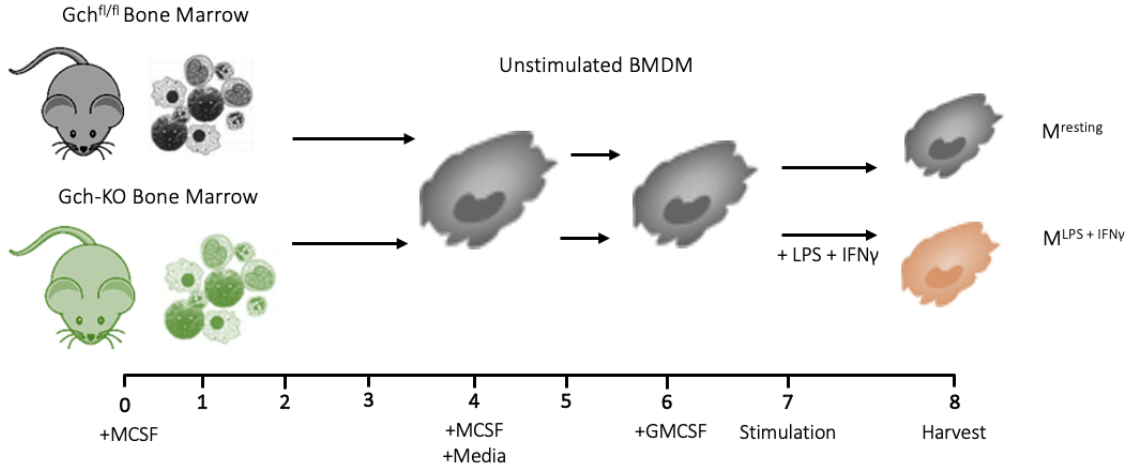



**Figure 3. 2 Schematic of Gch-KO BMDM culture protocol**

Bone marrow derived macrophages (BMDM) from Gch$^{fl/fl}$ and R26-CreER$^{T2}$Gch$^{fl/fl}$ mice were cultured over 8 days. On Days 1 and 3, cells were treated with 1.0 μM 4-hydroxytamoxifen (4-OHT) to induce *Gch1* deletion. On Day 4, cells were given 50% additional media containing MCSF. On Day 6, cells were treated with GMCSF. On Day 7 cells were stimulated with LPS/IFN-γ to polarise into inflammatory M$^{LPS/IFN\text{-}\gamma}$ state.

## 3.4 Results

### 3.4.1 *Gch1* is excised from R26-CreER$^{T2}$Gch$^{fl/fl}$ bone marrow derived macrophages

To investigate the effects of BH4 in bone marrow derived macrophages, a novel tamoxifen-inducible model of BH4 and nitric oxide (NO) deficiency was generated (Figure 3.3A-B). The predicted 1030 bp product was observed in Gch$^{fl/fl}$ mice. Upon tamoxifen induction, the 1392 bp KO allele was instead detected (Figure 3.3C). At the protein level, LPS/IFNγ induction increased iNOS and GTPCH levels in Gch$^{fl/fl}$ mice. In Gch-KO bone marrow derived macrophages, upon 4-hydroxytamoxifen (4-OHT) administration, there was an absence of GTPCH since *Gch1* gene had been deleted but iNOS protein levels were unaffected (Figure 3.3D). This effect was seen with both 0.1μM and 1μM 4-OHT administration.

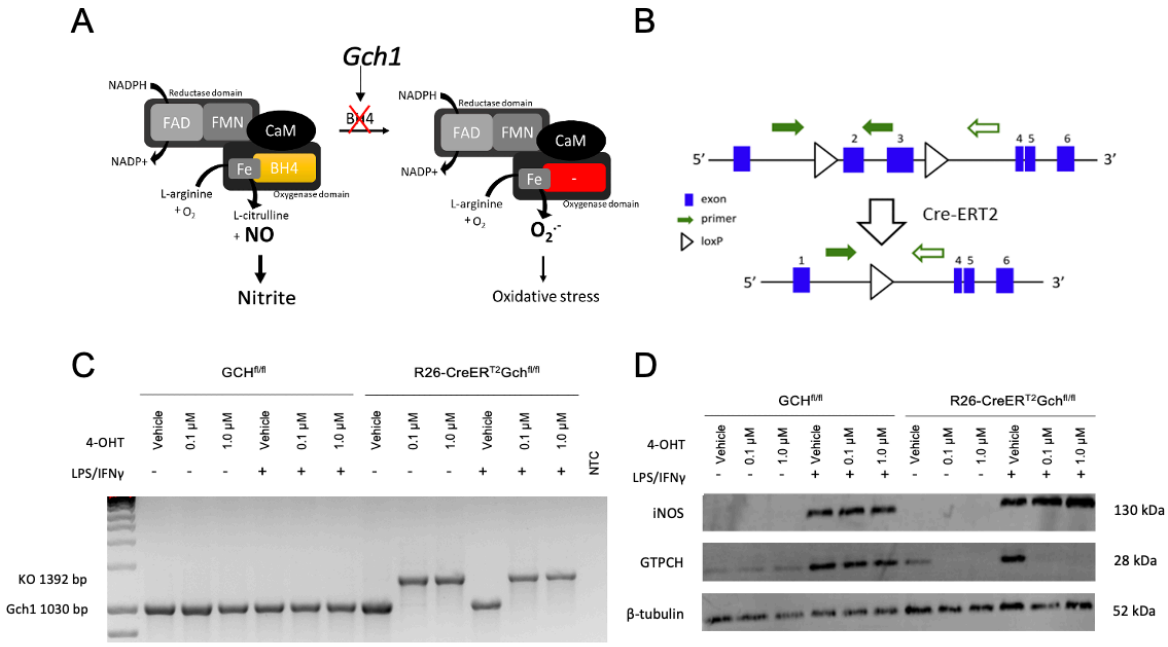



**Figure 3. 3 *Gch1* is excised from R26-CreER$^{T2}$ Gch$^{fl/fl}$ bone marrow derived macrophages**

(A) Scheme illustrating the role of BH4 as a NOS cofactor in redox biology. (B) Schematic detailing the excision of the critical exons (2 and 3) in *Gch1* due to the flanking loxP sites and the conditional activation of Cre-ER$^{T2}$ with tamoxifen in this murine model. C) PCR products from Gch$^{fl/fl}$ and R26-CreER$^{T2}$Gch$^{fl/fl}$ reactions were separated by electrophoresis. Floxed Gch1 products (1030 bp) were observed in Gch$^{fl/fl}$ samples and R26-CreER$^{T2}$Gch$^{fl/fl}$ samples not treated with 0.1μM or 1.0μM 4-hydroxytamoxifen with or without stimulation. Excised Gch1 products were observed in samples treated with 0.1μM or 1.0μM 4-hydroxytamoxifen regardless of LPS/IFNγ stimulation. In the presence of the Cre, a 1392 bp product is produced, confirming excision of the critical exons (n=3). (D) Western blot analysis of GTPCH and iNOS in R26-CreER$^{T2}$Gch$^{fl/fl}$ (Gch-KO) macrophages with and without 4-OHT treatment and with and without LPS/IFNγ stimulation (n=3) (Diotallevi et al, 2021).

### 3.4.2 R26-CreER$^{T2}$Gch$^{fl/fl}$ BMDMs have diminished BH4 and nitrite levels

Knockdown of the *Gch1* gene was confirmed by qPCR (Figure 3.4A). *Gch1* expression was upregulated >4-fold in M$^{LPS/IFN-\gamma}$. With tamoxifen treatment (0.1 μM, 1.0 μM 4-OHT), *Gch1* expression was undetectable in both unstimulated and LPS/IFNγ stimulated R26-CreER$^{T2}$Gch$^{fl/fl}$ (Gch-KO) macrophages (Figure 3.4A). This was similarly the case for BH4 levels (Figure 3.4B). Nitrite levels were diminished but detectable following 0.1 μM 4-OHT and further decreased with 1.0 μM 4-OHT. Therefore, we proceeded with 1.0 μM 4-OHT dose for subsequent experiments (Figure 3.4C).

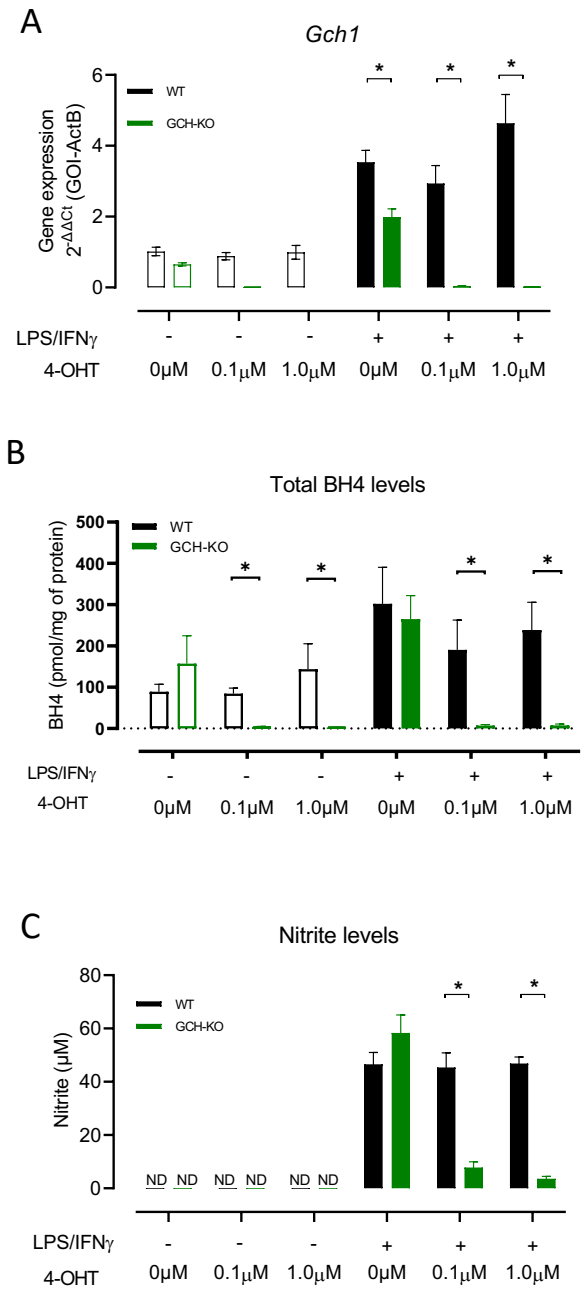



**Figure 3. 4 R26 CreER$^{T2}$Gch$^{fl/fl}$ BMDMs have diminished BH4 and nitrite levels**

(A) *Gch1* gene expression in Gch-KO cells measured by RT-qPCR with LPS/IFNγ stimulation and 0.1μM or 1.0μM 4-hydroxytamoxifen (4-OHT). (B) BH4 quantification in Gch-KO cells with and without 4-OHT treatment measured by HPLC. (C) Nitrite levels in supernatants from Gch-KO cells measured by Griess assay. Data are n=5-6 mean ± SEM. P values are calculated using a one-way ANOVA with Tukey's post-test (*P<0.05)

### 3.4.3 Characterisation of Gch-KO unstimulated and $M^{LPS/IFN\gamma}$

Polarisation states of $Gch^{fl/fl}$ and Gch-KO macrophages were compared by flow cytometry. Flow cytometry dot plots show the gating strategy and expression of CD11b and MHC II on cell surface of $Gch^{fl/fl}$ and Gch-KO macrophages (Figure 3.5A). Cell surface expression was quantified for CD11b+ and F4/80 expressing cells, which are generic markers for macrophages. The majority of cells had differentiated to macrophages, with 96% of cells expressed CD11b+ (Figure 3.5A-C). Of these, $M^{LPS/IFN\text{-}\gamma}$ had increased MHC II cell surface expression, a classic marker of macrophage activation (Figure 3.5D).

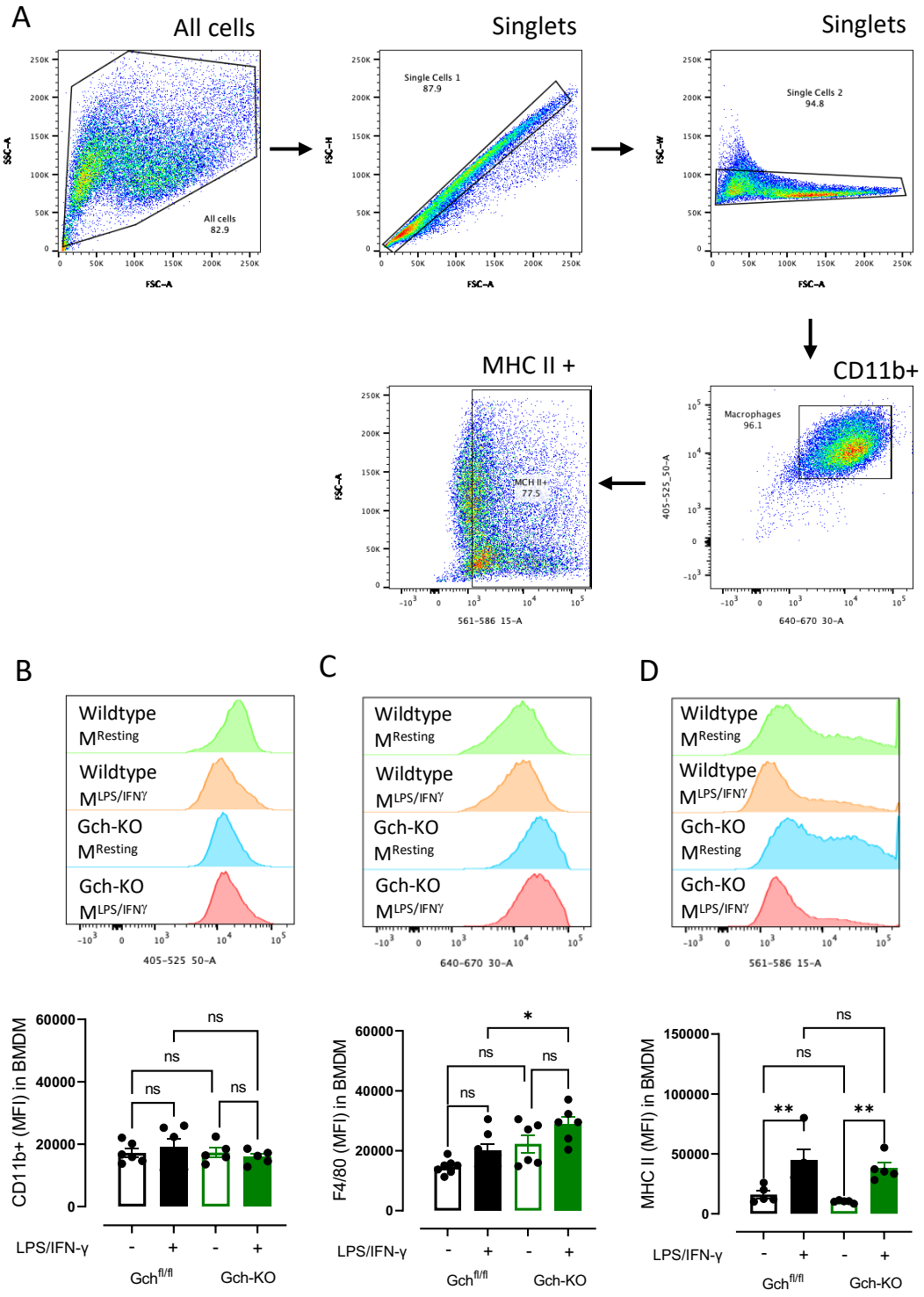



**Figure 3. 5 Characterisation of R26-CreER$^{T2}$Gch$^{fl/fl}$ unstimulated and M$^{LPS/IFN-\gamma}$**

(A) Flow cytometry dot plot gating strategy for identification of CD11b+F4/80+, and MHCII+ in M$^{LPS/IFN-\gamma}$. Cell counts for number of cells expressing (B) CD11b (C) F4/80 (D) MHC II. Data are n=5-6 mean ± SEM. P values are calculated using a one-way ANOVA with Tukey's post-test (*P<0.05, **P<0.01, ***P<0.001)

### 3.4.4 BH4-deficient $M^{LPS/IFN-\gamma}$ have increased IL1β cytokine release

*IL1β* gene expression and cytokine release were increased with LPS/IFN-γ stimulation in $Gch^{fl/fl}$ and Gch-KO macrophages (Figure 3.6A, B). There was a further increase in IL1β secretion in Gch-KO $M^{LPS/IFN-\gamma}$ (Figure 3.6B). As expected, *IL6* expression and cytokine release was increased with stimulation in both $Gch^{fl/fl}$ and KO $M^{LPS/IFN-\gamma}$ (Figure 3.6C-D). iNOS gene and protein expression were increased following stimulation in $Gch^{fl/fl}$ and KO $M^{LPS/IFN-\gamma}$ (Figure 3.6E). As expected, nitrite levels were not detectable in Gch-KO $M^{LPS/IFN-\gamma}$ as these cells lack the cofactor needed by iNOS to produce NO (Figure 3.6F).

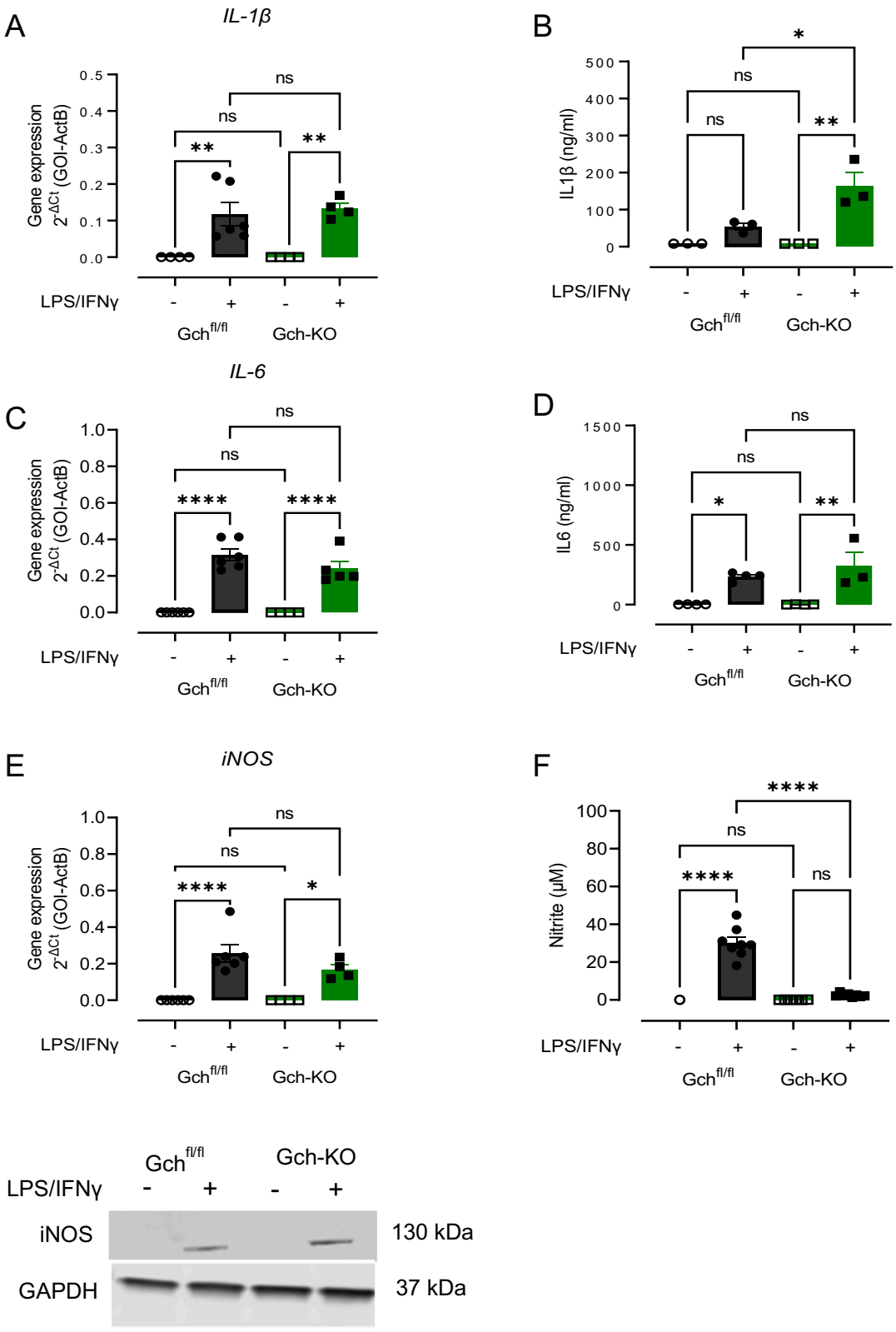



**Figure 3. 6 BH4-deficient M$^{LPS/IFN-\gamma}$ have increased inflammatory cytokine expression**

(A) *IL1β* gene expression in Gch-KO cells measured by RT-qPCR, (B) IL1β levels in supernatants from Gch-KO cells measured by ELISA. (C) *IL6* gene expression in Gch-KO cells measured by RT-qPCR, (D) IL6 levels in supernatants from Gch-KO cells measured by ELISA. western blot analysis of IRG1 in Gch-KO cells. (E) iNOS gene (upper panel) and protein (lower panel) expression in Gch-KO cells measured by RT-qPCR and western blot respectively (F) Nitrite levels in supernatants from Gch-KO cells measured by Griess assay. Data are n=3-6 mean ± SEM. P values are calculated using a one-way ANOVA with Tukey's post-test (*P<0.05, **P<0.01, ***P<0.001, ***P<0.0001)

### 3.4.5 BH4-deficient $M^{LPS/IFN\gamma}$ macrophages have increased mitochondrial respiration

For an initial insight into their mitochondrial metabolism, the Seahorse MitoStress test was performed on unstimulated and LPS/IFN-γ stimulated $Gch^{fl/fl}$ and Gch-KO macrophages. Seahorse traces for unstimulated and $M^{LPS/IFN-\gamma}$ are shown in Figures 3.7A-B, with analysis of the individual effects of the various compounds on oxygen consumption rate (OCR) shown in Figure 3.7C-F. Primarily glycolytic, $M^{LPS/IFN-\gamma}$ displayed low basal OCR levels (Figure 3.7C). Following addition of oligomycin, calculated ATP-linked OCR is decreased by 38% in Gch-KO $M^{LPS/IFN-\gamma}$ compared to $Gch^{fl/fl}$ (Figure 3.7D). Maximal OCR and spare capacity were increased in Gch-KO $M^{LPS/IFN-\gamma}$ compared to $Gch^{fl/fl}$, further indicating higher levels of mitochondrial respiration in Gch-KO $M^{LPS/IFN-\gamma}$ and that the switch to glycolysis was not complete (Figure 3.7E-F). Seahorse traces were comparable between Gch-KO and $Gch^{fl/fl}$Tie2cre macrophages (Figure 3.1A), as $M^{LPS/IFN-\gamma}$ macrophages from both models responded to Oligomycin and FCCP administration, suggesting higher mitochondrial respiration.

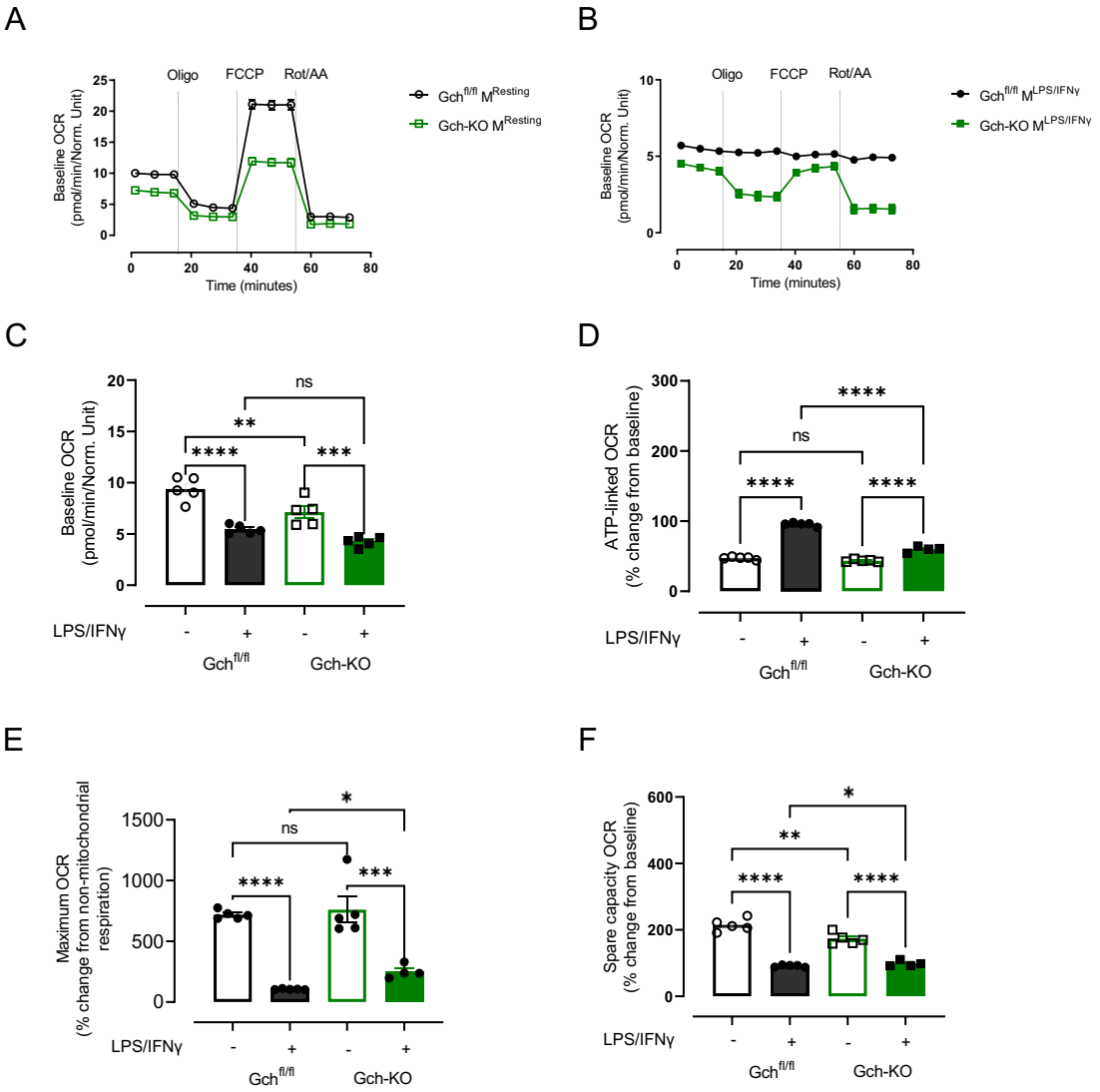



**Figure 3. 7 BH4-deficient $M^{LPS/IFN-\gamma}$ have increased mitochondrial respiration**

Oxygen consumption rate (OCR) measured using a XFe96 Seahorse analyser with sequential injection of Oligomycin, FCCP, and combined rotenone and antimycin A in (A) $Gch^{fl/fl}$ and Gch-KO unstimulated macrophages and (B) $Gch^{fl/fl}$ and GCH-KO $M^{LPS/IFN-\gamma}$ macrophages. Measurements were used to determine (C) basal, (D) ATP-linked OCR, (E) Spare capacity for mitochondrial respiration (F) Maximum OCR. Data are n=4-5 mean ± SEM. P values are calculated using a one-way ANOVA with Tukey's post-test (*P<0.05, **P<0.01, ***P<0.001, ****P<0.0001)

### 3.4.6 Production of the TCA cycle anti-inflammatory metabolite, itaconate, is increased in BH4-deficient $M^{LPS/IFN-\gamma}$ macrophages

A marker of macrophage activation, *Irg1* gene and protein expression increased with LPS/IFN-γ stimulation which, as previously reported in the GchTie2Cre model (Figure 3.8A, B) (Bailey et al., 2019). Loss of BH4 did not alter *Irg1* gene or protein expression, potentially due to the late 18h timepoint. However, when measuring the metabolite itaconate, in contrast to literature, there was a small but insignificant increase in intracellular itaconate levels in $Gch^{fl/fl}$ $M^{LPS/IFN-\gamma}$. This increase was more pronounced but again not significant when measuring extracellular itaconate levels (Figure 3.8C, D). Interestingly, there was a striking difference in both intracellular and extracellular itaconate in Gch-KO $M^{LPS/IFN-\gamma}$ macrophages compared to $Gch^{fl/fl}$ (Figure 3.8D). This indicated that loss of BH4 results in the increase of itaconate production that is independent of an increase in *Irg1* gene or protein expression.

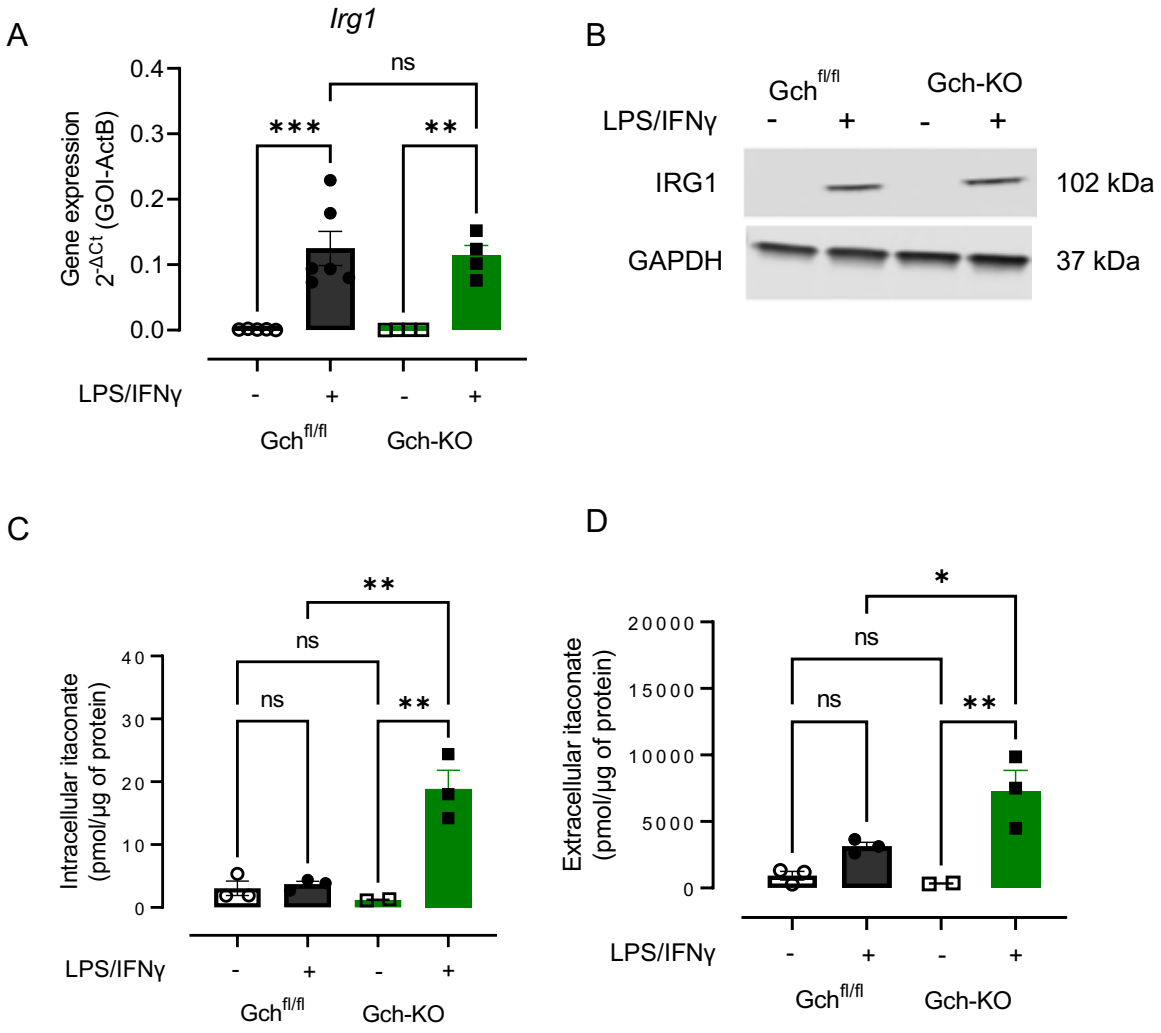



**Figure 3. 8 TCA cycle anti-inflammatory metabolite, itaconate, production is increased in BH4-deficient $M^{LPS/IFN-\gamma}$**

(A) *Irg1* gene expression in Gch-KO cells, (B) western blot analysis of IRG1 in Gch-KO cells. Concentration of itaconate measured by HPLC (C) intracellularly in Gch-KO cell pellets and (D) extracellularly in supernatants from Gch-KO cells. Data are n=4-6 mean ± SEM. P values are calculated using a one-way ANOVA with Tukey's post-test (*P<0.05, **P<0.01, ***P<0.001)

### 3.4.6 BH4-deficient $M^{LPS/IFN-\gamma}$ have increased glycolytic capacity

Having observed alterations in mitochondrial function, the Seahorse glycolytic rate assay was conducted to investigate glycolysis in $Gch^{fl/fl}$ and Gch-KO macrophages (Figure 3.9). As expected, the basal glycolytic rate in $Gch^{fl/fl}$ and Gch-KO $M^{LPS/IFN\gamma}$ was higher than $M^{Resting}$ (Figure 3.9A-C). There was also no significant difference in basal glycolytic rate in $Gch^{fl/fl}$ and Gch-KO $M^{LPS/IFN-\gamma}$ (Figure 3.9C). Electron transport chain Complex I and Complex III inhibitors, Rotenone and Antimycin (Rot/AA), prevent ATP production via oxidative phosphorylation (OXPHOS), and leaving only glycolysis available for ATP generation. Following Rot/AA treatment, ECAR is increased in Gch-KO $M^{LPS/IFN-\gamma}$ but remained unchanged in $Gch^{fl/fl}$ $M^{LPS/IFN-\gamma}$ (Figure 3.9B, D). This indicates that the Gch-KO $M^{LPS/IFN-\gamma}$ are less glycolytic, and supporting the finding that Gch-KO $M^{LPS/IFN-\gamma}$ have increased reliance on OXPHOS. There was a decrease in glycolytic reserve in $Gch^{fl/fl}$ macrophages upon activation which was not seen in Gch-KO macrophages (Figure 3.9E). However, post-DG acidification is decreased significantly in Gch-KO $M^{LPS/IFN-\gamma}$ indicating other non-mitochondrial sources of ECAR are present such as proton efflux via ion transporters or carbonic anhydrase activity which convert carbon dioxide and water to bicarbonate and H+ (Figure 3.9F).

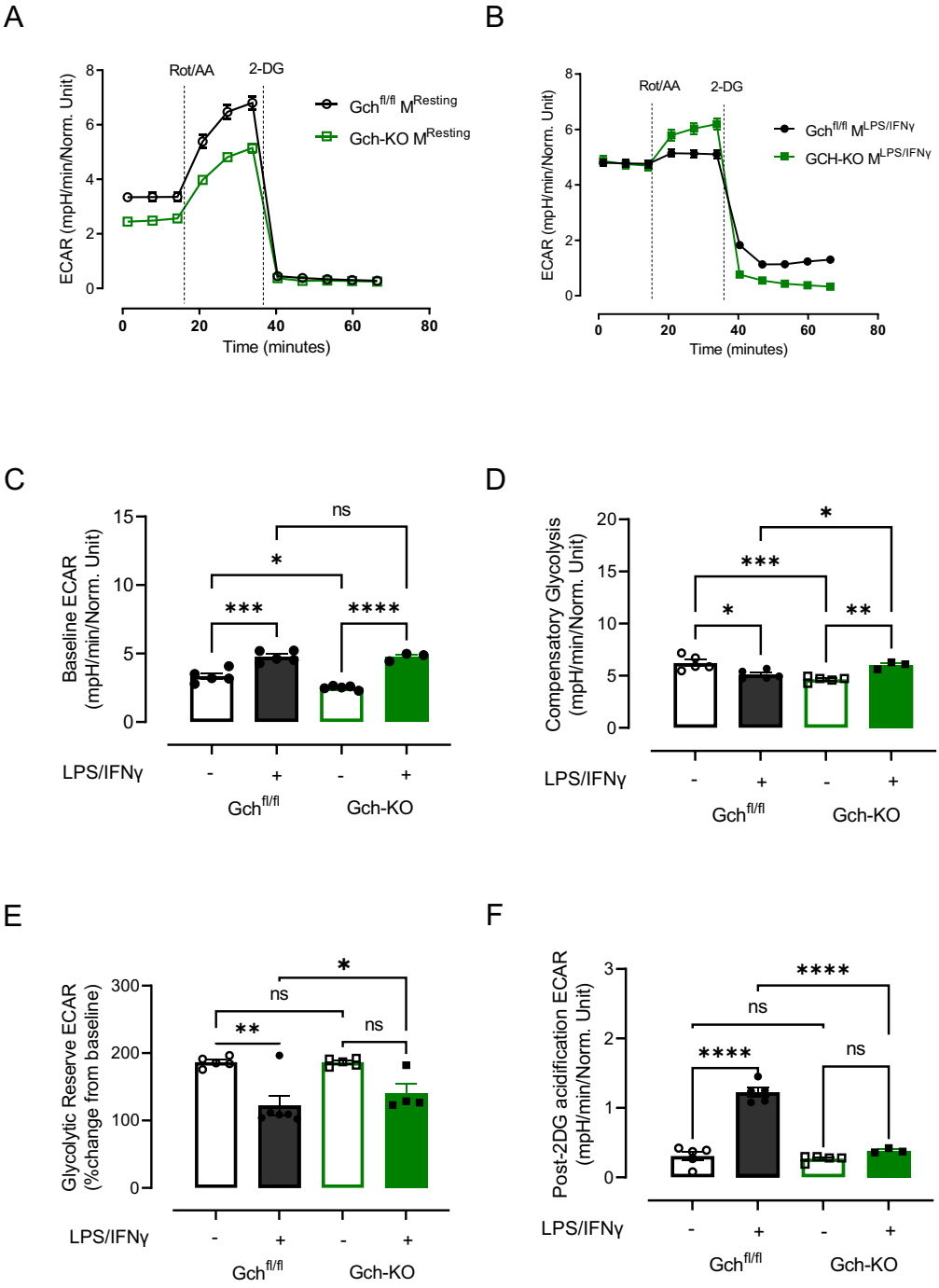



**Figure 3. 9 BH4-deficient $M^{LPS/IFN-\gamma}$ have increased glycolytic capacity**

Extracellular acidification rate (ECAR) measured using a XFe96 Seahorse analyser with sequential injection of combined rotenone and antimycin A (Rot/AA), next 2-deoxyglucose (2-DG) in (A) $Gch^{fl/fl}$ and Gch-KO unstimulated macrophages and (B) $Gch^{fl/fl}$ and Gch-KO $M^{LPS/IFN\gamma}$. Measurements were used to determine (C) basal OCR (D) compensatory glycolysis, (E) glycolytic reserve and (F) non-glycolytic acidification. Data are n=3-6 mean ± SEM. P values are calculated using a one-way ANOVA with Tukey's post-test (*P<0.05, **P<0.01, ***P<0.001, ****P<0.0001)

### 3.4.7 Abundance of glycolytic metabolites are decreased and Pentose Phosphate Pathway unchanged in BH4 deficient $M^{LPS/IFN\gamma}$

As changes in glycolytic rate had been observed, we interrogated a metabolomics dataset previously conducted on unstimulated and LPS/IFN-γ stimulated $Gch^{fl/fl}$Tie2Cre macrophages (Bailey et al., 2019). Accompanying a decrease in glycolytic rate in the Gch-KO $M^{LPS/IFN-\gamma}$, we saw a decrease in the metabolites in the glycolytic pathway (Figure 3.10A). In particular, there was a 30% decrease in glucose-6-phosphate, 60% decrease in DHAP, and 45% decrease in lactate levels (Figures 3.10B-D). The pentose phosphate pathway remained unchanged (Figure 3.10E-G).

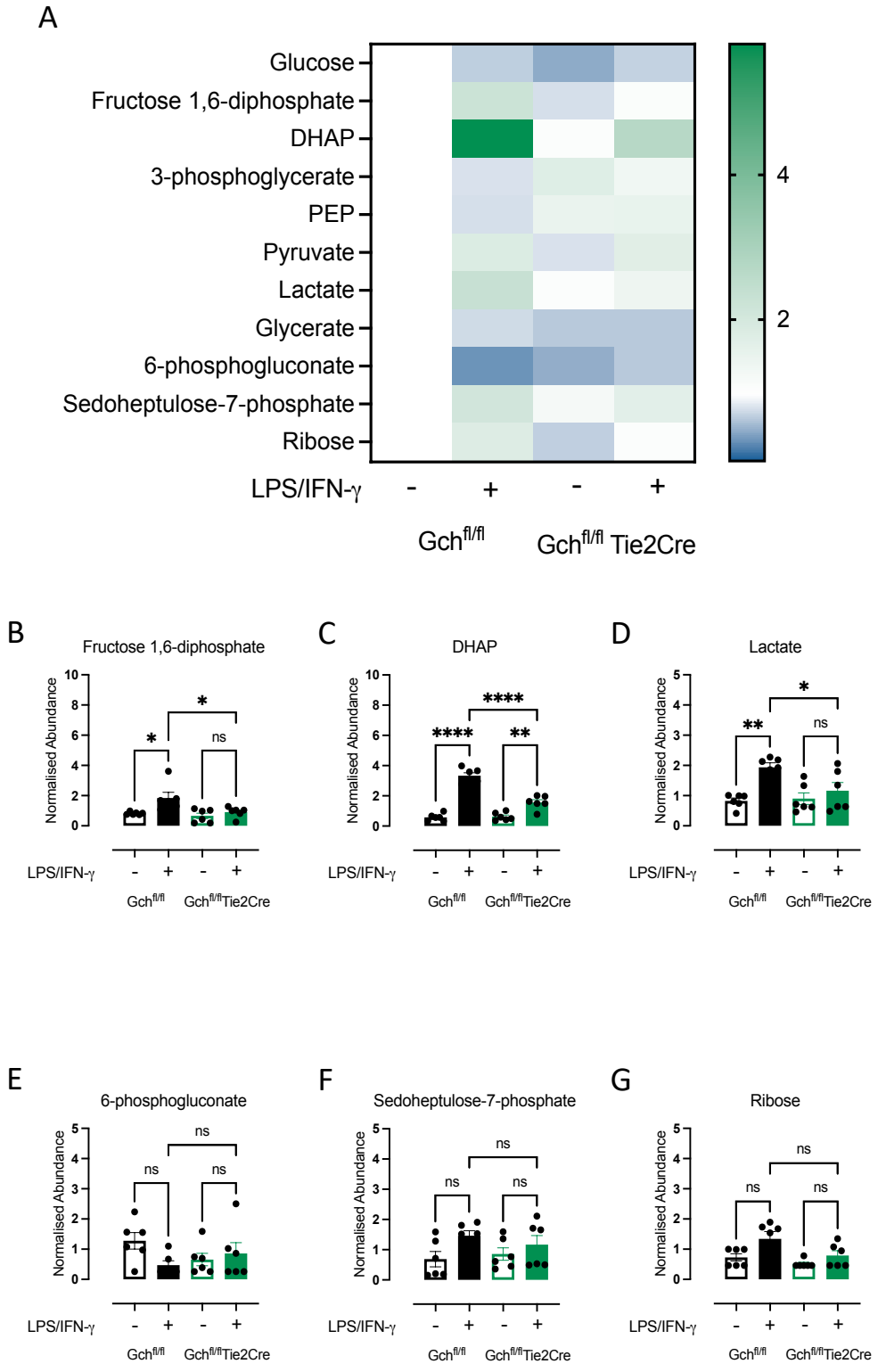



**Figure 3. 10 BH4-deficient $M^{LPS/IFN-\gamma}$ have decreased glycolytic and unchanged Pentose Phosphate Pathway metabolites**

(A) Fold change heatmap of glycolysis and pentose phosphate pathways relative to unstimulated $Gch^{fl/fl}$ macrophages (n=6)
(B) Fructose 1,6 diphosphate metabolite abundance (C) DHAP metabolite abundance (D) Lactate metabolite abundance (E) 6-phosphogluconate metabolite abundance (F) Sedoheptulose-7-phosphate metabolite abundance (G) Ribose metabolite abundance, in $Gch^{fl/fl}$ and $Gch^{fl/fl}$Tie2Cre macrophages unstimulated and LPS/IFN-ɣ macrophages
Data are n=6 mean ± SEM. P values are calculated using a one-way ANOVA with Tukey's post-test (*P<0.05, **P<0.01, ***P<0.001, ****P<0.0001)

### 3.4.8 BH4-deficient $M^{LPS/IFN-\gamma}$ have decreased expression of certain enzymes in the glycolytic pathway

Having shown alterations in glycolytic metabolites, we found *Slc2a1,* which encodes Glut1, the primary transporter of glucose into macrophages, was diminished in Gch-KO $M^{LPS/IFN-\gamma}$ (Figure 3.11A). Intracellular glucose measurements however remained unchanged (Figure 3.10A). Expression of *Hk2*, which encodes the first rate-limiting enzyme in the glycolytic pathway, was halved in Gch-KO $M^{LPS/IFN-\gamma}$ (Figure 3.11B), and its protein expression was almost undetectable by western blot (Figure 3.11C). This was consistent with findings in the glycolytic rate assay (Figure 3.9) and metabolomics (Figure 3.10) and suggests Gch-KO $M^{LPS/IFN-\gamma}$ have altered energy metabolism, gaining less energy from glycolysis, alongside increased OXPHOS as observed in Figure 3.7.

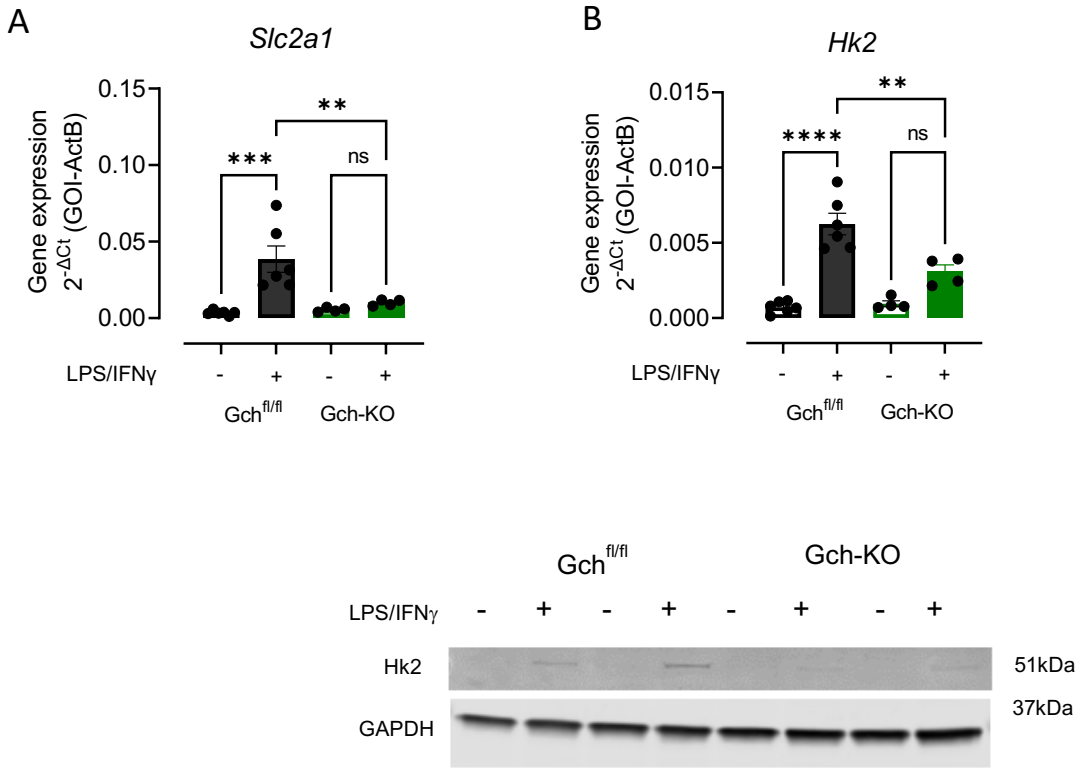



**Figure 3. 11 BH4-deficient $M^{LPS/IFN-\gamma}$ have decreased expression of certain enzymes in the glycolytic pathway**

(A) *Glut1* gene expression in Gch-KO cells measured by RT-qPCR (B) *Hk2* gene expression in Gch-KO cells measured by RT-qPCR and below western blot analysis of HK2 in Gch-KO cells (n=3). Gene of interest (GOI). Data are n=4-6 mean ± SEM. P values are calculated using a one-way ANOVA with Tukey's post-test (*P<0.05, **P<0.01, ***P<0.001, ****P<0.0001).

### 3.4.9 ATP generation via Glycolysis or OXPHOS in $Gch^{fl/fl}$ and BH4-deficient macrophages

We next sought to quantify ATP production from both glycolysis and OXPHOS using the Seahorse ATP rate assay (Figure 3.12). Quantification of ATP generation revealed that Gch-KO $M^{LPS/IFN-\gamma}$ were gaining less ATP from glycolysis (Figure 3.12A) and significantly more from OXPHOS (Figure 3.12B). Unstimulated Gch-KO macrophages had approximately 30% lower total ATP production compared to $Gch^{fl/fl}$, indicating lower metabolic activity. A difference in total ATP production was not observed in Gch-KO $M^{LPS/IFN-\gamma}$ (Figure 3.12C). Finally, as a ratio, Gch-KO $M^{LPS/IFN-\gamma}$ gain 5 times more energy from OXPHOS compared to $Gch^{fl/fl}$ $M^{LPS/IFN-\gamma}$ (Figure 3.12D). Overall, this demonstrates that BH4 is required for complete breaks in the TCA cycle to occur, resulting in increased OXPHOS and hence decreased reliance on glycolysis for ATP production.

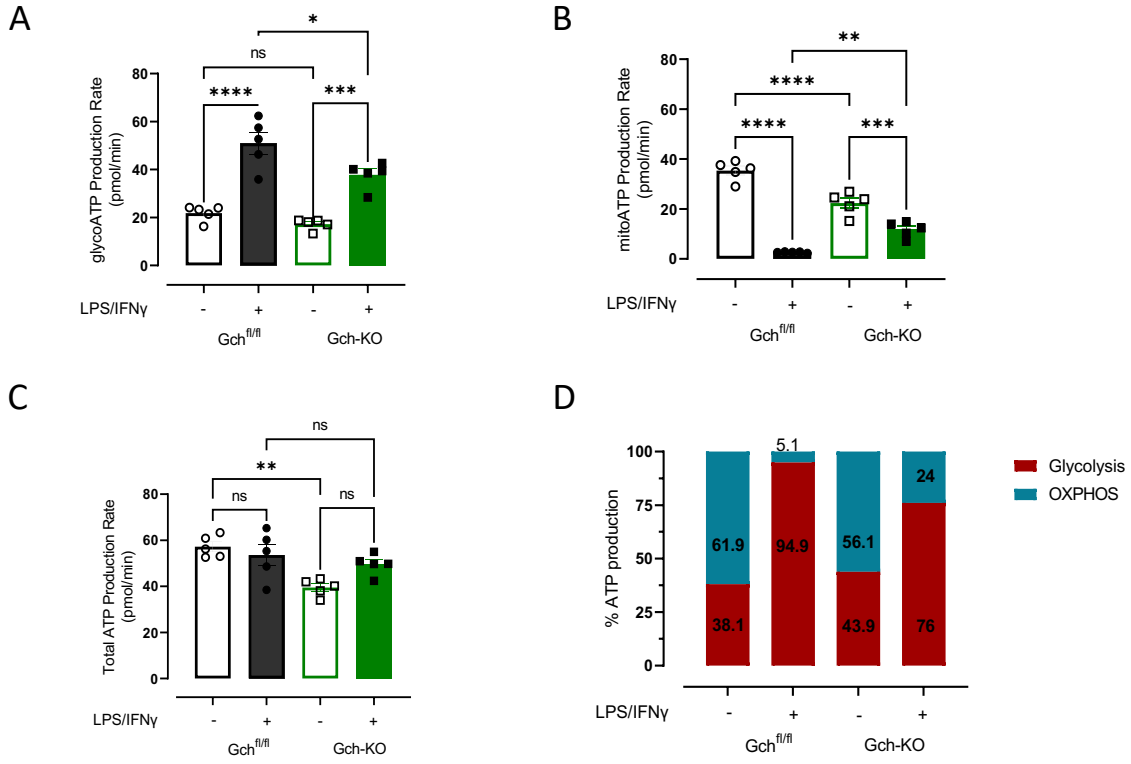



**Figure 3. 12 Ratio of ATP generated via Glycolysis or OXPHOS in Gch$^{fl/fl}$ and BH4-deficient macrophages**

ATP production rate measured using a XFe Seahorse analyser with sequential addition of Oligomycin and combined rotenone and antimycin A. Measurements were used to determine A) glycolytic ATP (glycoATP) production rate, B) Mitochondrial ATP (mitoATP) production rate (OXPHOS), C) Total ATP production rate and D) Percentage ATP production by glycolysis and OXPHOS in Gch$^{fl/fl}$ and Gch-KO M$^{Resting}$ M$^{LPS/IFN-\gamma}$ macrophages.
Data are n=4-5 mean ± SEM. P values are calculated using a one-way ANOVA with Tukey's post-test (*P<0.05, **P<0.01, ***P<0.001, ****P<0.0001).

### 3.4.10 BH4-deficient $M^{LPS/IFN-\gamma}$ do not use fatty acid oxidation for ATP production

We hypothesised that the increased TCA cycle flux in Gch-KO $M^{LPS/IFN-\gamma}$ may be supported by increased metabolism of other substrates. Apart from glycolysis, fatty acid metabolism and glutaminolysis also feed into the TCA cycle at citrate and α-ketoglutarate respectively. Using etomoxir, a fatty acid oxidation inhibitor, the cell's dependency on this pathway was determined. As expected, basal OCR was decreased in $M^{LPS/IFN-\gamma}$ macrophages (Figure 3.13A). Unstimulated Gch-KO macrophages FAO usage remained unchanged in Gch-KO macrophages and $M^{LPS/IFN-\gamma}$ were not dependant on FAO (Figure 3.13B).

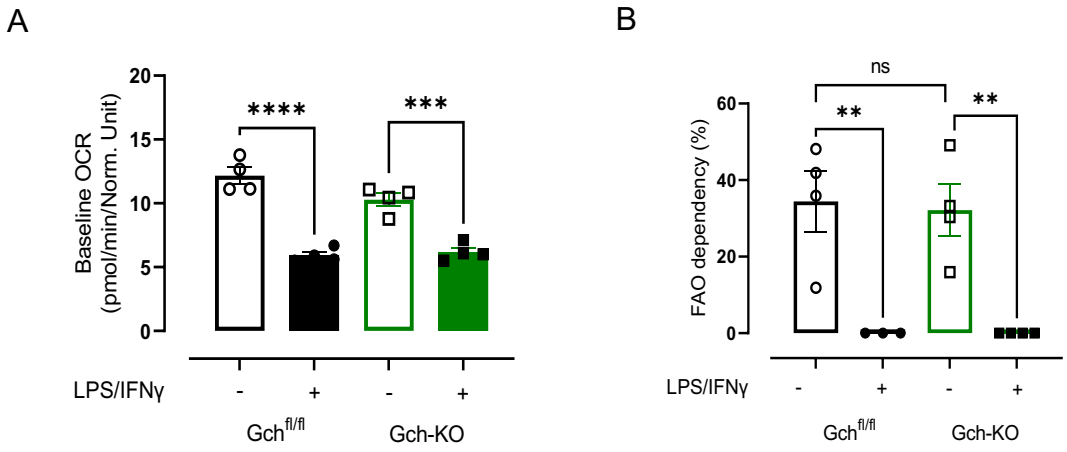



**Figure 3. 13 BH4-deficient $M^{LPS/IFN-\gamma}$ macrophages do not have increased mitochondrial respiration due to Fatty Acid Oxidation**

Oxygen consumption rate (OCR) measured using a XFe96 Seahorse analyser with sequential injection of Etomoxir, next combined bis-2-(5-phenylacetamido-1,3,4-thiadiazol-2-yl)ethyl sulfide (BPTES)/UK5099 to determine (A) Basal OCR, (B) Dependency on fatty acid oxidation (FAO) (%) in $Gch^{fl/fl}$ and Gch-KO $M^{Resting}$ $M^{LPS/IFN-\gamma}$ macrophages.
Data are n=3-4 mean ± SEM. P values are calculated using a one-way ANOVA with Tukey's post-test (*P<0.05, **P<0.01, ****P<0.0001)

### 3.4.11 Most fatty acid metabolism metabolites remain unchanged in BH4-deficient $M^{LPS/IFN-\gamma}$

Next, metabolites involved in fatty acid metabolism from the GchTie2Cre metabolomics dataset was interrogated (Figure 3.14A-I) (Bailey et al, 2019). Many metabolites in fatty acid synthesis and metabolism remained unchanged. However, we observed increases in 2-hydroxyglutarate and acetylcarnitine with stimulation in wildtype macrophages which were not observed with BH4 deficiency (Figure 3.14B, F). Furthermore, methylmalonate levels increased with stimulation in $Gch^{fl/fl}$ and further increased in Gch-KO $M^{LPS/IFN-\gamma}$ (Figure 3.14E).

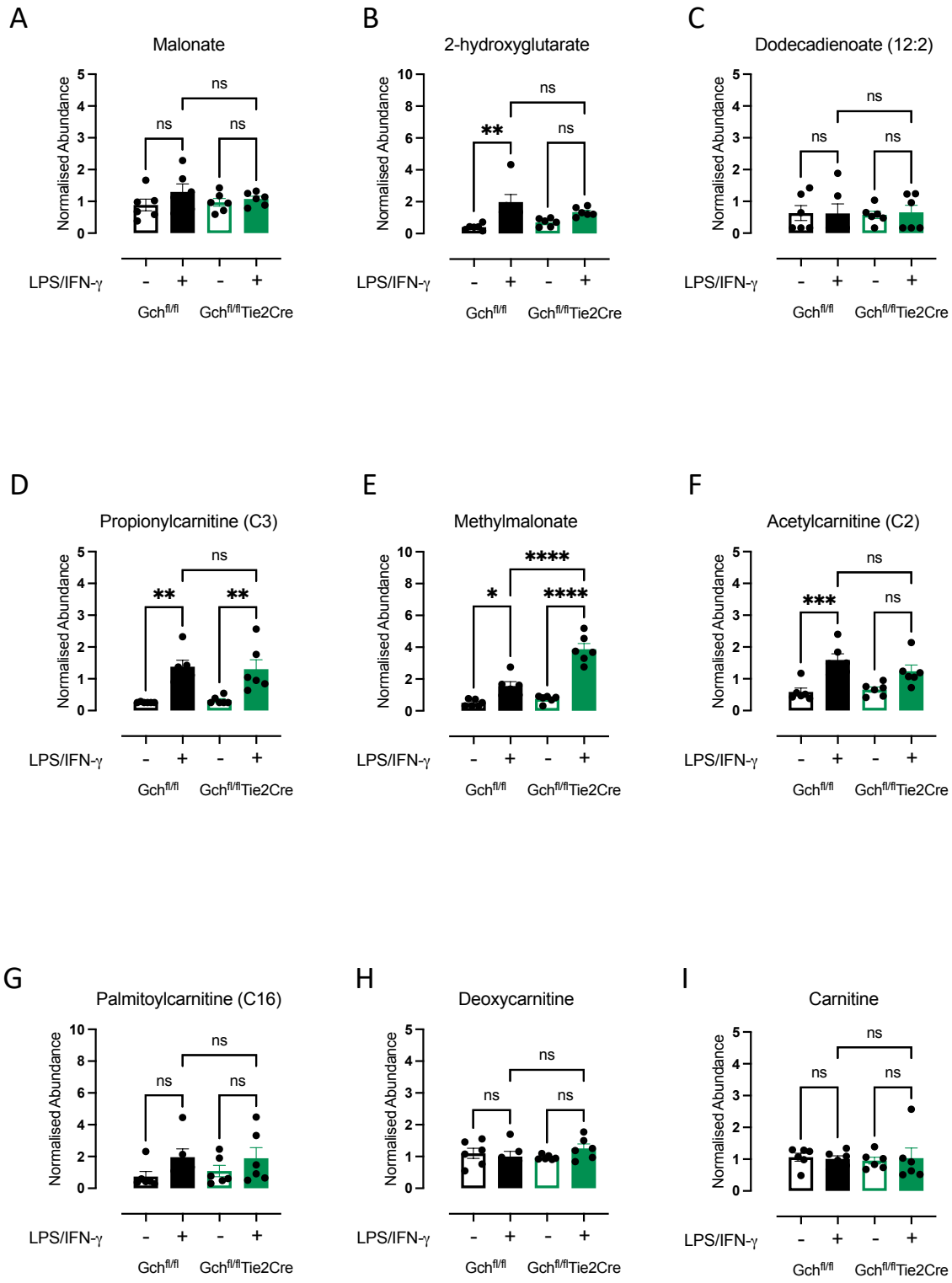



**Figure 3. 14 Metabolites involved in Fatty acid synthesis and metabolism in BH4-deficient macrophages**

(A) Malonate metabolite abundance (B) 2-hydroxyglutarate metabolite abundance (C) Dodocadienoate metabolite abundance (D) Propionylcarnitine metabolite abundance (E) Methylmalonate metabolite abundance (F) Acetylcarnitine metabolite abundance (G) Palmitoylcarnitine metabolite abundance (H) Deoxycarnitine metabolite abundance (I) Carnitine metabolite abundance in $Gch^{fl/fl}$ and $Gch^{fl/fl}$Tie2Cre macrophages unstimulated and LPS/IFN-ɣ macrophages. Data are n=6 mean ± SEM. P values are calculated using a one-way ANOVA with Tukey's post-test (*P<0.05, **P<0.01, ***P<0.001, ****P<0.0001)

### 3.4.12 BH4-deficient $M^{LPS/IFN-\gamma}$ have decreased eicosanoid levels

Eicosanoids link fatty acids and inflammation. Arachidonic acid, the precursor to prostaglandins, was significantly decreased in GchTie2Cre stimulated macrophages (Figure 3.15A). 13-HODE + 9-HODE increased with stimulation but this was not altered by loss of BH4 (Figure 3.15B). Prostaglandin E2 was increased with stimulation in $Gch^{fl/fl}$ macrophages but not in Gch-KO $M^{LPS/IFN-\gamma}$ (Figure 3.15C). Furthermore, 12-HHTrE, a lipid agonist of leukotriene B2 receptor which induces leukocyte chemotaxis during inflammation, was significantly decreased in Gch-KO $M^{LPS/IFN-\gamma}$ compared to $Gch^{fl/fl}$ (Figure 3.15D). Decreased levels of key eicosanoids suggest a less inflammatory profile despite unchanged fatty acid metabolism in BH4-deficient inflammatory macrophages.

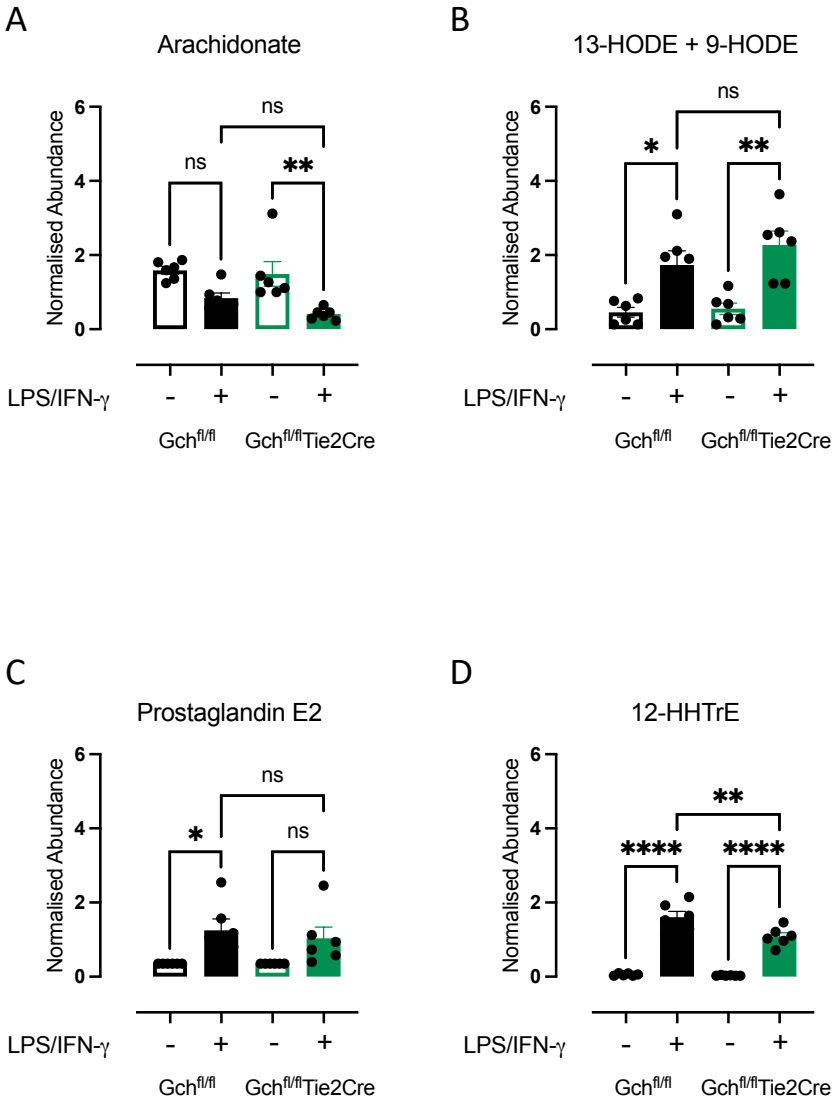



**Figure 3. 15 Metabolites involved in eicosanoid production**

(A) Arachidonate metabolite abundance (B) 13-HODE + 9-HODE metabolite abundance (C) Dodocadienoate metabolite abundance (D) Propionylcarnitine metabolite abundance.
Data are n=6 mean ± SEM. P values are calculated using a one-way ANOVA with Tukey's post-test (*P<0.05, **P<0.01, ***P<0.001, ****P<0.0001)

### 3.4.13 BH4-deficient $M^{LPS/IFN-\gamma}$ are more dependent on the Glutamine oxidation pathway

Glutamine feeds into the TCA cycle via α-ketoglutarate, after the first TCA cycle break. To test cell dependency on glutaminolysis, and if it contributes to increased OXPHOS observed in Gch-KO $M^{LPS/IFN-\gamma}$, macrophages were treated with a glutaminase inhibitor BPTES. Unstimulated macrophages Gch-KO macrophages were not more dependent on glutaminolysis (Figure 3.16A-B). Again, $Gch^{fl/fl}$ and Gch-KO $M^{LPS/IFN-\gamma}$ basal OCR was halved with LPS/IFNγ stimulation (Figure 3.16A). Gch-KO $M^{LPS/IFN-\gamma}$ were approximately 20% more dependent on glutaminolysis (Figure 3.16B).

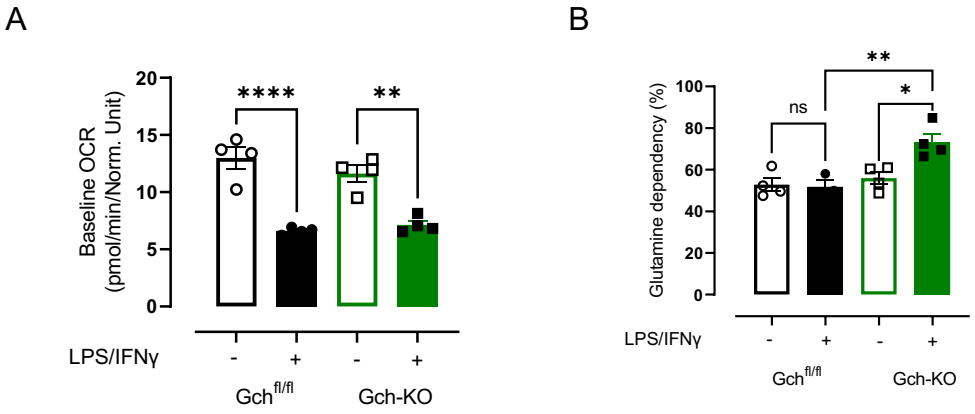



**Figure 3. 16 BH4-deficient $M^{LPS/IFN-\gamma}$ are more dependent on the glutaminolysis pathway**

Oxygen consumption rate (OCR) measured using a XFe96 Seahorse analyser with sequential injection of bis-2-(5-phenylacetamido-1,3,4-thiadiazol-2-yl)ethyl sulfide (BPTES) and combined Etomoxir and UK5099 to determine (A) basal OCR, (B) Dependency on glutamine (%) in $Gch^{fl/fl}$ and GCH-KO $M^{Resting}$ $M^{LPS/IFN-\gamma}$ macrophages. Data are n=4-5 mean ± SEM. P values are calculated using a one-way ANOVA with Tukey's post-test (*P<0.05, **P<0.01, ****P<0.0001)

### 3.4.14 Glutamine levels are unchanged in BH4-deficient $M^{LPS/IFN-\gamma}$ macrophages

Again, we analysed glutamine metabolism pathway in $Gch^{flfl}$Tie2Cre metabolomics dataset (Bailey et al., 2019). There were no changes in glutamine, glutamate or N-acetyl glutamine (Figure 3.17 A-B, D). N-acetyl glutamate levels doubled in $Gch^{fl/fl}$ macrophages upon stimulation but no changes were observed with BH4 deficiency (Figure 3.17C). This suggests that metabolite levels were unchanged although glutaminolysis activity was increased in Gch-KO $M^{LPS/IFN-\gamma}$ (Figure 3.16).

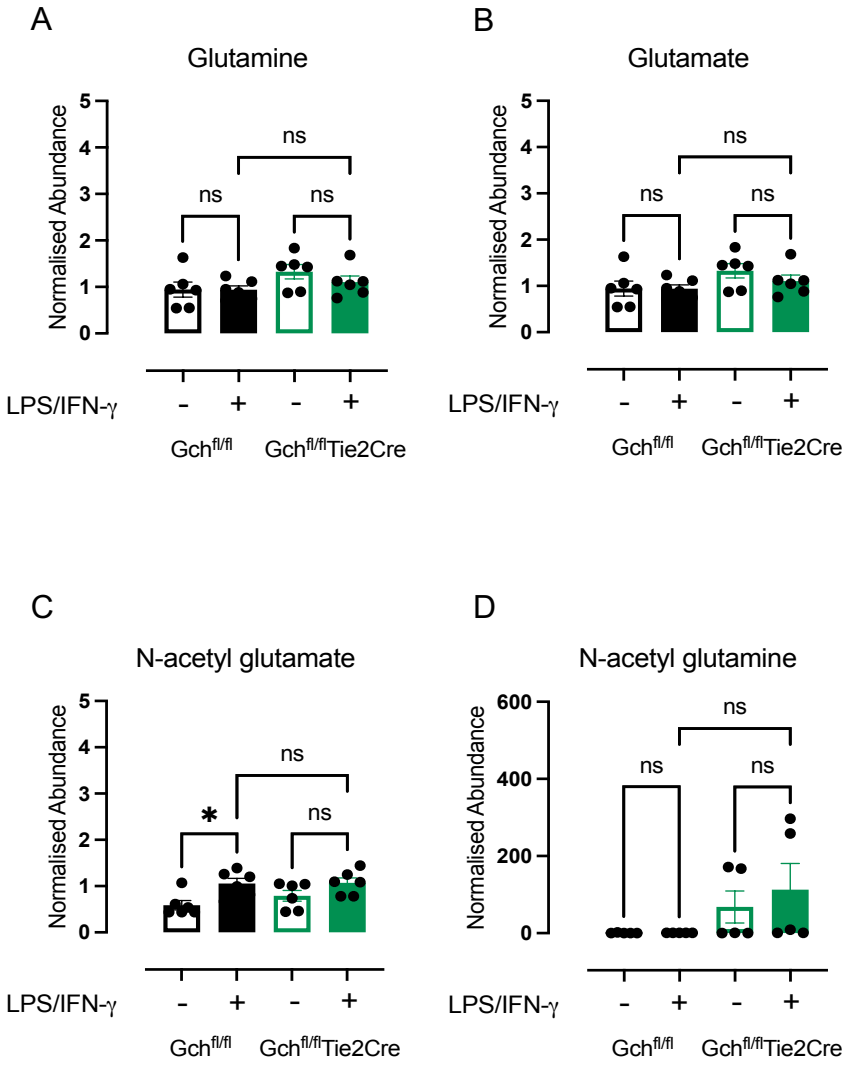



**Figure 3. 17 BH4-deficient $M^{LPS/IFN-\gamma}$ do not have increased glutamine levels**

(A) Glutamine metabolite abundance (B) Glutamate metabolite abundance (C) N-acetyl glutamate metabolite abundance (D) N-acetyl glutamine metabolite abundance, in $Gch^{fl/fl}$ and $Gch^{fl/fl}$Tie2Cre macrophages unstimulated and LPS/IFN-ɣ macrophages. Data are n=6 mean ± SEM. P values are calculated using a one-way ANOVA with Tukey's post-test (*P<0.05, **P<0.01, ***P<0.001)

## 3.5 Discussion

### 3.5.1 Overview

The importance of BH4 in the generation of nitric oxide (NO) by iNOS as part of the inflammatory response in macrophages is well established (Douglas et al., 2018; McNeill et al., 2015; McNeill et al., 2018). More recently, it has been recognised that NO has a role in the metabolic remodelling associated with the proinflammatory switch, particularly its regulation of the TCA cycle (Bailey et al., 2019; Palmieri, Gonzalez-Cotto, et al., 2020; Van den Bossche et al., 2016). A novel model of BH4 deficiency in bone marrow derived macrophages was generated. This revealed an incomplete glycolytic switch in BH4-deficient inflammatory macrophages, accompanied by additional reliance on OXPHOS, which may be supported by increased glutaminolysis. Although fatty acid metabolism overall appeared unchanged, abundance of inflammatory eicosanoids was decreased with loss of BH4. The TCA cycle metabolite, itaconate, was not only significantly increased in BH4-deficient inflammatory macrophages but was also secreted in large quantities. Although inflammation-linked metabolites were decreased, suggesting a shift towards a less inflammatory macrophage phenotype, pro-inflammatory cytokine production remained unchanged.

### 3.5.2 A novel mouse model of BH4 and NO deficiency

The R26-CreER$^{T2}$Gch$^{fl/fl}$ (Gch-KO) mouse model takes a new approach to *Gch1* excision. In contrast to the previously used GchTie2Cre model, the Gch-KO mouse has a global tamoxifen inducible deletion of *Gch1*. To achieve specificity, tamoxifen was administered to bone marrow cells in the petri dish following bone marrow isolation. This resulted in complete knockdown of *Gch1* in bone marrow derived macrophages. Furthermore, BH4 levels were undetectable in Gch-KO bone marrow derived macrophages. Nitrite levels were measured at 0-3μM , which is sufficiently low to gain insight into NO deficiency alongside

BH4. Baseline OCR of Gch-KO cells was consistently slightly lower than $Gch^{fl/fl}$ in Seahorse assays. This may be due to cells adapting to loss of BH4 immediately in the petri dish, whereas in the GchTie2Cre model, cells have time to adapt to this loss in vivo. BH4 deficiency could be lowering overall metabolism or mitochondrial function of the cell but this effect was not observed in the GchTie2Cre model (Bailey et al, 2019). In addition, Gch-KO and GchTie2Cre inflammatory macrophages both exhibited similarly increased IL1β levels and itaconate levels (20 pmol/μL) following LPS/IFNγ stimulation compared to $Gch^{fl/fl}$. Overall, the Gch-KO model has a comparable mitochondrial function to the GchTie2Cre model. It exhibits complete and consistent *Gch1* knockdown, reducing the number of animals used and costs, but in vivo experiments will be more difficult to achieve.

### 3.5.3 Loss of BH4 alters TCA substrate metabolism

Macrophages are often described as plastic immune cells demonstrated by their spectrum of polarisation states, with much literature focussing on the inflammatory $M^{LPS/IFN\text{-}\gamma}$ state. The glycolytic switch facilitates many functions of $M^{LPS/IFN\text{-}\gamma}$ macrophages including phagocytosis, secretion of pro-inflammatory cytokines and ROS production (Viola et al, 2019). However, with a complete switch they are unable to polarise into any other state, thereby losing their perceived plasticity (Van den Bossche et al., 2016). Our findings reinforce that BH4 is required for the glycolytic switch to completely occur. Indeed, it has been suggested that it is not inhibition of isocitrate dehydrogenase (IDH) activity but NO acting as an important intermediary signalling molecule to cause the first TCA cycle break (Jha et al., 2015; Palmieri, McGinity, et al., 2020). Instead of a break at IDH, which has yet to be conclusively proven, iNOS is required for alterations in α-ketoglutarate homeostasis (Ho Ping et al, 2012). Our group too has reported a reduction in IDH activity but not mRNA levels in $Nos2^{-/-}$ BMDMs (Bailey et al., 2019).

With loss of BH4 and NO, the incomplete glycolytic switch and increased reliance on OXPHOS suggests increased capacity for metabolic manipulation. This increased OXPHOS is accompanied by increased glutaminolysis which has been reproduced in the $Nos2^{-/-}$ model suggesting the effect is NO and not BH4 dependant (Palmieri, Gonzalez-Cotto, et al., 2020). Moreover, although there is approximately 20% dependence on glutaminolysis in BH4 deficient $M^{LPS/IFN\text{-}\gamma}$, this may not be sufficient to explain elevated TCA cycle flux. As glutamine levels were not altered in the GchTie2Cre metabolomics analysis it suggests the activity of the pathway is altered more than metabolite levels.

In contrast to glutaminolysis, there was no increased reliance on fatty acid oxidation in Gch-KO $M^{LPS/IFN\text{-}\gamma}$, which is understandable since the first TCA cycle break occurs after citrate and before α-ketoglutarate. However, there were differences in several fatty acid metabolites which were upregulated in $Gch^{fl/fl}$ but not BH4-deficient $M^{LPS/IFN\text{-}\gamma}$. The anti-inflammatory metabolite, 2-hydroxyglutarate, has been noted as one of the most induced immunometabolites in murine BMDM and hMDM following TLR-4 activation, accumulating after the initial inflammatory response (de Goede et al., 2022). Its abundance was increased in $Gch^{fl/fl}$ $M^{LPS/IFN\text{-}\gamma}$ but not in Gch-KO $M^{LPS/IFN\text{-}\gamma}$ indicating a less pro-inflammatory phenotype. Other fatty acid metabolites methylmalonate and acetylcarnitine were altered too, and associated with a proinflammatory response, but have not been studied in macrophages (de Souza Almeida et al., 2022; Gabbi et al., 2017; Jamali-Raeufy et al., 2021; Wang et al., 2020).

### 3.5.4 Metabolism drives Inflammation?

The glycolytic switch was first reported in a landmark study in dendritic cells (Krawczyk et al., 2010) and later in macrophages (Rodríguez-Prados et al., 2010). The studies demonstrated that this metabolic switch to glycolysis underpinned the activation of dendritic

cells and, importantly, this was required for the inflammatory response. With decreased glycolysis, and increased OXPHOS, we hypothesise that BH4-deficient macrophages would exhibit a decreased inflammatory response.

Levels of the anti-inflammatory TCA cycle metabolite itaconate were increased with loss of BH4. In the GchTie2Cre and *Nos2*$^{-/-}$ models, a similar 2-3-fold increase in intracellular itaconate levels were observed upon activation (Bailey et al, 2019). Similar findings were reported in another *Nos2*$^{-/-}$ model in both LPS treated BMDMs as well as from peritoneal lavage fluid of thioglycolate treated mice exposed to an IFN-γ 3 days later (Palmieri, Gonzalez-Cotto, et al., 2020).

Indeed, eicosanoids $PGE_2$ and 12-HHTrE levels were decreased in activated macrophages lacking BH4. Eicosanoids are 20-carbon oxidised fatty acid signalling molecules derived from arachidonate, or other similar polyunsaturated fatty acids, and carry a host of physiological functions including inflammation, pregnancy, pain and blood pressure regulation. Eicosanoids increase with TLR-4 pathway activation. Another group reported the levels of $PGE_2$ and $PGE_2$ formation were decreased by 80% after 12h and 74% after 24h post LPS/IFN-γ stimulation in *Nos2*$^{-/-}$ peritoneal murine macrophages (Marnett et al., 2000). Furthermore, resident peritoneal macrophages stimulated with zymosan, in the presence of a $PGE_2$ analog, had halved TNF-α levels and increased several fold IL10 production through IP, EP2 and EP4 receptor signalling (Shinomiya et al., 2001). The study neatly demonstrated the close connection between inflammatory eicosanoid and cytokine signalling.

In endothelial cells, NO has been shown to increase eicosanoid production through activation of prostaglandin H synthase (Davidge et al., 1995). In another study, M1-like mouse peritoneal macrophages had higher proportion of AA-derived eicosanoids compared to EPA-derived eicosanoids (Cui et al., 2022). In murine macrophage cell line J774, PGE2 and prostacyclin inhibited LPS-induced iNOS synthase levels (Marotta et al., 1992).

Furthermore, it was found that NO activates cyclooxygenase (COX) enzymes in RAW267 cells 30 years ago. Therefore, loss of NO production via loss of BH4 could result in reduced COX activation and hence less eicosanoids which corroborates our observations (Marnett et al., 2000; Mollace et al., 2005; Salvemini et al., 1993).

Despite this, IL1β secretion was increased, but IL6 remained the same Gch-KO $M^{LPS/IFN\text{-}\gamma}$ compared to wildtype. Palmeiri et al reported increased IL1β, IL6 and IL12 cytokine levels in NO-deficient stimulated macrophages, but no changes in TNF-α and IL10 (Palmieri, Gonzalez-Cotto, et al., 2020). Overall, this suggests BH4 or NO loss results in alterations in metabolism but not at the expense of the inflammatory response. More functional studies need to be carried out to confirm this such as phagocytosis and chemotaxis assays.

### 3.5.5 Itaconate – the anti-inflammatory metabolite in a pro-inflammatory macrophage

Itaconate has become recognised as one of the hallmarks of inflammatory macrophage polarisation, even though its exerts anti-inflammatory effects. Itaconate modulation by nitric oxide has been reproduced by two models of BH4 deficiency and NO deficiency, as described above (Bailey et al., 2019; Palmieri, Gonzalez-Cotto, et al., 2020).

Much of the literature on itaconate focuses on its role as an intracellular signalling metabolite. We were struck by the >100-fold higher levels of itaconate secreted from activated BMDMs compared to that measured intracellularly. In another study on BMDMs, secreted itaconate levels were also measured approx. 2-fold higher than intracellular itaconate 24h after LPS/IFN-γ exposure (Lampropoulou et al., 2016; Strelko et al., 2011). The potential paracrine and autocrine signalling roles of itaconate are an exciting area that remains to be explored. The mechanism by which itaconate is secreted from the cell is also unknown but that active transport out of the mitochondria and the cell is likely as itaconate is a polar molecule.

### 3.5.6 Future work

This chapter presents a novel inducible model of BH4 deficiency to build on previous findings in bone marrow derived macrophages. The study shows BH4 is required for a complete glycolytic switch to occur in inflammatory macrophages resulting in a reduced inflammatory macrophage phenotype. While the results suggest TCA cycle supplementation via glutaminolysis in BH4-deficient inflammatory macrophages, this finding needs to be confirmed. To gain a more thorough understanding, future investigations would include assessments of enzymatic activity, gene and protein expression levels and functional assays, particularly for glutamine. Functional assays such as bacteria killing, chemotaxis, foam cell formation will be useful in determining whether changes in inflammatory metabolites such as eicosanoids and itaconate indeed alter macrophage function. Intracellular and extracellular itaconate levels were increased with loss of BH4. The mechanism by which BH4 modulates itaconate is not understood but could be due to effects of NO on IRG1, or itaconate itself, or due to interactions between iNOS and IRG1. The role of extracellular itaconate is further explored in Chapter 6.

# Chapter 4

## Effects of hyperglycaemia on Wildtype and BH4-deficient macrophages

# Chapter 4: Effects of hyperglycaemia on WT and BH4 deficient macrophages

## 4.1 Introduction

Macrophages are highly adaptable immune cells whose behaviour and function are influenced by their surrounding microenvironment (Mantovani et al., 2008). High glucose has been shown to alter the inflammatory state of macrophages in vitro. A hallmark of both type 1 and type 2 diabetes, hyperglycaemia has been linked to impaired immune responses and reduced pathogen clearance by macrophages in diabetic patients (Ayala et al., 2019). This is important since diabetes is associated with increased morbidity and mortality from cardiovascular diseases and increased risk of infections and surgical complications.

Disturbed glucose homeostasis has been shown to increase production of inflammatory markers such as nitric oxide, IL6, IL1β and TNF-α (Ayala et al., 2019; Freemerman et al., 2014; Pavlou et al., 2018). Furthermore, with LPS/IFN-γ activation, macrophages increase glucose uptake via Glut1 to meet their increased energy needs (Freemerman et al., 2014). This generates ATP, as well as different metabolites involved in glucose metabolism that can generate mediators to support different macrophage functions. For example, the end product of glycolysis, lactate, enhanced MCT1 dependent oxidative transition in macrophages, resulting in a more reparative macrophage phenotype (Zhang et al., 2020). The glucose environment can also influence glucose metabolism and skew the shift to glycolysis or oxidative phosphorylation, which in turn can shift macrophage polarisation states and contribution to inflammation (Mantovani et al., 2008).

In Chapter 3, it was established that BH4-deficient macrophages have altered inflammatory and metabolic profile. Glycolytic pathway flux as well as gene expression and protein levels of glycolytic enzymes were decreased in BH4-deficient $M^{LPS/IFN-\gamma}$, whilst ATP production via OXPHOS was increased. In addition, levels of TCA cycle metabolite, itaconate, were increased in BH4-deficient $M^{LPS/IFN-\gamma}$. Itaconate has been shown to alkylate the glycolytic

enzyme, GAPDH, resulting in decreased enzyme activity and inhibition of the glycolytic pathway (Liao et al., 2019). In turn, GAPDH has been shown to result in post-translational repression of TNF-α (Millet et al., 2016). In essence, this shows how altered metabolite levels can lead to direct alterations of pro-inflammatory cytokine levels. Furthermore, it indicates how hyperglycaemia could alter the inflammatory, metabolic and functional state of macrophages.

Accordingly, we sought to investigate how high glucose treatment would alter the inflammatory profile of BH4-deficient macrophages.

## 4.2 Hypothesis and Aims

### 4.2.1 Hypothesis

High glucose treatment increases glycolysis and inflammatory gene expression and cytokine release in BH4-deficient macrophages.

### 4.2.2 Aims

Aim 1: To investigate how high glucose treatment alters the metabolic profile of BH4-deficient macrophages

Aim 2: To investigate how high glucose treatment alters the inflammatory profile of BH4-deficient macrophages

## 4.3 Methods

### 4.3.1 Cell culture

BMDM culture was performed as described in Section 2.2.1. In addition to the steps outlined before, to induce deletion of the *Gch1* gene, all cells were given 1 μM 4-hydroxytamoxifen (4-OHT) on Day 1 and Day 3 of culture (Figure 4.1). Cells were then stimulated with LPS/IFN-γ or IL4 for polarisation and stimulated with high glucose levels for 24h before harvest. To mimic normoglycemic or hyperglycaemic conditions, the culture medium contained 5mM or 20mM glucose levels for 24 hours.

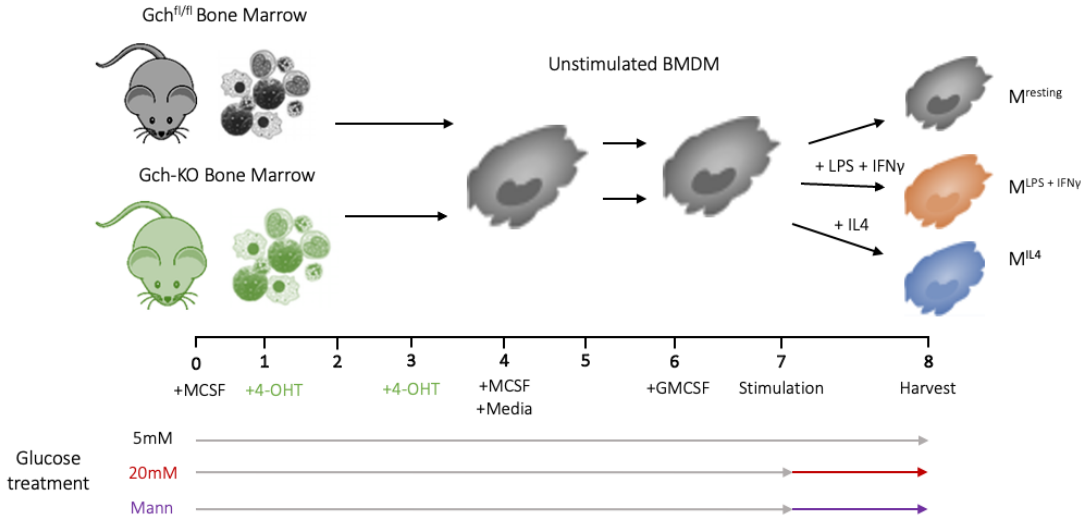



**Figure 4. 1 Gch$^{fl/fl}$ and R26Cre-ER$^{T2}$Gch$^{fl/fl}$ culture protocol**

Schematic showing culture of bone marrow derived macrophages from Gch$^{fl/fl}$ and R26Cre-ER$^{T2}$Gch$^{fl/fl}$ (Gch-KO) mice. Cells were cultured over 8 days. On Days 1 and 3, cells are treated with 1.0 μM 4-hydroxytamoxifen (4-OHT) to induce *Gch1* deletion. On Day 4, cells are given 50% additional media containing 50ng/ml MCSF. On Day 6, cells are treated with 10μg/ml GMCSF. On Day 7 cells are stimulated with LPS/IFN-γ to polarise into inflammatory M$^{LPS/IFN-γ}$ state or with IL-4 for reparative polarisation state M$^{IL4}$ . In addition, cells are left in normoglycaemia, stimulated with 20mM high glucose treatment or 5mM glucose+15mM Mannitol (Mann) for 24 hours before harvest.

## 4.4 Results

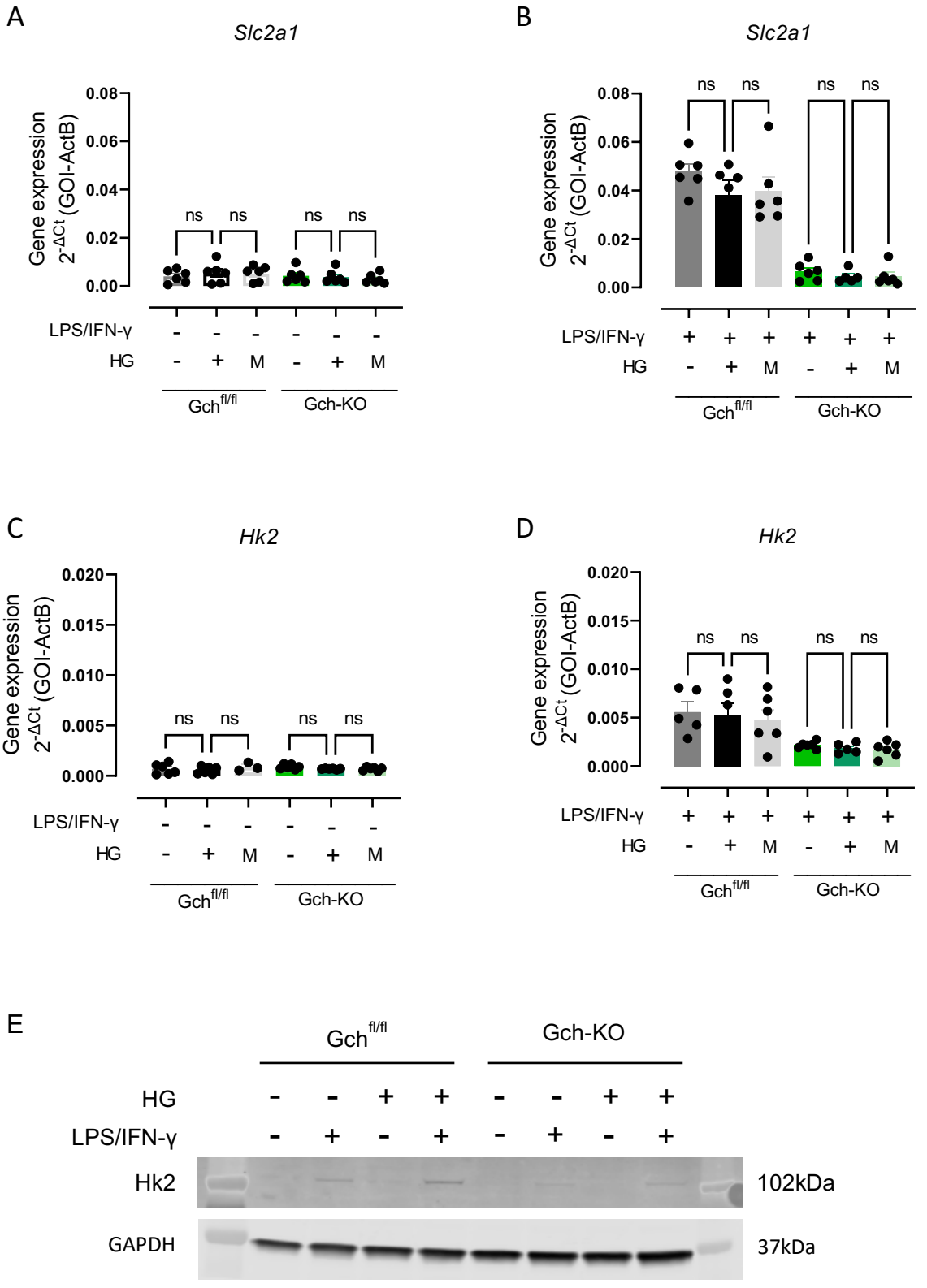
### 4.4.1 Glycolytic gene expression is unaltered in HG-treated $Gch^{fl/fl}$ and GCH-KO macrophages

To explore effects of HG treatment on glycolysis, we quantified *Slc2a1*expression (encodes GLUT1, the primary transporter of glucose into macrophages) and *Hk2* expression, (the first rate-limiting enzyme in the glycolytic pathway). HG treatment did not alter *Slc2a1* in $Gch^{fl/fl}$ or GCH-KO $M^{Resting}$ or $M^{LPS/IFN\text{-}\gamma}$ macrophages(Figure 4.2A-B). Similarly, *Hk2* expression, was unchanged in $Gch^{fl/fl}$ and GCH-KO $M^{Resting}$ and $M^{LPS/IFN\text{-}\gamma}$ macrophages (Figure 4.1C-D). HK2 protein expression appeared increased with HG-treatment but this did not reach significance in densitometric analysis (Figure 4.1E). Genotype differences seen previously with *Slc2a1*and *Glut1* expression were maintained in the presence of HG treatment. No changes were observed with Mannitol (M) treatment, the osmotic control for HG treatment.

**Figure 4. 2 *Slc2a1* and *Hk2* expression is unaltered with HG in $Gch^{fl/fl}$ and Gch-KO BMDMs**

A) qRT-PCR mRNA measurement of *Slc2a1* gene encoding GLUT-1 protein in $Gch^{fl/fl}$ and Gch-KO $M^{Resting}$ ± HG ± M (n=5-6).
B) qRT-PCR mRNA measurement of *Slc2a1* gene encoding GLUT-1 protein in $Gch^{fl/fl}$ and Gch-KO $M^{LPS/IFN\text{-}\gamma}$ ± HG ± M (n=5-6).
C) Hexokinase 2 (HK2) gene expression in $Gch^{fl/fl}$ and Gch-KO $M^{Resting}$ ± HG ± M (n=5-6).
D) Hexokinase 2 (HK2) gene expression in $Gch^{fl/fl}$ and Gch-KO $M^{LPS/IFN\text{-}\gamma}$ ± HG ± M (n=5-6)
E) Western blot analysis of Hexokinase 2 in WT and Gch-KO macrophages ± LPS/IFN-γ and ± HG (n=4).

High glucose (20mM, HG) treatment for 24h treatment; Mannitol treatment (5mM glucose + 15mM Mannitol) treatment for 24h as an osmotic control (M)
Data are n=4-6 mean ± SEM. P values are calculated using a one-way ANOVA with Tukey's post-test (ns = P>0.05, *P<0.05, **P<0.01, ***P<0.001)


A
Slc2a1
Gene expression
2-ΔCt (GOI-ActB)
0.08
0.06
0.04
0.02
0.00
ns ns ns ns
LPS/IFN-γ - - - - - -
HG - + M - + M
Gchfl/fl
Gch-KO
B
Slc2a1
Gene expression
2-ΔCt (GOI-ActB)
0.08
0.06
0.04
0.02
0.00
ns ns ns ns
LPS/IFN-γ + + + + + +
HG - + M - + M
Gchfl/fl
Gch-KO
C
Hk2
Gene expression
2-ΔCt (GOI-ActB)
0.020
0.015
0.010
0.005
0.000
ns ns ns ns
LPS/IFN-γ - - - - - -
HG - + M - + M
Gchfl/fl
Gch-KO
D
Hk2
Gene expression
2-ΔCt (GOI-ActB)
0.020
0.015
0.010
0.005
0.000
ns ns ns ns
LPS/IFN-γ + + + + + +
HG - + M - + M
Gchfl/fl
Gch-KO
E
Gchfl/fl
Gch-KO
HG - - + + - - + +
LPS/IFN-γ - + - + - + - +
Hk2
102kDa
GAPDH
37kDa

### 4.4.2 IL1β and IL6 levels are unaltered with HG in $Gch^{fl/fl}$ and Gch-KO BMDMs

Next, the inflammatory profile of HG-treated $Gch^{fl/fl}$ and Gch-KO macrophages was explored. *IL1b* expression and cytokine release were unchanged with HG-treatment in both unstimulated and stimulated $Gch^{fl/fl}$ and Gch-KO macrophages (Figure 4.3A-C). This was similarly true for *IL6* gene expression and cytokine release (Figure 4.3D-F). No changes were observed with Mannitol (M) treatment, the osmotic control for HG treatment.

**Figure 4. 3 IL1β and IL6 levels are unaltered with HG in $Gch^{fl/fl}$ and Gch-KO BMDMs**

A) IL1β gene expression in $Gch^{fl/fl}$ and Gch-KO $M^{Resting}$ ± HG ± M (n=5-6)

B) IL1β gene expression in $Gch^{fl/fl}$ and Gch-KO $M^{LPS/IFN\text{-}\gamma}$ ± HG ± M (n=5-6).

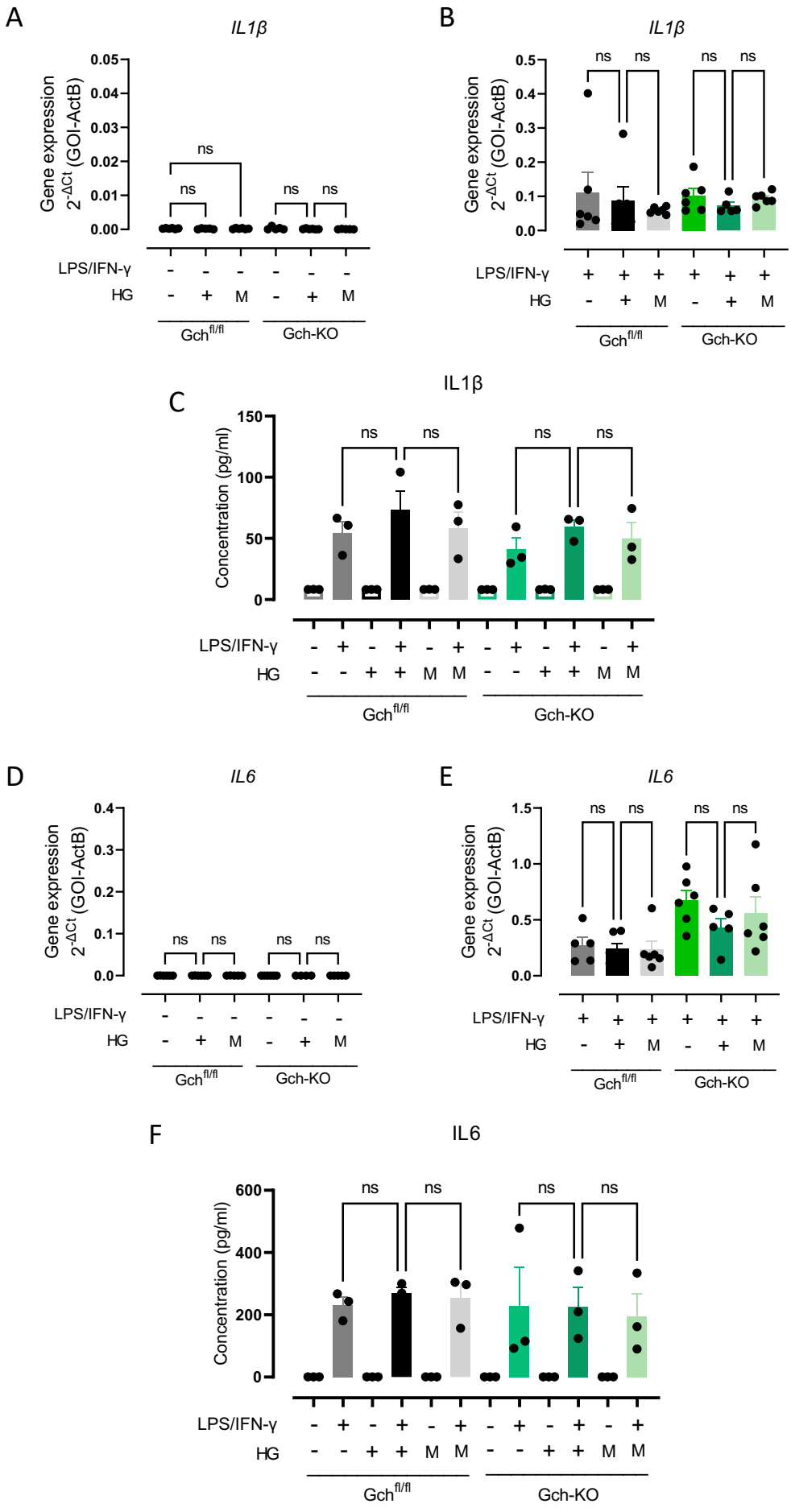
C) IL1β secretion in $Gch^{fl/fl}$ and Gch-KO macrophages ± LPS/IFN-γ and ± HG ± M (n=3)

D) IL6 gene expression in $Gch^{fl/fl}$ and Gch-KO $M^{Resting}$ ± HG ± M (n=5-6)

E) IL6 gene expression in $Gch^{fl/fl}$ and Gch-KO $M^{LPS/IFN\text{-}\gamma}$ ± HG ± M (n=5-6)

F) IL6 secretion $Gch^{fl/fl}$ and Gch-KO macrophages ± LPS/IFN-γ and ± HG ± M (n=3)

High glucose (20mM) treatment for 24h treatment; Mannitol treatment (5mM glucose + 15mM Mannitol) treatment for 24h as an osmotic control (M)
Data are n=3-6 mean ± SEM. P values are calculated using a one-way ANOVA with Tukey's post-test (ns = P>0.05, *P<0.05, **P<0.01, ***P<0.001)


A
IL1β
Gene expression
2-ΔCt (GOI-ActB)
0.05
0.04
0.03
0.02
0.01
0.00
ns
ns
ns
ns
LPS/IFN-γ - - - - - -
HG - + M - + M
Gch fl/fl
Gch-KO
B
IL1β
Gene expression
2-ΔCt (GOI-ActB)
0.5
0.4
0.3
0.2
0.1
0.0
ns ns ns ns
LPS/IFN-γ + + + + + +
HG - + M - + M
Gch fl/fl
Gch-KO
C
IL1β
Concentration (pg/ml)
150
100
50
0
ns ns ns ns
LPS/IFN-γ - + - + - + - + - + - +
HG - - + + M M - - + + M M
Gch fl/fl
Gch-KO
D
IL6
Gene expression
2-ΔCt (GOI-ActB)
0.4
0.3
0.2
0.1
0.0
ns ns ns ns
LPS/IFN-γ - - - - - -
HG - + M - + M
Gch fl/fl
Gch-KO
E
IL6
Gene expression
2-ΔCt (GOI-ActB)
1.5
1.0
0.5
0.0
ns ns ns ns
LPS/IFN-γ + + + + + +
HG - + M - + M
Gch fl/fl
Gch-KO
F
IL6
Concentration (pg/ml)
600
400
200
0
ns ns ns ns
LPS/IFN-γ - + - + - + - + - + - +
HG - - + + M M - - + + M M
Gch fl/fl
Gch-KO

### 4.4.3 NO production is unaltered with HG in $Gch^{fl/fl}$ and Gch-KO BMDMs

Nos2 gene expression and protein levels were unchanged with HG-treatment in $Gch^{fl/fl}$ and Gch-KO $M^{Resting}$ and $M^{LPS/IFN-\gamma}$ (Figure 4.4A-C). Nos2 (iNOS) protein levels did not change in $Gch^{fl/fl}$ and Gch-KO $M^{IL4}$ either (Figure 4.4C). Nitrite release was diminished in Gch-KO $M^{LPS/IFN-\gamma}$ as expected in a model of BH4 and NO deficiency. No changes in nitrite levels were observed in unstimulated and stimulated $Gch^{fl/fl}$ and Gch-KO macrophages with HG-treatment in $Gch^{fl/fl}$ and Gch-KO $M^{Resting}$ $M^{LPS/IFN-\gamma}$ (Figure 4.4D). However, previously observed genotype differences are maintained in the presence of HG treatment. No changes were observed with Mannitol (M) treatment, the osmotic control for HG treatment.

**Figure 4. 4 NO production is unaltered with HG in $Gch^{fl/fl}$ and Gch-KO BMDMs**

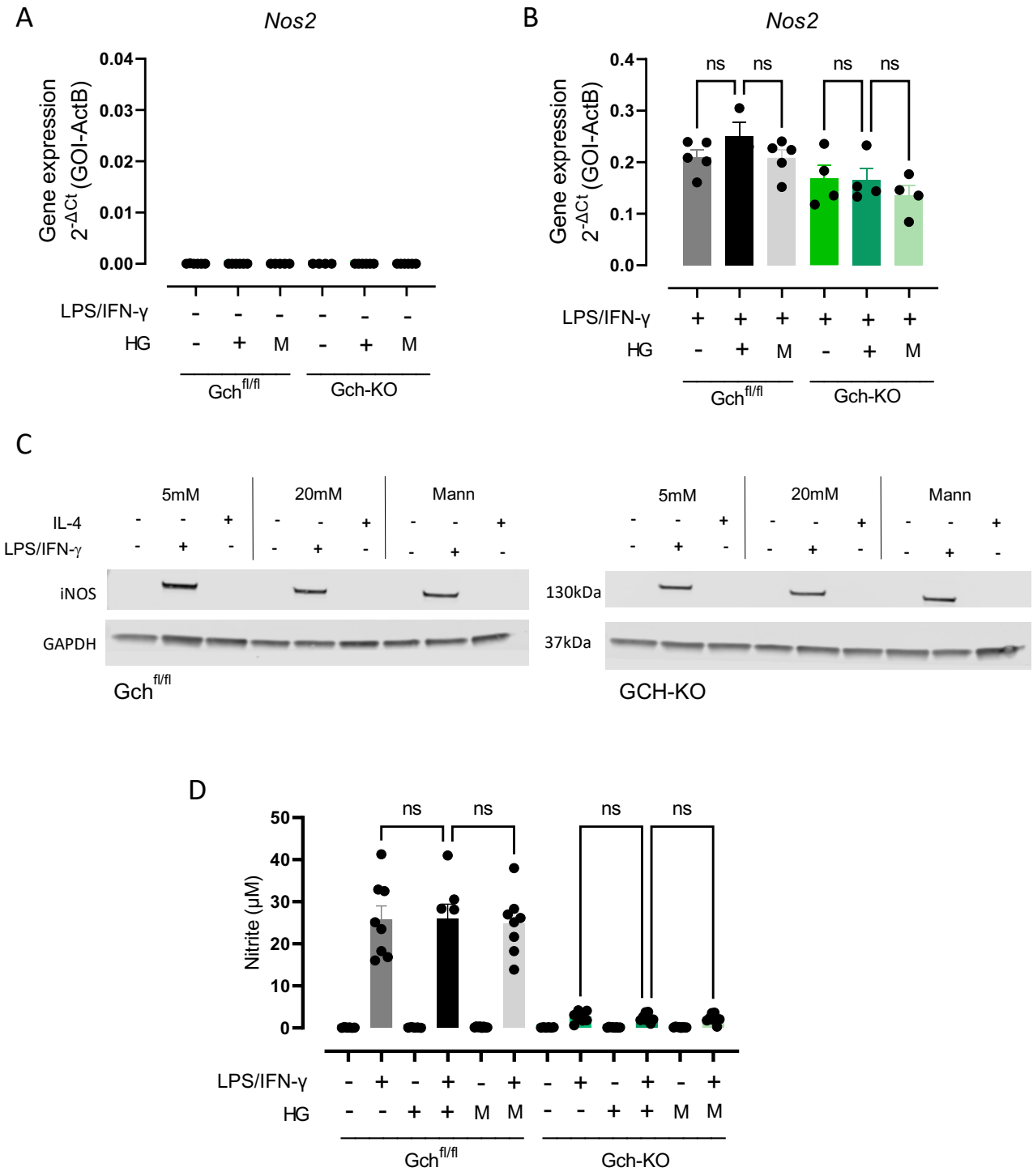
A) iNOS gene expression in $Gch^{fl/fl}$ and Gch-KO $M^{Resting}$ ± HG ± M (n=5-6)

B) iNOS gene expression in $Gch^{fl/fl}$ and Gch-KO $M^{LPS/IFN-\gamma}$ ± HG ± M (n=5-6)

C) Western blot analysis of iNOS in $Gch^{fl/fl}$ and Gch-KO ± LPS/IFN-γ and ± HG ± M (n=4)

D) Nitrite levels measured by Griess assay in $Gch^{fl/fl}$ and Gch-KO ± LPS/IFN-γ and ± HG ± M (n=4)

High glucose (20mM) treatment for 24h treatment; Mannitol treatment (5mM glucose + 15mM Mannitol) treatment for 24h as an osmotic control (M)
Data are n=4-6 mean ± SEM. P values are calculated using a one-way ANOVA with Tukey's post-test (ns = P>0.05, *P<0.05, **P<0.01, ***P<0.001)


A
Nos2
Gene expression
2-ΔCt (GOI-ActB)
0.04
0.03
0.02
0.01
0.00
LPS/IFN-γ
HG
Gchfl/fl
Gch-KO
B
Nos2
ns
0.4
0.3
0.2
0.1
0.0
C
5mM
20mM
Mann
IL-4
LPS/IFN-γ
iNOS
GAPDH
130kDa
37kDa
Gchfl/fl
GCH-KO
D
Nitrite (μM)
50
40
30
20
10
0

### 4.4.4 Irg1 expression and itaconate levels are unaltered HG in Gch$^{fl/fl}$ and Gch-KO BMDMs

With continued interest in itaconate production, IRG1 was unchanged with HG treatment in Gch$^{fl/fl}$ and Gch-KO M$^{Resting}$ and M$^{LPS/IFN-\gamma}$ (Figure 4.5A-C). IRG1 protein levels did not change in Gch$^{fl/fl}$ and Gch-KO M$^{IL4}$ either (Figure 4.5C). Increased itaconate levels in Gch-KO M$^{LPS/IFN-\gamma}$ compared to Gch$^{fl/fl}$ M$^{LPS/IFN-\gamma}$, as seen in Chapter 3, were maintained in the presence of HG treatment. Intracellular and extracellular itaconate levels were also unchanged in Gch$^{fl/fl}$ and Gch-KO macrophages with HG-treatment (Figure 4.5D-E). Increased levels of IRG1 and itaconate due to genotype were maintained in the presence of HG-treatment (Figure 4.5B and 4.5E).

**Figure 4. 5 Irg1 expression and itaconate levels are unaltered with HG in Gch$^{fl/fl}$ and Gch-KO BMDMs**

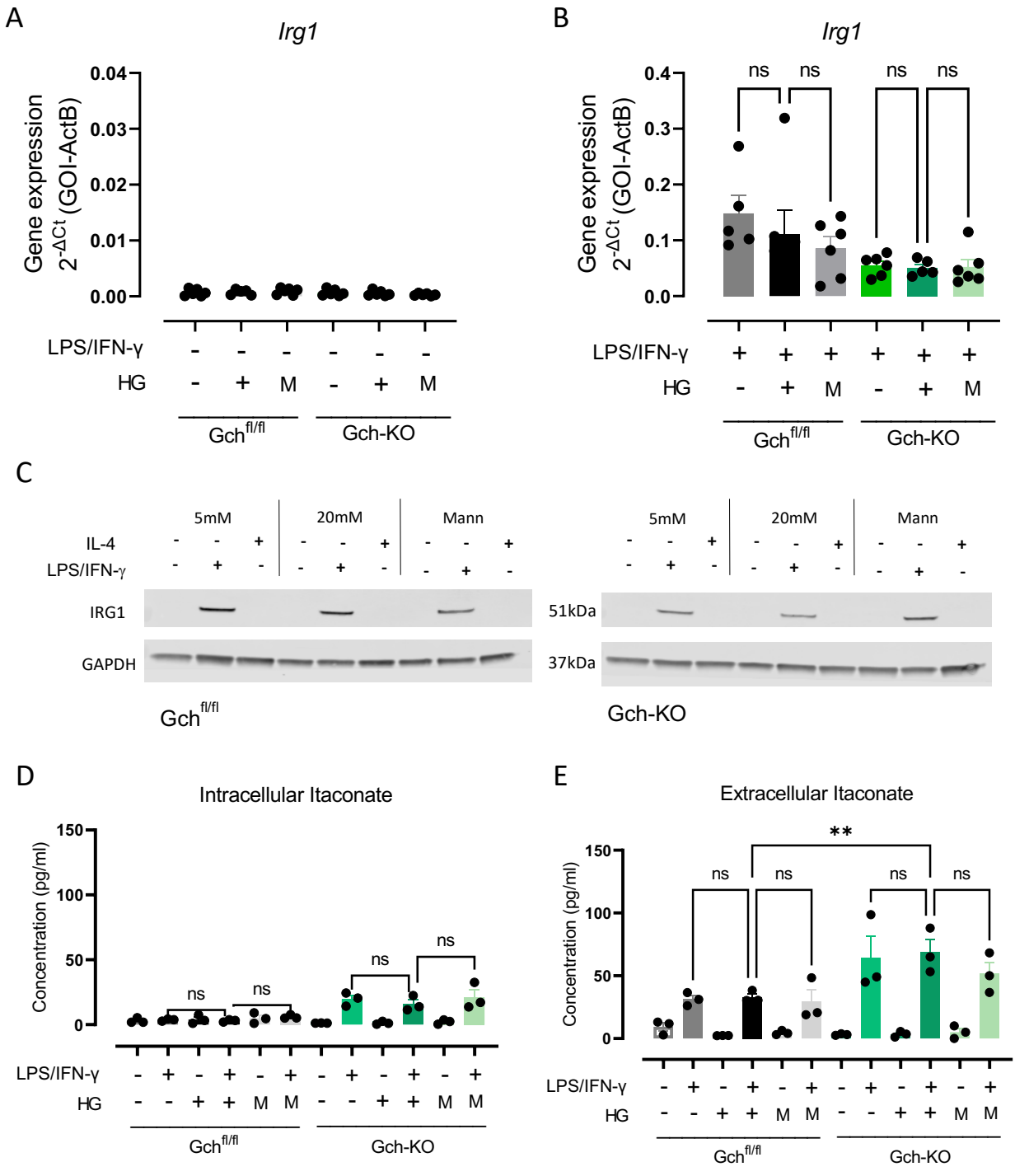
A) *Irg1* gene expression in Gch$^{fl/fl}$ and Gch-KO M$^{Resting}$ ± HG ± M (n=5-6)

B) *Irg1* gene expression in Gch$^{fl/fl}$ and Gch-KO M$^{LPS/IFN-\gamma}$ ± HG ± M (n=5-6)

C) Western blot analysis of IRG1 in Gch$^{fl/fl}$ and Gch-KO ± LPS/IFN-γ and ± HG ± M (n=4)

D) Intracellular itaconate levels measured by HPLC Gch$^{fl/fl}$ and Gch-KO ± LPS/IFN-γ and ± HG ± M (n=4)

High glucose (20mM) treatment for 24h treatment; Mannitol treatment (5mM glucose + 15mM Mannitol) treatment for 24h as an osmotic control (M)
Data are n=4-6 mean ± SEM. P values are calculated using a one-way ANOVA with Tukey's post-test (ns = P>0.05, *P<0.05, **P<0.01, ***P<0.001)


A
Irg1
Gene expression
2-ΔCt (GOI-ActB)
0.04
0.03
0.02
0.01
0.00
LPS/IFN-γ
HG
Gchfl/fl
Gch-KO
B
Irg1
ns
0.4
0.3
0.2
0.1
0.0
C
5mM
20mM
Mann
IL-4
LPS/IFN-γ
IRG1
GAPDH
51kDa
37kDa
D
Intracellular Itaconate
Concentration (pg/ml)
150
100
50
0
E
Extracellular Itaconate
**

### 4.4.5 Literature on hyperglycaemic macrophages reveal inconsistent results

As in vitro hyperglycaemia did not alter pro-inflammatory gene expression or cytokine release, we further interrogated the literature on hyperglycaemia in macrophages. This revealed that a range of models and treatments are used in the study of hyperglycaemic macrophages, which yield various results in inflammatory gene and protein expression. Selected studies are shown in Table 4.1.

| Model | Glucose | Stimulation | Findings | Ref |
|---|---|---|---|---|
| BMDM WT | 5 v 20mM | LPS + IFN-γ (16-18h) | **I:** →IL1β, → IL6, →iNOS, →NO, **M:** →Glut1, →Hk2, →IRG1, →itaconate | This study |
| BMDM C57BL/6 mice | 5 v 20mM | LPS + IFN-γ (16-18h) | **I:** ↑IL6, ↓Ym1, Fizz1 **M:** ↑succinate, ↑malate, ↑pyruvate, ↑ lactate | (Edgar et al., 2021) |
| BMDM C57BL/6 mice | 5.5 v 25 v 40mM for (3d+) 4d | LPS + IFN-γ (24h) | **I:** ↓IL-6 48h-HG (→ at 3,6,12,24h) in M1. ↓NO after 25mM 7d in M0 and M1 | (Ayala et al., 2019) |
| BMDM C57BL/6 mice. | 5.5 v 25-40mM for 24h or 7d | LPS + IFN-γ (24h) | **I:** →IL6 in 24h-HG M0. →IL6 in 24h-HG M1. →IL6 in 7d-HG M0. →IL6 in 7d-HG M1. ↑IL1β gene after 24h-HG and 7d-HG in M0 and M1. ↑IL1β after 24h-HG, not 48h-HG. ↓NO after 7d-HG in M1s.→NO after 24h | (Pavlou et al., 2018) |
| WT BMDM | 5 v 25mM (24h) | LPS (18h) | **I:** ↑iNOS gene expression in HG | (Parathath et al., 2011) |
| BMDM STZ-diabetic mice | 11mM (7d) | LPS +IFN-γ | **I:** ↓IL6 in diabetic M1, ↓TNF-α in diabetic M1, ↓NO, | (Sun et al., 2012) |
| BMDM STZ-diabetic mice | 5 v 20mM | LPS + IFN-γ (16-18h). | **I:** ↑IL6 →NO ↓Ym1 ↓Fizz1 | (Edgar et al., 2021) |
| BMDM Alloxan-diabetic mice | Alloxan; 5.5 v 25 v 40mM (24h v 48h v 7d) | LPS + IFN-γ (24h) | **I:** ↑IL6 in diabetic-M1s (7d). ↓ IL6 in HG-cultured diabetic-M1s (25mM & 40 mM) compared to NG-cultured diabetic M1s. ↑IL1β after 48h HG v 24h-HG in both diabetic and non-diabetic M1s. ↓NO levels in diabetic BMDM v WT. →NO in diabetic M0 or M1 with HG culture | (Ayala et al., 2019) |
| hMDM | 5 v 25mM (6 or 24h) | LPS + IFN-γ (6h). | **I:** ↑IL1β gene expression after 6h HG | (Moganti et al., 2017) |

Table 4. 1 Summary of selected studies on the effects of hyperglycaemia in macrophages

Summary of in vitro and in vivo hyperglycemia-induced changes in pro-inflammatory cytokine production or metabolism in different macrophage experimental models.
→no change, ↑ increased, ↓ decreased. NO = Nitric oxide. HG= High glucose. NG=Normal glucose. I = inflammatory markers. M=metabolic markers. STZ=streptozotocin. d=days.

## 4.5 Discussion

### 4.5.1 Overview

This study aimed to elucidate whether the metabolic or inflammatory profile of BH4-deficient macrophages would be altered with high glucose treatment stimulus. Although genotype differences were reproduced, high glucose treatment did not alter glycolytic gene expression or production of the anti-inflammatory metabolite itaconate. NO production and pro-inflammatory cytokine production also remained unaltered. In contrast to literature, wildtype macrophages too displayed unchanged inflammatory and metabolic profiles following HG treatment. However, a detailed literature search also revealed inconsistent findings on the inflammatory state of macrophages (IL6, IL1β, TNF-α, NO) potentially due to the variety of treatment models used. More consistent findings were observed in vivo, using diabetic mice, in comparison to in vitro high glucose treatment. Future work will focus on in vivo hyperglycaemia induced changes in macrophage metabolism.

### 4.5.2 HG as an inflammatory stimulus yields inconsistent results

Hyperglycaemia has been associated with increased inflammatory response in macrophages (Table 4.1). Despite this, HG-treatment did not alter inflammatory cytokine gene expression or secretion in WT or BH4-deficient macrophages. This was reported in another study where no changes were observed in IL1β cytokine levels even with 40mM HG treatment (Ayala et al., 2019). However, alterations in TNF-α were observed after 12-24 hours HG exposure, and IL6 levels increased after 48 hours HG exposure (Ayala et al., 2019). In another study, there were changes in IL1β but not in IL6 or iNOS expression and NO production. However, HG exposure for 7 days resulted in increased TNF-α in $M^{LPS/IFN\text{-}\gamma}$ (Pavlou et al., 2018). Finally, Edgar et al observed increased *IL6* gene expression, decreased *Ym1* and *Fizz1* expression and no changes in iNOS expression following 20mM exposure in murine BMDMs (Edgar et al., 2021).

HG treatment has also been tested in other macrophage models. In LPS-stimulated RAW 264 cells, 15mM glucose levels were sufficient to increase nitrite levels and iNOS protein. Additionally, proinflammatory cytokine release (IL1β, IL6) was increased with 48 hours exposure to 15mM or 25mM glucose levels; no changes were observed after 24 hours (Hua et al., 2012). In THP.1 cells, 24- and 48-hours exposure to 15mM glucose increased IL6 gene production (Devaraj et al., 2005). In human peripheral monocytes, 25mM glucose exposure did not yield inflammatory changes whereas 40mM glucose exposure increased IL1β, IL6 and TNF-α production (Akbari & Hassan-Zadeh, 2018). However other study showed human peripheral monocytes exposed to 35mM glucose levels only had increased TNF-α levels (Megawati et al., 2022).

In comparison, our study showed no changes in IL1β, IL6, iNOS or NO levels with 20mM high glucose treatment. This glucose concentration is commonly used but is on the lower range of what has been classed an in vitro high glucose stimulus experimentally, with other studies reaching up to 40mM glucose. Nonetheless, 20mM glucose levels are still higher than that seen in diabetic patients (>7.8mM glucose) (Moghissi et al., 2009; Umpierrez et al., 2012). When investigating the inflammatory profile of macrophages, many studies also looked at TNF-α levels, which will be included in follow up studies in the next chapter. Furthermore, we used 24 hours high glucose exposure time, which is also commonly used in the literature. Some studies see changes with 48 hours exposure or longer but also at shorter timepoints such as 12 hours. We chose 24-hour duration to study the effects of acute HG exposure, instead of 7 days HG exposure, as an example of prolonged HG-treatment. However, an even shorter duration may have been more appropriate considering blood glucose levels are increased 1-2 hours postprandial in diabetic individuals (Daenen et al., 2010).

### 4.5.3 Studies of HG as a metabolic stimulus report heterogenous results

Although there are no metabolic markers of specifically high glucose treatment, high glucose is expected to increase glycolysis, which is also a marker of inflammation, and there are known inflammation related metabolites. The majority of studies investigating the effects of high glucose on macrophage function focus on inflammatory markers and study metabolism superficially, if at all (Table 4.1). One study reported increased TCA cycle (succinate and malate) and glycolytic metabolites (lactate and pyruvate) following HG treatment in BMDMs (Edgar et al., 2021). This study also reported increased glycolysis ATP production rate, as measured by Seahorse, following acute 20 minutes exposure to glucose but not with 24 hours HG treatment. The ECAR and OCR readings also demonstrated a more glycolytic and less oxidative macrophage phenotype following HG treatment (Edgar et al., 2021). However, another study reported decreased glycolytic capacity of BMDMs exposed to high glucose for 24 hours and 7 days. Oxygen consumption rate was unchanged with short term and long term HG-treatment (Pavlou et al., 2018).

The most comprehensive look at metabolism was conducted in *Slc2a1* $^{-/-}$ macrophages, which lack the GLUT1 transporter and therefore display blunted glycolysis. *Slc2a1* $^{-/-}$ macrophages has reduced pro-inflammatory metabolites but increased ornithine and polyamines, which indicates an anti-inflammatory phenotype shift. Increased glutamine contribution to the TCA cycle was also observed in *Slc2a1* $^{-/-}$ resting macrophages. Decreased glycolysis in both $M^{Resting}$ and $M^{LPS/IFN\text{-}\gamma}$ decreased plaque stability (Freemerman et al., 2014). However, this study, although it links glucose metabolism and inflammatory response, it does not investigate HG treatment specifically.

### 4.5.4 In vitro vs in vivo hyperglycaemia – differences in models and methodology

After conducting a targeted and thorough literature review, it was apparent that a variety of glucose levels (5-40mM), stimuli (LPS, IFN-γ, LPS+IFN-γ, BCG, oxLDL), lengths of

stimulation (4h-7days) and models (BMDM, RAW cells, THP1, human monocytes) are used to study the effects of high glucose on macrophages. This could explain the variability in results, particularly the effects of high glucose on cytokine production. Moreover, even when comparing studies solely using murine BMDMs stimulated with LPS+IFN-γ for 18-24 hours, there are differences in IL6, IL1β, TNF-α, NO production reported (Table 4.1).

More consistent findings were reported in macrophages derived from diabetic mouse models, exposed to in vivo hyperglycaemia. BMDMs from STZ-induced diabetic mouse model had increased *IL6* gene expression, and decreased *Ym1* and *Fizz1* gene expression (Edgar et al., 2021). In another study, alloxan-diabetic macrophages had increased IL6 production as well as increased IL1β, and decreased TNF-α and NO production. Decreased lactate levels were also observed. These changes were present regardless of additional in vitro HG-treatment (Ayala et al., 2019).

Pro-inflammatory cytokines are the most commonly used and commonly altered markers of HG treatment. However, other markers of inflammation aside from pro-inflammatory cytokine and NO production could be upregulated with HG stimuli. These include superoxide production, hydrogen peroxide, and readouts of macrophage function. Our small study might have benefitted from studying these other readouts. In one study, the phagocytic capacity of BMDMs was not altered with HG-treatment but was decreased in alloxan-diabetic macrophages (Ayala et al., 2019). Furthermore, HG-treatment decreased hydrogen peroxide levels, regardless of macrophage activation and there was decreased TLR4 cell surface expression in the same study with both HG-treatment and alloxan-diabetes (Ayala et al., 2019). As mentioned earlier, decreased glycolysis has also been linked to decreased plaque stability (Freemerman et al., 2014). High glucose treatment also increased mouse monocyte adhesion to endothelial cells and oxLDL uptake was increased in BMDMs resulting in higher levels of foam cell formation (Edgar et al., 2021).

Overall, this suggests not only that in vivo hyperglycaemia yields more consistent changes in the inflammatory profile of macrophages but also that HG-treatment does not mimic the in vivo environment.

### 4.5.5 Future work

This chapter sought to investigate the effects of high glucose on the inflammatory and metabolic profile of wildtype and BH4-deficient macrophages. Finding limited changes, it is apparent that the literature in this area contains much variability, particularly with in vitro high glucose treatment. Furthermore, the effects of hyperglycaemia on metabolite levels in macrophages is not well studied. To follow on from these findings and observations, in Chapter 5 we will investigate the effects of in vivo hyperglycaemia with and without HG treatment on inflammatory markers, with a specific focus on macrophage metabolism.

# Chapter 5

## Hyperglycaemia induced changes in macrophage metabolism

# Chapter 5: Hyperglycaemia-induced changes in macrophage metabolism

## 5.1 Introduction

Trained immunity is a form of innate immune cell memory involving long term epigenetic and metabolic reprogramming. Innate immune cells, including macrophages, can adopt prolonged pro-inflammatory states after initial encounters with pathogens or other stimuli. Many stimuli such as bacilli Calmette-Guerin (BCG), β-glucan, oxLDL as well as hyperglycaemia have been reported to induce trained immunity in monocytes or macrophages. In diabetic patients it has been observed that even well controlled blood sugar levels do not mitigate increased risk of cardiovascular diseases including myocardial infarction (Gerstein et al., 2011). This could be explained by hyperglycaemic memory in innate immune cells which reportedly results in a heightened, more pro-inflammatory response in macrophages and increased risk of atherosclerosis development even after glucose levels have been normalised (Edgar et al., 2021).

Hyperglycaemia has been reported to directly alter cellular metabolism and immune cell function (Ayala et al., 2019; Edgar et al., 2021; Freemerman et al., 2014; Pavlou et al., 2018). Despite this, in the previous chapter, we found surprisingly few changes with high glucose treatment in murine BMDMs. However, the literature is variable on HG-treatment on the inflammatory profile of macrophages, and effects on macrophage metabolism are not well studied. Furthermore, in vivo hyperglycaemia demonstrated more consistent and disease-relevant findings compared to in vitro HG-treatment. To study the effects of HG-treatment and in vivo hyperglycaemia on the inflammatory and metabolic profile of macrophages, the βV59M mouse model of diabetes was used.

The βV59M-diabetic mouse is a transgenic mouse model expressing the human neonatal diabetes mutation (Kir6.2-V59M) resulting in alterations in the $K_{ATP}$ channels in pancreatic beta cells, which are well-known to regulate glucose stimulated insulin secretion (Brereton

et al., 2014). $K_{ATP}$ channels are open in normoglycemic conditions. High glucose promotes intracellular ATP formation which closes $K_{ATP}$ channels, resulting in membrane depolarisation and exocytosis of insulin. The Kir6.2-V59M mutation prevents closure of $K_{ATP}$ channels, and hence insulin secretion, which results in hyperglycaemia. As well as being an inducible model, the hyperglycaemia can be reversed in this model with the use of sulfonylurea drugs, although this feature was not used in this study. The βV59M model was developed by the laboratory of Dame Frances Ashcroft, and has been characterised and published on extensively (Brereton et al., 2014; Brereton et al., 2016; Haythorne et al., 2022; Haythorne et al., 2019). Of note, βV59M-diabetic mice are hyperglycaemic but do not have dyslipidaemia. This allows the effects of high glucose to be studied more specifically, which is difficult to achieve in more commonly used and more severe models of diabetes such as streptozotocin (STZ)-induced, alloxan induced, nonobese diabetic mice.

We hypothesised that in vivo hyperglycaemia would train macrophages to have an increased inflammatory response upon a second stimulus. Training can be induced with the same or a different inflammatory stimulus (Divangahi et al., 2021). In this study, two secondary inflammatory stimuli were used; high glucose (HG) treatment, LPS/IFNγ, as well as both (HG + LPS/IFNγ) in case of an additive effect or nulling effect. If hyperglycaemia is an inflammatory stimulus with training capacity, $M^{Resting}$ may appear to have an inflammatory or metabolic profile more similar to that of $M^{LPS/IFN\gamma}$. Furthermore, $M^{LPS/IFN\gamma}$ may display an even more pro-inflammatory phenotype.

## 5.2 Hypothesis and Aims

### 5.2.1 Hypothesis

In this chapter, it was hypothesised that in vivo hyperglycaemia increases pro-inflammatory cytokine release and induces training in $M^{Resting}$ and $M^{LPS/IFN\gamma}$. It was proposed that a metabolomics study would highlight the metabolic pathways underlying hyperglycaemia-induced effects. A particular focus was placed on TCA cycle substrates and inflammation related metabolites.

### 5.2.2 Aims

Aim 1: To investigate how hyperglycaemia alters macrophage inflammatory response

Aim 2: To investigate whether in vivo hyperglycaemia alters macrophage metabolism in response to LPS/IFNγ stimulation

Aim 3: To investigate the role of in vivo hyperglycaemia induces training in macrophages as seen by their metabolic profile

## 5.3 Methods

### 5.3.1 Cell culture

Cell culture protocol for the differentiation and polarisation of βV59M-diabetic bone marrow derived macrophages is outlined below (Figure 5.1). For more details on the βV59M-diabetic mouse model, see section 2.2.2.

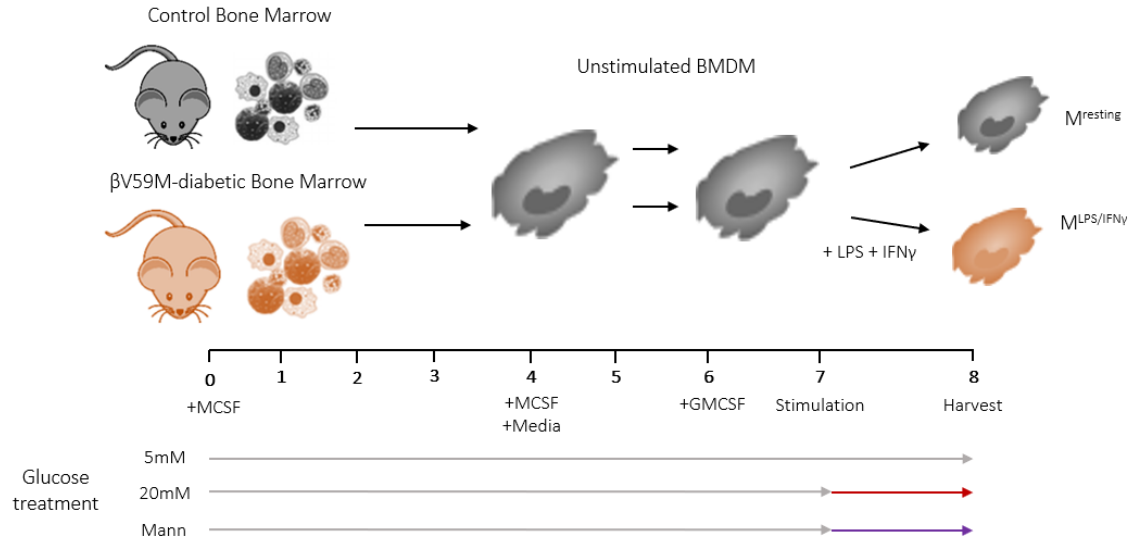



**Figure 5. 1 Schematic of βV5M-diabetic BMDM culture protocol**

Bone marrow derived macrophages from Control and βV5M-diabetic mice. Cells are cultured over 8 days. On Day 4, cells are given 50% additional media containing MCSF. On Day 6, cells are treated with GMCSF. On Day 7 cells are stimulated with LPS/IFN-γ to polarise into inflammatory $M^{LPS/IFN-\gamma}$ state. In addition, cells are left in normoglycaemia, stimulated with high glucose (20mM), or 5mM glucose+15mM Mannitol (Mann) as an osmotic control, for 24 hours before harvest.

### 5.3.2 Metabolomics sample preparation

Cells were harvested and pellets immediately frozen on dry ice and stored at -80 °C prior to shipping to Metabolon on dry ice. Samples were prepared by Metabolon using the automated MicroLab STAR® system from Hamilton Company. Proteins were precipitated with methanol, and the resulting extract divided into fractions for analysis by reverse phase (RP)/UPLCMS/MS methods with positive ion mode electrospray ionization (ESI), with

negative ion mode ESI, and HILIC/UPLC-MS/MS with negative ion mode ESI. All methods utilised a Waters ACQUITY ultra-performance liquid chromatography (UPLC) and a Thermo Scientific Q-Exactive high resolution/accurate mass spectrometer interfaced with a heated electrospray ionization (HESI-II) source and Orbitrap mass analyser operated at 35,000 mass resolution.

### 5.3.3 Metabolomics analysis

Raw data were extracted, peak-identified and QC processed using Metabolon's hardware and software built on a web-service platform using Microsoft's .NET technologies. Compounds were identified by comparison to library entries of purified standards or recurrent unknown entities. Metabolon maintains a library based on authenticated standards that contains the retention time/index (RI), mass to charge ratio (m/z), and chromatographic data (including MS/MS spectral data). Peaks were quantified using area-under-the-curve. Data were normalised to protein concentration as determined by Bradford assay. Two samples from diabetic $M^{LPS/IFN-\gamma}$ -HG treated macrophages were excluded from analysis due to low protein concentration measured by Bradford assay, performed by Metabolon. All other groups have full n=6 sample set. One-way ANOVA contrasts were used to identify metabolites that differed significantly ($P \leq 0.05$) between experimental groups.

Enrichment analysis and pathway analyses were conducted using MetaboAnalyst v5.0. Pathways highlighted were determined by comparison between Control $M^{LPS/IFN-\gamma}$ compared to Diabetic $M^{LPS/IFN-\gamma}$ +HG treatment. Metabolites were normalised by the median, log-transformed and scaled to prepare for data analysis. For enrichment analysis, metabolite set enrichment analysis (MSEA) is performed based on Kyoto Encyclopaedia of Genes and Genomes (KEGG) pathway database. Pathway analysis of the metabolomics dataset integrated pathway enrichment analysis and pathway topology analysis based on compounds in KEGG pathway library. Significance threshold was set at $P<0.05$.

## 5.4 Results

### 5.4.1 βV59M-diabetic mouse model

Upon tamoxifen treatment, βV59M-diabetic mice exhibited blood glucose of at least 20mM (Figure 5.2A). Blood glucose measurements for the majority of mice measured 30mM, which is the glucose monitor's maximum measurement (Figure 5.2A). The number of bone marrow derived macrophages derived from βV59M-diabetic mice was similar to that derived from WT mice (Figure 5.2B). Upon stimulation βV59M-diabetic $M^{LPS/IFN\text{-}\gamma}$ had increased nitrite levels compared to $M^{Resting}$, but were not altered with in vitro or in vivo hyperglycaemia (Figure 5.2C).

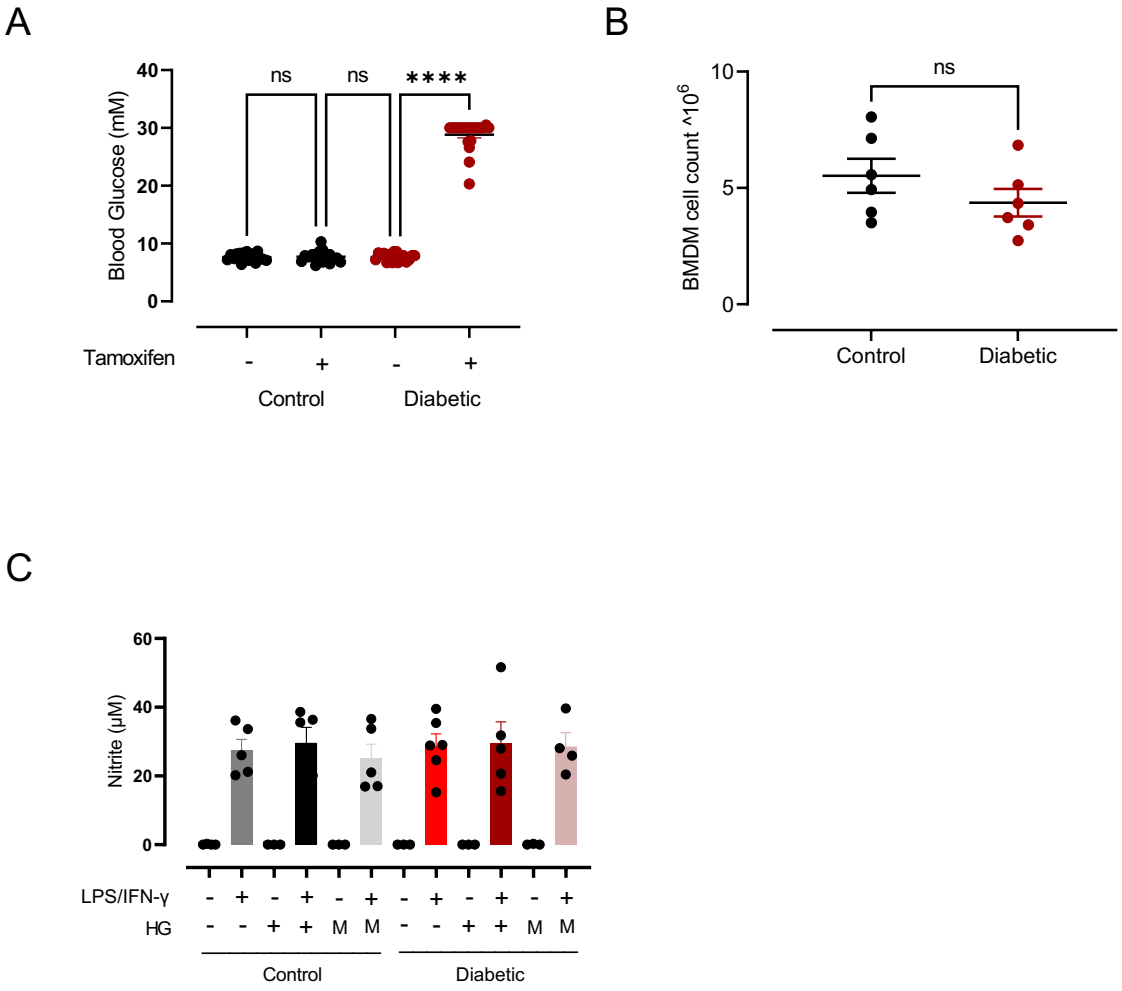



**Figure 5. 2 Overview of diabetic mouse model**

A) Blood glucose levels of βV59M-diabetic mouse model pre and post tamoxifen (1µM 4-OHT) administration which induces mutation to present insulin secretion in pancreatic beta cells (n=15)
B) BMDM cell counts from Control and βV59M-diabetic mice (n=6)
C) Nitrite levels in Control and βV59M-diabetic macrophages, $M^{LPS/IFN-\gamma}$, ± High Glucose (HG) treatment with Mannitol (M) as a control stimulus (n=4-6)
Data are mean ± SEM. P values are calculated using a one-way ANOVA with Tukey's post-test (****P<0.0001)

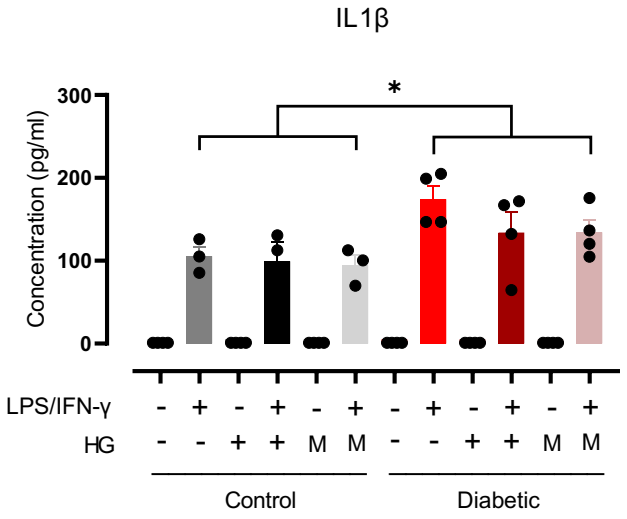
### 5.4.2 βV59M-diabetic mice have altered inflammatory profile

Upon stimulation, there was an increase in IL1β, IL6 and TNF-α cytokine release in both WT and βV59M-diabetic $M^{LPS/IFN-\gamma}$ (Figure 5.3A-C). There was a 37% increase in IL1β levels in the βV59M-diabetic $M^{LPS/IFN-\gamma}$ group (Figure 5.3A) but a decrease in TNF-α levels compared to the WT $M^{LPS/IFN-\gamma}$ group (Figure 5.3C). However, there were no changes in IL6 levels with in vitro or in vivo hyperglycaemia (Figure 5.3B). Overall, these results suggest in vivo, rather than in vitro, hyperglycaemia is driving any changes observed in inflammatory cytokine levels. Neither IL1β, IL6 nor TNF-a levels were altered with Mannitol treatment in comparison with non-HG-treated counterparts.

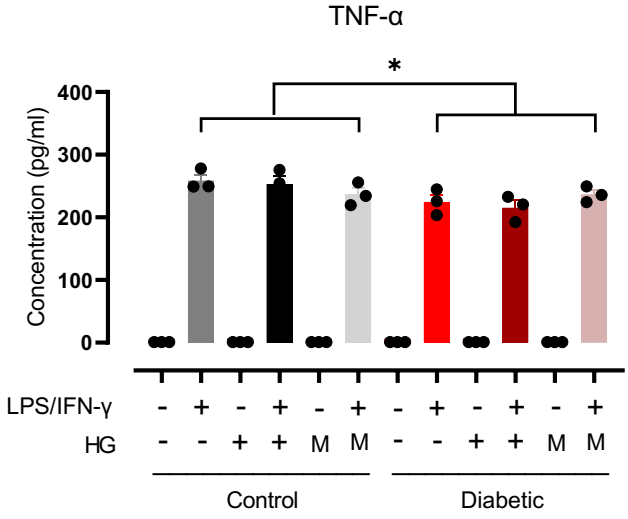
**Figure 5. 3 IL1β and TNF-α levels are increased in control and diabetic macrophages ± LPS/IFN-γ and ± HG**

A) IL1β secretion in unstimulated and LPS/IFN-ɣ stimulated Control and 2-week βV59M-diabetic macrophages cultured in 5mM and 20mM glucose levels (n=3-4)
B) IL6 secretion in unstimulated and LPS/IFN-ɣ stimulated Control and 2-week βV59M-diabetic macrophages cultured in 5mM and 20mM glucose levels (n=3-4)
C) TNF-α secretion in unstimulated and LPS/IFN-ɣ stimulated Control and 2-week βV59M-diabetic macrophages cultured in 5mM and 20mM glucose levels (n=3-4)
Data are n=3-4 mean ± SEM. Significance shown refers to a genotype change irrespective of HG treatment (Control $M^{LPS/IFN\gamma}$ v Diabetic $M^{LPS/IFN\gamma}$). P values are calculated using a one-way ANOVA with Tukey's post-test (*P<0.05, **P<0.01, ***P<0.001).

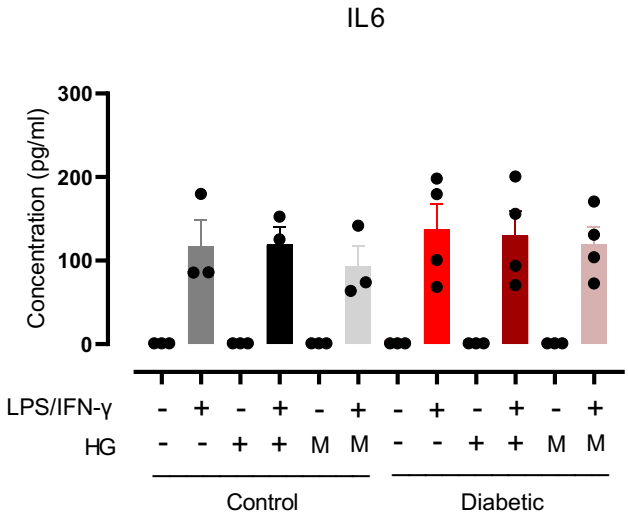
A


IL1β
*
Concentration (pg/ml)
300
200
100
0
LPS/IFN-γ - + - + - + - + - + - +
HG - - + + M M - - + + M M
Control
Diabetic

B


TNF-α
*
Concentration (pg/ml)
400
300
200
100
0
LPS/IFN-γ - + - + - + - + - + - +
HG - - + + M M - - + + M M
Control
Diabetic

C


IL6
Concentration (pg/ml)
300
200
100
0
LPS/IFN-γ - + - + - + - + - + - +
HG - - + + M M - - + + M M
Control
Diabetic

### 5.4.3 Itaconate levels are unaltered in βV59M-diabetic mice

Upon stimulation, there was a 2-3-fold increase in extracellular itaconate levels but no changes in intracellular itaconate levels in βV59M-diabetic mice (Figure 5.4A-B). There were no changes in intracellular or extracellular itaconate levels with in vitro or in vivo hyperglycaemia (Figure 5.4A-B).

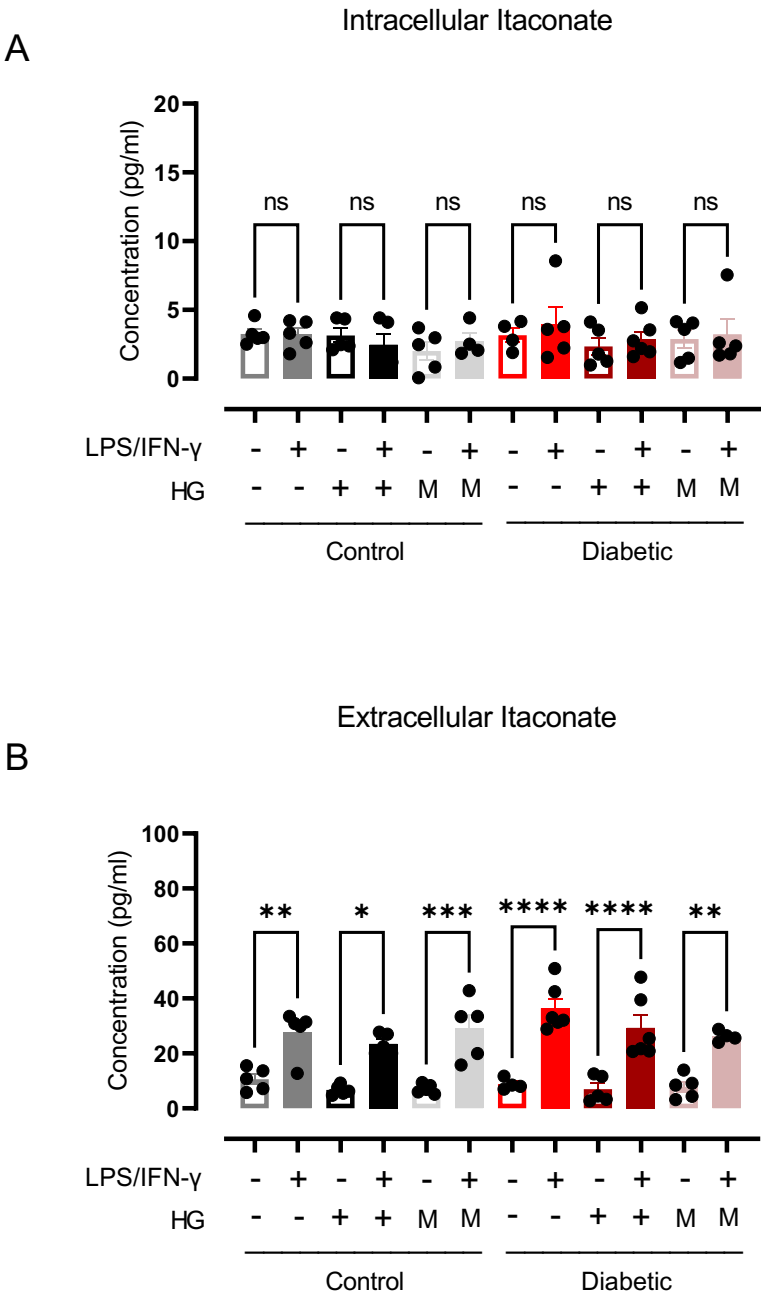



**Figure 5. 4 Itaconate levels are unchanged in control and diabetic macrophages ± LPS/IFN-γ and ± HG**

A) Intracellular itaconate levels measured by HPLC in LPS/IFN-ɣ stimulated HG-treated Control and 2-week βV59M-diabetic macrophages
B) Extracellular itaconate levels measured by HPLC in LPS/IFN-ɣ stimulated HG-treated Control and 2-week βV59M-diabetic macrophages
Data are n=4-6 mean ± SEM. P values are calculated using a one-way ANOVA with Tukey's post-test (*P<0.05, **P<0.01, ***P<0.001, ****P<0.0001)

### 5.4.4 Metabolomics analysis of Control and βV59M-diabetic macrophages

Based on initial changes in inflammatory cytokine release, we ran metabolomics analyses on 8 groups: Control and βV59M-diabetic macrophages ± LPS/IFN-γ and ± HG (Table 5.1). Note, βV59M-diabetic bone marrow have 2 weeks in vivo hyperglycaemia before exposure to culture conditions and stimuli.

This dataset was analysed with a view to answering 2 main questions:

1. Do diabetic macrophages respond differently to LPS/IFN-ɣ stimulation?
2. Does hyperglycaemia induce trained immunity in macrophages?

An overview of the data was gained with hierarchical clustering analysis (HCA), enrichment and pathway analyses, followed by in depth analysis of metabolic pathways. Metabolic pathways of interest were investigated (carbohydrate metabolism, fatty acid metabolism, glutamine metabolism) as well as pathways highlighted in the enrichment analysis (arginine metabolism, aspartate metabolism and sphingolipid metabolism). This workflow is shown in Figure 5.5.

| Control BMDM | βV59M-diabetic BMDM |
|---|---|
| 1. $M^{Resting}$ (-) HG | 5. $M^{Resting}$ (-) HG |
| 2. $M^{LPS/IFN-\gamma}$ (-) HG | 6.$M^{LPS/IFN-\gamma}$ (-) HG |
| 3. $M^{Resting}$ (+) HG | 7. $M^{Resting}$ (+) HG |
| 4.$M^{LPS/IFN-\gamma}$ (+) HG | 8.$M^{LPS/IFN-\gamma}$ (+) HG |

Table 5. 1 Samples sent for metabolomics analysis

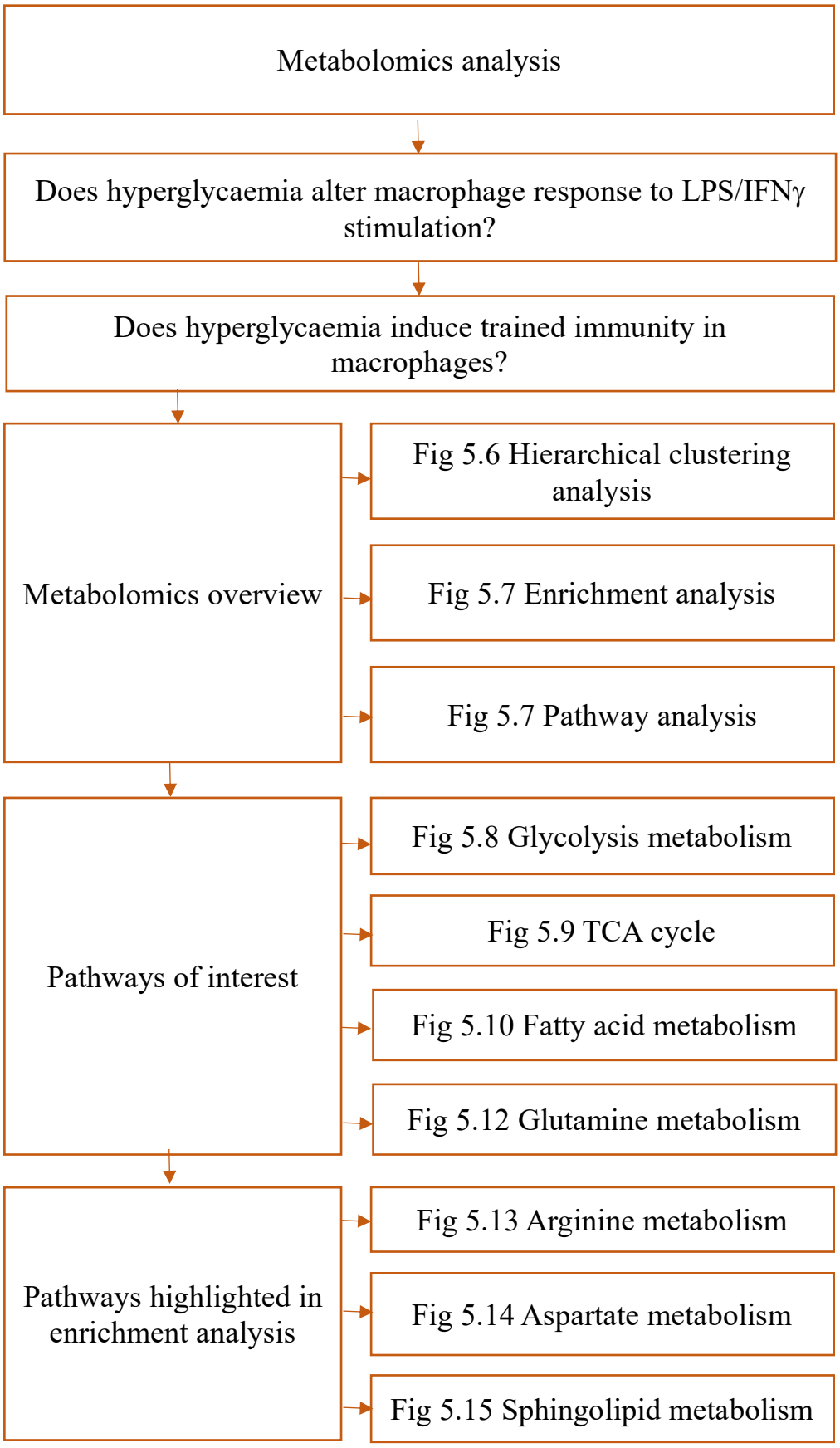



**Figure 5. 5 Metabolomics analysis workflow**

### 5.4.5 Hierarchical clustering analysis (HCA) of Control and βV59M-diabetic mice

To investigate the effects of hyperglycaemia on macrophage metabolism, metabolomics analysis was conducted on Control and βV59M-diabetic macrophages ± LPS/IFN-γ and ± HG stimuli. The highest level of clustering was due to LPS/IFN-γ stimulation (Figure 5.6).

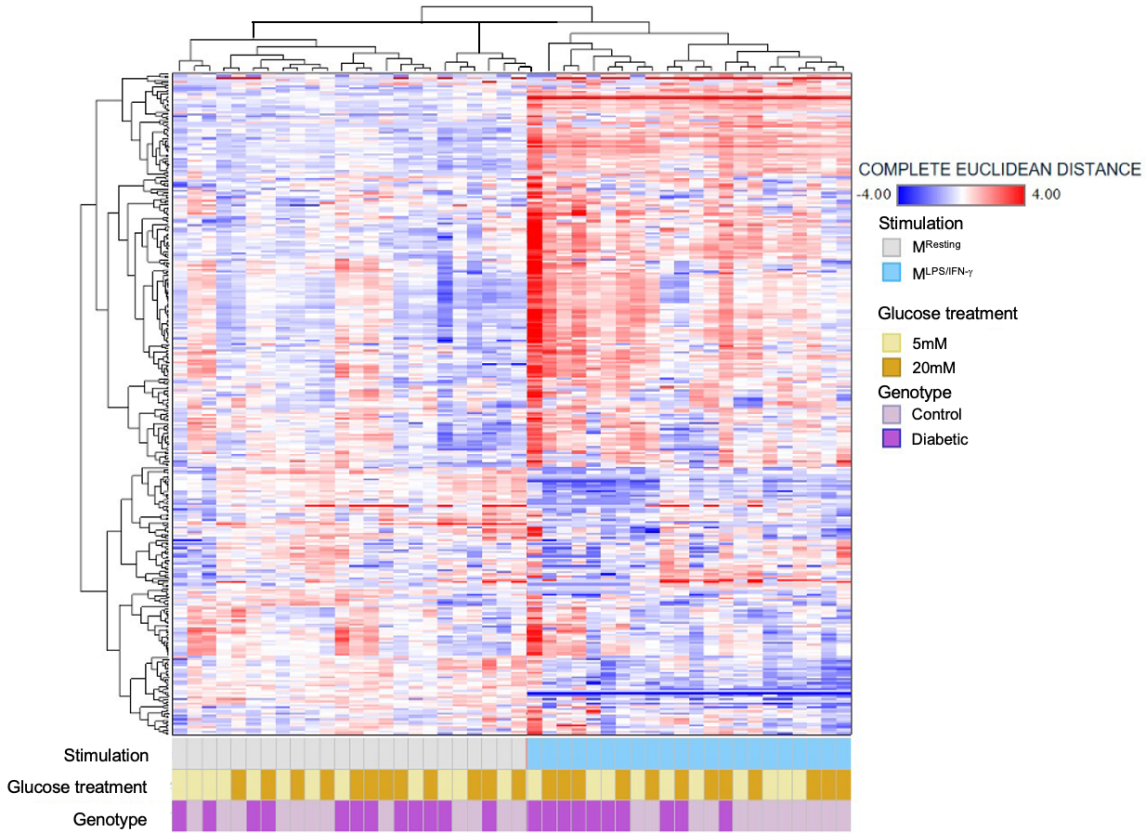



**Figure 5. 6 Hierarchical Clustering Analysis (HCA) of Control and βV59M-Diabetic macrophages samples based on stimulation, glucose treatment, and mouse genotype**

Samples are organized in columns and metabolites in rows. Increased metabolites compared to control are highlighted in red; decreased metabolites are highlighted in blue. Samples are further clustered by stimulation (LPS/IFNγ), in vitro glucose treatment and genotype (in vivo hyperglycaemia). HCA was performed by Metabolon.

### 5.4.6 Significantly altered metabolites in Control and βV59M-diabetic macrophages due to LPS/IFNγ and hyperglycaemia

As shown by hierarchical clustering, the greatest number of metabolite changes were due to stimulation (Table 5.2). Upon stimulation, the total number of metabolites changed was similar (180 metabolites) in both non-HG treated and HG-treated control and βV59M-diabetic macrophages (Table 5.2). The ratio of increased:decreased metabolites was 2:1 in Control $M^{Resting}$, Control $M^{LPS/IFN\text{-}\gamma}$ and 5mM βV59M-diabetic macrophages, but 5:1 in 5mM βV59M-diabetic macrophages. There were significantly more altered metabolites in $M^{LPS/IFN\text{-}\gamma}$ with in vivo hyperglycaemia (Table 5.3) than in HG-treatment (Table 5.4), but nonetheless fewer than with stimulation (Table 5.2). As hypothesised, this suggests that in vivo hyperglycaemia results in a greater number of metabolite changes compared to control, in comparison with in vitro HG-treatment.

| | | Metabolites (ANOVA p<0.05) | |
|---|---|---|---|
| Comparison | | Increased | Decreased |
| Control $M^{resting}$ vs Control $M^{LPS/IFN-\gamma}$ | −HG | 114 | 60 |
| | +HG | 103 | 65 |
| Diabetic $M^{resting}$ vs Diabetic $M^{LPS/IFN-\gamma}$ | −HG | 147 | 29 |
| | +HG | 146 | 54 |

Table 5. 2 Significantly altered metabolites due to LPS/IFN-ɣ stimulation in Control and βV59M-diabetic macrophages

| | | Metabolites (ANOVA p<0.05) | |
|---|---|---|---|
| Comparison | | Increased | Decreased |
| Control −HG vs Diabetic −HG | $M^{resting}$ | 2 | 7 |
| | $M^{LPS/IFN-\gamma}$ | 48 | 4 |
| Control +HG vs Diabetic +HG | $M^{resting}$ | 3 | 3 |
| | $M^{LPS/IFN-\gamma}$ | 39 | 4 |

Table 5. 3 Significantly altered metabolites due in Control and βV59M-diabetic macrophages

| | | Metabolites (ANOVA p<0.05) | |
|---|---|---|---|
| Comparison | | Increased | Decreased |
| Control −HG vs +HG | $M^{resting}$ | 11 | 0 |
| | $M^{LPS/IFN-\gamma}$ | 20 | 7 |
| βV59M-diabetic −HG vs +HG | $M^{resting}$ | 27 | 5 |
| | $M^{LPS/IFN-\gamma}$ | 6 | 8 |

Table 5. 4 Significantly altered metabolites due to HG-treatment in Control and βV59M-diabetic macrophages

### 5.4.7 Enrichment and pathway analysis

To gain an unbiased overview of the most changed pathways, enrichment analysis and pathway analysis of the metabolomics dataset was performed. The majority of pathways highlighted were related to glycolysis and the TCA cycle. Aside from already designated pathways of interest, arginine metabolism, aspartate metabolism and sphingomyelin metabolism were highlighted in the pathway analysis and subsequently followed up (Figure 5.7A-B).

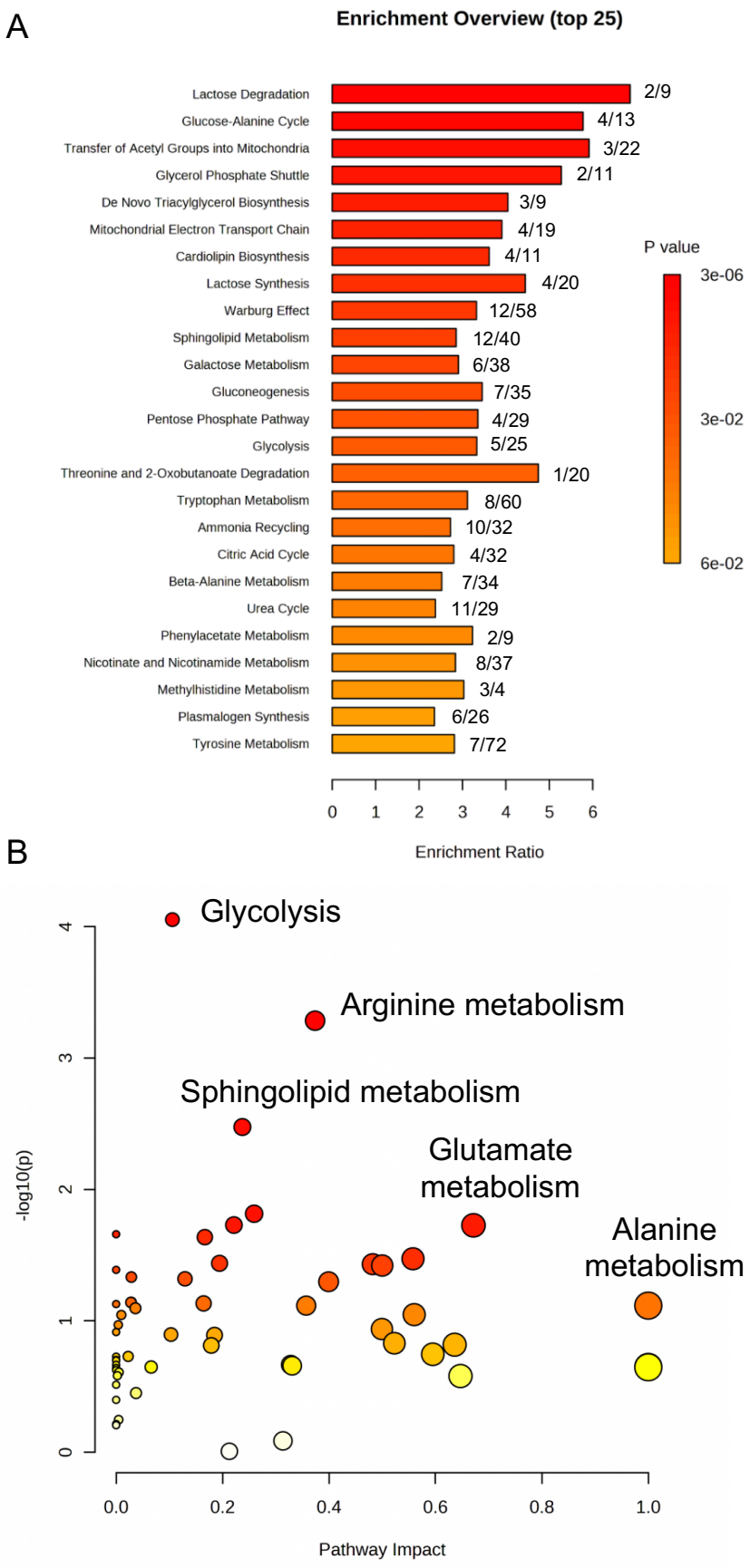



**Figure 5. 7 Enrichment analysis and pathway analysis**

A) Top 25 pathways highlighted, as well as number of metabolite hits per pathway, in enrichment analysis of Control $M^{LPS/IFN-\gamma}$ compared to Diabetic $M^{LPS/IFN-\gamma}$ +HG treatment.
B) Most impacted pathways highlighted by pathway analysis. Both analyses were conducted based on KEGG pathway database in MetaboAnalyst.

### 5.4.8 Glycolysis

Glucose levels were only increased following LPS/IFN-γ stimulation in HG-treated diabetic macrophages. HG-treatment doubled glucose levels in control and diabetic $M^{resting}$ and $M^{LPS/IFN-\gamma}$, possibly indicating increased glucose uptake. There were no glucose changes with genotype (in vivo hyperglycaemia) alone, but additional HG-treatment significantly increased glucose levels compared to the respective control group (Figure 5.8B). This demonstrates HG-treatment increased intracellular glucose levels. Furthermore, increase glucose levels indicated increased glucose uptake.

Dihydroxyacetone phosphate (DHAP) levels were increased 2-3 fold following LPS/IFN-γ stimulation in HG-treated control, non-HG-treated and HG-treated diabetic macrophages. HG-treatment doubled DHAP levels in control $M^{LPS/IFN-\gamma}$. Furthermore, there was a 1.8 fold increase in DHAP levels in diabetic $M^{LPS/IFN-\gamma}$ compared to control, which increased to 2.2 fold increase following additional HG-treatment (Figure 5.8C). 3-phosphoglycerate, PEP and glycerate levels were decreased in $M^{LPS/IFN-\gamma}$ but this did not reach significance (Figure 5.8A). Lactate levels were not altered following LPS/IFN-γ stimulation or due to in vivo hyperglycaemia. They did increase with HG-treatment in control $M^{LPS/IFN-\gamma}$ and following both in vivo and HG-treatment in diabetic $M^{LPS/IFN-\gamma}$ (Figure 5.8D).

In the Pentose Phosphate pathway, sedoheptulose levels increased with stimulation in control and diabetic $M^{LPS/IFN-\gamma}$. Levels did not change with genotype or HG-treatment (Figure 5.8E). Furthermore, phosphate levels only increased with stimulation in diabetic $M^{LPS/IFN-\gamma}$ (Figure 5.8F). This potentially suggests the PPP is increased with stimulation and this is normalised following an additional HG stimulus.

Overall, these findings suggest that in vivo hyperglycaemia and HG-treatment increase glycolysis in both resting and inflammatory macrophages. Furthermore, macrophages

exposed to in vivo hyperglycaemia have increased levels of key glycolytic metabolites suggesting an enhanced glycolytic phenotype.

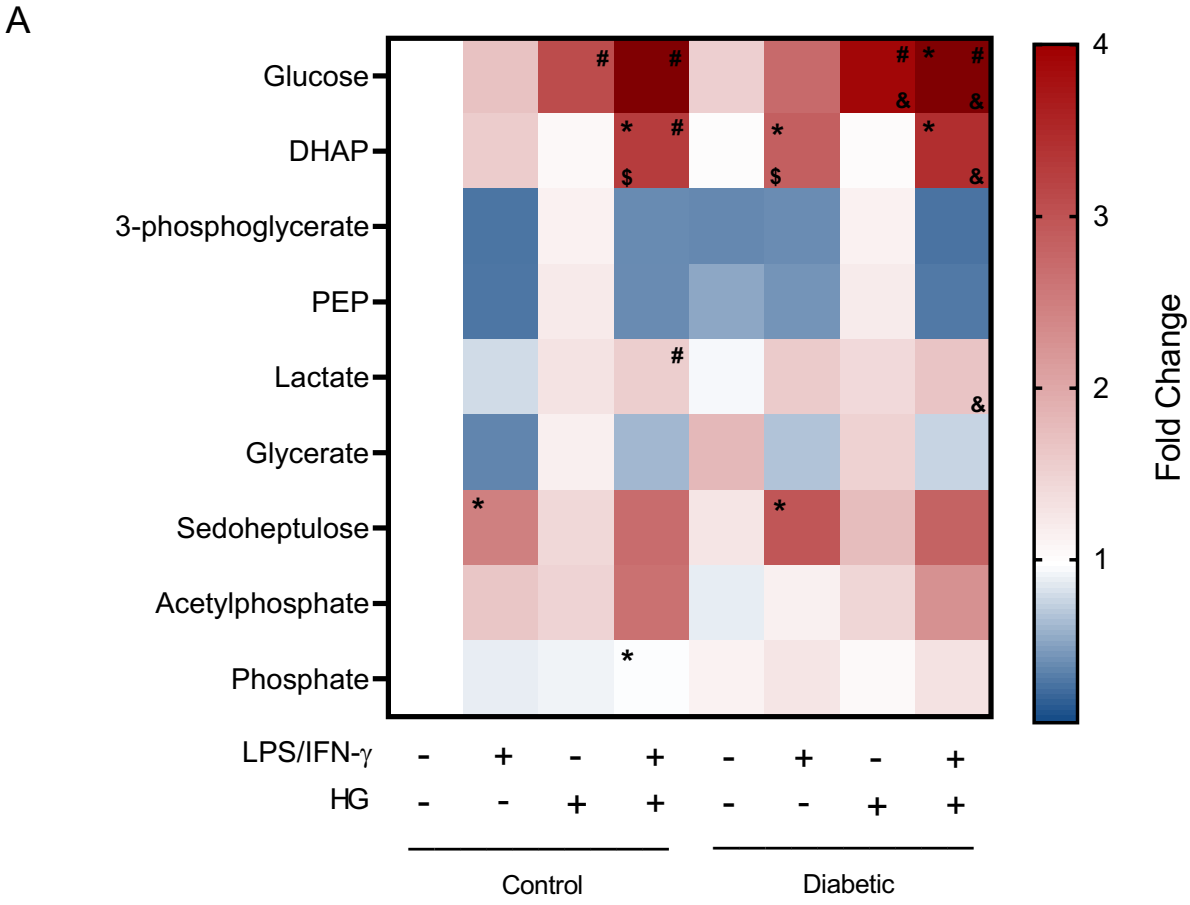
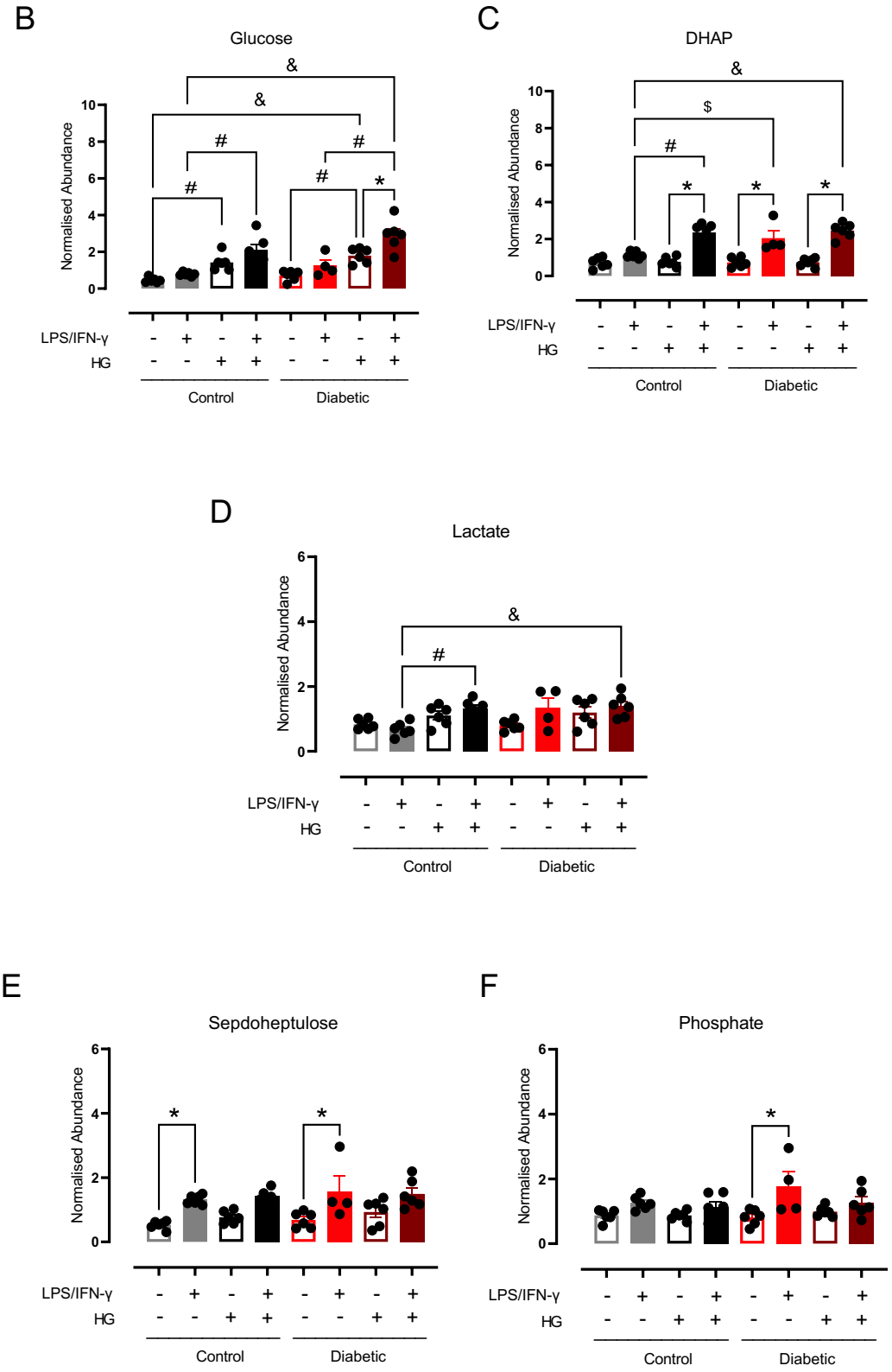



**Figure 5. 8 Glycolysis in control and diabetic macrophages ± LPS/IFN-γ and ± HG**

A) Fold change heatmap of glycolysis and pentose phosphate pathways relative to non-HG-treated unstimulated control macrophages
B) Glucose metabolite abundance
C) DHAP metabolite abundance
D) Lactate metabolite abundance
E) Sedoheptulose metabolite abundance
F) Phosphate metabolite abundance

in Control and βV59M-diabetic ± LPS/IFN-γ and ± HG. Data are n=4-6, mean ± SEM. P values are calculated using a one-way ANOVA with Tukey's post-test.

Heatmap notation:
(*) indicates P<0.05 for LPS/IFNγ stimulation vs control within the same genotype and HG-treatment
(#) indicates P<0.05 for HG-treatment vs control within the same genotype and polarisation state
($) indicates P<0.05 for genotype difference (control v diabetic)
(&) indicates P<0.05 for both in vivo hyperglycaemia + HG-treatment within the same polarisation state


B
Glucose
Normalised Abundance
LPS/IFN-γ
HG
Control
Diabetic
C
DHAP
Normalised Abundance
LPS/IFN-γ
HG
Control
Diabetic
D
Lactate
Normalised Abundance
LPS/IFN-γ
HG
Control
Diabetic
E
Sepdoheptulose
Normalised Abundance
LPS/IFN-γ
HG
Control
Diabetic
F
Phosphate
Normalised Abundance
LPS/IFN-γ
HG
Control
Diabetic

### 5.4.9 TCA cycle

In the resting macrophage, glycolysis feeds into the TCA cycle. In the inflammatory macrophage, breaks in the TCA cycle render it non-functional and lead to an accumulation of citrate and itaconate. Inflammation related metabolites, citrate and itaconate levels, were increased following LPS/IFN-γ stimulation in control and diabetic macrophages regardless of genotype and HG-treatment (Figure 5.9A-C). There were no changes in any other metabolites due to LPS/IFN-γ stimulation, HG-treatment or genotype (Figure 5.9A). This suggests the broken TCA cycle is not altered by hyperglycaemia. Finally, aconitate levels decreased in resting diabetic macrophages, although this did not reach significance (Figure 5.9A).

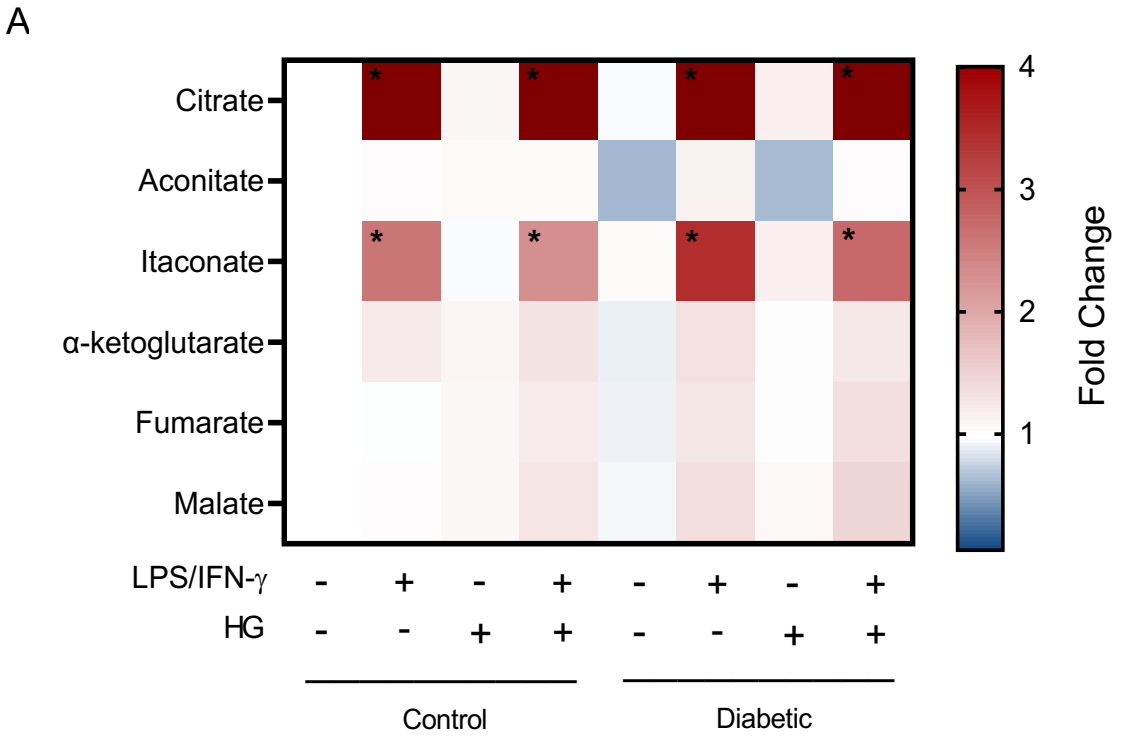
Overall, this suggests in vivo hyperglycaemia and HG-treatment does not alter the TCA cycle.

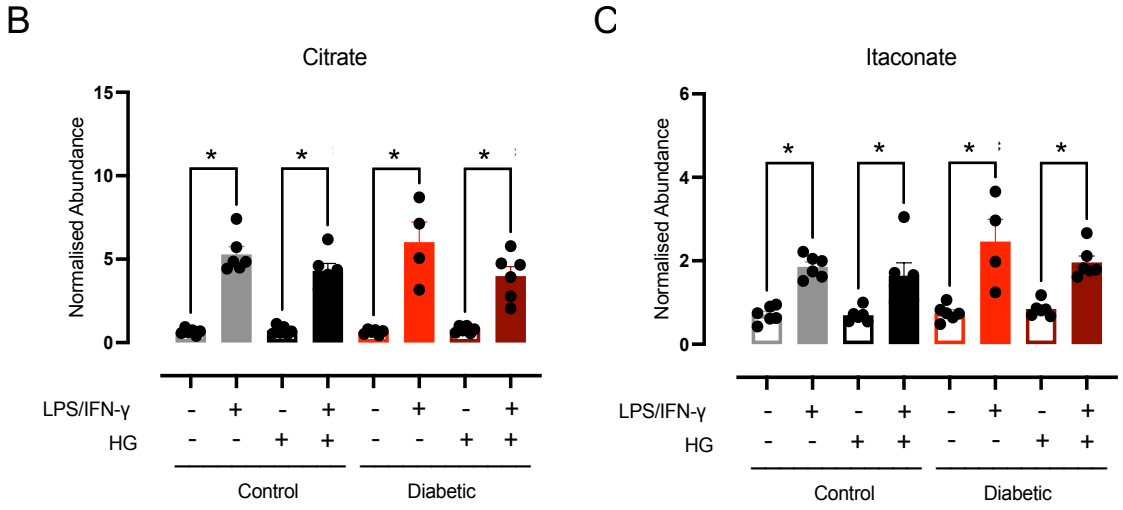
**Figure 5. 9 TCA cycle overview of control and diabetic macrophages ± LPS/IFN-γ and ± HG**

A) Fold change heatmap of TCA cycle metabolites relative to non-HG-treated unstimulated Control macrophages
B) Citrate metabolite abundance
C) Itaconate metabolite abundance

in Control and βV59M-diabetic unstimulated and LPS/IFN-ɣ, HG-treated macrophages
Data are n=4-6 mean ± SEM. P values are calculated using a one-way ANOVA with Tukey's post test

Heatmap notation:
(*) indicates P<0.05 for LPS/IFNγ stimulation vs control within the same genotype and HG-treatment


A
Citrate
Aconitate
Itaconate
α-ketoglutarate
Fumarate
Malate
LPS/IFN-γ
HG
Control
Diabetic
Fold Change
4
3
2
1


B
Citrate
Normalised Abundance
15
10
5
0
LPS/IFN-γ
HG
Control
Diabetic
C
Itaconate
Normalised Abundance
6
4
2
0
LPS/IFN-γ
HG
Control
Diabetic

### 5.4.10 Fatty acid metabolism

Fatty acids enter the TCA cycle at citrate. Furthermore DHAP, levels of which were increased with hyperglycaemia, is a key substrate in the de novo lipogenesis pathway. Although most lipids involved in fatty acid metabolism were increased with stimulation, this only reached significance in deoxycarnitine. There were no alterations in any other metabolites associated with fatty acid metabolism following in vivo hyperglycaemia or HG-treatment or LPS/IFN-γ stimulation (Figure 5.10A-E).

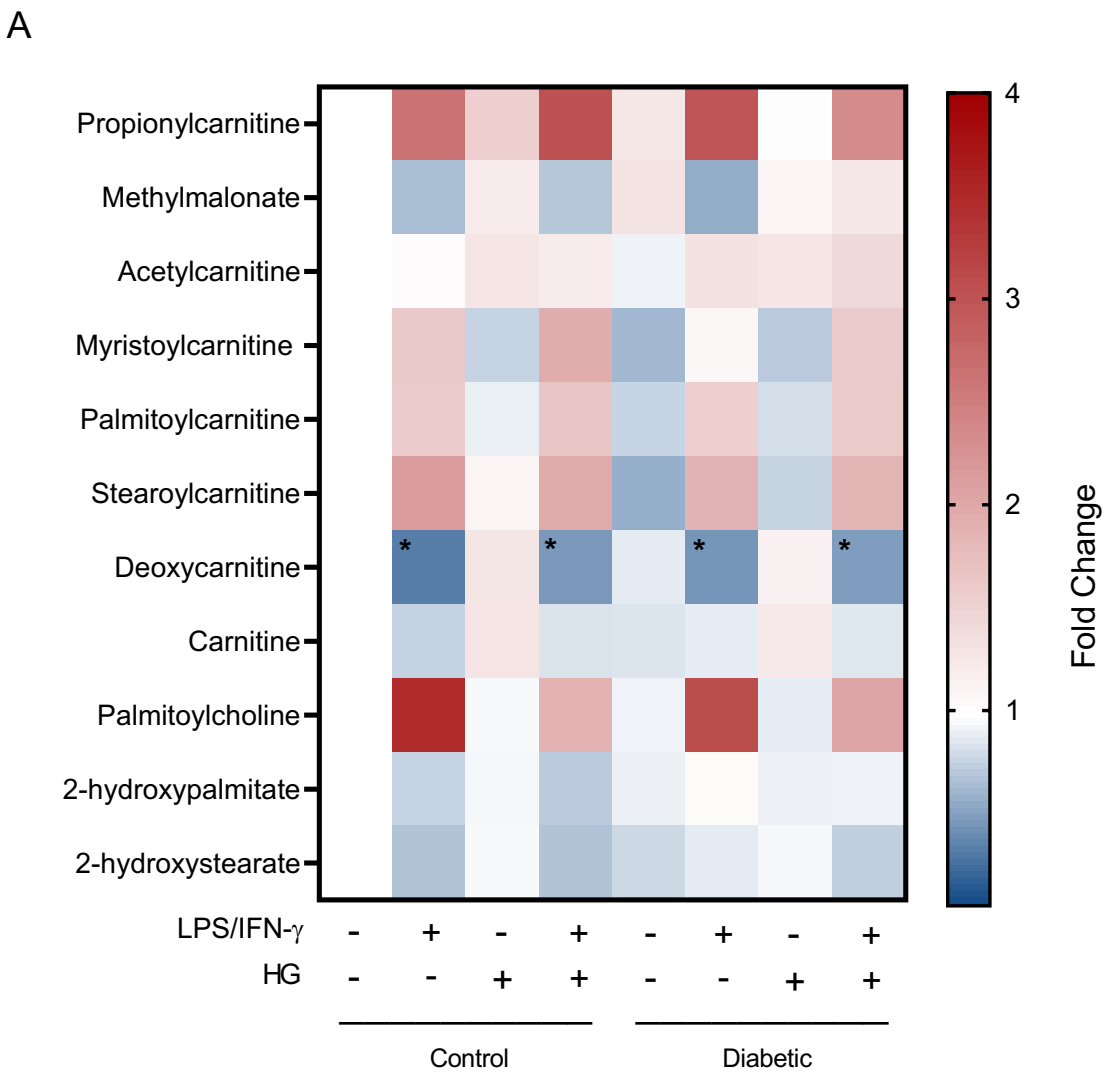
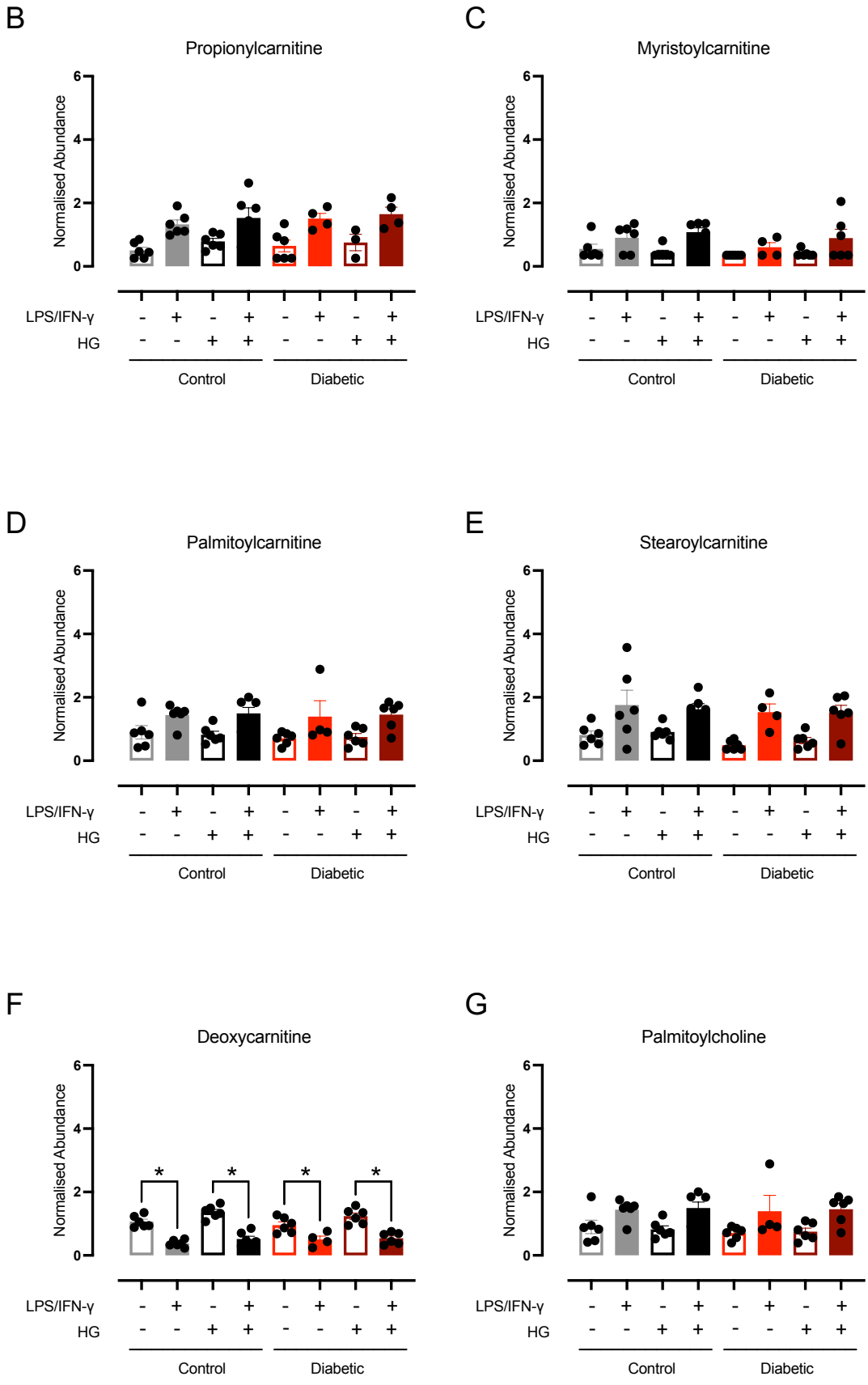



**Figure 5. 10 Fatty acid metabolism in control and diabetic macrophages ± LPS/IFN-γ and ± HG**

A) Fold change heatmap of Fatty acid metabolites relative to non-HG-treated unstimulated Control macrophages
B) Propionylcarnitine metabolite abundance
C) Myristoylcarnitine metabolite abundance
D) Palmitoylcarnitine metabolite abundance
E) Stearoylcarnitine metabolite abundance
F) Deoxycarnitine metabolite abundance
G) Palmitoylcholine metabolite abundance

in Control and βV59M-diabetic ± LPS/IFN-γ and ± HG. Data are n=4-6, mean ± SEM. P values are calculated using a one-way ANOVA with Tukey's post-test.

Heatmap notation:
(*) indicates P<0.05 for LPS/IFNγ vs control within the same genotype and HG-treatment


B
Propionylcarnitine
C
Myristoylcarnitine
D
Palmitoylcarnitine
E
Stearoylcarnitine
F
Deoxycarnitine
G
Palmitoylcholine
Normalised Abundance
0
2
4
6
LPS/IFN-γ
HG
- + - + - + - +
- - + + - - + +
Control
Diabetic
*

### 5.4.11 Eicosanoids

Arachidonate levels were not altered with LPS/IFN-γ stimulation, in vivo hyperglycaemia or HG-treatment (Figure 5.11A). Further down the eicosanoid synthesis pathway, 13-HODE, 9-HODE and 12-HHTrE levels increased significantly with LPS/IFN-γ stimulation but remained unaltered following in vivo hyperglycaemia and/or HG-treatment (Figure 5.11B-C).

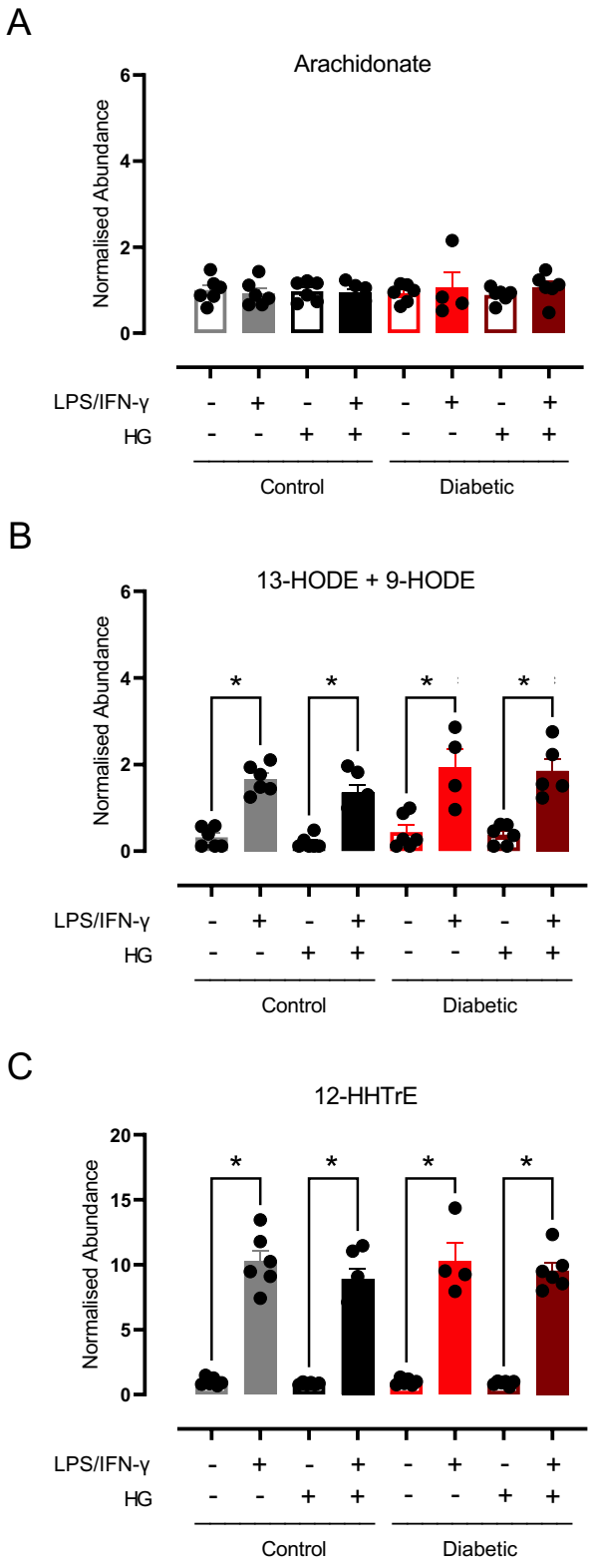



**Figure 5. 11 Eicosanoids in control and diabetic macrophages ± LPS/IFN-γ and ± HG**

A) Arachidonate metabolite abundance
B) 13-HODE + 9-HODE metabolite abundance
C) 12-HHTrE metabolite abundance

in Control and βV59M-diabetic ± LPS/IFN-γ and ± HG. Data are n=4-6, mean ± SEM. P values are calculated using a one-way ANOVA with Tukey's post-test (*P<0.05).

### 5.4.12 Glutamine metabolism

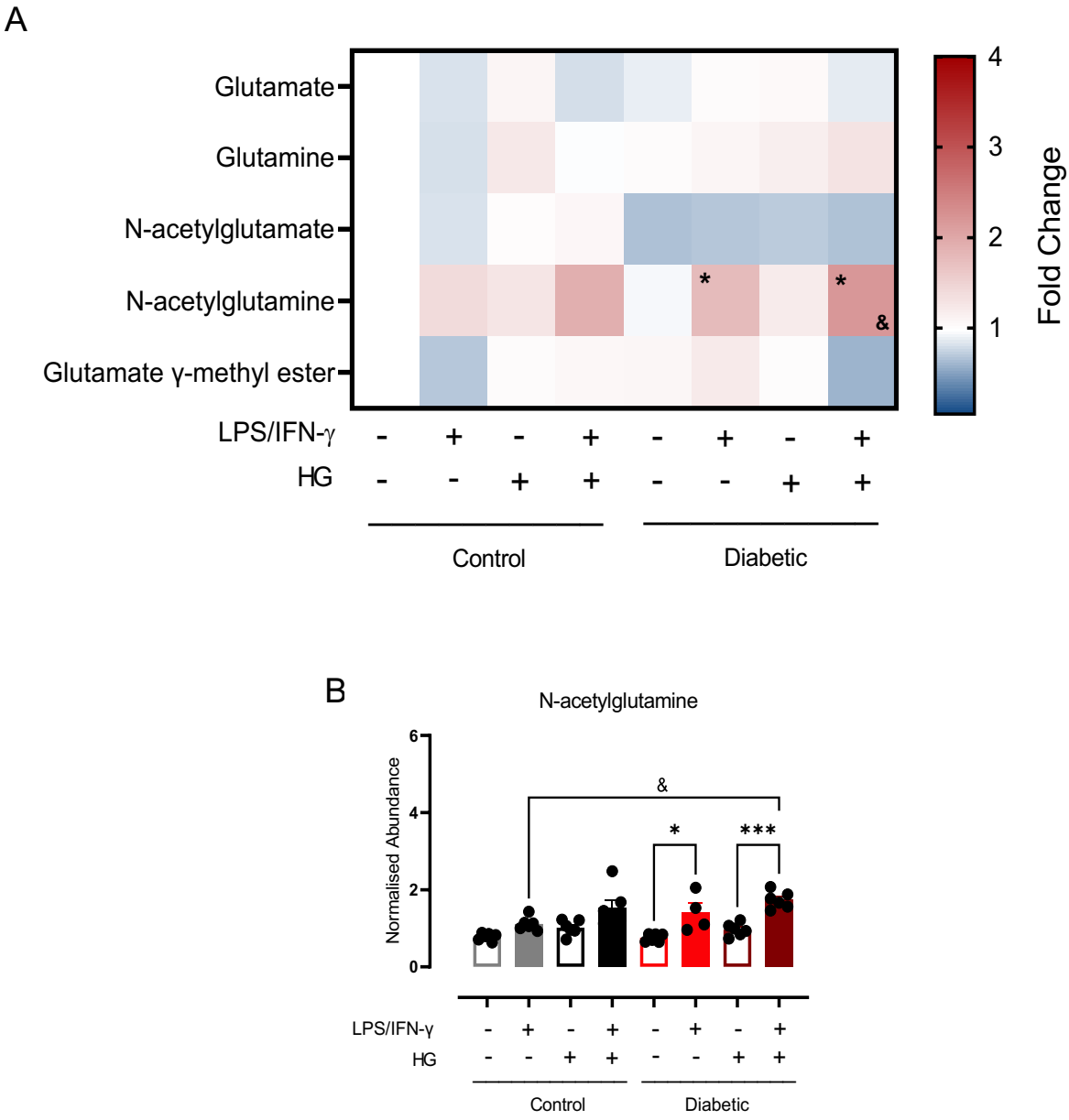
N-acetylglutamine levels increased following LPS/IFN-γ stimulation in diabetic macrophages (Figure 5.14A-B). Levels also increased with both in vivo hyperglycaemia and HG-treatment (Figure 5.14A-B). There were no changes in any other metabolites involved in glutaminolysis in response to LPS/IFN-γ stimulation, HG-treatment or genotype (Figure 5.9A). This suggests there are minimal changes in glutaminolysis with hyperglycaemia.

**Figure 5. 12 Glutamine metabolism in control and diabetic macrophages ± LPS/IFN-γ and ± HG**

A) Fold change heatmap of glutamate metabolism relative to non-HG-treated unstimulated Control macrophages
B) N-acetylglutamine metabolite abundance

in Control and βV59M-diabetic ± LPS/IFN-γ and ± HG. Data are n=4-6, mean ± SEM. P values are calculated using a one-way ANOVA with Tukey's post-test.

Heatmap notation:
(*) indicates $P<0.05$ for LPS/IFNγ stimulation vs control within the same genotype and HG-treatment
(&) indicates $P<0.05$ for both in vivo hyperglycaemia + HG-treatment within the same polarisation state


A
Glutamate
Glutamine
N-acetylglutamate
N-acetylglutamine
Glutamate γ-methyl ester
LPS/IFN-γ
HG
Control
Diabetic
Fold Change
4
3
2
1
*
*
&
B
N-acetylglutamine
Normalised Abundance
6
4
2
0
&
*
***
LPS/IFN-γ
HG
Control
Diabetic

### 5.4.13 Arginine metabolism

2-oxoarginine levels were only increased following LPS/IFN-γ stimulation in HG-treated diabetic macrophages (Figure 5.13A-B). Citrulline is a classical marker of macrophage activation. Citrulline levels increased at least 50 fold following LPS/IFN-γ stimulation in control and diabetic macrophages regardless of genotype and HG-treatment (Figure 5.13B). Trans-4-hydroxyproline levels decreased by 42% in HG-treated control $M^{LPS/IFN-\gamma}$ (Figure 5.13C).

There were no changes in any other metabolites involved in arginine metabolism due to LPS/IFN-γ stimulation, HG-treatment or genotype (Figure 5.13A).

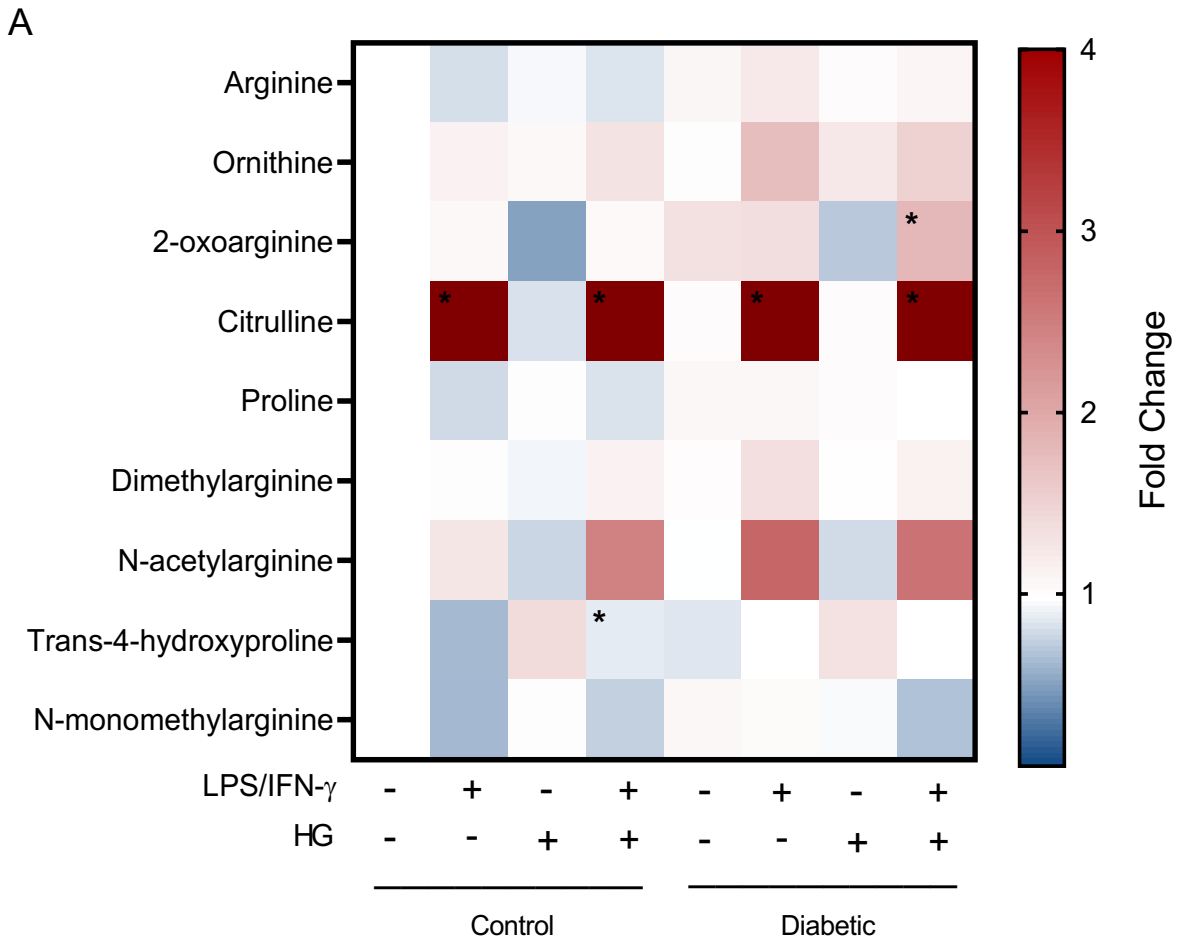
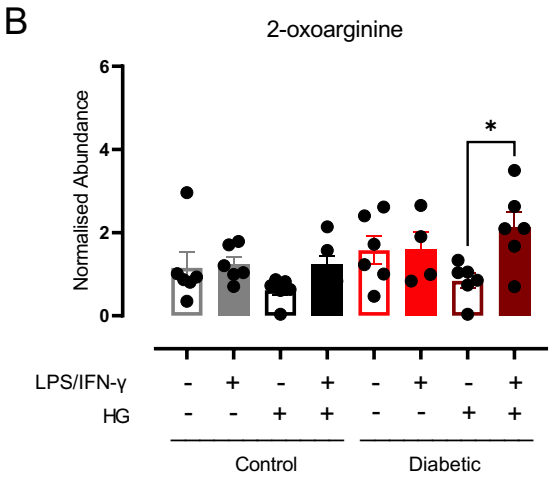


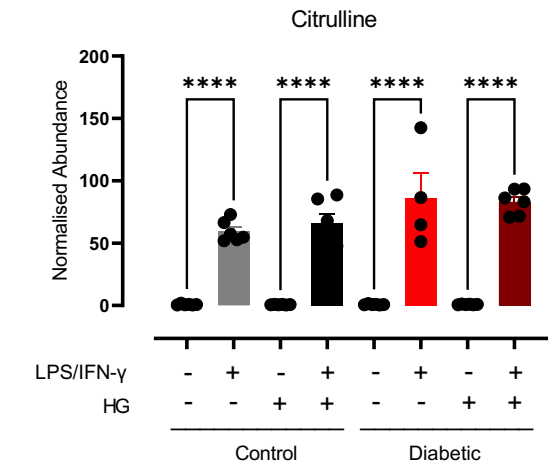

**Figure 5. 13 Arginine metabolism in control and diabetic macrophages ± LPS/IFN-γ and ± HG**

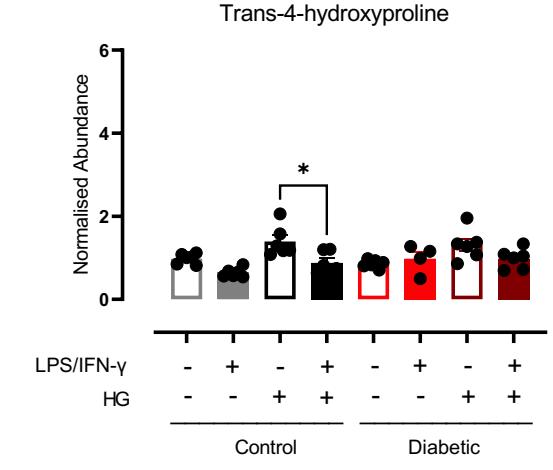
A) Fold change heatmap of arginine metabolism relative to non-HG-treated unstimulated Control macrophages
B) 2-oxoarginine metabolite abundance
C) Citrulline sphingomyelin metabolite abundance
D) Trans-4-hydroxyproline metabolite abundance

in Control and βV59M-diabetic ± LPS/IFN-γ and ± HG. Data are n=4-6, mean ± SEM. P values are calculated using a one-way ANOVA with Tukey's post-test.

Heatmap notation:
(*) indicates P<0.05 for LPS/IFNγ stimulation vs control within the same genotype and HG-treatment


B
2-oxoarginine
Normalised Abundance
6
4
2
0
*
LPS/IFN-γ
HG
- + - + - + - +
- - + + - - + +
Control
Diabetic


C
Citrulline
Normalised Abundance
200
150
100
50
0
****
****
****
****
LPS/IFN-γ
HG
- + - + - + - +
- - + + - - + +
Control
Diabetic


D
Trans-4-hydroxyproline
Normalised Abundance
6
4
2
0
*
LPS/IFN-γ
HG
- + - + - + - +
- - + + - - + +
Control
Diabetic

### 5.4.14 Aspartate metabolism

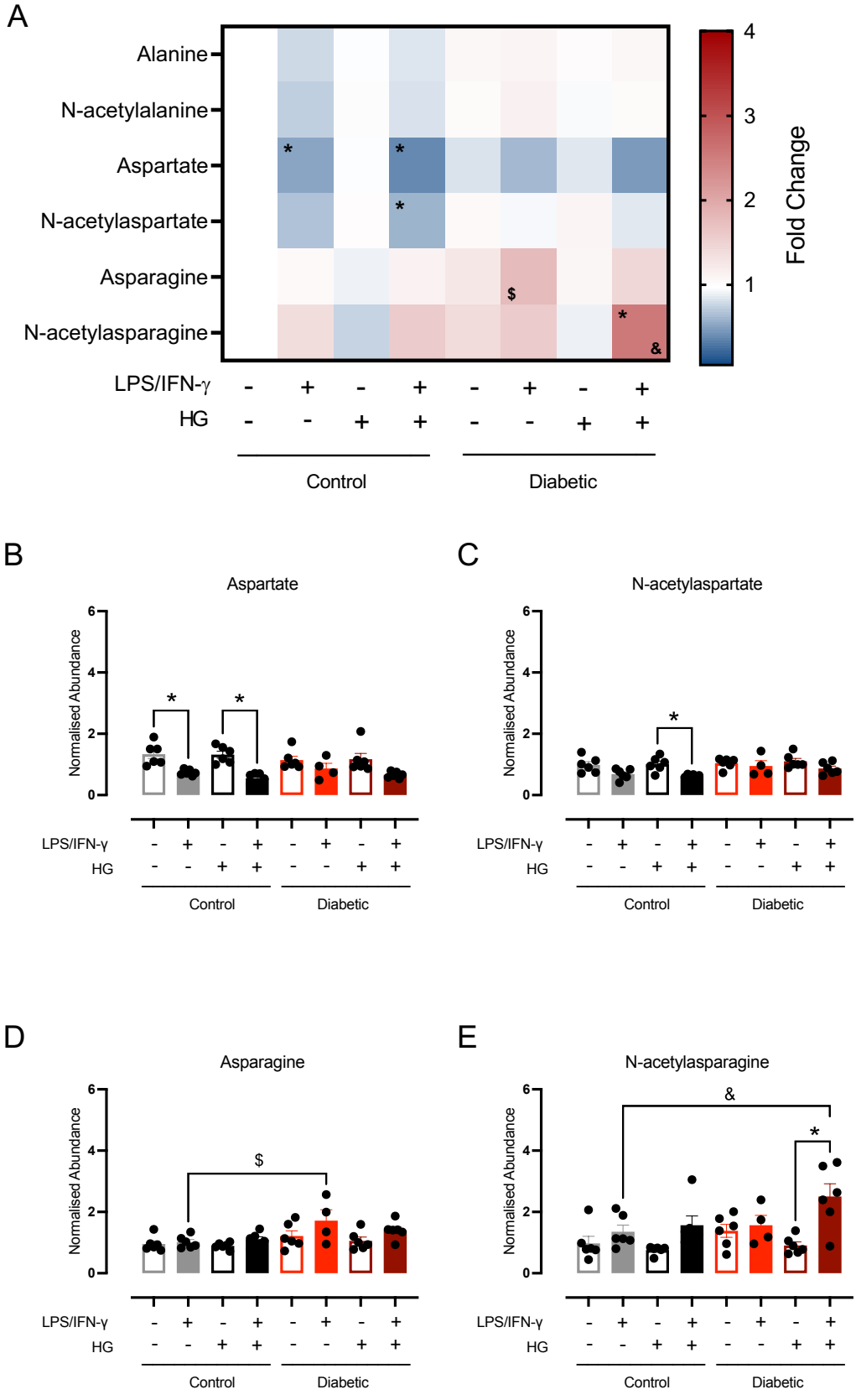
Aspartate levels decreased by at least 40% following LPS/IFN-γ stimulation in control regardless of HG-treatment (Figure 5.14A-B). Overall, there were no strong indication of hyperglycaemia induced changes in the alanine metabolism pathway. There was a consistent decrease in aspartate levels following LPS/IFN-γ stimulation which was not replicated in diabetic macrophages. Furthermore, asparagine levels increase but alanine levels were not altered (Figure 5.14A). N-acetylaspartate decreased by at least 40% following LPS/IFN-γ stimulation in HG-treated control macrophages (Figure 5.14C). Asparagine levels were not altered with LPS/IFN-γ stimulation. However, asparagine increased with genotype (in vivo hyperglycaemia) in diabetic $M^{LPS/IFN-\gamma}$ (Figure 5.14D). N-acetylasparagine levels increased LPS/IFN-γ stimulation in HG-treated diabetic macrophages (Figure 5.14E). There were no changes with genotype (in vivo hyperglycaemia) alone, but additional HG-treatment significantly increased glucose levels compared to the respective control group (Figure 5.14E).

**Figure 5. 14 Aspartate metabolism in control and diabetic macrophages ± LPS/IFN-γ and ± HG**

A) Fold change heatmap of Aspartate relative to non-HG-treated unstimulated Control macrophages (n=4-6)
B) Aspartate metabolite abundance
C) N-acetylaspartate metabolite abundance
D) Asparagine metabolite abundance
E) N-acetyl-asparagine metabolite abundance

in Control and βV59M-diabetic ± LPS/IFN-γ and ± HG. Data are n=4-6, mean ± SEM. P values are calculated using a one-way ANOVA with Tukey's post-test.

Heatmap notation:
(*) indicates P<0.05 for LPS/IFNγ stimulation vs control within the same genotype and HG-treatment
($) indicates P<0.05 for genotype difference (control v diabetic)
(&) indicates P<0.05 for both in vivo hyperglycaemia + HG-treatment within the same polarisation state


A
Alanine
N-acetylalanine
Aspartate
N-acetylaspartate
Asparagine
N-acetylasparagine
LPS/IFN-γ
HG
Control
Diabetic
Fold Change
B
Aspartate
C
N-acetylaspartate
D
Asparagine
E
N-acetylasparagine
Normalised Abundance

### 5.4.15 Sphingomyelin metabolism

Stearoyl sphingomyelin, behenoyl sphingomyelin, SM 17:1/16:0, SM 18:1/20:0 and SM 18:1/22:1increased with LPS/IFN-γ stimulation in diabetic macrophages (Figure 5.15 A-C, E, H-I). In addition to LPS/IFN-γ stimulation, SM-18:1/14:1 and SM 18:2/16:0 levels were also increased with HG-stimulation (Figure 5.15 F-G). SM18:1/18:1 levels increased only following LPS/IFN-γ stimulation in HG-treated diabetic macrophages (Figure 5.15G). Overall, this demonstrates in vivo hyperglycaemia alters macrophages response to LPS/IFN-γ stimulation to increase sphingomyelin levels.

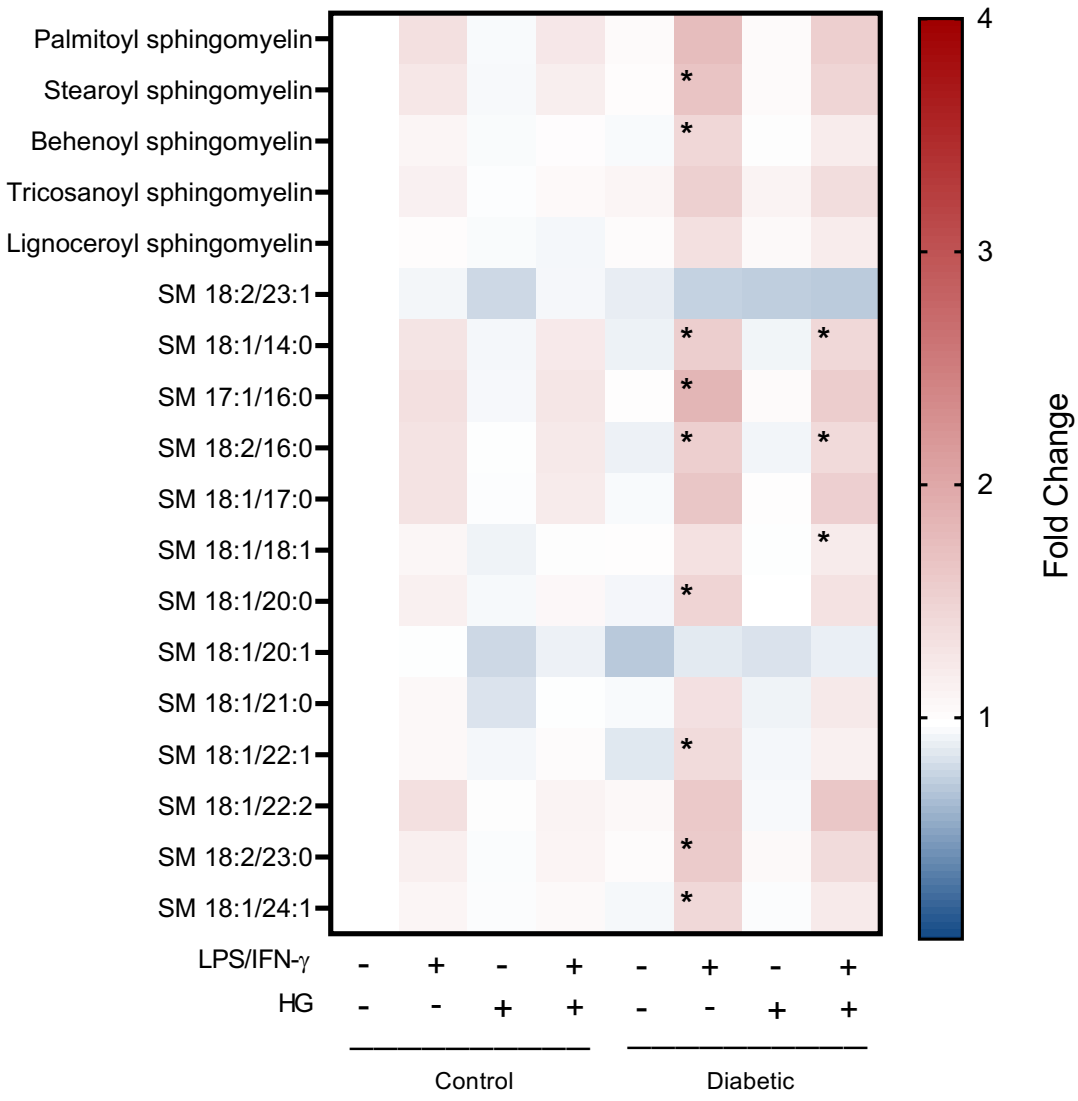
**Figure 5. 15 Sphingomyelins of control and diabetic macrophages ± LPS/IFN-γ and ± HG**

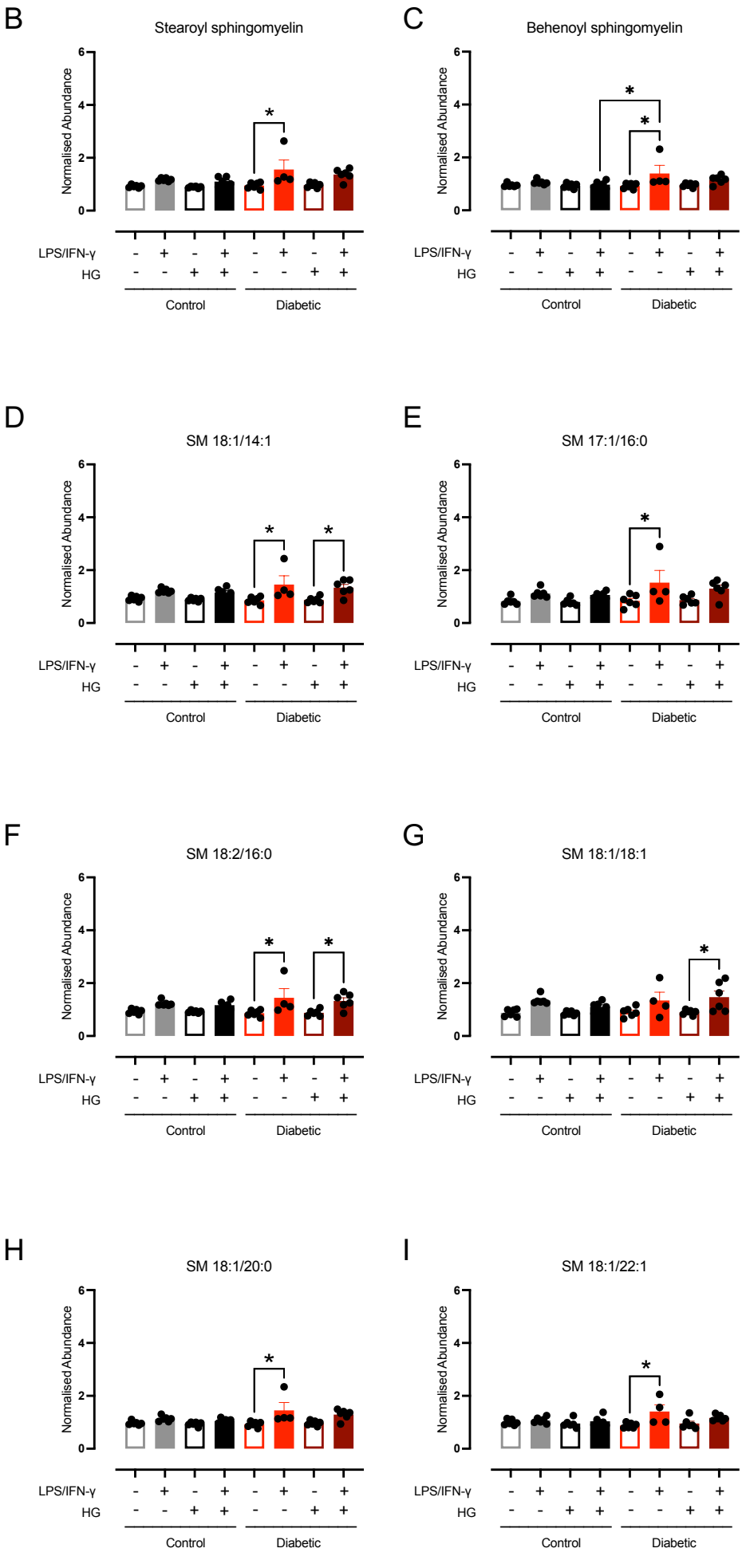
A) Fold change heatmap of Sphingomyelins relative to non-HG-treated unstimulated Control macrophages (n=4-6)
B) Stearoyl sphingomyelin metabolite abundance
C) Behenoyl sphingomyelin metabolite abundance
D) SM 18:1/14:1 metabolite abundance
E) SM 17:1/16:0 metabolite abundance
F) SM 18:2/16:0 metabolite abundance
G) SM 18:1/18:1 metabolite abundance
H) SM 18:1/20:0 metabolite abundance
I) SM 18:1/22:1 metabolite abundance

in Control and βV59M-diabetic ± LPS/IFN-γ and ± HG. Data are n=4-6, mean ± SEM. P values are calculated using a one-way ANOVA with Tukey's post-test.

Heatmap notation:
(*) indicates P<0.05 for LPS/IFNγ stimulation vs control within the same genotype and HG-treatment

A


Palmitoyl sphingomyelin
Stearoyl sphingomyelin
Behenoyl sphingomyelin
Tricosanoyl sphingomyelin
Lignoceroyl sphingomyelin
SM 18:2/23:1
SM 18:1/14:0
SM 17:1/16:0
SM 18:2/16:0
SM 18:1/17:0
SM 18:1/18:1
SM 18:1/20:0
SM 18:1/20:1
SM 18:1/21:0
SM 18:1/22:1
SM 18:1/22:2
SM 18:2/23:0
SM 18:1/24:1
LPS/IFN-γ - + - + - + - +
HG - - + + - - + +
Control
Diabetic
4
3
2
1
Fold Change


B
Stearoyl sphingomyelin
C
Behenoyl sphingomyelin
D
SM 18:1/14:1
E
SM 17:1/16:0
F
SM 18:2/16:0
G
SM 18:1/18:1
H
SM 18:1/20:0
I
SM 18:1/22:1
Normalised Abundance
0
2
4
6
LPS/IFN-γ
HG
Control
Diabetic
*

## 5.5 Discussion

### 5.5.1 Overview

This study investigated the effects of in vivo hyperglycaemia on the inflammatory and metabolic profile of macrophages using the βV59M-diabetic mouse model. After observing alterations in pro-inflammatory cytokine release in diabetic BMDMs, metabolomics analysis of control and diabetic BMDMs ± LPS/IFN-γ and ± HG was conducted. The dataset revealed an overall increase in glycolysis in diabetic BMDMs, with further increases observed with LPS/IFN-γ stimulation and HG-treatment. However, there were no changes observed in other TCA cycle substrates (fatty acids, glutamine, alanine) or arginine metabolism. Interestingly, sphingomyelins were consistently increased in diabetic $M^{LPS/IFN\text{-}\gamma}$. Overall, although there was some evidence of hyperglycaemia induced priming of macrophages, changes in metabolite levels were modest suggesting the greatest hyperglycaemia-induced differences lie elsewhere such as in enzymatic activity or in the epigenome.

### 5.5.2 Hyperglycaemia alters macrophage inflammatory profile

In the previous chapter, HG-treatment alone did not alter pro-inflammatory cytokine release leading to the hypothesis in vivo hyperglycaemia may instead trigger these changes. Indeed IL1β levels increased and TNF-α levels decreased with in vivo hyperglycaemia, whilst IL6 secretion did not change. Similarly, in a study with alloxan-diabetic mouse model, IL1β levels were also increased and TNF-α levels decreased (Ayala et al., 2019). The mechanism by which hyperglycaemia may alter IL1β and TNF-α levels is unclear. In contrast, Thiem et al demonstrated unchanged TNF-α levels in the bone marrow but increased TNF-α secretion in STZ-diabetic bone marrow derived macrophages. This study also did not see any changes in IL6 secretion in STZ-diabetic macrophages (Thiem et al., 2021). Furthermore, NO production was also unaltered with hyperglycaemia and HG-treatment in our study. Whilst

in alloxan-diabetic mice, decreased NO production was reported, in STZ-diabetic mice NO production was not measured and iNOS gene expression was unaltered (Ayala et al., 2019; Edgar et al., 2021).

In addition, inflammation-associated metabolites also remained unchanged with HG-treatment and in vivo hyperglycaemia. As expected, citrate, itaconate, citrulline and eicosanoids were increased with LPS/IFN-γ stimulation, but remained unaltered with hyperglycaemia exposure. Another study demonstrated increases in the proinflammatory metabolite succinate, malate and markers of glycolysis: lactate and pyruvate in diabetic $M^{LPS/IFN-\gamma}$ (Edgar et al., 2021). Although succinate and pyruvate were not measured in our metabolomics dataset, no changes were observed in malate or lactate.

### 5.5.3 Hyperglycaemia alters macrophage response to stimulation

Glycolysis and sphingomyelins were the main metabolic pathways altered in βV59M-diabetic $M^{LPS/IFN-\gamma}$. Increased glycolysis was also reported in another metabolomics study in STZ-diabetic macrophages (Edgar et al., 2021). However, other studies have in fact shown in vivo hyperglycaemia can impair glucose uptake and glycolysis in macrophages (Ayala et al., 2019; Matsuura et al., 2022). Furthermore, increased glycolytic flux, such as after LPS/IFN-γ stimulation, is theorised to result in an upregulation of the pentose phosphate pathway in $M^{LPS/IFN-\gamma}$, but we did not consistently observe increased abundance of metabolites in the pentose phosphate pathway (Viola et al., 2019). An intermediary in the glycolytic pathway, DHAP was one of the most altered metabolites in our study. Glycolytic metabolites downstream of DHAP were decreased, even though DHAP levels increased with hyperglycaemia. Although DHAP also feeds into de novo lipogenesis pathway, metabolites in this pathway or fatty acid metabolism generally were also not altered.

Next, sphingomyelins were consistently increased in diabetic macrophages. Although, sphingolipids have not been studied well in hyperglycaemic macrophages, they have been

associated with type 2 diabetes, and shown to mediate loss of insulin sensitivity and the elevated pro-inflammatory state characteristic of diabetes (Ross et al., 2014; Russo et al., 2013). Sphingomyelins (SM) are the most abundant sphingolipids in cells synthesised from ceramides and phosphocholine by SM synthases (SMS) (Taniguchi & Okazaki, 2014). SMS1 KO mice demonstrated decreased glucose tolerance due to impaired mitochondrial function as well as decreased body weight and fat tissue mass indicating general metabolic abnormality (Yano et al., 2011; Yano et al., 2013). Furthermore, in a study on lipid species and cardiovascular health, sphingomyelin and ceramides had the strongest association with mortality; 32% of the participants were also diabetic (Sigruener et al., 2014). This suggests that although sphingolipids play a role in diabetes, the molecular mechanisms of the pathway and enzyme regulation need further exploration (Hannun & Obeid, 2018).

### 5.5.4 Hyperglycaemia induces priming in macrophages

The two pillars of trained immunity are epigenetic and metabolic reprogramming. This chapter focussed solely on the latter. Our results suggest hyperglycaemia induces priming of macrophages, rather than training, demonstrated by a heightened glycolytic response. In both priming and training there is a heightened inflammatory response upon a second stimulus However, after the first stimulus, the inflammatory state of the trained macrophage returns back to baseline, whereas primed macrophages retain the inflammatory state (Divangahi et al., 2021). A retained inflammatory state is observed in βV59M-diabetic $M^{LPS/IFN\text{-}\gamma}$ exposed to normoglycaemia. Following a secondary HG stimulus, an additive effect is observed in diabetic macrophages, such as that seen in priming.

Hyperglycaemia-induced training in macrophages have been shown to be supported by some metabolic changes, as discussed above, although much focus was placed on epigenetic changes (Edgar et al., 2021). This could be since metabolism was not in the scope of these studies but also because the major reproducible findings lie in the epigenome. Furthermore,

any linked metabolism changes could lie in the metabolic flux, enzymatic activity or at the transcriptional level of metabolic enzymes and less so in the levels of metabolites themselves. We found even the most enriched pathways in our metabolomics yielded modest results, suggesting limited hyperglycaemia-induced changes, in our experimental setup, in metabolite levels of BMDMs.

### 5.5.5 Experimental Design

Finally, the length of HG stimulation may alter training of macrophages. βV59M-diabetic macrophages were exposed to two weeks in vivo hyperglycaemia followed by 7 days normoglycemic culture (rest) and followed by 24 hours HG treatment. In the trained immunity model developed by Edgar et al, IL6 gene expression increased after 4 days HG culture, followed by 6 days rest and IL1β gene expression increased after 7 days HG exposure followed by 3 days' rest. No secondary HG stimulus was given (Edgar et al., 2021). In this study, aside from in vivo hyperglycaemia, we also used a secondary stimulus of LPS/IFN-γ to understand changes in diabetic $M^{LPS/IFN\text{-}\gamma}$, as well as HG-treatment. Trained immunity has been demonstrated with both the same and as well as a different secondary stimuli to the original stimulus (Netea et al., 2020). Having either HG, LPS/IFN-γ or both showed a double inflammatory stimulus hit is still not enough to cause dramatic metabolic changes in our model. Other stimuli which may have been shown to induce trained immunity include oxLDL, β-glucan and BCG. LPS is a reasonable model here since diabetic patients are more prone to infections.

### 5.5.6 Is hyperglycaemia alone sufficient to induce long term metabolic changes?

This study used the βV59M-diabetic mouse model to study the effects of hyperglycaemia on macrophage metabolism. This was on the background of several studies reporting altered macrophage metabolism with in vitro HG which could not be reproduced in Chapter 4. Our

findings in this chapter also differ to hyperglycaemia-induced effects observed in other diabetic mouse models (Ayala et al., 2019; Edgar et al., 2021; Grosick et al., 2018; Pavlou et al., 2018). The βV59M-diabetic mouse model is used for the first time in the study of BMDMs. This model does not exhibit high triglyceride or high cholesterol levels commonly seen in more commonly used, and more severe, diabetic models (Brereton et al., 2014). This suggests hyperglycaemia alone, without dyslipidaemia, or insulin resistance, may not be sufficient to cause significant metabolic or trained effects. It has also been suggested that the effects of diabetes on macrophage training or metabolism are due to insulin deficiency instead of hyperglycaemia (Lachmandas et al., 2015; Matsuura et al., 2022).

### 5.5.7 Future work

This chapter first demonstrated in vivo hyperglycaemia alters inflammatory cytokine production in BMDMs, regardless of subsequent normoglycemic culture or HG stimulation. A metabolomics study to investigate the metabolic changes supporting this effect, yielded few metabolic targets and alterations were largely limited to glycolysis and sphingomyelins. Understanding enzymatic activity, protein levels and metabolic flux may provide more insight into the macrophage metabolism dynamics. Overall, hyperglycaemia appeared to prime rather than train macrophages, although epigenetics of the cell still need to be investigated. Also, to understand if hyperglycaemia-induced inflammatory and metabolic changes have functional consequence, studies such as chemotaxis assays, foam cell formation, phagocytosis assays and seahorse studies should be conducted.

# Chapter 6

# The role of exogenous itaconate on vascular function

## Chapter 6: The role of exogenous itaconate on vascular function

### 6.1 Introduction

Itaconate is an important immunoregulatory metabolite. Notably, itaconate exhibits high polarity and low electrophilicity that result in weak cell permeability. Research on itaconate is divided into the use of IRG1-/- macrophages to understand signalling pathways mediated by itaconate, and the effects of itaconate via the use of itaconate derivatives to explore the role of itaconate as a therapeutic. Itaconate derivatives are used to enhance cell permeability with 4-octyl itaconate (4-OI) and dimethyl itaconate (DI) the most commonly used. The structures of 4-OI and DI are shown in Figure 6.1 and their properties are summarised by Lin et al (Lin et al., 2021).

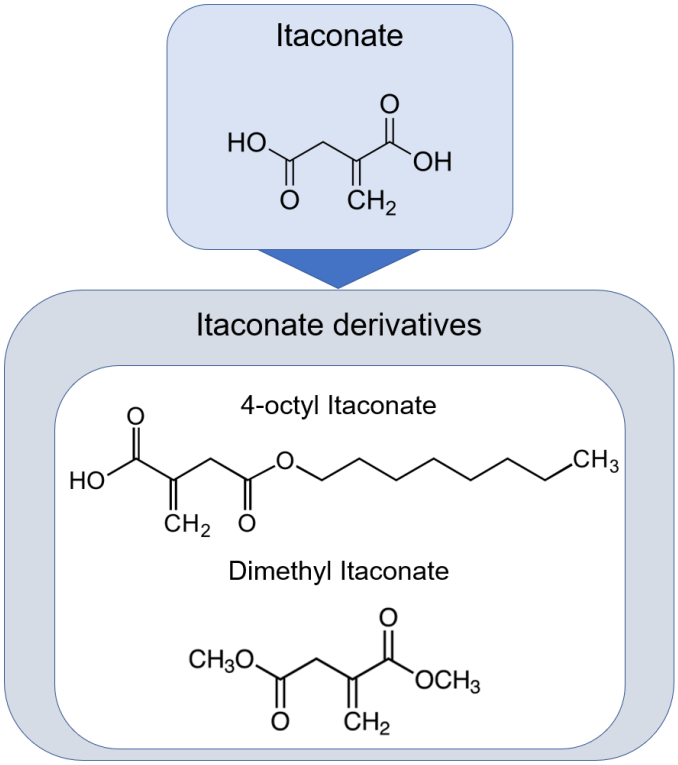



**Figure 6. 1 The structure of itaconate itaconate derivatives: 4-octyl itaconate (4-OI) and dimethyl itaconate (DI)**

Itaconate is a naturally occurring metabolite produced during the breakdown of glucose in the TCA cycle. Levels of itaconate are typically low under physiological conditions but increase significantly to low millimolar levels in activated macrophages in response to many inflammatory stimuli (Strelko et al., 2011). Stimulation with LPS increases the expression of aconitate decarboxylase 1 (*ACOD1* also known as *IRG1*) which encodes the enzyme ACOD1 (also known as CAD and IRG1). High induction of ACOD1 diverts cis-aconitate away from the TCA cycle, repurposing it for itaconate production. Itaconate inhibits succinate dehydrogenase (SDH) leading to the accumulation of succinate, a metabolite with pro-inflammatory properties; succinate has been shown to suppress IL6, TNF-α and NO production (Tannahill et al., 2013). The role of the succinate receptor 1 (SUNCR1) on macrophage function is less clear as SUNCR1 deficiency has been shown to promote a proinflammatory response in macrophages and activation of SUNCR1 resulted in a more anti-inflammatory macrophage phenotype (Harber et al., 2020; Keiran et al., 2019). Itaconate is metabolised into itaconyl-coenzyme A (coA) which acts on mitochondrial coA B12 to decrease activity of methylmalonyl-CoA mutase (MUT) and production of MUT-dependant branched-chain amino acids (Cordes & Metallo, 2021).

Aside from SDH inhibition, itaconate also exerts effects through several other mechanisms. Itaconate covalently binds to Keap1 cysteine 151 to disassociate the Keap1-NRF2 complex and promote NRF2 migration to the nucleus. NRF2 activation induces expression of anti-inflammatory proteins, suppresses pro-inflammatory cytokine production and inhibits NF-κB signalling pathway (Mills et al., 2018). Furthermore, itaconate increases activating transcription factor (ATF3) levels which translocate to the nucleus to inhibit Iκbζ mRNA levels (Bambouskova et al., 2018). Itaconate depletes the NLRP3-NEK7 complex through dicarboxypropylation of NLRP3 resulting in inhibition of NLRP3-dependant IL1β production (Mills et al., 2018). Moreover, itaconate can form itaconyl-coenzyme A and also

can alkylate cysteine 22 residues on GAPDH and cysteine 73 and 339 on ALDOA to inhibit glycolysis (Bambouskova et al., 2021; Liao et al., 2019). Most recently, itaconate has also been shown to bind to ten-eleven translocation (TET) family DNA dioxygenases to suppress LPS-induced inflammation and 4-OI has been shown to inhibit Janus Kinase 1 (JAK1) activation and suppress M2 polarisation (L. L. Chen et al., 2022).

With its anti-inflammatory and anti-oxidant effects, itaconate is a promising candidate in the treatment of many diseases including cardiovascular inflammation (Table 6.1). Several studies have already reported on the use of itaconate or its derivatives in preventing cardiac damage as well as enhancing repair following ischaemia reperfusion injury of the heart (Table 6.1). Although molecular mechanistic differences have been described between itaconate and its derivatives due to their electrophilic chemistry, the majority, if not all have shown beneficial effect on oxidative damage and inflammation, which are both key drivers of many cardiovascular diseases. There are currently no active clinical trials investigating itaconate or its derivatives in any inflammatory conditions, but this is most likely since research into its therapeutic use is in early stages. Therefore, we aimed to investigate the role of ACOD1 in clinical cohorts of cardiovascular disease patients. We used the oxHVF cohort as a large study on patients with cardiovascular disease. These findings brought to light results which were followed up in mice mechanistically.

| Organ | Findings |
|---|---|
| Heart  | • DI intravenous infusion during ischemia reduces myocardial infarct size (Lampropoulou et al, 2016)<br>• DI loaded PCL nanofibers promote tissue repair, improve LV function and reduce infarct area (Nakkala et al, 2021)<br>• NIPAM-gel promotes heart repair via angiogenesis, apoptosis inhibition, improved cardiac stem cell retention (Cui et al, 2019)<br>• DI protects against cardiotoxicity induced by doxorubicin, an anti-tumour drug (Shan et al, 2019) |
| Vessels  | • 4-OI pre-treatment inhibits high glucose-induced ROS production, lipid peroxidation, mitochondrial depolarisation in HUVECs (Tang et al, 2019)<br>• 4-OI inhibits abdominal aortic aneurysm formation through inhibition of vascular inflammation via activation of Nrf2 (Song et al, 2020)<br>• DI treatment of transient middle cerebral artery occlusion decreases neurologic deficit score and toxic conversion of microglia (Zhang et al, 2019) |
| Immune system  | • 4-OI inhibit pathogenic viruses including SARS-Cov2, HSV, VACV, and Zika Virus through activation of NRF2 (Olagnier et al, 2020)<br>• 4-OI inhibits pro-Inflammatory cytokine production in PBMCs of Systemic Lupus Erythematosus Patients (Tang et al, 2018)<br>• Itaconate, 4-OI and DI reduces interferon responses and inflammation in influenza A virus infection (Sohail et al, 2022)<br>• IRG1 expression in myeloid cells prevents immunopathology during M.Tubersclerosis infection (Nair et al, 2018)<br>• DI alleviates the Inflammatory Responses of Macrophages in Sepsis through Nrf2 (Zhang et al, 2021)<br>• Itaconate limits Zika virus infection by promoting an antiviral metabolic state in neurons (Daniels et al, 2019) |
| Lungs  | • 4-OI prevents lung damage caused by MRSA bacteremia through Nrf2/ARE pathway activation (Liu et al, 2021)<br>• 4-OI alleviates LPS-Induced Acute Lung Injury and inflammation by inhibiting ROS mediated signalling pathways (Li et al, 2020)<br>• DI protects against pulmonary fibrosis via alleviation of fibroblast–myofibroblast differentiation by increasing Nrf2 expression level and decreasing TXNIP expression level (Han et al, 2021)<br>• Itaconate has anti-fibrotic effects and is crucial in controlling the severity of lung fibrosis (Ogger et al, 2020) |
| Brain  | • Itaconate reduces ROS/RNS to improve neurological function and traumatic brain injury survival (Cordes et al, 2020)<br>• Itaconate suppresses neuroinflammation providing chronic pain relief (Ren et al, 2022) |
| Liver  | • 4-OI significantly improved liver injury and hepatocyte cell death after I/R via Nrf2 activation (Yi et al, 2020)<br>• 4-OI attenuates carbon tetrachloride-induced hepatic injury via oxidative stress and inflammatory response regulation (Li et al, 2021)<br>• Itaconate suppresses glycolysis resulting in decreased visceral fat in liver (Sakai et al, 2004) |
| Kidney  | • Itaconate protects against acute kidney injury via Nrf2 activation (Zhu et al, 2021)<br>• 4-OI protects against renal fibrosis via inhibition of TGF-b/Smad pathway, autophagy and reduced generation of ROS (Tian et al, 2020) |
| Reproductive  | • DI protects against LPS-induced endometritis by inhibition of TLR4/NFκB and activation of Nrf2/HO-1 (Xu et al, 2020)<br>• DI protects against LPS-induced mastitis in mice by activating Nrf2 and inhibiting NFκB signalling pathways (Zhao et al, 2019) |
| Bone  | • 4-OI protects osteoblasts from hydrogen peroxide-induced oxidative injury via Nrf2 activation (Zheng et al, 2020)<br>• 4-OI inhibits osteoclastogenesis by suppressing Hrd1 and activating Nrf2 signalling (Sun et al, 2019) |
| Eyes  | • 4-OI against inflammatory response in angiotensin II-induced oxidative stress in human primary retinal pigment epithelium (Fu et al, 2021)<br>• DI protects against fungal keratitis by activating the Nrf2/HO-1 signalling pathway (Gu et al, 2020) |
| Skin  | • DI ameliorates disease severity in experimental autoimmune encephalomyelitis through neuroinflammation suppression (Kuo et al, 2020) |

Table 6. 1 Therapeutic evidence of itaconate and its derivatives in various models of disease. 4-octyl itaconate (4-OI); Dimethyl itaconate (DI)

## 6.2 Hypothesis and aims

### 6.2.1 Hypothesis

It was hypothesised that increases in ACOD1 expression or itaconate levels result in improved outcomes in cardiovascular disease patients. Upon observing improved vascular function in the internal mammary artery of patients with ACOD1 SNP, it was hypothesised that itaconate treatment improves vascular function in mouse aorta.

### 6.2.2 Aims

Aim 1: To test the association of ACOD1 with cardiovascular phenotypes in patients with advanced coronary artery disease

Aim 2: To investigate the role of itaconate on vascular function

## 6.3 Methods

### 6.3.1 The Oxford Heart, Vessels & Fat cohort

The OX-HVF (Oxford Heart, Vessels & Fat) cohort comprises several clinical studies, including ART Vascular, Bypass Grafts, AdipoRedox, and ORFAN. Together, these studies allow a multi-level approach to understand the mechanisms of cardiovascular diseases. By investigating cardiovascular disease pathogenesis from different perspectives, the OX-HVF cohort provides a unique and powerful platform. Its strength lies in the ability to access human tissue, including vessels, myocardial and fat biopsies, DNA, plasma, and other samples, as well as extensive non-invasive cardiovascular phenotyping, such as cardiovascular computed tomography angiography and ultrasound. In this chapter, we only utilize data from the AdipoRedox study (REC11/SC/0140).

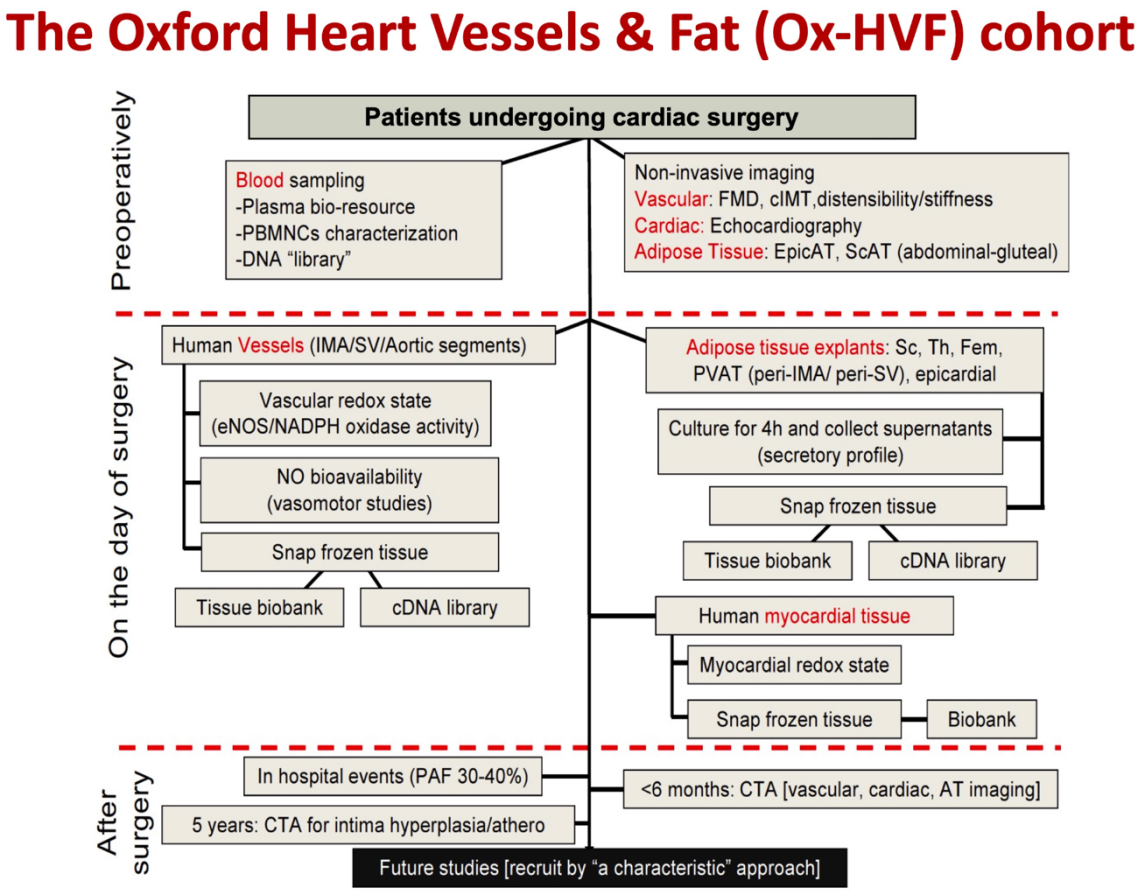



**Figure 6. 2 The Oxford Heart Vessels and Fat (OxHVF) cohort work flow.**

More information on the oxHVF cohort can be found on the domain https://oxhvf.com

### 6.3.2 The AdipoRedox study

The AdipoRedox study (15/09/2011 to current; REC: 11/SC/140), aims to investigate the interactions among fat tissue, vascular tissue, and heart muscle to determine whether aspects of these interactions can predict the outcomes of coronary artery bypass grafting operation (CABG). The study includes 663 male and female patients over the age of 18 who have been diagnosed with cardiovascular disease and scheduled for CABG or valve replacement/repair surgery. All patients provided informed consent to participate in the study and met the inclusion criteria (Table 6.2).

| Inclusion criteria | Exclusion criteria |
|---|---|
| Male or Female | Individuals with active infectious, auto-immune or idiopathic diseases |
| Aged over 18 years or above | Individuals with active malignancy |
| Diagnosed with cardiovascular disease | Individuals with end-stage liver or renal failure |
| Scheduled for CABG or valve/repair surgery | Individuals with recent unstable coronary syndrome |
| | Individuals taking non-steroidal or anti-inflammatory drugs |

Table 6. 2 Summary of population inclusion and exclusion criteria

Upon recruitment, patients underwent a thorough medical history evaluation that included information on traditional risk factors for cardiovascular disease, family history of cardiovascular diseases, heart failure classification, angina pectoris grading, and cardiovascular medication profile. The patients also underwent non-invasive echo-based imaging studies, BMI, waist and hip circumference measurements, and provided fasting blood samples, which were used for plasma and serum isolation and then snap-frozen for

subsequent experiments. All patient demographics and post-surgery outcomes collected are in the appendix.

### 6.3.3 Sample collection and superoxide

Before surgery, fasting blood samples were collected and processed by oxHVF staff. During surgery, pedicle left IMA tissue was collected by the surgeon and transferred in Krebs Henseleit buffer (KHB; NaCl 120mM, KCl 4.7mM, $CaCl_2$ 2.5mM, $MgSO_4$ 1.2mM, $KH_2PO_4$ 1.2mM, $NaHCO_3$ 25mM, glucose 5.5mM, pH=7.4, oxygenated for 5 min (95% $O_2$/5% $CO_2$)). On the same day, adipose tissue surrounding the vessel was removed, IMA was cut into rings and used for luminometry experiments conducted by oxHVF staff.

### 6.3.4 Measurement of superoxide production

Luminometry experiments on IMA vessels included superoxide generation, as well as the specific generation of NADPH oxidases and uncoupled eNOS. To measure NADPH-stimulated superoxide, vessels were stimulated with 100 μM NADPH after recording the baseline signal, resulting in saturation of the NADPH-oxidases molecules, and acting as a chemical surrogate marker of NADPH-oxidase activity. Production of $O_2^{\cdot-}$ was measured using a lucigenin (5 μmol/L)-enhanced chemiluminescence assay. The difference in intracellular $O_2^{\cdot-}$ generation before and after addition of L-NAME was calculated to assess the coupling status of endothelial nitric oxide synthase (eNOS) (Antoniades et al., 2006).

### 6.3.5 oxHVF cohort Genome wide SNP array

Patients were genotyped with the genome-wide single nucleotide polymorphism (SNP) array UK Biobank Axiom Array (Affymetrix) by oxHVF staff. Details of genotyping and primary quality control of samples and SNPs described previously (Kotanidis, 2021). In total, 881 samples and 800,000 SNPs per person were identified and fulfilled all quality criteria for subsequent analysis.

### 6.3.6 Wire myography in mouse aorta

#### 6.3.6.1 Animals

Male C57BL/6J mice were used for aorta isolation and housed in groups of 2-5, in individually ventilated cages at the Functional Genetics Facility (FGF), a specific pathogen free environment, at the Wellcome Centre for Human Genetics, Oxford. Temperatures were maintained at 20-22 °C with 12-hour light/dark cycles and mice were given access to standard chow diet (Teklad global 16% protein diet, Harlan Laboratories) and sterile water ad libitum.

#### 6.3.6.2 Isometric Tension Vasomotor Studies

To assess vasomotor function in aortas, isometric tension studies in a wire myograph (MultiMyograph 610M, Danish Myo Technology, Denmark) were carried out. Mice were first culled with overdose of isoflurane by inhalation, the chest cavity opened and the system circulation was flushed gently with 5 ml ice-cold PBS. Next, the thoracic aorta was dissected with 2 mm aortic rings mounted on a wire myograph using tungsten wires (100 μm diameter; Goodfellows, UK); myograph chambers contained 5ml ice-cold Krebs solution gassed with 95% $O_2$/5% $CO_2$. Vessels were left to equilibrate for 30 minutes at 37°C before optimal tension was set to 25 mN. Vessel viability was assessed using 60 mM KCl which causes contraction during maximal depolarisation. Concentration-response contraction curves were generated using cumulative half-log concentrations of phenylephrine (1 nM to 10 μM), a potent vasoconstrictor. Following this, vessels were washed at least three times with fresh Krebs Henseleit buffer (KHB [in mmol/l]: NaCl 120, KCl 4.7, MgSO4 1.2, KH2PO4 1.2, CaCl2 2.5, NaHCO3 25, glucose 5.5).and left to equilibrate for 30 minutes, before being precontracted to approximately 90% maximal tension with phenylephrine. Acetylcholine was used to stimulated endothelium-dependant vasodilation through increasing cumulative concentrations (1 nM to 10 μM). Responses

were expressed as a percentage of the precontracted tension. Finally, the NO donor sodium nitroprusside (SNP) was used to test endothelium-independent smooth muscle relaxation in the presence of L-NAME. All pharmacological drugs were pre-incubated at least 30 minutes before the dose-response curves were determined. Apamin was used at 50 nM, charybdotoxin at 100 nM, 1H-(1,2,4)oxadiazolo[4,3-a]quinoxalin-1-one (ODQ) at 500 nM, indomethacin at 10 μM, and L-NAME at 100 μM.. All drugs used were purchased from Sigma Chemical Company except ODQ (Cayman Europe).

Vasomotor studies were performed in collaboration with Dr Surawee Chuaphichai from the Channon group.

## 6.4 Results

### 6.4.1 Demographics of study participants

Out of the 630 patients taking part in the AdipoRedox study, 85% were male, 94% were Caucasian, with a mean age of 66.5 years. The majority of participants had additional cardiovascular risk factors including hypertension (74%), hypercholesterolemia (82%), history of smoking (53%) and family history of cardiovascular disease (58%). Furthermore, the majority of participants were taking medication including statins (88%), ACE inhibitors (52%), beta blockers (70%), aspirin (85%), and a significant number were taking nitrates (42%) and clopidogrel (30%) (Table 6.3).

| Table 6. 3 Demographics of study participants | |
|---|---|
| No of patients | 630 |
| Men/Women | 540/90 |
| Age, years | 66.5 ± 0.39 |
| Ethnicity | 94% Caucasian |
| Risk factors, n (%) | |
| • Hypertension | 467 (74) |
| • Hypercholesterolemia | 517 (82) |
| • Smokers/ex-smokers | 67/333 (10/53) |
| • Diabetes Mellitus | 141 (22) |
| • Family history of CVD | 363 (58) |
| • Body mass index, kg/m2 | 28.7 |
| • Triglycerides, mmol/L | 1.82 ± 0.22 |
| • Cholesterol, mmol/L | 4.45 ± 0.16 |
| • High-density lipoprotein, mol/L | 16.9 or 1.15 |
| • HbA1c | 7.2 ± 0.167 |
| Medication, n (%) | |
| • Statins | 555 (88) |
| • Angiotensin converting enzyme inhibitors | 326 (52) |
| • Calcium channel blockers | |
| • Angiotensin receptor blockers | 82 (13) |
| • Beta-blockers | 446 (70) |
| • Nitrates | 267 (42) |
| • Aspirin | 535 (85) |
| • Clopidogrel | 186 (30) |
| • Diuretics | 101 (16) |

### 6.4.2 Study design and analysis workflow of oxHVF cohort to identify ACOD1 SNP

Association tests were carried out using 881 patient samples to identify potential causal ACOD1 associations. Out of 184 SNPs identified, 61 ACOD1 SNPs that are within ±2Kb range of ACOD1 gene and are in overlap with the SNPs on UCSC genome browser were selected for testing (Figure 6.3).

Spearman's correlation test was first performed on 105 non-experimental traits/patient demographics. Next, SNPs were verified with at least one significant association to cardiovascular related traits including redox signalling, vascular inflammation and vascular function measures. Mann-Whitney test was used for the 56 experimental measurements. Non-experimental and experimental measures are listed in the appendix. Association tests were carried out using both additive model as well as recessive models with the p-value threshold of 0.05. Overall, we identified 16 associations across 7 SNPs (Figure 6.3). Positions and functions of these 7 SNPs as well as the associations are listed in Table 6.4. Due to their associations, the most promising SNPs were Rs17470171 and Rs17385627 which are in linkage disequilibrium. ACOD1 Rs17470171 was followed up as it had the highest number of positive and negative associations.

This analysis was performed by Dr Murray Polkinghorne from the Antoniades group in the Department of Cardiovascular Medicine.

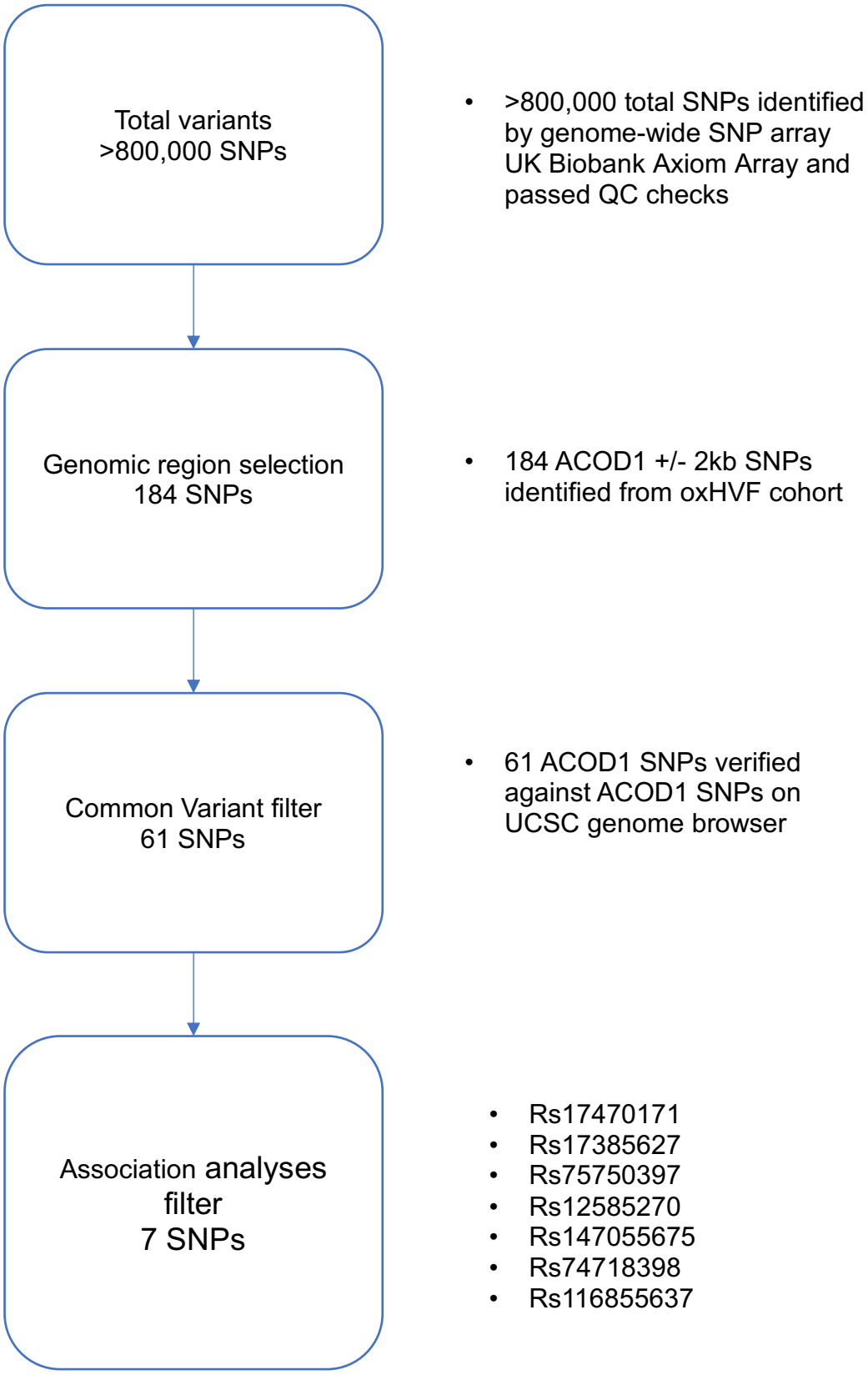



**Figure 6. 3 ACOD1 SNPs identification workflow**

| SNP (Effect genotypes) | Position | Function | Sig. Positive Associations | Sig Negative Associations |
|---|---|---|---|---|
| Rs17470171* (CA/AA) | Upstream 1835bp from ACOD1 start position | enhancer | IMA resting & NADPH O2- | IMA LNAME O2-, Max Relax (BK) |
| Rs17385627* (TA/AA) | Intronic - 5070bp | enhancer | IMA resting & NADPH O2- | IMA LNAME O2- |
| Rs75750397** (CG/GG) | Intronic – 700bp | unknown | None | SV Vas2870 O2-, Plasma TNF-α |
| Rs12585270** (CT/TT) | Intronic – 2879bp | unknown | None | SV Vas2870 O2-, Plasma TNF-α |
| Rs147055675 (AG/GG) | Coding – 9400bp | missense | Plasma Wnt5a | SV NADPH O2- |
| Rs74718398 (GA/AA) | Intronic – 3494bp | unknown | EC50 PE & LogEC50 PE, DPP4 activity | None |
| Rs116855637 (AG/GG) | Coding – 8485bp | missense | EC50 PE & LogEC50 PE, DPP4 activity | None |

**Table 6. 4 Position, function and associations found for 7 identified ACOD1 SNPs**

UCSC genome browser session showing ACOD1 SNPs is available
https://genome.ucsc.edu/s/faseeha/ACOD1_SNPs

(*) and (**) indicate ACOD1 SNPs in linkage disequilibrium.
IMA = Internal Mammary Artery, SV= saphenous vein, DPP4 = Dipeptidyl-peptidase 4, NADPH = nicotinamide adenine dinucleotide phosphate

### 6.4.3 ACOD1 Rs17470171 is associated with increased superoxide production

To test the association of *ACOD1* rs17470171 variant on endothelial cell function, datasets on superoxide production from internal mammary artery rings were interrogated. These revealed significantly increased levels of superoxide in carriers of the ACOD1 rs17470171 allele (Figure 6.4A). This increase was due to NAPDH-oxidase activity (Figure 6.4B) as well as eNOS uncoupling (Figure 6.4C).

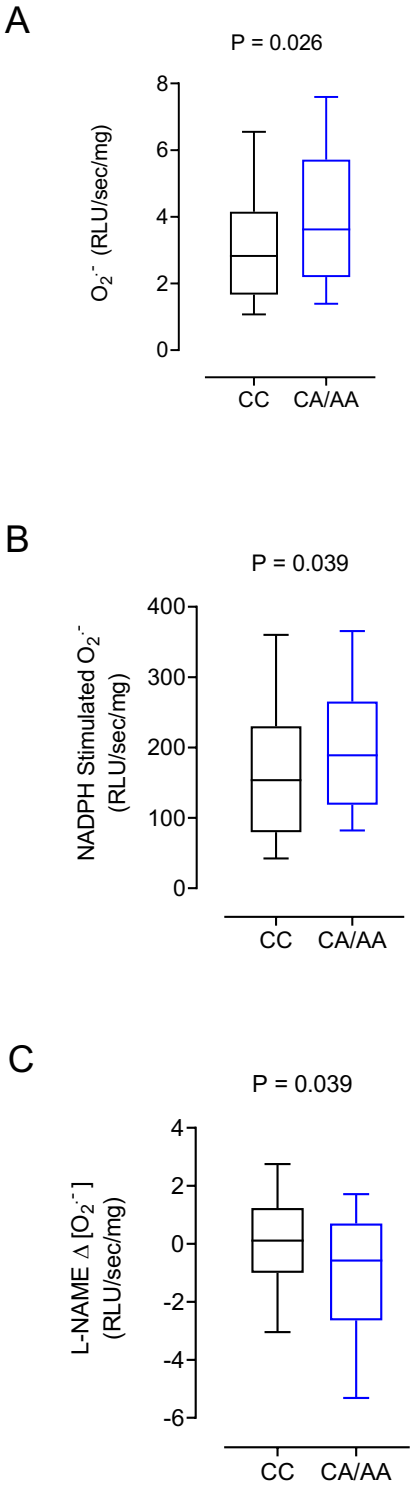



**Figure 6. 4 ACOD1 rs17470171 is associated with increased superoxide production in IMA of patients**

Association between A) Basal superoxide production in human IMAs (n=304). B) NAPDH-stimulated superoxide production in IMA (n=290). C) N(G)-Nitro-L-arginine methyl ester (L-NAME) inhibitable superoxide O2 .- production (n=265). CC indicates the reference genotype. Both heterozygous (CA) and homozygous (AA) mutations are counted as effect genotypes.
Data are mean ± SD. *P* values calculated using Mann Whitney test.

### 6.4.4 ACOD1 Rs17470171 is associated with improved vasorelaxation

To test the association between of ACOD1 rs17470171 variant and endothelial cell function, ex vivo organ bath measurements of endothelial cell function in internal mammary artery rings were conducted as before. These revealed significantly increased vasorelaxation in response to the vasodilator bradykinin in carriers of the ACOD1 rs17470171 allele (Figure 6.5A). No difference in response to endothelium-independent dilator, sodium nitroprusside (SNP) was observed (Figure 6.5B).

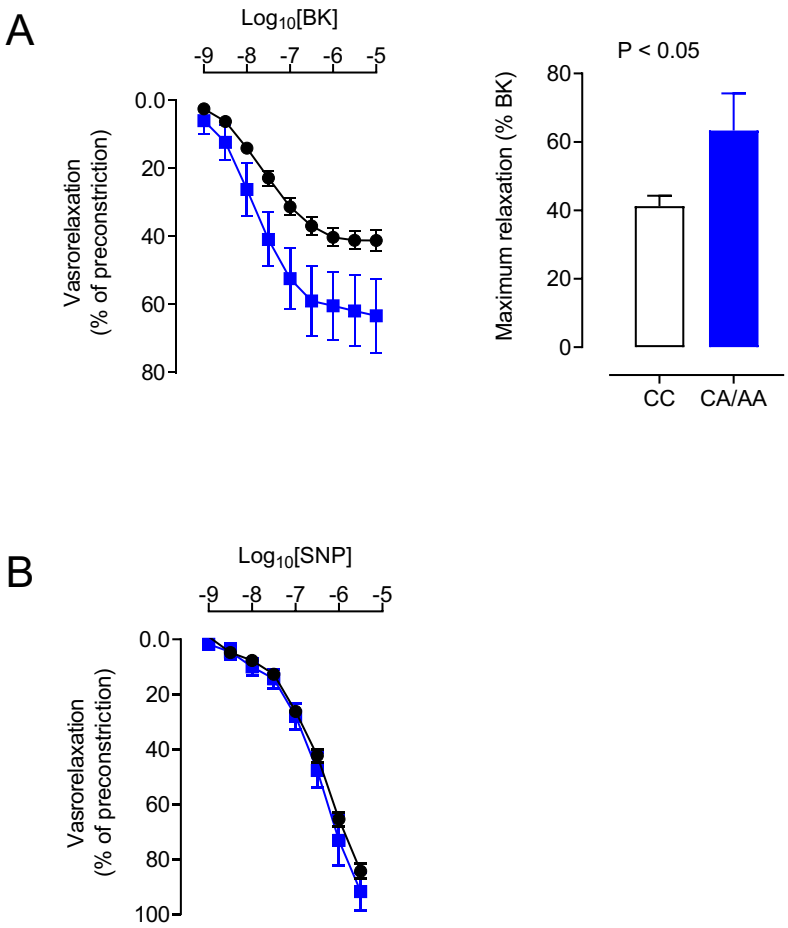



**Figure 6. 5 ACOD1 rs17470171 is associated with improved vasorelaxation in IMA of patients**

Vasorelaxation curves of phenylephrine precontracted human vessels in response to, A) bradykinin (BK; endothelium-dependent, $n$ = 71), and (B) sodium nitroprusside (SNP; endothelium-independent, $n$ = 77). CC indicates the reference genotype. Both heterozygous (CA) and homozygous (AA) mutations are counted as effect genotypes. Data are mean ± SD. $P$ values calculated using Mann Whitney test (*$P$<0.05).

### 6.4.5 4-octyl itaconate treatment blunts preconstriction in mouse aorta

We next sought to explore the effects of itaconate on wildtype mouse aorta. As expected, mouse aortas contracted in the presence of phenylephrine (Figure 6.6A). Maximal vasoconstriction to 60mM KCl (non-receptor mediated contraction) was comparable between DMSO treated and 4-OI treated wildtype aortas (Figure 6.6B). With 1mM 4-OI pre-incubation, receptor-mediated vasoconstriction to phenylephrine was diminished (Figure 6.6A, Figure 6.6C), an effect not observed in the control group. This blunting effect was reversible after extensive (>7) washes with Krebs Henseleit Buffer. This suggests the vessel's relaxing capacity is not impaired by 4-OI. This relaxant effect is reproduced in the presence of an endothelium derived contracting factor prostaglandin F2α (PGF2α, (1 nM to 10 μM)), demonstrating this response is not specific to phenylephrine or $\alpha_1$adrenoreceptor signaling. Loss of constriction induced by 4-OI treatment was not normalized in the presence of non-selective nitric oxide synthase (NOS) inhibitor, L-NAME (100μM).

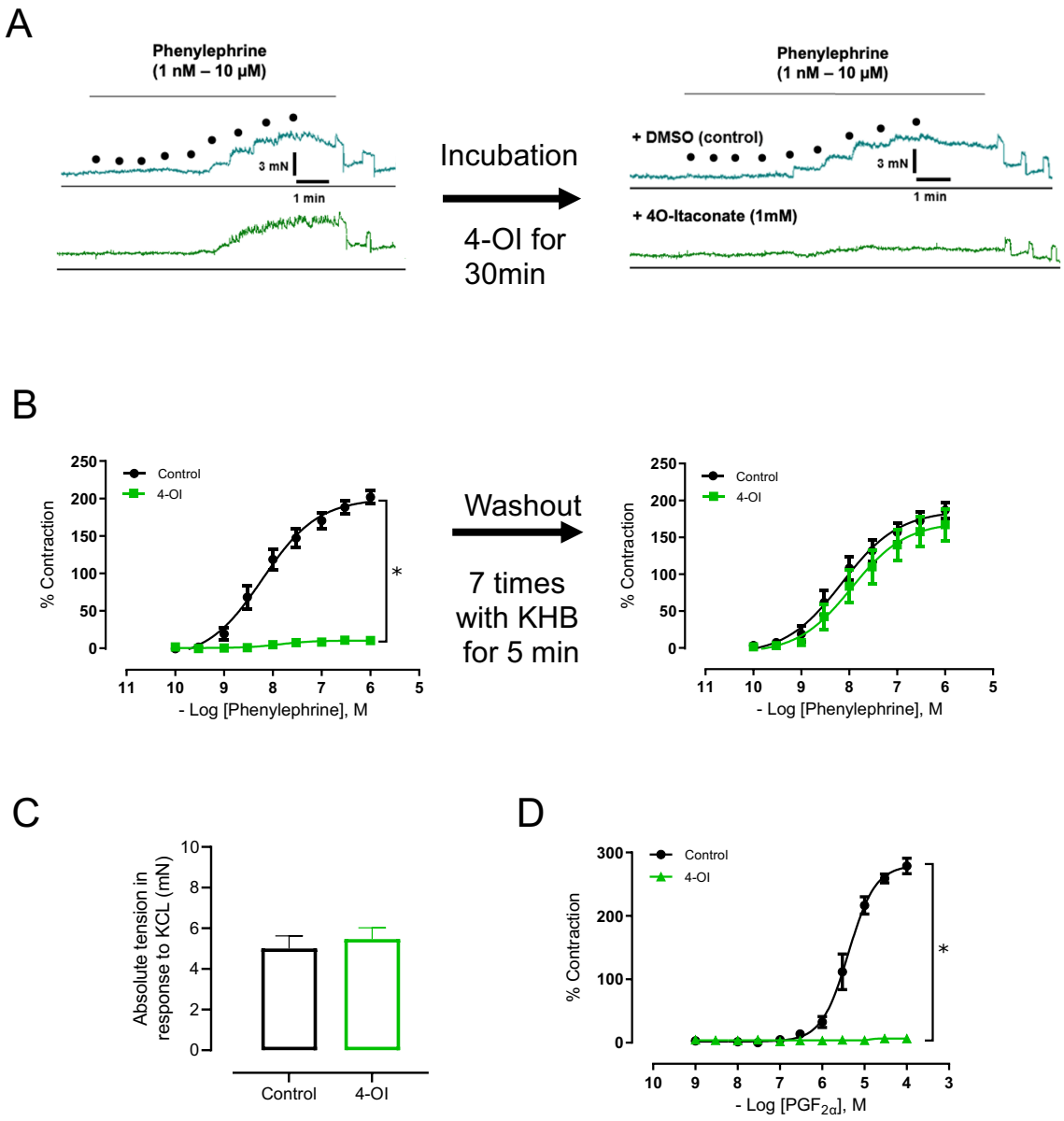



**Figure 6. 6 4-OI treatment prevents preconstriction in mouse aorta**

A) Original trace showing relaxant effect of 4-octyl itaconate (4-OI, 30min) on WT mouse aorta B) Absolute tension in aorta in response to KCL showing the vessels are healthy and equally responsive. C) Vasoconstriction in response to phenylephrine (PE), alone or with 4-OI treatment. This effect is reversible. D) Vasoconstriction in response to PGF-2α, alone or 4-OI treatment. Data are mean ± SEM n=6-8 per group. *P <0.05.

### 6.4.6 4-octyl itaconate prevents 222reconstruction via endothelium independent mechanisms in mouse aorta

To determine the mechanism underlying 4-OI mediated loss of constriction in mouse aortas, relaxation curves in response to 4-OI were compared (Figure 6.7A). Responses to exogenous 4-OI were comparable in the presence of the cyclooxygenase inhibitor, Indomethacin (10 μM), and the NOS inhibitor, L-NAME (100 μM). (Figure 6.7B). Furthermore, again in the presence of Indomethacin and L-NAME, addition of apamin and charybdotoxin (EDHF blockers) vasodilation was not altered with 4-OI treatment (Figure 6.7C). Addition of soluble guanylyl cyclase (sGC) inhibitor ODQ to indomethacin and L-NAME treatment did not alter relaxation response in the presence of 4-OI (Figure 6.7D). Surprisingly, in the presence of Indomethacin, L-NAME, Apamin, Charybdotoxin and ODQ, which inhibit all the major pathways for endothelium-derived vasodilation, there was no effect on vasodilation following 4-OI treatment (Figure 6.7E). The concentration of ODQ used was sufficient to block sGC and its downstream signaling pathway and hence block exogenous NO (SNP) (Figure 6.7F). Overall, this suggests 4-OI mediated loss of constriction in mouse aortas is endothelium independent, and could be occurring through mechanisms in smooth muscle cells.

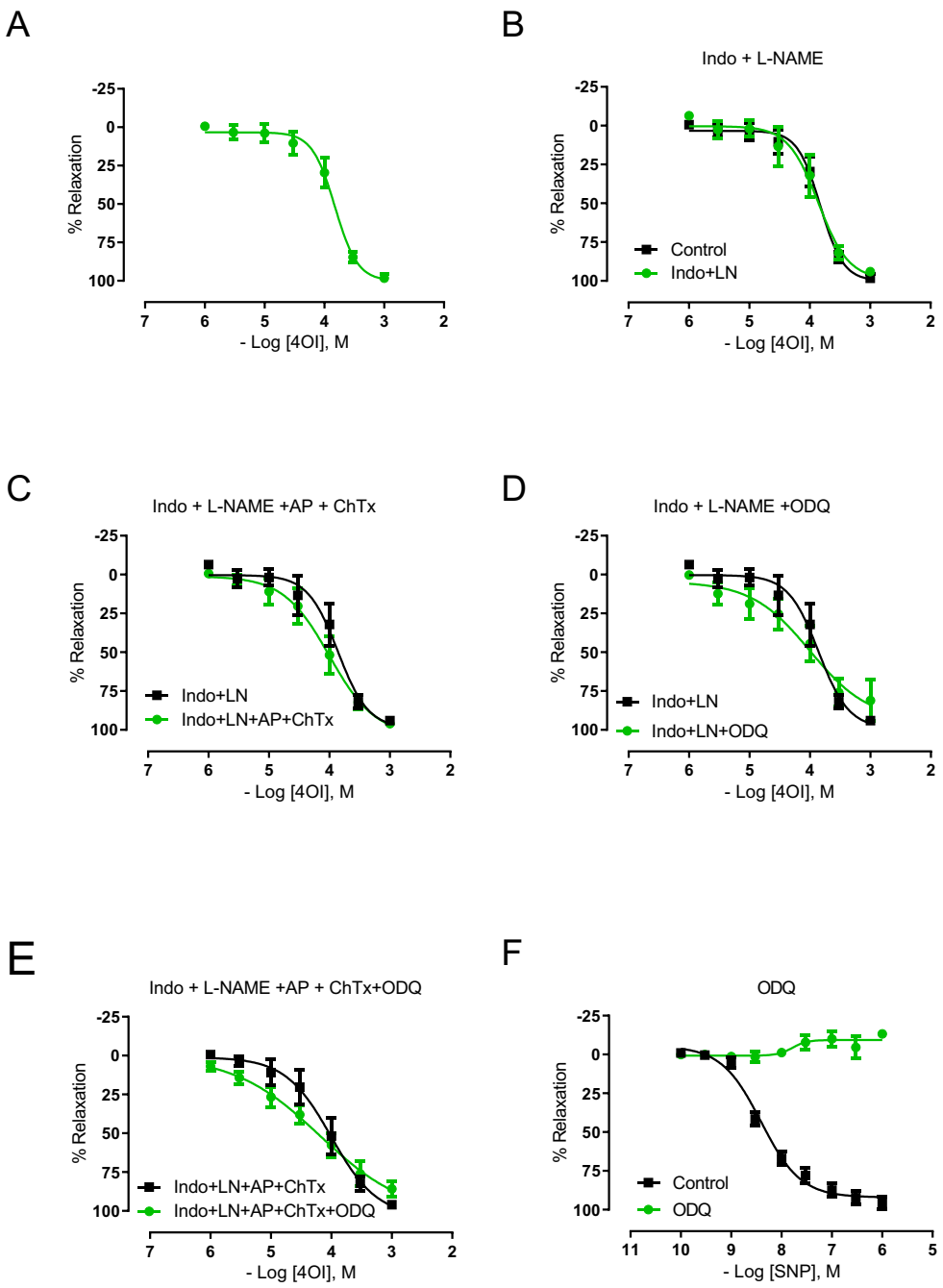



**Figure 6. 7 4-OI prevents preconstriction via endothelium independent mechanisms in mouse aorta**

A) Vasodilation in response to 4-OI. B) Vasodilation in response to 4-OI in the presence of Indomethacin, L-NAME. C) Vasodilation in response to 4-OI in the presence of Indomethacin, L-NAME, Apamin, and Charybdotoxin. D) Vasodilation in response to 4-OI in the presence of Indomethacin, L-NAME and ODQ. E) Vasodilation in response to 4-OI in the presence of Indomethacin, L-NAME, Apamin, and Charybdotoxin and ODQ. F) Vasodilation in response to inhibitor of soluble guanylyl cyclase, ODQ, in the absence of 4-OI showing that vessels are able to constrict. Data are mean ± SEM. n=6-8.

Drugs used:

Indomethacin, Cox inhibitor; L-NAME, eNOS inhibitor; Apamin, calcium-activated potassium channel blocker; Charybdotoxin, voltage dependent potassium channel blocker; ODQ, non-competitive inhibitor of soluble guanylyl cyclase

### 6.4.7 Octanol prevents preconstriction to a lesser extent to 4-octyl itaconate in mouse aortas and independent of the endothelium

4-OI diffuses into cells where it is cleaved by esterases to octanol and itaconate. To test whether 4-OI mediated loss of constriction were due to itaconate or the effects of the 4-OI derivative, mouse aortas were incubated in octanol and itaconate. Maximal vasoconstriction to 60mM KCl (non-receptor mediated contraction) was comparable between untreated and octanol-treated wildtype aortas (Figure 6.8A). Following PE-mediated vasoconstriction, 1mM octanol incubation caused a 50% reduction in contraction (Figure 6.8B). Concentration response curves of the negative control, octanol (Figure 6.8C). This suggests 4-OI mediated loss of constriction is at least partly due to octanol.

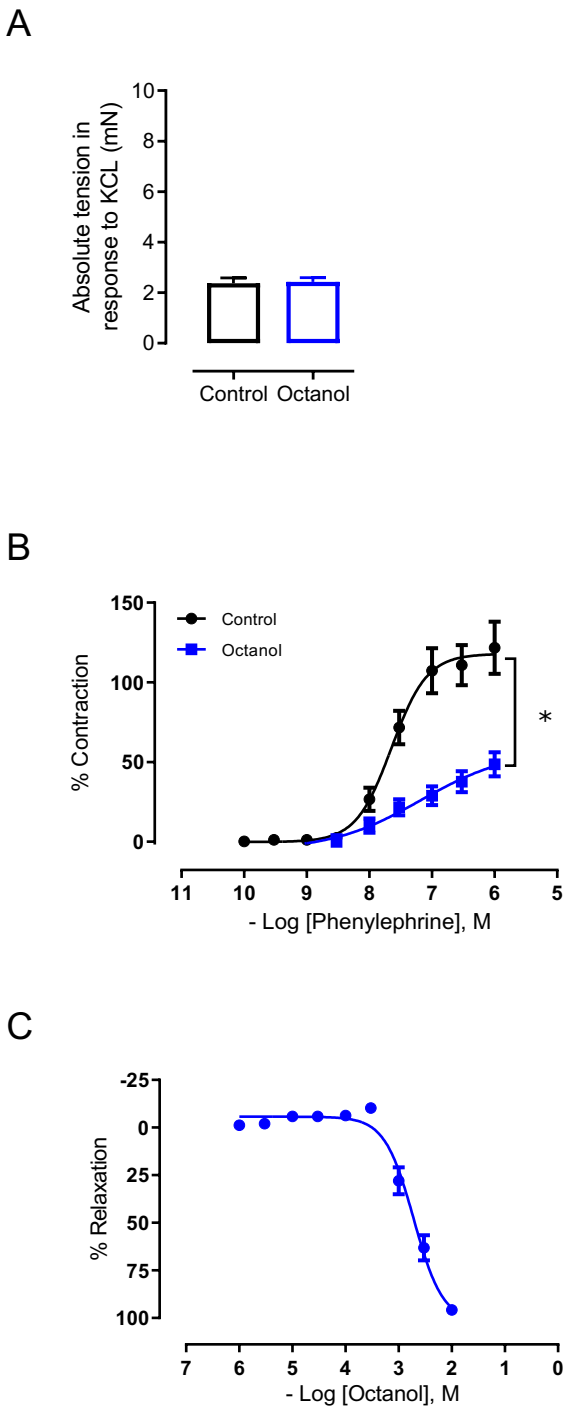



**Figure 6. 8 Octanol prevents preconstriction to a lesser extent to 4-OI in mouse aortas and independent of the endothelium**

A) Absolute tension in aorta in response to potassium chloride (KCL) showing the vessels are healthy and equally responsive B) Vasoconstriction in response to PE, alone or with 1mM octanol treatment. This effect is reversible with extensive washing. C) Dose response to 1mM octanol treatment. Data are mean ± SEM. n=6-8 per group, *P <0.05.

### 6.4.8 Itaconate prevents preconstriction less potently than 4-octyl itaconate and independent of endothelium

Maximal vasoconstriction to 60mM KCl (non-receptor mediated contraction) was comparable between untreated and itaconate treated wildtype aortas (Figure 6.9A). With 1mM itaconate pre-incubation, receptor-mediated vasoconstriction to phenylephrine was reduced by 30%, an effect not observed in control group (Figure 6.9B). Similarly, to 4-OI, this effect was reversible with after extensive (>7) washes with Krebs Hensleit Buffer (Figure 6.9A). Loss of constriction induced by itaconate treatment was not normalised in the presence of non-selective nitric oxide synthase (NOS) inhibitor, L-NAME (100μM), indicating the relaxant effect is again not mediated by tonic eNOS-derived vasodilation (Figure 6.9C).

Concentration response curves of exogenous itaconate in isolated aortic rings from Wildtype mice revealed an Ec50 of 6.67 mM compared to 4-OI (Figure 6.9D). This shows 4-OI is approximately 40-fold more potent than itaconate, although its effects are driven in large part by octanol. In the absence of the endothelium, itaconate-mediated loss of vasoconstriction in mouse aortic rings remained unchanged, indicating its effects are not endothelium dependent (Figure 6.9E).

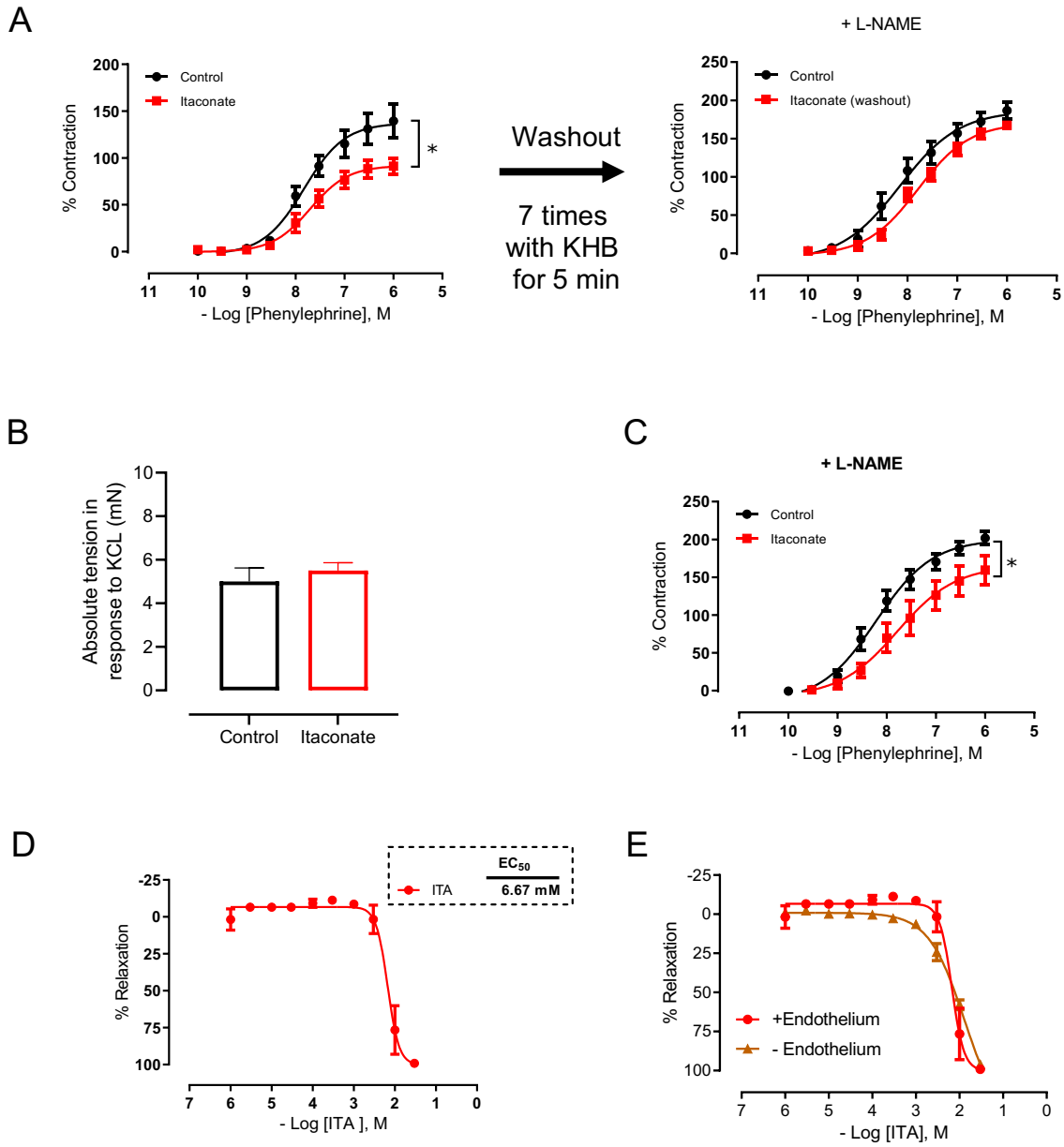
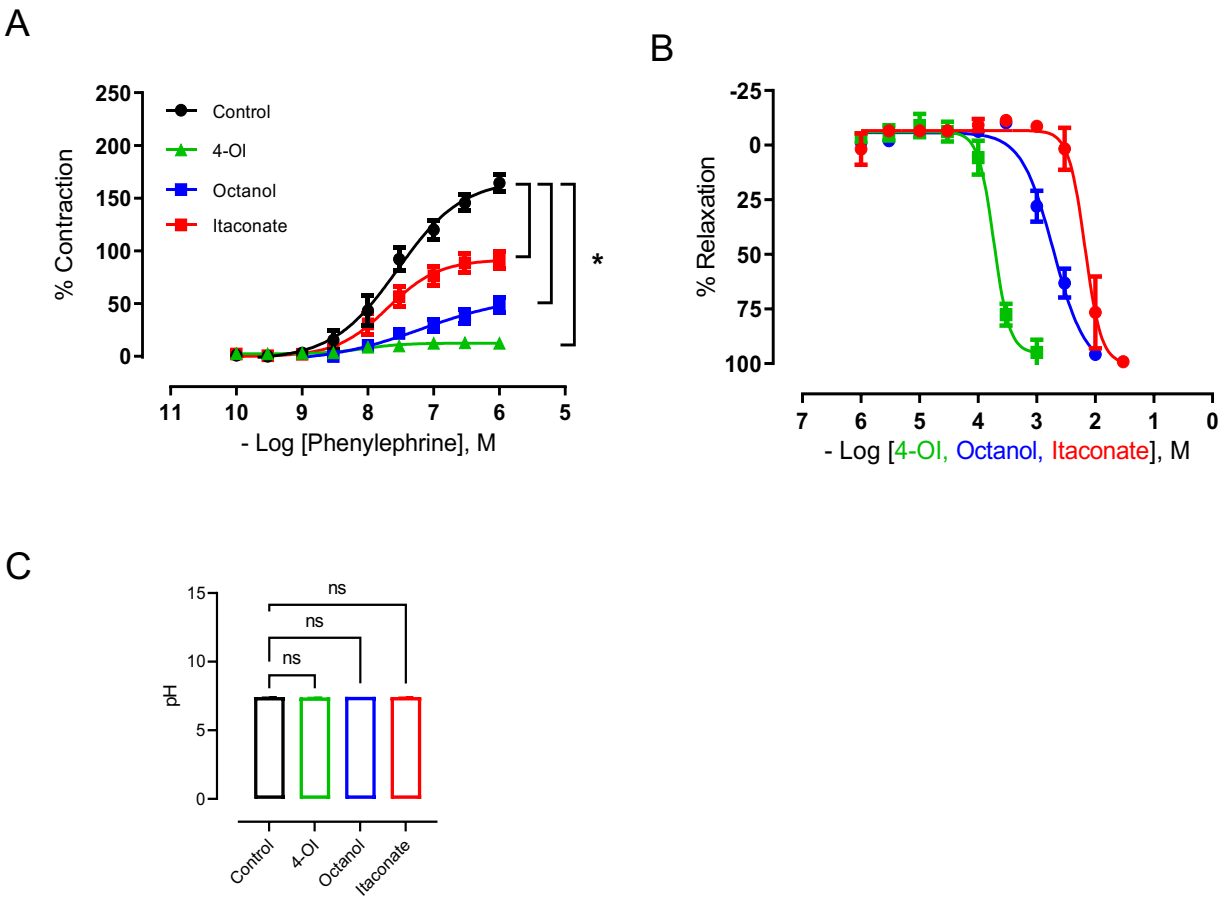



**Figure 6. 9 Itaconate causes loss of vasoconstriction less potently than 4-OI and independent of endothelium**

A) Vasoconstriction in response to phenylephrine (PE), alone or with 1mM itaconate treatment. This effect is reversible with extensive washing. B) Absolute tension in aorta in response to potassium chloride (KCL) showing the vessels are healthy and equally responsive. C) Vasoconstriction in response to PE, alone or with 1mM itaconic acid treatment in the presence of eNOS inhibitor, L-NAME. D) Dose response to itaconic acid treatment. E) Loss of constriction in response to itaconic acid treatment in intact or endothelium-denuded WT aortas. Data are mean ± SEM, *P <0.05. n=6-8 per group).

### 6.4.9 Itaconate and Octanol mediated loss of constriction have additive effect

4-OI and its components itaconate and octanol prevented constriction in mouse aorta. PE-induced vasoconstriction was reduced by 30-40% in the presence of itaconate, 60-70% in the presence of octanol and 100% blunted in the presence of 4-OI (Figure 6.10A). Furthermore, 4-OI was 18 times more potent than octanol and 44 times more potent than itaconate (Figure 6.10B). Unlike 4-OI, neither itaconate nor octanol caused complete blunting of constriction. This indicates itaconate and octanol have an additive effect. Finally, the effects observed are not due to changes in pH (Figure 6.10C).




| | Control | 4-OI | Octanol | Itaconate |
|---|---|---|---|---|
| Mean | 7.4175 | 7.4 | 7.4375 | 7.4175 |
| SD | 0.017078251 | 0.008164966 | 0.009574 | 0.005 |
| SEM | 0.008539126 | 0.004082483 | 0.004787 | 0.0025 |

**Figure 6. 10 Loss of vasoconstriction by itaconate and octanol have an additive effect**

A) Vasoconstriction in response to PE, alone or with 1mM itaconic acid, 1mM octanol or 1mM 4-OI treatment B) Vasodilation in response to octanol treatment. C) The effect of 1mM itaconic acid, 1mM octanol, 1mM 4-octyl itaconate on pH in myograph chamber. Data are mean ± SEM. n=6-8 per group, RmANOVA, *P <0.05.

## 6.5 Discussion

### 6.5.1 Overview

In this chapter, we show that *ACOD1* minor allele rs17470171 is associated with altered redox state and improved vascular function in patients with cardiovascular disease. To investigate the implications of this finding, mouse aortas were treated with itaconate or its derivative: 4-octyl itaconate (4-OI). Itaconate and octanol mediated loss of constriction was revealed to be additive, with 4-OI, comparatively the most potent. This effect was not endothelium dependent indicating the effects are mediated by vascular smooth muscle cells. To date, the therapeutic benefits of itaconate have almost exclusively been associated with the immune response and its anti-inflammatory effects. Therefore, this novel finding opens the door to investigating non-immune response focussed roles for this small but influential metabolite, in endothelial cells and vascular smooth muscle cells.

### 6.5.2 ACOD1 in cardiovascular disease

This study found that the *ACOD1* rs17470171 variant, linked to increased *ACOD1* expression, is associated with increased superoxide production via NOX enzymes and improved vascular function. This SNP has previously only been linked to inflammation. Although, in another study, ACOD1 rs17470171 and rs17385627 were associated with the immune response activation to hepatitis B vaccination in Chinese Han population (X. Liu et al., 2017). ACOD1 rs17385627 was not identified in the oxHVF SNP array analysis as customisation of this SNP array predated identification of this SNP.

In 2019, Chen et al elucidated the crystal structure of both human and murine ACOD1, which mediates itaconate production. This study reported 6 missense polymorphisms of which 6 are rare variants and directly affect ACOD1 enzyme active site to reduce activity (Chen et al., 2019). Furthermore, Chen et al hypothesised increased ACOD1 function

would be associated with decreased disease risk, supporting the association identified in the oxHVF AdipoRedox study.

Although the oxHVF AdipoRedox study is a valuable resource, it has several limitations. There is no healthy control group as the study is composed entirely of patients with advanced cardiovascular disease. Furthermore, there is a lack of diversity in the recruited patient cohort as 85% are male and 94% are of Caucasian heritage. There was no bias in the recruitment process. However, this may be due to the population demographics of the area serviced by the hospital, or the subset of patients willing to consent to being part of the study.

### 6.5.3 Is itaconate a vasodilator?

This study demonstrates that itaconate treatment has a concentration-dependant effect in mice vasculature. From the data currently, it cannot be concluded whether itaconate is a vasodilator or inhibits vasoconstriction which results in vasodilation. To shed light on this, further studies would need to be carried out targeting vasorelaxation and vasoconstriction signalling. It has previously been shown that succinate can induce relaxation in endothelium-intact aortic rings from Wistar rats that were pre-contracted with phenylephrine, with the maximum effect observed at a concentration of 10 mmol/L (Leite et al., 2016). In our study, we revealed the itaconate concentration needed for complete loss of contractility was 30 mmol/L.

Itaconate-mediated loss of constriction was not affected by removal of the endothelium indicating endothelium-independent mechanism of action. In contrast, our observations of improved vasorelaxation in human internal mammary arteries with ACOD1 rs17470171 variant were endothelium-dependent. This could be due to a species difference or artery difference as well as a difference due to healthy versus diseased vessels. Furthermore, there may be effects of ACOD1 aside from itaconate production which may result in differing

response to exogenous itaconate treatment. Itaconate-mediated loss of constriction would need to be tested in human vessels. Since itaconate-mediated loss of constriction is observed within minutes of exposure, this suggests regulation by G protein-coupled receptors (GPCRs), ion channels or calcium signalling.

Furthermore, the succinate GPCR, GPR91 (or SUNCR1), has been implicated in vascular function. Vascular function studies in GPR91-deficient mice had reduced succinate-mediated vascular relaxation suggesting endothelium dependent relaxation is due to GPR91 signalling. Also, removal of the endothelium reduced succinate-induced relaxation but not completely, suggesting a combination of endothelium dependent and independent effects (Leite et al., 2016). Unlike succinate, there is currently no known receptor for itaconate. In fact, many metabolites including malonate, oxaloacetate and α-ketoglutarate are agonists to varying degrees for GPR91 (He et al., 2004; Trauelsen et al., 2017). Non-metabolite agonists and antagonists for GPR91 also exist and with the determination of humanised GPR91, the selective antagonist NF-56-EJ40 has been reported (Haffke et al., 2019). Furthermore, M2 macrophages have high expression of GPR91. Extracellular succinate has also been shown to hyperpolarise primary human M2 macrophages compared to M1 via GPR91-activated Gq signalling (Trauelsen et al., 2021).

Due to its structural similarity with succinate, itaconate too is reportedly an agonist for GPR91 and its effects therefore may be mediated by GPR91 signalling (Trauelsen et al., 2017). However, our findings suggest an endothelium independent role of itaconate mediated effects on vasoconstriction and GPR91 is expressed by endothelial cells but not vascular smooth muscle cells. The effects of itaconate on vascular function may be due to other GPCRs or ion channels and calcium signalling as mentioned previously.

### 6.5.4 Itaconate or itaconate derivatives

Itaconate has considerable therapeutic potential due to its broad range of anti-inflammatory effects, stability and much pre-clinical evidence showing promising results (Shi et al., 2022). To enhance the permeability of this polar metabolite, an esterified derivative 4-octyl itaconate was used to assess the effects of itaconate on vascular function. Short incubation (<30min) with 4-OI caused complete loss of constriction in mouse aortas. Further investigation revealed this was mediated in part by octanol. Indeed, octanol and heptanol were shown to be reversible vascular smooth muscle cell gap junction channel inhibitors ($10^{-4}$ to $10^{-3}$ mol/L) following 15min incubation in Wistar rats (Dantas et al., 1999; Leite & Webb, 2001).

The combination of octanol and itaconate leads to an additive loss of constriction, as neither alone is able to completely blunt constriction, indicating that 4-OI has different effects than itaconate alone. In a study by Swain et al, the ability of different itaconate derivatives (4-OI, 4-EI, and DI) to produce intracellular itaconate was compared. This study demonstrated that treatment with 4-OI at concentrations higher than 125 μM only increased intracellular itaconate levels by 20% (Mills et al., 2018; Swain et al., 2020). Furthermore, although 4-OI triggers KEAP1-mediated NRF2 driven (KEAP1-NRF2) responses, similarly to itaconate, 4-OI exhibits a far greater response. In contrast to exogenous itaconate, 4-OI stabilises the NRF2 protein and can induce NRF2 induction without an additional inflammatory stimulus (i.e. LPS) (Swain et al., 2020). 4-OI is also significantly more electrophilic compared to itaconate, which is important since it is itaconate's electrophilicity which allows it to modify cysteine residues and alter protein structure and function (Swain et al., 2020). Although the mechanism of 4-OI or itaconate mediated loss of vasoconstriction is unlikely to be through NRF2-driven effects, this is a major mechanism of action associated with itaconate's immunological effects, and a mechanistic difference exists.

A recent study used itaconate and 4-OI to demonstrate both block M2 polarisation with a dose dependent decrease in classical M2 marker gene expression *Fizz1* and *Pparg* following 4-OI and itaconate treatment in BMDMs (Runtsch et al., 2022). *Arg1* and *Mrc1* mRNA was decreased with 4-OI treatment but not with itaconate treatment. Other studies too have shown non-derivatised itaconate can increase intracellular itaconate levels at high concentrations, indicating its uptake (Bambouskova et al., 2021; Li et al., 2023; Swain et al., 2020). Therefore, non-derivatised itaconate should be used wherever possible. Where derivatives are used, an appropriate derivative control in addition to a vehicle control should be used, such as octanol as well as DMSO in the case of 4-OI.

### 6.5.5 Itaconate as a potential therapeutic

This study suggests that itaconate's potential as a therapeutic agent or target extends beyond its inflammatory effects, as it exhibits vasodilatory properties. This finding could pave the way for itaconate to be used as a new target in the treatment of hypertension, where vasodilators are used to reduce resistance to blood flow through arteries and reduce blood pressure. To further investigate this, it is necessary to observe itaconate-mediated loss of vasoconstriction in resistance vessels such as mesenteric arteries, which can adjust blood flow to the digestive system depending on metabolic demands of the body, in effect contributing to overall blood pressure control (Intengan & Schiffrin, 2000). Assessment of itaconate's effects in animal models of hypertension would also provide valuable insight, for example, if treatment of itaconate in vivo or ex vivo rescues vascular function and blood pressure. Vessels from other disease models such as from diabetic or atherosclerotic models could also be assessed.

Aside from hypertension, itaconate could also play a key role in sepsis, which is characterised by a heightened immune response to infection and has been linked to Nrf2 previously (Thimmulappa et al., 2006). Hypotension is a complication of sepsis and can be

due to the release of inflammatory mediators which can cause vasodilation. We have shown previously that itaconate is secreted from macrophages in inflammatory conditions, and therefore could act as a vasodilator to contribute to a hypotensive state during sepsis. To test this blood pressure of IRG1$^{-/-}$ mice with sepsis could be assessed. Moreover, IRG1 inhibitors could be developed and used in models of sepsis. Although not measured in patients with sepsis, itaconate plasma levels were increased in early rheumatoid patients, which is another inflammatory condition, and itaconate levels here had the same predictive power as C-reactive protein (Daly et al., 2020). Furthermore, 4-OI has been suggested as a potential therapy for sepsis based on network pharmacology and molecular docking technology (M. Chen et al., 2022).

In our study, due to its low cell permeability, mouse aortas were incubated with a relatively high dose of 1mM itaconate. It is not clear whether this is a physiologically relevant dose. Although itaconate levels systemically are unlikely to be so high, even in the case of sepsis, it is plausible that in a localised area with macrophages in close contact with vessels, millimolar levels of itaconate can be reached. Other studies have reported using even higher doses of itaconate with RAW264.7 cells treated with 3mM itaconate in vitro in one study and another only observing decreased IL1β in BMDMs after pretreatment with 5mM itaconate (Bambouskova et al., 2021; Li et al., 2023).

### 6.5.6 Future work

This chapter first established that ACOD1 SNPs are associated with redox signalling and vascular function in patients with cardiovascular disease in the oxHVF cohort. Other large datasets could also be investigated such as UKBiobank to see if alternative associations are found. Next we observed itaconate-mediated loss of vasoconstriction in mouse aorta. The mechanism of action of this finding is not yet known. To explore, we would in the first instance investigate voltage gated potassium channels, gap junctions and calcium

signalling. In case it is receptor mediated, we would check cAMP signalling pathway and also use GPR91 agonists and antagonists. These studies could be compared alongside succinate too and other metabolites. Molecular studies could be followed up with treated smooth muscle cells as well as endothelial cells with itaconate. For example, coculture studies with macrophages and endothelial cells and smooth muscle cells could provide insights into the secreted role of itaconate in vessels. Furthermore, as mentioned in Chapter 3, it is also not yet known how itaconate is entering cells, and in this case, whether this occurs or differs between endothelial or smooth muscle cells.

Apart from mechanistic studies, to test its capacity as a therapeutic, itaconate treatment could be tested on diseased vessels from mouse models of hypertension, atherosclerosis or sepsis. Furthermore, vascular function studies could be carried out in IRG1$^{-/-}$ mice aorta as well as *Irg1* overexpressing mice, and particularly in a disease model. For example, *Irg1* overexpressing mice treated with angiotensin II, high fat diet or streptozotocin and assessed to see if IRG1 is protective. Importantly, it is recommended that itaconate be used in studies wherever possible. If more potent derivatives are needed, they are best used alongside the appropriate derivative controls.

# Chapter 7

# Final Discussion

# Chapter 7: Final Discussion

## 7.1 Original hypotheses and aims

Previous work from the group showed BH4 modulates mitochondrial respiration and TCA cycle metabolites. Using a new model of BH4 deficiency, we aimed to investigate the impact of this on other pathways (glycolysis, fatty acid oxidation, glutaminolysis) feeding into the TCA cycle. After observing alterations in cell bioenergetics and inflammatory status, BH4-deficient macrophages were placed in high glucose, which is an inflammatory and metabolic stimulus. In vitro hyperglycaemia yielded few changes but in vivo hyperglycaemia was hypothesised to cause more profound alterations in the inflammatory and metabolic profile of macrophages following a secondary stimulus. Finally, with its known anti-inflammatory and anti-oxidant roles, it was hypothesised that *ACOD1*, the gene encoding enzyme CAD which produces the immunometabolite itaconate, would be associated with cardiovascular disease outcomes.

## 7.2 Key findings

1. BH4 is required for the TCA cycle breaks and a complete glycolytic switch to occur in inflammatory macrophages. The resulting increased OXPHOS may be supported by increased glutaminolysis.
2. Loss of BH4 results in an overall less inflammatory macrophage phenotype with decreased levels of pro-inflammatory metabolites, such as eicosanoids, and increased levels of anti-inflammatory metabolites, such as itaconate.
3. In vitro hyperglycaemic stimulus alone (24h) has minimal effects on the inflammatory or metabolic profile of macrophages.
4. In vivo hyperglycaemia followed by a secondary inflammatory stimulus alters pro-inflammatory cytokine release and increases glycolysis and sphingomyelin metabolism.

5. *ACOD1* minor allele rs17470171 is associated with altered redox state and improved vascular function in patients with cardiovascular disease.
6. Itaconate treatment causes a loss of constriction in mouse aortas via endothelium independent mechanisms, suggesting a non-immune related role for itaconate.

### 7.3 Perspectives and future directions

Immunometabolism has become a rapidly expanding field of research over the past decade, providing invaluable insights into the intricate interplay between metabolism and immune responses. A characteristic of $M^{LPS/IFN\text{-}\gamma}$ macrophages is breaks in TCA cycle resulting in a glycolytic switch. The prevailing hypothesis suggests these breaks are at isocitrate dehydrogenase and succinate dehydrogenase. Our findings, in BH4-deficient macrophages, support an alternative hypothesis that nitric oxide mediates the first break at isocitrate dehydrogenase and is a key intermediate in the metabolic switch. This calls for a re-interpretation of the metabolic shifts during macrophage polarisation with the role of NO in mind.

The repolarisation of inflammatory macrophages to the reparative phenotype can have important implications in the treatment of inflammatory diseases. Our findings in BH4-deficient macrophages focus on $M^{LPS/IFN\text{-}\gamma}$ macrophages which appear to have a reduced inflammatory phenotype. In future studies, it is important to compare these macrophages to $M^{IL4}$ macrophages to understand if BH4-deficient $M^{LPS/IFN\text{-}\gamma}$ are more $M^{IL4}$-like or not fully $M^{LPS/IFN\text{-}\gamma}$- like. Furthermore, our findings and much of the literature, are based on LPS/IFN-γ stimulated macrophages when macrophages are exposed to a variety of stimuli including oxLDL, TNF-α, VEGF which may induce macrophage phenotype more relevant to the disease being studied. Finally, and crucially, a broader approach that encompasses subsets beyond the M1 and M2 paradigm is needed when studying macrophage phenotypes.

Although we have aimed to refer to macrophages by the stimulus, this is largely still within the M1 and M2 or inflammatory and reparative macrophage phenotype paradigm.

Whilst BH4-deficient inflammatory macrophages displayed a reduced pro-inflammatory response, it was hypothesised that βV59M-diabetic macrophages would have an enhanced pro-inflammatory phenotype. This was somewhat supported by increased IL1β levels, increased abundance of glycolytic metabolites and sphingomyelins. However, findings on the inflammatory and metabolic profile of both BH4-deficient macrophages and βV59M-diabetic macrophages need to be followed up by functional studies to ascertain if they translate into any functional outcomes. This is particularly true since there are discrepancies between metabolic profile and inflammatory cytokine release of macrophages. Although BH4-deficient macrophages are suggested to have less inflammatory phenotype, increased IL1β levels are measured. Furthermore, although βV59M-diabetic macrophages are suggested to have an enhanced inflammatory phenotype, decreased levels of TNF-α are noted.

Hyperglycaemic memory is intriguing simply as a concept, that innate immune cells retain a memory, and also with a view to answering a clinical paradox, that lowering blood glucose levels does not alter the cardiovascular prognosis of diabetic patients. The βV59M model is a neonatal model of diabetes which allows for the study of hyperglycaemia-induced sensitising, priming or even induction of trained immunity in macrophages but linking any findings in this model to type 2 diabetic patients would be a challenge. Furthermore, whether the changes observed in hyperglycaemic macrophages are significant will depend on future functional studies. Hyperglycaemia alone may have limited effects, secondary measures of diabetes, such as increased triglyceride levels may be needed to induce training and would be relevant to Type 2 diabetes.

The metabolomics study on βV59M-diabetic macrophages was an investigation of in vitro and in vitro hyperglycaemia-induced effects on macrophage metabolism. Both the metabolomics studies on BH4-deficient macrophages and βV59M-diabetic macrophages are limited by the static nature. Metabolomics provides a snapshot of the metabolome at the timepoint chosen and does not provide information on metabolic flux. In both datasets, changes in metabolites were relatively muted in known upregulated pathways. For example, the pentose phosphate pathway is known to be upregulated in inflammatory macrophages but the abundance of metabolites in the pathway remained unchanged in both datasets. This suggests the changes lie in the enzymatic expression or activity. Integration of proteomics, enzymatic activity assays or metabolic flux to metabolomics datasets would allow tracking of substrates and provide more insights to the metabolic profile of BH4-deficient and βV59M-diabetic macrophages. In the case of βV59M-diabetic macrophages, a study on their transcriptomic or epigenetic profile would have provided greater insights into if training was indeed induced with hyperglycaemia.

Aside from investigating intracellular metabolites, it is clear that future studies should also focus on the secretome of macrophages and function of secreted metabolites. In the case of itaconate, it remains to be understood how or why itaconate is secreted from the cell. With the discovery of metabolite sensing GPCRs, there may be an itaconate receptor or itaconate may act on known receptors such as the succinate sensing receptor, GPR91. Over the past decades our understanding of metabolites has grown from their being simple intermediaries in metabolic pathways, to intracellular signalling molecules and now to having potential autocrine and paracrine signalling roles. Understanding more about extracellular signalling roles may provide novel pathways to target for therapy.

One significant challenge in the area of immunometabolism is translatability. While metabolic rewiring occurs in mice, more research is needed to determine whether the same

phenomenon occurs in human macrophages. Additionally, in mice, the metabolic phenotype of macrophages is significantly influenced by nitric oxide (NO). While BH4 is needed for NO production, human inflammatory macrophages produce little to no nitric oxide in vitro. Understanding how NO affects metabolic differences between human and mice requires further investigation. Furthermore, modulating metabolic pathways in humans has the potential for off-target effects on other tissues. Although this is a challenge, drugs that target cell metabolism, such as methotrexate and rapamycin, are currently in use at low doses clinically. To achieve specificity, the property of macrophages as professional phagocytosing cells could also be exploited for drug delivery purposes, such as through the use of nanoparticles or pro-drugs.

### 7.4 Final remarks

In conclusion, this study highlights the potential of altering macrophage metabolism as a means of potentially modifying their function in the development of inflammatory diseases. Specifically, the study shows that the loss of tetrahydrobiopterin (BH4) in macrophages can alter their bioenergetics, resulting in a less inflammatory phenotype. Furthermore, the study investigated the impact of hyperglycaemia on macrophages, revealing that it primes macrophages to have altered inflammatory and metabolic profile. Finally, the study reveals a potential non-immune related role for the immunometabolite, itaconate, which was found to be secreted in large quantities by macrophages. While the study sheds light on the potential of targeting macrophage metabolism to modify their function, further studies are required to determine if these metabolic changes translate into functional outcomes.

## References


Abu-Soud, H. M., Gachhui, R., Raushel, F. M., & Stuehr, D. J. (1997). The ferrous-dioxy complex of neuronal nitric oxide synthase. Divergent effects of L-arginine and tetrahydrobiopterin on its stability. *J Biol Chem*, *272*(28), 17349-17353. https://doi.org/10.1074/jbc.272.28.17349

Abu-Soud, H. M., & Stuehr, D. J. (1993). Nitric oxide synthases reveal a role for calmodulin in controlling electron transfer. *Proc Natl Acad Sci U S A*, *90*(22), 10769-10772. https://doi.org/10.1073/pnas.90.22.10769

Akbari, M., & Hassan-Zadeh, V. (2018). Hyperglycemia Affects the Expression of Inflammatory Genes in Peripheral Blood Mononuclear Cells of Patients with Type 2 Diabetes. *Immunol Invest*, *47*(7), 654-665. https://doi.org/10.1080/08820139.2018.1480031

Allen, B. G., & Walsh, M. P. (1994). The biochemical basis of the regulation of smooth-muscle contraction. *Trends Biochem Sci*, *19*(9), 362-368. https://doi.org/10.1016/0968-0004(94)90112-0

Alving, A. S., Carson, P. E., Flanagan, C. L., & Ickes, C. E. (1956). Enzymatic deficiency in primaquine-sensitive erythrocytes. *Science*, *124*(3220), 484-485. https://doi.org/10.1126/science.124.3220.484-a

Antoniades, C., Shirodaria, C., Warrick, N., Cai, S., de Bono, J., Lee, J., Leeson, P., Neubauer, S., Ratnatunga, C., Pillai, R., Refsum, H., & Channon, K. M. (2006). 5-methyltetrahydrofolate rapidly improves endothelial function and decreases superoxide production in human vessels: effects on vascular tetrahydrobiopterin availability and endothelial nitric oxide synthase coupling. *Circulation*, *114*(11), 1193-1201. https://doi.org/10.1161/circulationaha.106.612325

Arts, R. J., Novakovic, B., Ter Horst, R., Carvalho, A., Bekkering, S., Lachmandas, E., Rodrigues, F., Silvestre, R., Cheng, S. C., Wang, S. Y., Habibi, E., Gonçalves, L. G., Mesquita, I., Cunha, C., van Laarhoven, A., van de Veerdonk, F. L., Williams, D. L., van der Meer, J. W., Logie, C., . . . Netea, M. G. (2016). Glutaminolysis and Fumarate Accumulation Integrate Immunometabolic and Epigenetic Programs in Trained Immunity. *Cell Metab*, *24*(6), 807-819. https://doi.org/10.1016/j.cmet.2016.10.008

Arts, R. J. W., Carvalho, A., La Rocca, C., Palma, C., Rodrigues, F., Silvestre, R., Kleinnijenhuis, J., Lachmandas, E., Gonçalves, L. G., Belinha, A., Cunha, C., Oosting, M., Joosten, L. A. B., Matarese, G., van Crevel, R., & Netea, M. G. (2016). Immunometabolic Pathways in BCG-Induced Trained Immunity. *Cell Rep*, *17*(10), 2562-2571. https://doi.org/10.1016/j.celrep.2016.11.011

Ayala, T. S., Tessaro, F. H. G., Jannuzzi, G. P., Bella, L. M., Ferreira, K. S., & Martins, J. O. (2019). High Glucose Environments Interfere with Bone Marrow-Derived Macrophage Inflammatory Mediator Release, the TLR4 Pathway and Glucose Metabolism. *Sci Rep*, *9*(1), 11447. https://doi.org/10.1038/s41598-019-47836-8

Baardman, J., Verberk, S. G. S., Prange, K. H. M., van Weeghel, M., van der Velden, S., Ryan, D. G., Wüst, R. C. I., Neele, A. E., Speijer, D., Denis, S. W., Witte, M. E., Houtkooper, R. H., O'Neill L, A., Knatko, E. V., Dinkova-Kostova, A. T., Lutgens, E., de Winther, M. P. J., & Van den Bossche, J. (2018). A Defective Pentose Phosphate Pathway Reduces Inflammatory Macrophage Responses during Hypercholesterolemia. *Cell Rep*, *25*(8), 2044-2052.e2045. https://doi.org/10.1016/j.celrep.2018.10.092

Bafana, R., Sivanesan, S., & Pandey, R. A. (2017). Itaconic Acid Production by Filamentous Fungi in Starch-Rich Industrial Residues. *Indian J Microbiol*, *57*(3), 322-328. https://doi.org/10.1007/s12088-017-0661-5

Bahrar, H., Bekkering, S., Stienstra, R., Netea, M. G., & Riksen, N. P. (2023). Innate immune memory in cardiometabolic disease. *Cardiovasc Res*. https://doi.org/10.1093/cvr/cvad030

Bailey, J. D., Diotallevi, M., Nicol, T., McNeill, E., Shaw, A., Chuaiphichai, S., Hale, A., Starr, A., Nandi, M., Stylianou, E., McShane, H., Davis, S., Fischer, R., Kessler, B. M., McCullagh, J., Channon, K. M., & Crabtree, M. J. (2019). Nitric Oxide Modulates Metabolic

Remodeling in Inflammatory Macrophages through TCA Cycle Regulation and Itaconate Accumulation. *Cell Rep*, *28*(1), 218-230.e217. https://doi.org/10.1016/j.celrep.2019.06.018

Bailey, J. D., Shaw, A., McNeill, E., Nicol, T., Diotallevi, M., Chuaiphichai, S., Patel, J., Hale, A., Channon, K. M., & Crabtree, M. J. (2020). Isolation and culture of murine bone marrow-derived macrophages for nitric oxide and redox biology. *Nitric Oxide*, *100-101*, 17-29. https://doi.org/10.1016/j.niox.2020.04.005

Bambouskova, M., Gorvel, L., Lampropoulou, V., Sergushichev, A., Loginicheva, E., Johnson, K., Korenfeld, D., Mathyer, M. E., Kim, H., Huang, L. H., Duncan, D., Bregman, H., Keskin, A., Santeford, A., Apte, R. S., Sehgal, R., Johnson, B., Amarasinghe, G. K., Soares, M. P., . . . Artyomov, M. N. (2018). Electrophilic properties of itaconate and derivatives regulate the IκBζ-ATF3 inflammatory axis. *Nature*, *556*(7702), 501-504. https://doi.org/10.1038/s41586-018-0052-z

Bambouskova, M., Potuckova, L., Paulenda, T., Kerndl, M., Mogilenko, D. A., Lizotte, K., Swain, A., Hayes, S., Sheldon, R. D., Kim, H., Kapadnis, U., Ellis, A. E., Isaguirre, C., Burdess, S., Laha, A., Amarasinghe, G. K., Chubukov, V., Roddy, T. P., Diamond, M. S., . . . Artyomov, M. N. (2021). Itaconate confers tolerance to late NLRP3 inflammasome activation. *Cell Rep*, *34*(10), 108756. https://doi.org/10.1016/j.celrep.2021.108756

Baup, S. (1836). Ueber eine neue Pyrogen-Citronensäure, und über Benennung der Pyrogen-Säuren überhaupt. *Annalen der Pharmacie*, *19*(1), 29-38.

Bentzon, J. F., Otsuka, F., Virmani, R., & Falk, E. (2014). Mechanisms of plaque formation and rupture. *Circ Res*, *114*(12), 1852-1866. https://doi.org/10.1161/circresaha.114.302721

Berka, V., Yeh, H. C., Gao, D., Kiran, F., & Tsai, A. L. (2004). Redox function of tetrahydrobiopterin and effect of L-arginine on oxygen binding in endothelial nitric oxide synthase. *Biochemistry*, *43*(41), 13137-13148. https://doi.org/10.1021/bi049026j

BHF. (2023). British Heart Foundation UK Fact Sheet. https://www.bhf.org.uk/-/media/files/for-professionals/research/heart-statistics/bhf-cvd-statistics-uk-factsheet.pdf?rev=e771367bf0654a4dae85cbc9dbefae17&hash=76C0182379BB6EE118EC6F76FA35A158

Brereton, M. F., Iberl, M., Shimomura, K., Zhang, Q., Adriaenssens, A. E., Proks, P., Spiliotis, II, Dace, W., Mattis, K. K., Ramracheya, R., Gribble, F. M., Reimann, F., Clark, A., Rorsman, P., & Ashcroft, F. M. (2014). Reversible changes in pancreatic islet structure and function produced by elevated blood glucose. *Nat Commun*, *5*, 4639. https://doi.org/10.1038/ncomms5639

Brereton, M. F., Rohm, M., Shimomura, K., Holland, C., Tornovsky-Babeay, S., Dadon, D., Iberl, M., Chibalina, M. V., Lee, S., Glaser, B., Dor, Y., Rorsman, P., Clark, A., & Ashcroft, F. M. (2016). Hyperglycaemia induces metabolic dysfunction and glycogen accumulation in pancreatic β-cells. *Nat Commun*, *7*, 13496. https://doi.org/10.1038/ncomms13496

Caslin, H. L., Taruselli, M. T., Haque, T., Pondicherry, N., Baldwin, E. A., Barnstein, B. O., & Ryan, J. J. (2018). Inhibiting Glycolysis and ATP Production Attenuates IL-33-Mediated Mast Cell Function and Peritonitis. *Front Immunol*, *9*, 3026. https://doi.org/10.3389/fimmu.2018.03026

Chen, F., Lukat, P., Iqbal, A. A., Saile, K., Kaever, V., van den Heuvel, J., Blankenfeldt, W., Büssow, K., & Pessler, F. (2019). Crystal structure of cis-aconitate decarboxylase reveals the impact of naturally occurring human mutations on itaconate synthesis. *Proc Natl Acad Sci U S A*, *116*(41), 20644-20654. https://doi.org/10.1073/pnas.1908770116

Chen, L. L., Morcelle, C., Cheng, Z. L., Chen, X., Xu, Y., Gao, Y., Song, J., Li, Z., Smith, M. D., Shi, M., Zhu, Y., Zhou, N., Cheng, M., He, C., Liu, K. Y., Lu, G., Zhang, L., Zhang, C., Zhang, J., . . . Ye, D. (2022). Itaconate inhibits TET DNA dioxygenases to dampen inflammatory responses. *Nat Cell Biol*, *24*(3), 353-363. https://doi.org/10.1038/s41556-022-00853-8

Chen, M., Su, W., Chen, F., Lai, T., Liu, Y., & Yu, D. (2022). Mechanisms underlying the therapeutic effects of 4-octyl itaconate in treating sepsis based on network pharmacology and molecular docking. *Front Genet*, *13*, 1056405. https://doi.org/10.3389/fgene.2022.1056405

Cheng, S. C., Quintin, J., Cramer, R. A., Shepardson, K. M., Saeed, S., Kumar, V., Giamarellos-Bourboulis, E. J., Martens, J. H., Rao, N. A., Aghajanirefah, A., Manjeri, G. R., Li, Y., Ifrim, D. C., Arts, R. J., van der Veer, B. M., Deen, P. M., Logie, C., O'Neill, L. A., Willems, P., . . . Netea, M. G. (2014). mTOR- and HIF-1α-mediated aerobic glycolysis as metabolic basis for trained immunity. *Science*, *345*(6204), 1250684. https://doi.org/10.1126/science.1250684

Chuaiphichai, S., Crabtree, M. J., McNeill, E., Hale, A. B., Trelfa, L., Channon, K. M., & Douglas, G. (2017). A key role for tetrahydrobiopterin-dependent endothelial NOS regulation in resistance arteries: studies in endothelial cell tetrahydrobiopterin-deficient mice. *Br J Pharmacol*, *174*(8), 657-671. https://doi.org/10.1111/bph.13728

Chuaiphichai, S., McNeill, E., Douglas, G., Crabtree, M. J., Bendall, J. K., Hale, A. B., Alp, N. J., & Channon, K. M. (2014). Cell-autonomous role of endothelial GTP cyclohydrolase 1 and tetrahydrobiopterin in blood pressure regulation. *Hypertension*, *64*(3), 530-540. https://doi.org/10.1161/hypertensionaha.114.03089

Cleeter, M. W., Cooper, J. M., Darley-Usmar, V. M., Moncada, S., & Schapira, A. H. (1994). Reversible inhibition of cytochrome c oxidase, the terminal enzyme of the mitochondrial respiratory chain, by nitric oxide. Implications for neurodegenerative diseases. *FEBS Lett*, *345*(1), 50-54. https://doi.org/10.1016/0014-5793(94)00424-2

Collins, P., Griffith, T. M., Henderson, A. H., & Lewis, M. J. (1986). Endothelium-derived relaxing factor alters calcium fluxes in rabbit aorta: a cyclic guanosine monophosphate-mediated effect. *J Physiol*, *381*, 427-437. https://doi.org/10.1113/jphysiol.1986.sp016336

Cordes, T., & Metallo, C. M. (2021). Itaconate Alters Succinate and Coenzyme A Metabolism via Inhibition of Mitochondrial Complex II and Methylmalonyl-CoA Mutase. *Metabolites*, *11*(2). https://doi.org/10.3390/metabo11020117

Cordes, T., Michelucci, A., & Hiller, K. (2015). Itaconic acid: the surprising role of an industrial compound as a mammalian antimicrobial metabolite. *Annual review of nutrition*, *35*, 451-473.

Corraliza, I. M., Soler, G., Eichmann, K., & Modolell, M. (1995). Arginase induction by suppressors of nitric oxide synthesis (IL-4, IL-10 and PGE2) in murine bone-marrow-derived macrophages. *Biochem Biophys Res Commun*, *206*(2), 667-673. https://doi.org/10.1006/bbrc.1995.1094

Crabtree, M. J., Tatham, A. L., Al-Wakeel, Y., Warrick, N., Hale, A. B., Cai, S., Channon, K. M., & Alp, N. J. (2009). Quantitative regulation of intracellular endothelial nitric-oxide synthase (eNOS) coupling by both tetrahydrobiopterin-eNOS stoichiometry and biopterin redox status: insights from cells with tet-regulated GTP cyclohydrolase I expression. *J Biol Chem*, *284*(2), 1136-1144. https://doi.org/10.1074/jbc.M805403200

Crabtree, M. J., Tatham, A. L., Hale, A. B., Alp, N. J., & Channon, K. M. (2009). Critical role for tetrahydrobiopterin recycling by dihydrofolate reductase in regulation of endothelial nitric-oxide synthase coupling: relative importance of the de novo biopterin synthesis versus salvage pathways. *J Biol Chem*, *284*(41), 28128-28136. https://doi.org/10.1074/jbc.M109.041483

Crasso, G. L. (1840). Untersuchungen über das Verhalten der Citronsäure in höherer Temperatur und die daraus hervorgehenden Produkte. *Justus Liebigs Annalen der Chemie*, *34*(1), 53-84.

Cui, J., Shan, K., Yang, Q., Chen, W., Feng, N., & Chen, Y. Q. (2022). Eicosanoid production by macrophages during inflammation depends on the M1/M2 phenotype. *Prostaglandins Other Lipid Mediat*, *160*, 106635. https://doi.org/10.1016/j.prostaglandins.2022.106635

Cui, X., Tang, J., Hartanto, Y., Zhang, J., Bi, J., Dai, S., Qiao, S. Z., Cheng, K., & Zhang, H. (2018). NIPAM-based Microgel Microenvironment Regulates the Therapeutic Function of Cardiac Stromal Cells. *ACS Appl Mater Interfaces*, *10*(44), 37783-37796. https://doi.org/10.1021/acsami.8b09757

Daenen, S., Sola-Gazagnes, A., M'Bemba, J., Dorange-Breillard, C., Defer, F., Elgrably, F., Larger, E., & Slama, G. (2010). Peak-time determination of post-meal glucose excursions in insulin-treated diabetic patients. *Diabetes Metab*, *36*(2), 165-169. https://doi.org/10.1016/j.diabet.2009.12.002

Daly, R., Blackburn, G., Best, C., Goodyear, C. S., Mudaliar, M., Burgess, K., Stirling, A., Porter, D., McInnes, I. B., Barrett, M. P., & Dale, J. (2020). Changes in Plasma Itaconate Elevation in Early Rheumatoid Arthritis Patients Elucidates Disease Activity Associated Macrophage Activation. *Metabolites*, *10*(6). https://doi.org/10.3390/metabo10060241

Daniels, B. P., Kofman, S. B., Smith, J. R., Norris, G. T., Snyder, A. G., Kolb, J. P., Gao, X., Locasale, J. W., Martinez, J., Gale, M., Jr., Loo, Y. M., & Oberst, A. (2019). The Nucleotide Sensor ZBP1 and Kinase RIPK3 Induce the Enzyme IRG1 to Promote an Antiviral Metabolic State in Neurons. *Immunity*, *50*(1), 64-76.e64. https://doi.org/10.1016/j.immuni.2018.11.017

Dantas, M. F., Urban, M., Spray, D., Catelli De Carvalho, M. H., & Passaglia, R. D. (1999). Increased acetylcholine-induced vasodilation in pregnant rats: A role for gap junctional communication. *Hypertension*, *34*(4 Pt 2), 937-942. https://doi.org/10.1161/01.hyp.34.4.937

Davidge, S. T., Baker, P. N., Laughlin, M. K., & Roberts, J. M. (1995). Nitric oxide produced by endothelial cells increases production of eicosanoids through activation of prostaglandin H synthase. *Circ Res*, *77*(2), 274-283. https://doi.org/10.1161/01.res.77.2.274

de Goede, K. E., Harber, K. J., Gorki, F. S., Verberk, S. G. S., Groh, L. A., Keuning, E. D., Struys, E. A., van Weeghel, M., Haschemi, A., de Winther, M. P. J., van Dierendonck, X., & Van den Bossche, J. (2022). d-2-Hydroxyglutarate is an anti-inflammatory immunometabolite that accumulates in macrophages after TLR4 activation. *Biochim Biophys Acta Mol Basis Dis*, *1868*(9), 166427. https://doi.org/10.1016/j.bbadis.2022.166427

de Souza Almeida, R. R., Bobermin, L. D., Parmeggiani, B., Wartchow, K. M., Souza, D. O., Gonçalves, C. A., Wajner, M., Leipnitz, G., & Quincozes-Santos, A. (2022). Methylmalonic acid induces inflammatory response and redox homeostasis disruption in C6 astroglial cells: potential glioprotective roles of melatonin and resveratrol. *Amino Acids*, *54*(11), 1505-1517. https://doi.org/10.1007/s00726-022-03191-z

Devaraj, S., Venugopal, S. K., Singh, U., & Jialal, I. (2005). Hyperglycemia induces monocytic release of interleukin-6 via induction of protein kinase c-{alpha} and -{beta}. *Diabetes*, *54*(1), 85-91. https://doi.org/10.2337/diabetes.54.1.85

Dewberry, R., Holden, H., Crossman, D., & Francis, S. (2000). Interleukin-1 receptor antagonist expression in human endothelial cells and atherosclerosis. *Arterioscler Thromb Vasc Biol*, *20*(11), 2394-2400. https://doi.org/10.1161/01.atv.20.11.2394

Dinarello, C. A. (2011). Interleukin-1 in the pathogenesis and treatment of inflammatory diseases. *Blood*, *117*(14), 3720-3732. https://doi.org/10.1182/blood-2010-07-273417

Diotallevi, M., Ayaz, F., Nicol, T., & Crabtree, M. J. (2021). Itaconate as an inflammatory mediator and therapeutic target in cardiovascular medicine. *Biochem Soc Trans*, *49*(5), 2189-2198. https://doi.org/10.1042/bst20210269

Divangahi, M., Aaby, P., Khader, S. A., Barreiro, L. B., Bekkering, S., Chavakis, T., van Crevel, R., Curtis, N., DiNardo, A. R., Dominguez-Andres, J., Duivenvoorden, R., Fanucchi, S., Fayad, Z., Fuchs, E., Hamon, M., Jeffrey, K. L., Khan, N., Joosten, L. A. B., Kaufmann, E., . . . Netea, M. G. (2021). Trained immunity, tolerance, priming and differentiation: distinct immunological processes. *Nat Immunol*, *22*(1), 2-6. https://doi.org/10.1038/s41590-020-00845-6

Donnarumma, E., Bhushan, S., Bradley, J. M., Otsuka, H., Donnelly, E. L., Lefer, D. J., & Islam, K. N. (2016). Nitrite Therapy Ameliorates Myocardial Dysfunction via H2S and Nuclear Factor-Erythroid 2-Related Factor 2 (Nrf2)-Dependent Signaling in Chronic Heart Failure. *J Am Heart Assoc*, *5*(8). https://doi.org/10.1161/jaha.116.003551

Douglas, G., Hale, A. B., Patel, J., Chuaiphichai, S., Al Haj Zen, A., Rashbrook, V. S., Trelfa, L., Crabtree, M. J., McNeill, E., & Channon, K. M. (2018). Roles for endothelial cell and macrophage Gch1 and tetrahydrobiopterin in atherosclerosis progression. *Cardiovasc Res*, *114*(10), 1385-1399. https://doi.org/10.1093/cvr/cvy078

Doyle, A. G., Herbein, G., Montaner, L. J., Minty, A. J., Caput, D., Ferrara, P., & Gordon, S. (1994). Interleukin-13 alters the activation state of murine macrophages in vitro: comparison with interleukin-4 and interferon-gamma. *Eur J Immunol*, *24*(6), 1441-1445. https://doi.org/10.1002/eji.1830240630

Edgar, L., Akbar, N., Braithwaite, A. T., Krausgruber, T., Gallart-Ayala, H., Bailey, J., Corbin, A. L., Khoyratty, T. E., Chai, J. T., Alkhalil, M., Rendeiro, A. F., Ziberna, K., Arya, R., Cahill, T. J., Bock, C., Laurencikiene, J., Crabtree, M. J., Lemieux, M. E., Riksen, N. P., . . . Choudhury, R. P. (2021). Hyperglycemia Induces Trained Immunity in Macrophages and Their Precursors and Promotes Atherosclerosis. *Circulation*, *144*(12), 961-982. https://doi.org/10.1161/circulationaha.120.046464

Edwards, G., Dora, K. A., Gardener, M. J., Garland, C. J., & Weston, A. H. (1998). K+ is an endothelium-derived hyperpolarizing factor in rat arteries. *Nature*, *396*(6708), 269-272. https://doi.org/10.1038/24388

El-Osta, A., Brasacchio, D., Yao, D., Pocai, A., Jones, P. L., Roeder, R. G., Cooper, M. E., & Brownlee, M. (2008). Transient high glucose causes persistent epigenetic changes and altered gene expression during subsequent normoglycemia. *J Exp Med*, *205*(10), 2409-2417. https://doi.org/10.1084/jem.20081188

ElAzzouny, M., Tom, C. T., Evans, C. R., Olson, L. L., Tanga, M. J., Gallagher, K. A., Martin, B. R., & Burant, C. F. (2017). Dimethyl Itaconate Is Not Metabolized into Itaconate Intracellularly. *J Biol Chem*, *292*(12), 4766-4769. https://doi.org/10.1074/jbc.C117.775270

Everts, B., Amiel, E., van der Windt, G. J., Freitas, T. C., Chott, R., Yarasheski, K. E., Pearce, E. L., & Pearce, E. J. (2012). Commitment to glycolysis sustains survival of NO-producing inflammatory dendritic cells. *Blood*, *120*(7), 1422-1431. https://doi.org/10.1182/blood-2012-03-419747

Fan, J., Liu, Y., Su, S., Cao, Y., & Yu, Y. (2021). New conditions of HPLC analysis for separation and quantification of simple organic acids of tricarboxylic acid cycle in psoriasis. *Acta Chromatographica*, *33*(4), 322-332. https://doi.org/https://doi.org/10.1556/1326.2020.00838

Fanucchi, S., Domínguez-Andrés, J., Joosten, L. A. B., Netea, M. G., & Mhlanga, M. M. (2021). The Intersection of Epigenetics and Metabolism in Trained Immunity. *Immunity*, *54*(1), 32-43. https://doi.org/10.1016/j.immuni.2020.10.011

Fitzgerald, K. A., & Kagan, J. C. (2020). Toll-like Receptors and the Control of Immunity. *Cell*, *180*(6), 1044-1066. https://doi.org/10.1016/j.cell.2020.02.041

Fitzgerald, K. A., Rowe, D. C., Barnes, B. J., Caffrey, D. R., Visintin, A., Latz, E., Monks, B., Pitha, P. M., & Golenbock, D. T. (2003). LPS-TLR4 signaling to IRF-3/7 and NF-kappaB involves the toll adapters TRAM and TRIF. *J Exp Med*, *198*(7), 1043-1055. https://doi.org/10.1084/jem.20031023

Freemerman, A. J., Johnson, A. R., Sacks, G. N., Milner, J. J., Kirk, E. L., Troester, M. A., Macintyre, A. N., Goraksha-Hicks, P., Rathmell, J. C., & Makowski, L. (2014). Metabolic reprogramming of macrophages: glucose transporter 1 (GLUT1)-mediated glucose metabolism drives a proinflammatory phenotype. *J Biol Chem*, *289*(11), 7884-7896. https://doi.org/10.1074/jbc.M113.522037

Fu, X., Wu, M., & Zhou, X. (2021). Protective effects of 4-octyl itaconate against inflammatory response in angiotensin II-induced oxidative stress in human primary retinal pigment epithelium. *Biochem Biophys Res Commun*, *557*, 77-84. https://doi.org/10.1016/j.bbrc.2021.03.113

Fujisaka, S. (2021). The role of adipose tissue M1/M2 macrophages in type 2 diabetes mellitus. *Diabetol Int*, *12*(1), 74-79. https://doi.org/10.1007/s13340-020-00482-2

Fukuzumi, M., Shinomiya, H., Shimizu, Y., Ohishi, K., & Utsumi, S. (1996). Endotoxin-induced enhancement of glucose influx into murine peritoneal macrophages via GLUT1. *Infect Immun*, *64*(1), 108-112. https://doi.org/10.1128/iai.64.1.108-112.1996

Gabbi, P., Ribeiro, L. R., Jessié Martins, G., Cardoso, A. S., Haupental, F., Rodrigues, F. S., Machado, A. K., Sperotto Brum, J., Medeiros Frescura Duarte, M. M., Schetinger, M. R., da Cruz, I. B., Flávia Furian, A., Oliveira, M. S., Dos Santos, A. R., Royes, L. F., Fighera, M. R., & de Freitas, M. L. (2017). Methylmalonate Induces Inflammatory and Apoptotic Potential: A Link to Glial Activation and Neurological Dysfunction. *J Neuropathol Exp Neurol*, *76*(3), 160-178. https://doi.org/10.1093/jnen/nlw121

Gerstein, H. C., Miller, M. E., Genuth, S., Ismail-Beigi, F., Buse, J. B., Goff, D. C., Jr., Probstfield, J. L., Cushman, W. C., Ginsberg, H. N., Bigger, J. T., Grimm, R. H., Jr., Byington, R. P.,

Rosenberg, Y. D., & Friedewald, W. T. (2011). Long-term effects of intensive glucose lowering on cardiovascular outcomes. *N Engl J Med*, *364*(9), 818-828. https://doi.org/10.1056/NEJMoa1006524

Gimbrone, M. A., Jr., & García-Cardeña, G. (2016). Endothelial Cell Dysfunction and the Pathobiology of Atherosclerosis. *Circ Res*, *118*(4), 620-636. https://doi.org/10.1161/circresaha.115.306301

Goldstein, J. L., Ho, Y. K., Basu, S. K., & Brown, M. S. (1979). Binding site on macrophages that mediates uptake and degradation of acetylated low density lipoprotein, producing massive cholesterol deposition. *Proc Natl Acad Sci U S A*, *76*(1), 333-337. https://doi.org/10.1073/pnas.76.1.333

Gordon, S. (2008). Elie Metchnikoff: father of natural immunity. *Eur J Immunol*, *38*(12), 3257-3264. https://doi.org/10.1002/eji.200838855

Grosick, R., Alvarado-Vazquez, P. A., Messersmith, A. R., & Romero-Sandoval, E. A. (2018). High glucose induces a priming effect in macrophages and exacerbates the production of pro-inflammatory cytokines after a challenge. *J Pain Res*, *11*, 1769-1778. https://doi.org/10.2147/jpr.S164493

Gu, L., Lin, J., Wang, Q., Li, C., Peng, X., Fan, Y., Lu, C., Lin, H., Niu, Y., Zhu, G., & Zhao, G. (2020). Dimethyl itaconate protects against fungal keratitis by activating the Nrf2/HO-1 signaling pathway. *Immunol Cell Biol*, *98*(3), 229-241. https://doi.org/10.1111/imcb.12316

Guria, S., Hoory, A., Das, S., Chattopadhyay, D., & Mukherjee, S. (2023). Adipose tissue macrophages and their role in obesity-associated insulin resistance: an overview of the complex dynamics at play. *Biosci Rep*, *43*(3). https://doi.org/10.1042/bsr20220200

Haffke, M., Fehlmann, D., Rummel, G., Boivineau, J., Duckely, M., Gommermann, N., Cotesta, S., Sirockin, F., Freuler, F., Littlewood-Evans, A., Kaupmann, K., & Jaakola, V. P. (2019). Structural basis of species-selective antagonist binding to the succinate receptor. *Nature*, *574*(7779), 581-585. https://doi.org/10.1038/s41586-019-1663-8

Han, Y. Y., Gu, X., Yang, C. Y., Ji, H. M., Lan, Y. J., Bi, Y. Q., Si, R., Qu, J., Cheng, M. H., & Gao, J. (2021). Protective effect of dimethyl itaconate against fibroblast-myofibroblast differentiation during pulmonary fibrosis by inhibiting TXNIP. *J Cell Physiol*, *236*(11), 7734-7744. https://doi.org/10.1002/jcp.30456

Hannun, Y. A., & Obeid, L. M. (2018). Sphingolipids and their metabolism in physiology and disease. *Nat Rev Mol Cell Biol*, *19*(3), 175-191. https://doi.org/10.1038/nrm.2017.107

Harber, K. J., de Goede, K. E., Verberk, S. G. S., Meinster, E., de Vries, H. E., van Weeghel, M., de Winther, M. P. J., & Van den Bossche, J. (2020). Succinate Is an Inflammation-Induced Immunoregulatory Metabolite in Macrophages. *Metabolites*, *10*(9). https://doi.org/10.3390/metabo10090372

Haschemi, A., Kosma, P., Gille, L., Evans, C. R., Burant, C. F., Starkl, P., Knapp, B., Haas, R., Schmid, J. A., Jandl, C., Amir, S., Lubec, G., Park, J., Esterbauer, H., Bilban, M., Brizuela, L., Pospisilik, J. A., Otterbein, L. E., & Wagner, O. (2012). The sedoheptulose kinase CARKL directs macrophage polarization through control of glucose metabolism. *Cell Metab*, *15*(6), 813-826. https://doi.org/10.1016/j.cmet.2012.04.023

Haythorne, E., Lloyd, M., Walsby-Tickle, J., Tarasov, A. I., Sandbrink, J., Portillo, I., Exposito, R. T., Sachse, G., Cyranka, M., Rohm, M., Rorsman, P., McCullagh, J., & Ashcroft, F. M. (2022). Altered glycolysis triggers impaired mitochondrial metabolism and mTORC1 activation in diabetic β-cells. *Nat Commun*, *13*(1), 6754. https://doi.org/10.1038/s41467-022-34095-x

Haythorne, E., Rohm, M., van de Bunt, M., Brereton, M. F., Tarasov, A. I., Blacker, T. S., Sachse, G., Silva Dos Santos, M., Terron Exposito, R., Davis, S., Baba, O., Fischer, R., Duchen, M. R., Rorsman, P., MacRae, J. I., & Ashcroft, F. M. (2019). Diabetes causes marked inhibition of mitochondrial metabolism in pancreatic β-cells. *Nat Commun*, *10*(1), 2474. https://doi.org/10.1038/s41467-019-10189-x

He, W., Miao, F. J., Lin, D. C., Schwandner, R. T., Wang, Z., Gao, J., Chen, J. L., Tian, H., & Ling, L. (2004). Citric acid cycle intermediates as ligands for orphan G-protein-coupled receptors. *Nature*, *429*(6988), 188-193. https://doi.org/10.1038/nature02488

Holman, R. R., Paul, S. K., Bethel, M. A., Matthews, D. R., & Neil, H. A. (2008). 10-year follow-up of intensive glucose control in type 2 diabetes. *N Engl J Med*, *359*(15), 1577-1589. https://doi.org/10.1056/NEJMoa0806470

Honold, L., & Nahrendorf, M. (2018). Resident and Monocyte-Derived Macrophages in Cardiovascular Disease. *Circ Res*, *122*(1), 113-127. https://doi.org/10.1161/circresaha.117.311071

Hooftman, A., Angiari, S., Hester, S., Corcoran, S. E., Runtsch, M. C., Ling, C., Ruzek, M. C., Slivka, P. F., McGettrick, A. F., Banahan, K., Hughes, M. M., Irvine, A. D., Fischer, R., & O'Neill, L. A. J. (2020). The Immunomodulatory Metabolite Itaconate Modifies NLRP3 and Inhibits Inflammasome Activation. *Cell Metab*, *32*(3), 468-478.e467. https://doi.org/10.1016/j.cmet.2020.07.016

Horecker, B. L. (2002). The pentose phosphate pathway. *J Biol Chem*, *277*(50), 47965-47971. https://doi.org/10.1074/jbc.X200007200

Horng, T., Barton, G. M., Flavell, R. A., & Medzhitov, R. (2002). The adaptor molecule TIRAP provides signalling specificity for Toll-like receptors. *Nature*, *420*(6913), 329-333. https://doi.org/10.1038/nature01180

Hua, K.-F., Wang, S.-H., Dong, W.-C., Lin, C.-Y., Ho, C.-L., & Wu, T.-H. (2012). High glucose increases nitric oxide generation in lipopolysaccharide-activated macrophages by enhancing activity of protein kinase C-α/δ and NF-κB. *Inflammation Research*, *61*, 1107-1116.

Huang, S. C., Everts, B., Ivanova, Y., O'Sullivan, D., Nascimento, M., Smith, A. M., Beatty, W., Love-Gregory, L., Lam, W. Y., O'Neill, C. M., Yan, C., Du, H., Abumrad, N. A., Urban, J. F., Jr., Artyomov, M. N., Pearce, E. L., & Pearce, E. J. (2014). Cell-intrinsic lysosomal lipolysis is essential for alternative activation of macrophages. *Nat Immunol*, *15*(9), 846-855. https://doi.org/10.1038/ni.2956

Huang, X., Lu, X., Li, Y., Li, X., & Li, J. J. (2014). Improving itaconic acid production through genetic engineering of an industrial Aspergillus terreus strain. *Microb Cell Fact*, *13*, 119. https://doi.org/10.1186/s12934-014-0119-y

Ignarro, L. J. (2000). *Nitric oxide: biology and pathobiology*. Academic press.

Ignarro, L. J., Harbison, R. G., Wood, K. S., & Kadowitz, P. J. (1986). Activation of purified soluble guanylate cyclase by endothelium-derived relaxing factor from intrapulmonary artery and vein: stimulation by acetylcholine, bradykinin and arachidonic acid. *J Pharmacol Exp Ther*, *237*(3), 893-900.

Intengan, H. D., & Schiffrin, E. L. (2000). Structure and mechanical properties of resistance arteries in hypertension: role of adhesion molecules and extracellular matrix determinants. *Hypertension*, *36*(3), 312-318. https://doi.org/10.1161/01.hyp.36.3.312

Jamali-Raeufy, N., Alizadeh, F., Mehrabi, Z., Mehrabi, S., & Goudarzi, M. (2021). Acetyl-L-carnitine confers neuroprotection against lipopolysaccharide (LPS) -induced neuroinflammation by targeting TLR4/NFκB, autophagy, inflammation and oxidative stress. *Metab Brain Dis*, *36*(6), 1391-1401. https://doi.org/10.1007/s11011-021-00715-6

Jha, A. K., Huang, S. C., Sergushichev, A., Lampropoulou, V., Ivanova, Y., Loginicheva, E., Chmielewski, K., Stewart, K. M., Ashall, J., Everts, B., Pearce, E. J., Driggers, E. M., & Artyomov, M. N. (2015). Network integration of parallel metabolic and transcriptional data reveals metabolic modules that regulate macrophage polarization. *Immunity*, *42*(3), 419-430. https://doi.org/10.1016/j.immuni.2015.02.005

Jones, K. A., Wong, G. Y., Jankowski, C. J., Akao, M., & Warner, D. O. (1999). cGMP modulation of Ca2+ sensitivity in airway smooth muscle. *Am J Physiol*, *276*(1), L35-40. https://doi.org/10.1152/ajplung.1999.276.1.L35

Kanamasa, S., Dwiarti, L., Okabe, M., & Park, E. Y. (2008). Cloning and functional characterization of the cis-aconitic acid decarboxylase (CAD) gene from Aspergillus terreus. *Appl Microbiol Biotechnol*, *80*(2), 223-229. https://doi.org/10.1007/s00253-008-1523-1

Kang, K., Bachu, M., Park, S. H., Kang, K., Bae, S., Park-Min, K. H., & Ivashkiv, L. B. (2019). IFN-γ selectively suppresses a subset of TLR4-activated genes and enhancers to potentiate

macrophage activation. *Nat Commun*, *10*(1), 3320. https://doi.org/10.1038/s41467-019-11147-3

Keating, S. T., Groh, L., Thiem, K., Bekkering, S., Li, Y., Matzaraki, V., van der Heijden, C., van Puffelen, J. H., Lachmandas, E., Jansen, T., Oosting, M., de Bree, L. C. J., Koeken, V., Moorlag, S., Mourits, V. P., van Diepen, J., Strienstra, R., Novakovic, B., Stunnenberg, H. G., . . . Riksen, N. P. (2020). Rewiring of glucose metabolism defines trained immunity induced by oxidized low-density lipoprotein. *J Mol Med (Berl)*, *98*(6), 819-831. https://doi.org/10.1007/s00109-020-01915-w

Keating, S. T., Groh, L., van der Heijden, C., Rodriguez, H., Dos Santos, J. C., Fanucchi, S., Okabe, J., Kaipananickal, H., van Puffelen, J. H., Helder, L., Noz, M. P., Matzaraki, V., Li, Y., de Bree, L. C. J., Koeken, V., Moorlag, S., Mourits, V. P., Domínguez-Andrés, J., Oosting, M., . . . Riksen, N. P. (2020). The Set7 Lysine Methyltransferase Regulates Plasticity in Oxidative Phosphorylation Necessary for Trained Immunity Induced by β-Glucan. *Cell Rep*, *31*(3), 107548. https://doi.org/10.1016/j.celrep.2020.107548

Keiran, N., Ceperuelo-Mallafré, V., Calvo, E., Hernández-Alvarez, M. I., Ejarque, M., Núñez-Roa, C., Horrillo, D., Maymó-Masip, E., Rodríguez, M. M., Fradera, R., de la Rosa, J. V., Jorba, R., Megia, A., Zorzano, A., Medina-Gómez, G., Serena, C., Castrillo, A., Vendrell, J., & Fernández-Veledo, S. (2019). SUCNR1 controls an anti-inflammatory program in macrophages to regulate the metabolic response to obesity. *Nat Immunol*, *20*(5), 581-592. https://doi.org/10.1038/s41590-019-0372-7

Kelly, B., & O'Neill, L. A. (2015). Metabolic reprogramming in macrophages and dendritic cells in innate immunity. *Cell Res*, *25*(7), 771-784. https://doi.org/10.1038/cr.2015.68

Kolliniati, O., Ieronymaki, E., Vergadi, E., & Tsatsanis, C. (2022). Metabolic Regulation of Macrophage Activation. *J Innate Immun*, *14*(1), 51-68. https://doi.org/10.1159/000516780

Kotanidis, C. (2021). Developing new biomarkers for cardiovascular disease
The prognostic potential of oxidative stress, and perivascular adipose tissue phenotyping. *Thesis*.

Krawczyk, C. M., Holowka, T., Sun, J., Blagih, J., Amiel, E., DeBerardinis, R. J., Cross, J. R., Jung, E., Thompson, C. B., Jones, R. G., & Pearce, E. J. (2010). Toll-like receptor-induced changes in glycolytic metabolism regulate dendritic cell activation. *Blood*, *115*(23), 4742-4749. https://doi.org/10.1182/blood-2009-10-249540

Kuo, P. C., Weng, W. T., Scofield, B. A., Paraiso, H. C., Brown, D. A., Wang, P. Y., Yu, I. C., & Yen, J. H. (2020). Dimethyl itaconate, an itaconate derivative, exhibits immunomodulatory effects on neuroinflammation in experimental autoimmune encephalomyelitis. *J Neuroinflammation*, *17*(1), 138. https://doi.org/10.1186/s12974-020-01768-7

Lachmandas, E., Vrieling, F., Wilson, L. G., Joosten, S. A., Netea, M. G., Ottenhoff, T. H., & van Crevel, R. (2015). The effect of hyperglycaemia on in vitro cytokine production and macrophage infection with Mycobacterium tuberculosis. *PLoS One*, *10*(2), e0117941. https://doi.org/10.1371/journal.pone.0117941

Lamas, S., Marsden, P. A., Li, G. K., Tempst, P., & Michel, T. (1992). Endothelial nitric oxide synthase: molecular cloning and characterization of a distinct constitutive enzyme isoform. *Proc Natl Acad Sci U S A*, *89*(14), 6348-6352. https://doi.org/10.1073/pnas.89.14.6348

Lampropoulou, V., Sergushichev, A., Bambouskova, M., Nair, S., Vincent, E. E., Loginicheva, E., Cervantes-Barragan, L., Ma, X., Huang, S. C., Griss, T., Weinheimer, C. J., Khader, S., Randolph, G. J., Pearce, E. J., Jones, R. G., Diwan, A., Diamond, M. S., & Artyomov, M. N. (2016). Itaconate Links Inhibition of Succinate Dehydrogenase with Macrophage Metabolic Remodeling and Regulation of Inflammation. *Cell Metab*, *24*(1), 158-166. https://doi.org/10.1016/j.cmet.2016.06.004

Leite, L. N., Gonzaga, N. A., Simplicio, J. A., do Vale, G. T., Carballido, J. M., Alves-Filho, J. C., & Tirapelli, C. R. (2016). Pharmacological characterization of the mechanisms underlying the vascular effects of succinate. *Eur J Pharmacol*, *789*, 334-343. https://doi.org/10.1016/j.ejphar.2016.07.045

Leite, R., & Webb, R. C. (2001). Increased dilator response to heptanol and octanol in aorta from DOCA-salt-hypertensive rats. *Pharmacology*, *62*(1), 29-35. https://doi.org/10.1159/000056069

Li, R., Yang, W., Yin, Y., Ma, X., Zhang, P., & Tao, K. (2021). 4-OI Attenuates Carbon Tetrachloride-Induced Hepatic Injury via Regulating Oxidative Stress and the Inflammatory Response. *Front Pharmacol*, *12*, 651444. https://doi.org/10.3389/fphar.2021.651444

Li, W., Li, Y., Kang, J., Jiang, H., Gong, W., Chen, L., Wu, C., Liu, M., Wu, X., Zhao, Y., & Ren, J. (2023). 4-octyl itaconate as a metabolite derivative inhibits inflammation via alkylation of STING. *Cell Rep*, *42*(3), 112145. https://doi.org/10.1016/j.celrep.2023.112145

Li, Y., Chen, X., Zhang, H., Xiao, J., Yang, C., Chen, W., Wei, Z., Chen, X., & Liu, J. (2020). 4-Octyl Itaconate Alleviates Lipopolysaccharide-Induced Acute Lung Injury in Mice by Inhibiting Oxidative Stress and Inflammation. *Drug Des Devel Ther*, *14*, 5547-5558. https://doi.org/10.2147/dddt.S280922

Liao, S. T., Han, C., Xu, D. Q., Fu, X. W., Wang, J. S., & Kong, L. Y. (2019). 4-Octyl itaconate inhibits aerobic glycolysis by targeting GAPDH to exert anti-inflammatory effects. *Nat Commun*, *10*(1), 5091. https://doi.org/10.1038/s41467-019-13078-5

Libby, P. (2013). Mechanisms of acute coronary syndromes and their implications for therapy. *N Engl J Med*, *368*(21), 2004-2013. https://doi.org/10.1056/NEJMra1216063

Lin, J., Ren, J., Gao, D. S., Dai, Y., & Yu, L. (2021). The Emerging Application of Itaconate: Promising Molecular Targets and Therapeutic Opportunities. *Front Chem*, *9*, 669308. https://doi.org/10.3389/fchem.2021.669308

Liu, G., Wu, Y., Jin, S., Sun, J., Wan, B. B., Zhang, J., Wang, Y., Gao, Z. Q., Chen, D., Li, S., Pang, Q., & Wang, Z. (2021). Itaconate ameliorates methicillin-resistant Staphylococcus aureus-induced acute lung injury through the Nrf2/ARE pathway. *Ann Transl Med*, *9*(8), 712. https://doi.org/10.21037/atm-21-1448

Liu, P. S., Wang, H., Li, X., Chao, T., Teav, T., Christen, S., Di Conza, G., Cheng, W. C., Chou, C. H., Vavakova, M., Muret, C., Debackere, K., Mazzone, M., Huang, H. D., Fendt, S. M., Ivanisevic, J., & Ho, P. C. (2017). α-ketoglutarate orchestrates macrophage activation through metabolic and epigenetic reprogramming. *Nat Immunol*, *18*(9), 985-994. https://doi.org/10.1038/ni.3796

Liu, X., Zhang, L., Wu, X. P., Zhu, X. L., Pan, L. P., Li, T., Yan, B. Y., Xu, A. Q., Li, H., & Liu, Y. (2017). Polymorphisms in IRG1 gene associated with immune responses to hepatitis B vaccination in a Chinese Han population and function to restrain the HBV life cycle. *J Med Virol*, *89*(7), 1215-1223. https://doi.org/10.1002/jmv.24756

Liu, Y., Xu, R., Gu, H., Zhang, E., Qu, J., Cao, W., Huang, X., Yan, H., He, J., & Cai, Z. (2021). Metabolic reprogramming in macrophage responses. *Biomark Res*, *9*(1), 1. https://doi.org/10.1186/s40364-020-00251-y

Ma, J., & Chen, X. (2020). Anti-inflammatory Therapy for Coronary Atherosclerotic Heart Disease: Unanswered Questions Behind Existing Successes. *Front Cardiovasc Med*, *7*, 631398. https://doi.org/10.3389/fcvm.2020.631398

Mantovani, A., Allavena, P., Sica, A., & Balkwill, F. (2008). Cancer-related inflammation. *Nature*, *454*(7203), 436-444. https://doi.org/10.1038/nature07205

Mantovani, A., Biswas, S. K., Galdiero, M. R., Sica, A., & Locati, M. (2013). Macrophage plasticity and polarization in tissue repair and remodelling. *J Pathol*, *229*(2), 176-185. https://doi.org/10.1002/path.4133

Marnett, L. J., Wright, T. L., Crews, B. C., Tannenbaum, S. R., & Morrow, J. D. (2000). Regulation of prostaglandin biosynthesis by nitric oxide is revealed by targeted deletion of inducible nitric-oxide synthase. *J Biol Chem*, *275*(18), 13427-13430. https://doi.org/10.1074/jbc.275.18.13427

Marotta, P., Sautebin, L., & Di Rosa, M. (1992). Modulation of the induction of nitric oxide synthase by eicosanoids in the murine macrophage cell line J774. *Br J Pharmacol*, *107*(3), 640-641. https://doi.org/10.1111/j.1476-5381.1992.tb14499.x

Martínez-Reyes, I., & Chandel, N. S. (2020). Mitochondrial TCA cycle metabolites control physiology and disease. *Nat Commun*, *11*(1), 102. https://doi.org/10.1038/s41467-019-13668-3

Matoba, T., Shimokawa, H., Kubota, H., Morikawa, K., Fujiki, T., Kunihiro, I., Mukai, Y., Hirakawa, Y., & Takeshita, A. (2002). Hydrogen peroxide is an endothelium-derived

hyperpolarizing factor in human mesenteric arteries. *Biochem Biophys Res Commun*, *290*(3), 909-913. https://doi.org/10.1006/bbrc.2001.6278

Matsuda, K., Lozinskaya, I., & Cox, R. H. (1997). Augmented contributions of voltage-gated Ca2+ channels to contractile responses in spontaneously hypertensive rat mesenteric arteries. *Am J Hypertens*, *10*(11), 1231-1239. https://doi.org/10.1016/s0895-7061(97)00225-2

Matsuura, Y., Shimizu-Albergine, M., Barnhart, S., Kramer, F., Hsu, C. C., Kothari, V., Tang, J., Gharib, S. A., Kanter, J. E., Abel, E. D., Tian, R., Shao, B., & Bornfeldt, K. E. (2022). Diabetes Suppresses Glucose Uptake and Glycolysis in Macrophages. *Circ Res*, *130*(5), 779-781. https://doi.org/10.1161/circresaha.121.320060

McNeill, E., Crabtree, M. J., Sahgal, N., Patel, J., Chuaiphichai, S., Iqbal, A. J., Hale, A. B., Greaves, D. R., & Channon, K. M. (2015). Regulation of iNOS function and cellular redox state by macrophage Gch1 reveals specific requirements for tetrahydrobiopterin in NRF2 activation. *Free Radic Biol Med*, *79*, 206-216. https://doi.org/10.1016/j.freeradbiomed.2014.10.575

McNeill, E., Stylianou, E., Crabtree, M. J., Harrington-Kandt, R., Kolb, A. L., Diotallevi, M., Hale, A. B., Bettencourt, P., Tanner, R., O'Shea, M. K., Matsumiya, M., Lockstone, H., Müller, J., Fletcher, H. A., Greaves, D. R., McShane, H., & Channon, K. M. (2018). Regulation of mycobacterial infection by macrophage Gch1 and tetrahydrobiopterin. *Nat Commun*, *9*(1), 5409. https://doi.org/10.1038/s41467-018-07714-9

Megawati, E. R., Meutia, N., & Lubis, L. D. (2022). The effect of hyperglycaemia on the macrophages in the cell culture. *Folia Morphol (Warsz)*, *81*(2), 387-393. https://doi.org/10.5603/FM.a2021.0017

Michel, T., & Feron, O. (1997). Nitric oxide synthases: which, where, how, and why? *J Clin Invest*, *100*(9), 2146-2152. https://doi.org/10.1172/jci119750

Michelucci, A., Cordes, T., Ghelfi, J., Pailot, A., Reiling, N., Goldmann, O., Binz, T., Wegner, A., Tallam, A., Rausell, A., Buttini, M., Linster, C. L., Medina, E., Balling, R., & Hiller, K. (2013). Immune-responsive gene 1 protein links metabolism to immunity by catalyzing itaconic acid production. *Proc Natl Acad Sci U S A*, *110*(19), 7820-7825. https://doi.org/10.1073/pnas.1218599110

Millet, P., Vachharajani, V., McPhail, L., Yoza, B., & McCall, C. E. (2016). GAPDH Binding to TNF-α mRNA Contributes to Posttranscriptional Repression in Monocytes: A Novel Mechanism of Communication between Inflammation and Metabolism. *J Immunol*, *196*(6), 2541-2551. https://doi.org/10.4049/jimmunol.1501345

Mills, E. L., Ryan, D. G., Prag, H. A., Dikovskaya, D., Menon, D., Zaslona, Z., Jedrychowski, M. P., Costa, A. S. H., Higgins, M., Hams, E., Szpyt, J., Runtsch, M. C., King, M. S., McGouran, J. F., Fischer, R., Kessler, B. M., McGettrick, A. F., Hughes, M. M., Carroll, R. G., . . . O'Neill, L. A. (2018). Itaconate is an anti-inflammatory metabolite that activates Nrf2 via alkylation of KEAP1. *Nature*, *556*(7699), 113-117. https://doi.org/10.1038/nature25986

Moganti, K., Li, F., Schmuttermaier, C., Riemann, S., Klüter, H., Gratchev, A., Harmsen, M. C., & Kzhyshkowska, J. (2017). Hyperglycemia induces mixed M1/M2 cytokine profile in primary human monocyte-derived macrophages. *Immunobiology*, *222*(10), 952-959. https://doi.org/10.1016/j.imbio.2016.07.006

Moghissi, E. S., Korytkowski, M. T., DiNardo, M., Einhorn, D., Hellman, R., Hirsch, I. B., Inzucchi, S. E., Ismail-Beigi, F., Kirkman, M. S., & Umpierrez, G. E. (2009). American Association of Clinical Endocrinologists and American Diabetes Association consensus statement on inpatient glycemic control. *Diabetes Care*, *32*(6), 1119-1131. https://doi.org/10.2337/dc09-9029

Mollace, V., Muscoli, C., Masini, E., Cuzzocrea, S., & Salvemini, D. (2005). Modulation of prostaglandin biosynthesis by nitric oxide and nitric oxide donors. *Pharmacol Rev*, *57*(2), 217-252. https://doi.org/10.1124/pr.57.2.1

Moncada, S., & Erusalimsky, J. D. (2002). Does nitric oxide modulate mitochondrial energy generation and apoptosis? *Nat Rev Mol Cell Biol*, *3*(3), 214-220. https://doi.org/10.1038/nrm762

Moncada, S., Gryglewski, R., Bunting, S., & Vane, J. R. (1976). An enzyme isolated from arteries transforms prostaglandin endoperoxides to an unstable substance that inhibits platelet aggregation. *Nature*, *263*(5579), 663-665. https://doi.org/10.1038/263663a0
Moore, K. J., Sheedy, F. J., & Fisher, E. A. (2013). Macrophages in atherosclerosis: a dynamic balance. *Nat Rev Immunol*, *13*(10), 709-721. https://doi.org/10.1038/nri3520
Mosser, D. M., & Edwards, J. P. (2008). Exploring the full spectrum of macrophage activation. *Nat Rev Immunol*, *8*(12), 958-969. https://doi.org/10.1038/nri2448
Munder, M., Eichmann, K., & Modolell, M. (1998). Alternative metabolic states in murine macrophages reflected by the nitric oxide synthase/arginase balance: competitive regulation by CD4+ T cells correlates with Th1/Th2 phenotype. *J Immunol*, *160*(11), 5347-5354.
Murray, P. J., Allen, J. E., Biswas, S. K., Fisher, E. A., Gilroy, D. W., Goerdt, S., Gordon, S., Hamilton, J. A., Ivashkiv, L. B., Lawrence, T., Locati, M., Mantovani, A., Martinez, F. O., Mege, J. L., Mosser, D. M., Natoli, G., Saeij, J. P., Schultze, J. L., Shirey, K. A., . . . Wynn, T. A. (2014). Macrophage activation and polarization: nomenclature and experimental guidelines. *Immunity*, *41*(1), 14-20. https://doi.org/10.1016/j.immuni.2014.06.008
Nagareddy, P. R., Murphy, A. J., Stirzaker, R. A., Hu, Y., Yu, S., Miller, R. G., Ramkhelawon, B., Distel, E., Westerterp, M., Huang, L. S., Schmidt, A. M., Orchard, T. J., Fisher, E. A., Tall, A. R., & Goldberg, I. J. (2013). Hyperglycemia promotes myelopoiesis and impairs the resolution of atherosclerosis. *Cell Metab*, *17*(5), 695-708. https://doi.org/10.1016/j.cmet.2013.04.001
Nahrendorf, M., & Swirski, F. K. (2016). Abandoning M1/M2 for a Network Model of Macrophage Function. *Circ Res*, *119*(3), 414-417. https://doi.org/10.1161/circresaha.116.309194
Nair, S., Huynh, J. P., Lampropoulou, V., Loginicheva, E., Esaulova, E., Gounder, A. P., Boon, A. C. M., Schwarzkopf, E. A., Bradstreet, T. R., Edelson, B. T., Artyomov, M. N., Stallings, C. L., & Diamond, M. S. (2018). Irg1 expression in myeloid cells prevents immunopathology during M. tuberculosis infection. *J Exp Med*, *215*(4), 1035-1045. https://doi.org/10.1084/jem.20180118
Nakkala, J. R., Yao, Y., Zhai, Z., Duan, Y., Zhang, D., Mao, Z., Lu, L., & Gao, C. (2021). Dimethyl Itaconate-Loaded Nanofibers Rewrite Macrophage Polarization, Reduce Inflammation, and Enhance Repair of Myocardic Infarction. *Small*, *17*(17), e2006992. https://doi.org/10.1002/smll.202006992
Nankabirwa, V., Tumwine, J. K., Mugaba, P. M., Tylleskär, T., & Sommerfelt, H. (2015). Child survival and BCG vaccination: a community based prospective cohort study in Uganda. *BMC Public Health*, *15*, 175. https://doi.org/10.1186/s12889-015-1497-8
Netea, M. G., Domínguez-Andrés, J., Barreiro, L. B., Chavakis, T., Divangahi, M., Fuchs, E., Joosten, L. A. B., van der Meer, J. W. M., Mhlanga, M. M., Mulder, W. J. M., Riksen, N. P., Schlitzer, A., Schultze, J. L., Stabell Benn, C., Sun, J. C., Xavier, R. J., & Latz, E. (2020). Defining trained immunity and its role in health and disease. *Nat Rev Immunol*, *20*(6), 375-388. https://doi.org/10.1038/s41577-020-0285-6
O'Neill, L. A., Kishton, R. J., & Rathmell, J. (2016). A guide to immunometabolism for immunologists. *Nat Rev Immunol*, *16*(9), 553-565. https://doi.org/10.1038/nri.2016.70
Ogger, P. P., Albers, G. J., Hewitt, R. J., O'Sullivan, B. J., Powell, J. E., Calamita, E., Ghai, P., Walker, S. A., McErlean, P., Saunders, P., Kingston, S., Molyneaux, P. L., Halket, J. M., Gray, R., Chambers, D. C., Maher, T. M., Lloyd, C. M., & Byrne, A. J. (2020). Itaconate controls the severity of pulmonary fibrosis. *Sci Immunol*, *5*(52). https://doi.org/10.1126/sciimmunol.abc1884
Olagnier, D., Farahani, E., Thyrsted, J., Blay-Cadanet, J., Herengt, A., Idorn, M., Hait, A., Hernaez, B., Knudsen, A., Iversen, M. B., Schilling, M., Jørgensen, S. E., Thomsen, M., Reinert, L. S., Lappe, M., Hoang, H. D., Gilchrist, V. H., Hansen, A. L., Ottosen, R., . . . Holm, C. K. (2020). SARS-CoV2-mediated suppression of NRF2-signaling reveals potent antiviral and anti-inflammatory activity of 4-octyl-itaconate and dimethyl fumarate. *Nat Commun*, *11*(1), 4938. https://doi.org/10.1038/s41467-020-18764-3

Orecchioni, M., Ghosheh, Y., Pramod, A. B., & Ley, K. (2019). Macrophage Polarization: Different Gene Signatures in M1(LPS+) vs. Classically and M2(LPS-) vs. Alternatively Activated Macrophages. *Front Immunol*, *10*, 1084. https://doi.org/10.3389/fimmu.2019.01084

Pace, J. L., Russell, S. W., Schreiber, R. D., Altman, A., & Katz, D. H. (1983). Macrophage activation: priming activity from a T-cell hybridoma is attributable to interferon-gamma. *Proc Natl Acad Sci U S A*, *80*(12), 3782-3786. https://doi.org/10.1073/pnas.80.12.3782

Palmieri, E. M., Gonzalez-Cotto, M., Baseler, W. A., Davies, L. C., Ghesquière, B., Maio, N., Rice, C. M., Rouault, T. A., Cassel, T., Higashi, R. M., Lane, A. N., Fan, T. W., Wink, D. A., & McVicar, D. W. (2020). Nitric oxide orchestrates metabolic rewiring in M1 macrophages by targeting aconitase 2 and pyruvate dehydrogenase. *Nat Commun*, *11*(1), 698. https://doi.org/10.1038/s41467-020-14433-7

Palmieri, E. M., McGinity, C., Wink, D. A., & McVicar, D. W. (2020). Nitric Oxide in Macrophage Immunometabolism: Hiding in Plain Sight. *Metabolites*, *10*(11). https://doi.org/10.3390/metabo10110429

Palmieri, E. M., Menga, A., Martín-Pérez, R., Quinto, A., Riera-Domingo, C., De Tullio, G., Hooper, D. C., Lamers, W. H., Ghesquière, B., McVicar, D. W., Guarini, A., Mazzone, M., & Castegna, A. (2017). Pharmacologic or Genetic Targeting of Glutamine Synthetase Skews Macrophages toward an M1-like Phenotype and Inhibits Tumor Metastasis. *Cell Rep*, *20*(7), 1654-1666. https://doi.org/10.1016/j.celrep.2017.07.054

Parathath, S., Grauer, L., Huang, L. S., Sanson, M., Distel, E., Goldberg, I. J., & Fisher, E. A. (2011). Diabetes adversely affects macrophages during atherosclerotic plaque regression in mice. *Diabetes*, *60*(6), 1759-1769. https://doi.org/10.2337/db10-0778

Park, B. S., Song, D. H., Kim, H. M., Choi, B. S., Lee, H., & Lee, J. O. (2009). The structural basis of lipopolysaccharide recognition by the TLR4-MD-2 complex. *Nature*, *458*(7242), 1191-1195. https://doi.org/10.1038/nature07830

Patel, S., & Santani, D. (2009). Role of NF-kappa B in the pathogenesis of diabetes and its associated complications. *Pharmacol Rep*, *61*(4), 595-603. https://doi.org/10.1016/s1734-1140(09)70111-2

Patra, K. C., & Hay, N. (2014). The pentose phosphate pathway and cancer. *Trends Biochem Sci*, *39*(8), 347-354. https://doi.org/10.1016/j.tibs.2014.06.005

Patsouris, D., Li, P. P., Thapar, D., Chapman, J., Olefsky, J. M., & Neels, J. G. (2008). Ablation of CD11c-positive cells normalizes insulin sensitivity in obese insulin resistant animals. *Cell Metab*, *8*(4), 301-309. https://doi.org/10.1016/j.cmet.2008.08.015

Pavlou, S., Lindsay, J., Ingram, R., Xu, H., & Chen, M. (2018). Sustained high glucose exposure sensitizes macrophage responses to cytokine stimuli but reduces their phagocytic activity. *BMC Immunol*, *19*(1), 24. https://doi.org/10.1186/s12865-018-0261-0

Peace, C. G., & O'Neill, L. A. (2022). The role of itaconate in host defense and inflammation. *J Clin Invest*, *132*(2). https://doi.org/10.1172/jci148548

Prast, H., & Philippu, A. (2001). Nitric oxide as modulator of neuronal function. *Prog Neurobiol*, *64*(1), 51-68. https://doi.org/10.1016/s0301-0082(00)00044-7

Price, J. V., Russo, D., Ji, D. X., Chavez, R. A., DiPeso, L., Lee, A. Y., Coers, J., & Vance, R. E. (2019). IRG1 and Inducible Nitric Oxide Synthase Act Redundantly with Other Interferon-Gamma-Induced Factors To Restrict Intracellular Replication of Legionella pneumophila. *mBio*, *10*(6). https://doi.org/10.1128/mBio.02629-19

Puchalska, P., Huang, X., Martin, S. E., Han, X., Patti, G. J., & Crawford, P. A. (2018). Isotope Tracing Untargeted Metabolomics Reveals Macrophage Polarization-State-Specific Metabolic Coordination across Intracellular Compartments. *iScience*, *9*, 298-313. https://doi.org/10.1016/j.isci.2018.10.029

Qin, W., Qin, K., Zhang, Y., Jia, W., Chen, Y., Cheng, B., Peng, L., Chen, N., Liu, Y., Zhou, W., Wang, Y. L., Chen, X., & Wang, C. (2019). S-glycosylation-based cysteine profiling reveals regulation of glycolysis by itaconate. *Nat Chem Biol*, *15*(10), 983-991. https://doi.org/10.1038/s41589-019-0323-5

Qin, W., Zhang, Y., Tang, H., Liu, D., Chen, Y., Liu, Y., & Wang, C. (2020). Chemoproteomic Profiling of Itaconation by Bioorthogonal Probes in Inflammatory Macrophages. *J Am Chem Soc*, *142*(25), 10894-10898. https://doi.org/10.1021/jacs.9b11962

Qualls, J. E., Subramanian, C., Rafi, W., Smith, A. M., Balouzian, L., DeFreitas, A. A., Shirey, K. A., Reutterer, B., Kernbauer, E., Stockinger, S., Decker, T., Miyairi, I., Vogel, S. N., Salgame, P., Rock, C. O., & Murray, P. J. (2012). Sustained generation of nitric oxide and control of mycobacterial infection requires argininosuccinate synthase 1. *Cell Host Microbe*, *12*(3), 313-323. https://doi.org/10.1016/j.chom.2012.07.012

Rajendran, P., Rengarajan, T., Thangavel, J., Nishigaki, Y., Sakthisekaran, D., Sethi, G., & Nishigaki, I. (2013). The vascular endothelium and human diseases. *Int J Biol Sci*, *9*(10), 1057-1069. https://doi.org/10.7150/ijbs.7502

Reddy, M. A., Zhang, E., & Natarajan, R. (2015). Epigenetic mechanisms in diabetic complications and metabolic memory. *Diabetologia*, *58*(3), 443-455. https://doi.org/10.1007/s00125-014-3462-y

Ren, J., Yu, L., Lin, J., Ma, L., Gao, D. S., Sun, N., Liu, Y., Fang, L., Cheng, Z., Sun, K., & Yan, M. (2022). Dimethyl itaconate inhibits neuroinflammation to alleviate chronic pain in mice. *Neurochem Int*, *154*, 105296. https://doi.org/10.1016/j.neuint.2022.105296

Ridker, P. M., Everett, B. M., Thuren, T., MacFadyen, J. G., Chang, W. H., Ballantyne, C., Fonseca, F., Nicolau, J., Koenig, W., Anker, S. D., Kastelein, J. J. P., Cornel, J. H., Pais, P., Pella, D., Genest, J., Cifkova, R., Lorenzatti, A., Forster, T., Kobalava, Z., . . . Glynn, R. J. (2017). Antiinflammatory Therapy with Canakinumab for Atherosclerotic Disease. *N Engl J Med*, *377*(12), 1119-1131. https://doi.org/10.1056/NEJMoa1707914

Riksen, N. P., & Netea, M. G. (2021). Immunometabolic control of trained immunity. *Mol Aspects Med*, *77*, 100897. https://doi.org/10.1016/j.mam.2020.100897

Robert, T., & Friebel, S. (2016). Itaconic acid–a versatile building block for renewable polyesters with enhanced functionality. *Green Chemistry*, *18*(10), 2922-2934.

Robin, E. D., Murphy, B. J., & Theodore, J. (1984). Coordinate regulation of glycolysis by hypoxia in mammalian cells. *J Cell Physiol*, *118*(3), 287-290. https://doi.org/10.1002/jcp.1041180311

Rodríguez-Prados, J. C., Través, P. G., Cuenca, J., Rico, D., Aragonés, J., Martín-Sanz, P., Cascante, M., & Boscá, L. (2010). Substrate fate in activated macrophages: a comparison between innate, classic, and alternative activation. *J Immunol*, *185*(1), 605-614. https://doi.org/10.4049/jimmunol.0901698

Ross, J. S., Russo, S. B., Chavis, G. C., & Cowart, L. A. (2014). Sphingolipid regulators of cellular dysfunction in Type 2 diabetes mellitus: a systems overview. *Clin Lipidol*, *9*(5), 553-569.

Roth, G. A., Mensah, G. A., Johnson, C. O., Addolorato, G., Ammirati, E., Baddour, L. M., Barengo, N. C., Beaton, A. Z., Benjamin, E. J., Benziger, C. P., Bonny, A., Brauer, M., Brodmann, M., Cahill, T. J., Carapetis, J., Catapano, A. L., Chugh, S. S., Cooper, L. T., Coresh, J., . . . Fuster, V. (2020). Global Burden of Cardiovascular Diseases and Risk Factors, 1990-2019: Update From the GBD 2019 Study. *J Am Coll Cardiol*, *76*(25), 2982-3021. https://doi.org/10.1016/j.jacc.2020.11.010

Runtsch, M. C., Angiari, S., Hooftman, A., Wadhwa, R., Zhang, Y., Zheng, Y., Spina, J. S., Ruzek, M. C., Argiriadi, M. A., McGettrick, A. F., Mendez, R. S., Zotta, A., Peace, C. G., Walsh, A., Chirillo, R., Hams, E., Fallon, P. G., Jayamaran, R., Dua, K., . . . O'Neill, L. A. J. (2022). Itaconate and itaconate derivatives target JAK1 to suppress alternative activation of macrophages. *Cell Metab*, *34*(3), 487-501.e488. https://doi.org/10.1016/j.cmet.2022.02.002

Russo, S. B., Ross, J. S., & Cowart, L. A. (2013). Sphingolipids in obesity, type 2 diabetes, and metabolic disease. *Handb Exp Pharmacol*(216), 373-401. https://doi.org/10.1007/978-3-7091-1511-4_19

Ryan, D. G., & O'Neill, L. A. J. (2020). Krebs Cycle Reborn in Macrophage Immunometabolism. *Annu Rev Immunol*, *38*, 289-313. https://doi.org/10.1146/annurev-immunol-081619-104850

Saeed, S., Quintin, J., Kerstens, H. H., Rao, N. A., Aghajanirefah, A., Matarese, F., Cheng, S. C., Ratter, J., Berentsen, K., van der Ent, M. A., Sharifi, N., Janssen-Megens, E. M., Ter Huurne, M., Mandoli, A., van Schaik, T., Ng, A., Burden, F., Downes, K., Frontini, M., . . .

Stunnenberg, H. G. (2014). Epigenetic programming of monocyte-to-macrophage differentiation and trained innate immunity. *Science*, *345*(6204), 1251086. https://doi.org/10.1126/science.1251086

Sakai, A., Kusumoto, A., Kiso, Y., & Furuya, E. (2004). Itaconate reduces visceral fat by inhibiting fructose 2,6-bisphosphate synthesis in rat liver. *Nutrition*, *20*(11-12), 997-1002. https://doi.org/10.1016/j.nut.2004.08.007

Salvemini, D., Misko, T. P., Masferrer, J. L., Seibert, K., Currie, M. G., & Needleman, P. (1993). Nitric oxide activates cyclooxygenase enzymes. *Proc Natl Acad Sci U S A*, *90*(15), 7240-7244. https://doi.org/10.1073/pnas.90.15.7240

Shan, Q., Li, X., Zheng, M., Lin, X., Lu, G., Su, D., & Lu, X. (2019). Protective effects of dimethyl itaconate in mice acute cardiotoxicity induced by doxorubicin. *Biochem Biophys Res Commun*, *517*(3), 538-544. https://doi.org/10.1016/j.bbrc.2019.07.046

Shi, X., Zhou, H., Wei, J., Mo, W., Li, Q., & Lv, X. (2022). The signaling pathways and therapeutic potential of itaconate to alleviate inflammation and oxidative stress in inflammatory diseases. *Redox Biol*, *58*, 102553. https://doi.org/10.1016/j.redox.2022.102553

Shin, J. H., Yang, J. Y., Jeon, B. Y., Yoon, Y. J., Cho, S. N., Kang, Y. H., Ryu, D. H., & Hwang, G. S. (2011). (1)H NMR-based metabolomic profiling in mice infected with Mycobacterium tuberculosis. *J Proteome Res*, *10*(5), 2238-2247. https://doi.org/10.1021/pr101054m

Shinomiya, S., Naraba, H., Ueno, A., Utsunomiya, I., Maruyama, T., Ohuchida, S., Ushikubi, F., Yuki, K., Narumiya, S., Sugimoto, Y., Ichikawa, A., & Oh-ishi, S. (2001). Regulation of TNFalpha and interleukin-10 production by prostaglandins I(2) and E(2): studies with prostaglandin receptor-deficient mice and prostaglandin E-receptor subtype-selective synthetic agonists. *Biochem Pharmacol*, *61*(9), 1153-1160. https://doi.org/10.1016/s0006-2952(01)00586-x

Sigruener, A., Kleber, M. E., Heimerl, S., Liebisch, G., Schmitz, G., & Maerz, W. (2014). Glycerophospholipid and sphingolipid species and mortality: the Ludwigshafen Risk and Cardiovascular Health (LURIC) study. *PLoS One*, *9*(1), e85724. https://doi.org/10.1371/journal.pone.0085724

Singh, V. P., Bali, A., Singh, N., & Jaggi, A. S. (2014). Advanced glycation end products and diabetic complications. *Korean J Physiol Pharmacol*, *18*(1), 1-14. https://doi.org/10.4196/kjpp.2014.18.1.1

Soehnlein, O., & Libby, P. (2021). Targeting inflammation in atherosclerosis - from experimental insights to the clinic. *Nat Rev Drug Discov*, *20*(8), 589-610. https://doi.org/10.1038/s41573-021-00198-1

Sohail, A., Iqbal, A. A., Sahini, N., Chen, F., Tantawy, M., Waqas, S. F. H., Winterhoff, M., Ebensen, T., Schultz, K., Geffers, R., Schughart, K., Preusse, M., Shehata, M., Bähre, H., Pils, M. C., Guzman, C. A., Mostafa, A., Pleschka, S., Falk, C., . . . Pessler, F. (2022). Itaconate and derivatives reduce interferon responses and inflammation in influenza A virus infection. *PLoS Pathog*, *18*(1), e1010219. https://doi.org/10.1371/journal.ppat.1010219

Song, H., Xu, T., Feng, X., Lai, Y., Yang, Y., Zheng, H., He, X., Wei, G., Liao, W., Liao, Y., Zhong, L., & Bin, J. (2020). Itaconate prevents abdominal aortic aneurysm formation through inhibiting inflammation via activation of Nrf2. *EBioMedicine*, *57*, 102832. https://doi.org/10.1016/j.ebiom.2020.102832

Soto-Heredero, G., Gómez de Las Heras, M. M., Gabandé-Rodríguez, E., Oller, J., & Mittelbrunn, M. (2020). Glycolysis - a key player in the inflammatory response. *Febs j*, *287*(16), 3350-3369. https://doi.org/10.1111/febs.15327

Stein, M., Keshav, S., Harris, N., & Gordon, S. (1992). Interleukin 4 potently enhances murine macrophage mannose receptor activity: a marker of alternative immunologic macrophage activation. *J Exp Med*, *176*(1), 287-292. https://doi.org/10.1084/jem.176.1.287

Stitham, J., Midgett, C., Martin, K. A., & Hwa, J. (2011). Prostacyclin: an inflammatory paradox. *Front Pharmacol*, *2*, 24. https://doi.org/10.3389/fphar.2011.00024

Strelko, C. L., Lu, W., Dufort, F. J., Seyfried, T. N., Chiles, T. C., Rabinowitz, J. D., & Roberts, M. F. (2011). Itaconic acid is a mammalian metabolite induced during macrophage activation. *J Am Chem Soc*, *133*(41), 16386-16389. https://doi.org/10.1021/ja2070889

Sugimoto, M., Sakagami, H., Yokote, Y., Onuma, H., Kaneko, M., Mori, M., Sakaguchi, Y., Soga, T., & Tomita, M. (2012). Non-targeted metabolite profiling in activated macrophage secretion. *Metabolomics*, *8*, 624-633.

Sun, C., Sun, L., Ma, H., Peng, J., Zhen, Y., Duan, K., Liu, G., Ding, W., & Zhao, Y. (2012). The phenotype and functional alterations of macrophages in mice with hyperglycemia for long term. *J Cell Physiol*, *227*(4), 1670-1679. https://doi.org/10.1002/jcp.22891

Sun, X., Zhang, B., Pan, X., Huang, H., Xie, Z., Ma, Y., Hu, B., Wang, J., Chen, Z., & Shi, P. (2019). Octyl itaconate inhibits osteoclastogenesis by suppressing Hrd1 and activating Nrf2 signaling. *Faseb j*, *33*(11), 12929-12940. https://doi.org/10.1096/fj.201900887RR

Swain, A., Bambouskova, M., Kim, H., Andhey, P. S., Duncan, D., Auclair, K., Chubukov, V., Simons, D. M., Roddy, T. P., Stewart, K. M., & Artyomov, M. N. (2020). Comparative evaluation of itaconate and its derivatives reveals divergent inflammasome and type I interferon regulation in macrophages. *Nat Metab*, *2*(7), 594-602. https://doi.org/10.1038/s42255-020-0210-0

Tang, C., Tan, S., Zhang, Y., Dong, L., & Xu, Y. (2019). Activation of Keap1-Nrf2 signaling by 4-octyl itaconate protects human umbilical vein endothelial cells from high glucose. *Biochem Biophys Res Commun*, *508*(3), 921-927. https://doi.org/10.1016/j.bbrc.2018.12.032

Tang, C., Wang, X., Xie, Y., Cai, X., Yu, N., Hu, Y., & Zheng, Z. (2018). 4-Octyl Itaconate Activates Nrf2 Signaling to Inhibit Pro-Inflammatory Cytokine Production in Peripheral Blood Mononuclear Cells of Systemic Lupus Erythematosus Patients. *Cell Physiol Biochem*, *51*(2), 979-990. https://doi.org/10.1159/000495400

Taniguchi, M., & Okazaki, T. (2014). The role of sphingomyelin and sphingomyelin synthases in cell death, proliferation and migration-from cell and animal models to human disorders. *Biochim Biophys Acta*, *1841*(5), 692-703. https://doi.org/10.1016/j.bbalip.2013.12.003

Tannahill, G. M., Curtis, A. M., Adamik, J., Palsson-McDermott, E. M., McGettrick, A. F., Goel, G., Frezza, C., Bernard, N. J., Kelly, B., Foley, N. H., Zheng, L., Gardet, A., Tong, Z., Jany, S. S., Corr, S. C., Haneklaus, M., Caffrey, B. E., Pierce, K., Walmsley, S., . . . O'Neill, L. A. (2013). Succinate is an inflammatory signal that induces IL-1β through HIF-1α. *Nature*, *496*(7444), 238-242. https://doi.org/10.1038/nature11986

Tardif, J. C., Kouz, S., Waters, D. D., Bertrand, O. F., Diaz, R., Maggioni, A. P., Pinto, F. J., Ibrahim, R., Gamra, H., Kiwan, G. S., Berry, C., López-Sendón, J., Ostadal, P., Koenig, W., Angoulvant, D., Grégoire, J. C., Lavoie, M. A., Dubé, M. P., Rhainds, D., . . . Roubille, F. (2019). Efficacy and Safety of Low-Dose Colchicine after Myocardial Infarction. *N Engl J Med*, *381*(26), 2497-2505. https://doi.org/10.1056/NEJMoa1912388

Tesfamariam, B., & Halpern, W. (1988). Endothelium-dependent and endothelium-independent vasodilation in resistance arteries from hypertensive rats. *Hypertension*, *11*(5), 440-444. https://doi.org/10.1161/01.hyp.11.5.440

Thapa, B., & Lee, K. (2019). Metabolic influence on macrophage polarization and pathogenesis. *BMB Rep*, *52*(6), 360-372. https://doi.org/10.5483/BMBRep.2019.52.6.140

Thiem, K., Keating, S. T., Netea, M. G., Riksen, N. P., Tack, C. J., van Diepen, J., & Stienstra, R. (2021). Hyperglycemic Memory of Innate Immune Cells Promotes In Vitro Proinflammatory Responses of Human Monocytes and Murine Macrophages. *J Immunol*, *206*(4), 807-813. https://doi.org/10.4049/jimmunol.1901348

Thimmulappa, R. K., Lee, H., Rangasamy, T., Reddy, S. P., Yamamoto, M., Kensler, T. W., & Biswal, S. (2006). Nrf2 is a critical regulator of the innate immune response and survival during experimental sepsis. *J Clin Invest*, *116*(4), 984-995. https://doi.org/10.1172/jci25790

Thöny, B., Auerbach, G., & Blau, N. (2000). Tetrahydrobiopterin biosynthesis, regeneration and functions. *Biochem J*, *347 Pt 1*(Pt 1), 1-16.

Tian, F., Wang, Z., He, J., Zhang, Z., & Tan, N. (2020). 4-Octyl itaconate protects against renal fibrosis via inhibiting TGF-β/Smad pathway, autophagy and reducing generation of

reactive oxygen species. *Eur J Pharmacol*, *873*, 172989. https://doi.org/10.1016/j.ejphar.2020.172989
Touyz, R. M., Alves-Lopes, R., Rios, F. J., Camargo, L. L., Anagnostopoulou, A., Arner, A., & Montezano, A. C. (2018). Vascular smooth muscle contraction in hypertension. *Cardiovasc Res*, *114*(4), 529-539. https://doi.org/10.1093/cvr/cvy023
Trauelsen, M., Hiron, T. K., Lin, D., Petersen, J. E., Breton, B., Husted, A. S., Hjorth, S. A., Inoue, A., Frimurer, T. M., Bouvier, M., O'Callaghan, C. A., & Schwartz, T. W. (2021). Extracellular succinate hyperpolarizes M2 macrophages through SUCNR1/GPR91-mediated Gq signaling. *Cell Rep*, *35*(11), 109246. https://doi.org/10.1016/j.celrep.2021.109246
Trauelsen, M., Rexen Ulven, E., Hjorth, S. A., Brvar, M., Monaco, C., Frimurer, T. M., & Schwartz, T. W. (2017). Receptor structure-based discovery of non-metabolite agonists for the succinate receptor GPR91. *Mol Metab*, *6*(12), 1585-1596. https://doi.org/10.1016/j.molmet.2017.09.005
Umpierrez, G. E., Hellman, R., Korytkowski, M. T., Kosiborod, M., Maynard, G. A., Montori, V. M., Seley, J. J., & Van den Berghe, G. (2012). Management of hyperglycemia in hospitalized patients in non-critical care setting: an endocrine society clinical practice guideline. *J Clin Endocrinol Metab*, *97*(1), 16-38. https://doi.org/10.1210/jc.2011-2098
Van den Bossche, J., Baardman, J., Otto, N. A., van der Velden, S., Neele, A. E., van den Berg, S. M., Luque-Martin, R., Chen, H. J., Boshuizen, M. C., Ahmed, M., Hoeksema, M. A., de Vos, A. F., & de Winther, M. P. (2016). Mitochondrial Dysfunction Prevents Repolarization of Inflammatory Macrophages. *Cell Rep*, *17*(3), 684-696. https://doi.org/10.1016/j.celrep.2016.09.008
van der Heijden, C., Keating, S. T., Groh, L., Joosten, L. A. B., Netea, M. G., & Riksen, N. P. (2020). Aldosterone induces trained immunity: the role of fatty acid synthesis. *Cardiovasc Res*, *116*(2), 317-328. https://doi.org/10.1093/cvr/cvz137
van der Heijden, C., Noz, M. P., Joosten, L. A. B., Netea, M. G., Riksen, N. P., & Keating, S. T. (2018). Epigenetics and Trained Immunity. *Antioxid Redox Signal*, *29*(11), 1023-1040. https://doi.org/10.1089/ars.2017.7310
van Diepen, J. A., Thiem, K., Stienstra, R., Riksen, N. P., Tack, C. J., & Netea, M. G. (2016). Diabetes propels the risk for cardiovascular disease: sweet monocytes becoming aggressive? *Cell Mol Life Sci*, *73*(24), 4675-4684. https://doi.org/10.1007/s00018-016-2316-9
Vats, D., Mukundan, L., Odegaard, J. I., Zhang, L., Smith, K. L., Morel, C. R., Wagner, R. A., Greaves, D. R., Murray, P. J., & Chawla, A. (2006). Oxidative metabolism and PGC-1beta attenuate macrophage-mediated inflammation. *Cell Metab*, *4*(1), 13-24. https://doi.org/10.1016/j.cmet.2006.05.011
Viola, A., Munari, F., Sánchez-Rodríguez, R., Scolaro, T., & Castegna, A. (2019). The Metabolic Signature of Macrophage Responses. *Front Immunol*, *10*, 1462. https://doi.org/10.3389/fimmu.2019.01462
Virchow, R. (1989). Cellular pathology. As based upon physiological and pathological histology. Lecture XVI--Atheromatous affection of arteries. 1858. *Nutr Rev*, *47*(1), 23-25. https://doi.org/10.1111/j.1753-4887.1989.tb02747.x
von Rokitansky, K. F. (1854). *A manual of pathological anatomy* (Vol. 1). Sydenham society.
Wang, S., Xu, J., Zheng, J., Zhang, X., Shao, J., Zhao, L., & Hao, J. (2020). Anti-Inflammatory and Antioxidant Effects of Acetyl-L-Carnitine on Atherosclerotic Rats. *Med Sci Monit*, *26*, e920250. https://doi.org/10.12659/msm.920250
Warburg, O., Wind, F., & Negelein, E. (1927). THE METABOLISM OF TUMORS IN THE BODY. *J Gen Physiol*, *8*(6), 519-530. https://doi.org/10.1085/jgp.8.6.519
Wei, C. C., Wang, Z. Q., Hemann, C., Hille, R., & Stuehr, D. J. (2003). A tetrahydrobiopterin radical forms and then becomes reduced during Nomega-hydroxyarginine oxidation by nitric-oxide synthase. *J Biol Chem*, *278*(47), 46668-46673. https://doi.org/10.1074/jbc.M307682200

Wei, X., Song, H., Yin, L., Rizzo, M. G., Sidhu, R., Covey, D. F., Ory, D. S., & Semenkovich, C. F. (2016). Fatty acid synthesis configures the plasma membrane for inflammation in diabetes. *Nature*, *539*(7628), 294-298. https://doi.org/10.1038/nature20117

WHO. (2021). *Cardiovascular diseases (CVDs) Fact Sheet*. https://www.who.int/news-room/fact-sheets/detail/cardiovascular-diseases-(cvds)

Willerson, J. T., & Ridker, P. M. (2004). Inflammation as a cardiovascular risk factor. *Circulation*, *109*(21 Suppl 1), Ii2-10. https://doi.org/10.1161/01.Cir.0000129535.04194.38

Wynn, T. A., Chawla, A., & Pollard, J. W. (2013). Macrophage biology in development, homeostasis and disease. *Nature*, *496*(7446), 445-455. https://doi.org/10.1038/nature12034

Xu, M., Jiang, P., Sun, H., Yuan, X., Gao, S., Guo, J., Zhao, C., Hu, X., Liu, X., & Fu, Y. (2020). Dimethyl itaconate protects against lipopolysaccharide-induced endometritis by inhibition of TLR4/NF-κB and activation of Nrf2/HO-1 signaling pathway in mice. *Iran J Basic Med Sci*, *23*(9), 1239-1244. https://doi.org/10.22038/ijbms.2020.44151.10346

Yanagisawa, M., Kurihara, H., Kimura, S., Tomobe, Y., Kobayashi, M., Mitsui, Y., Yazaki, Y., Goto, K., & Masaki, T. (1988). A novel potent vasoconstrictor peptide produced by vascular endothelial cells. *Nature*, *332*(6163), 411-415. https://doi.org/10.1038/332411a0

Yano, M., Watanabe, K., Yamamoto, T., Ikeda, K., Senokuchi, T., Lu, M., Kadomatsu, T., Tsukano, H., Ikawa, M., Okabe, M., Yamaoka, S., Okazaki, T., Umehara, H., Gotoh, T., Song, W. J., Node, K., Taguchi, R., Yamagata, K., & Oike, Y. (2011). Mitochondrial dysfunction and increased reactive oxygen species impair insulin secretion in sphingomyelin synthase 1-null mice. *J Biol Chem*, *286*(5), 3992-4002. https://doi.org/10.1074/jbc.M110.179176

Yano, M., Yamamoto, T., Nishimura, N., Gotoh, T., Watanabe, K., Ikeda, K., Garan, Y., Taguchi, R., Node, K., Okazaki, T., & Oike, Y. (2013). Increased oxidative stress impairs adipose tissue function in sphingomyelin synthase 1 null mice. *PLoS One*, *8*(4), e61380. https://doi.org/10.1371/journal.pone.0061380

Yi, Z., Deng, M., Scott, M. J., Fu, G., Loughran, P. A., Lei, Z., Li, S., Sun, P., Yang, C., Li, W., Xu, H., Huang, F., & Billiar, T. R. (2020). Immune-Responsive Gene 1/Itaconate Activates Nuclear Factor Erythroid 2-Related Factor 2 in Hepatocytes to Protect Against Liver Ischemia-Reperfusion Injury. *Hepatology*, *72*(4), 1394-1411. https://doi.org/10.1002/hep.31147

Yona, S., Kim, K. W., Wolf, Y., Mildner, A., Varol, D., Breker, M., Strauss-Ayali, D., Viukov, S., Guilliams, M., Misharin, A., Hume, D. A., Perlman, H., Malissen, B., Zelzer, E., & Jung, S. (2013). Fate mapping reveals origins and dynamics of monocytes and tissue macrophages under homeostasis. *Immunity*, *38*(1), 79-91. https://doi.org/10.1016/j.immuni.2012.12.001

Yoo, H. C., Yu, Y. C., Sung, Y., & Han, J. M. (2020). Glutamine reliance in cell metabolism. *Exp Mol Med*, *52*(9), 1496-1516. https://doi.org/10.1038/s12276-020-00504-8

Zhang, D., Lu, Z., Zhang, Z., Man, J., Guo, R., Liu, C., & Wang, J. (2019). A likely protective effect of dimethyl itaconate on cerebral ischemia/reperfusion injury. *Int Immunopharmacol*, *77*, 105924. https://doi.org/10.1016/j.intimp.2019.105924

Zhang, D., Tang, Z., Huang, H., Zhou, G., Cui, C., Weng, Y., Liu, W., Kim, S., Lee, S., Perez-Neut, M., Ding, J., Czyz, D., Hu, R., Ye, Z., He, M., Zheng, Y. G., Shuman, H. A., Dai, L., Ren, B., . . . Zhao, Y. (2019). Metabolic regulation of gene expression by histone lactylation. *Nature*, *574*(7779), 575-580. https://doi.org/10.1038/s41586-019-1678-1

Zhang, J., Muri, J., Fitzgerald, G., Gorski, T., Gianni-Barrera, R., Masschelein, E., D'Hulst, G., Gilardoni, P., Turiel, G., Fan, Z., Wang, T., Planque, M., Carmeliet, P., Pellerin, L., Wolfrum, C., Fendt, S. M., Banfi, A., Stockmann, C., Soro-Arnáiz, I., . . . De Bock, K. (2020). Endothelial Lactate Controls Muscle Regeneration from Ischemia by Inducing M2-like Macrophage Polarization. *Cell Metab*, *31*(6), 1136-1153.e1137. https://doi.org/10.1016/j.cmet.2020.05.004

Zhang, S., Jiao, Y., Li, C., Liang, X., Jia, H., Nie, Z., & Zhang, Y. (2021). Dimethyl Itaconate Alleviates the Inflammatory Responses of Macrophages in Sepsis. *Inflammation*, *44*(2), 549-557. https://doi.org/10.1007/s10753-020-01352-4

Zhao, C., Jiang, P., He, Z., Yuan, X., Guo, J., Li, Y., Hu, X., Cao, Y., Fu, Y., & Zhang, N. (2019). Dimethyl itaconate protects against lippolysacchride-induced mastitis in mice by activating MAPKs and Nrf2 and inhibiting NF-κB signaling pathways. *Microb Pathog*, *133*, 103541. https://doi.org/10.1016/j.micpath.2019.05.024

Zheng, Y., Chen, Z., She, C., Lin, Y., Hong, Y., Shi, L., Zhang, Y., Cao, P., & Xu, X. (2020). Four-octyl itaconate activates Nrf2 cascade to protect osteoblasts from hydrogen peroxide-induced oxidative injury. *Cell Death Dis*, *11*(9), 772. https://doi.org/10.1038/s41419-020-02987-9

Zhu, D., Zhao, Y., Luo, Y., Qian, X., Zhang, Z., Jiang, G., & Guo, F. (2021). Irg1-itaconate axis protects against acute kidney injury via activation of Nrf2. *Am J Transl Res*, *13*(3), 1155-1169.

# Appendices

Appendix A – Other parameters measured in oxHVF cohort participants

| DEMOGRAPHICS | | REDOX measurements | COHORT-WIDE MEASUREMENTS | OUTCOMES |
|---|---|---|---|---|
| Age | AMIODARONE | SV_RESTING_02 | IL6_pg_per_mL_SERUM | DEATH |
| gender | INSULIN | SV_NADPH_O2 | TNFa_pg_per_mL_SERUM | DEATH_TIME |
| ETHNICITY | METFORMIN | SV_LNAME_O2 | Wnt5a_EDTA_(ng/ml) | DEATH_CAUSE |
| HYPERTENSION | SULFONYLUREA | SV_VAS_INHIBITABLE_O2- | SFRP5_EDTA_(ng/ml) | CV_DEATH |
| duration_of_HYPERTENSION_YEARS | DPPIV_INHIBITOR | IMA_RESTING_O2 | IGF-1 _(ng/ml)_EDTA | CV_DEATH_TIME |
| HYPERCHOLESTEROLEMIA | GLP1_ANALOGUE | IMA_NADPH_O2 | ENDOTHELIN_(fmol/ml)_EDTA | CARDIAC_DEATH |
| duration_of_HYPERCHOLESTEROL | GLIFLOZIN_CLASS | IMA_LNAME_O2 | BNP_(pg/ml)_CITRATE | CARDIAC_DEATH_TIME |
| DIABETES | THIAZOLIDINEDIONE | IMA_VAS_INHIBITABLE_O2- | hsCRP_(mg/L)_CITRATE | DOD_FOLLOW-UP |
| duration_of_DIABETES | ANY_ORAL_HYPOGLYCEMIC | EC50 PE | GLUCOSE_(mg/dL)_SERUM | SURGERY_DATE |
| SMOKING | Hb_1 (g/dl) | LogEC50 PE | INSULIN_(mU/mL)_SERUM | HF(I500, I501, I509)_APC_MASTER_DATABASE_ID |
| PACK_YEARS (duration) | WhiteCellCount_1 | EC50 Ach | HOMA-IR | HF(I500, I501, I509)_PRE_OP |
| FAMILY_HISTORY | Platelets_1 | LogEC50 Ach | PCT_SERUM_UG/L | HF(I500, I501, I509)_POST_OP |
| HEIGHT | Urea_1 (mmol/L) | Maximum Relaxation (Ach) | Cholesterol_serum_mM | HF(I500, I501, I509)_TIME |
| WEIGHT | Creatinine_1 (umol/lt) | EC50 BK | Triglycerides_serum_mM | I500_POST_OP |
| BMI | CC | LogEC50 BK | HDL_serum_mM | I500_TIME |
| Waist | Na_1 mmol/l | Maximum Relaxation (BK) | LDL_serum_mM | I501_POST_OP |
| Hip | K_1 mmol/l | EC50 SNP | HDLR | I501_TIME |
| Waist_to_Hip | Glucose_1 (mmol/l) | LogEC50 SNP | NHC | I509_POST_OP |
| CCS_class | HbA1c (%) | RAA_Resting_O2 | DPP4_ACTIVITY_SERUM_pmol_substrate_min | I509_TIME |
| NYHA_class | Cholesterol_1 (mmol/L) | MYOCARDIUM_NADPH_STIM_O2_10MIN | MME_RELPPIA_ATE | AMI(I210-2, I214, I219)_POST_OP |
| Aortic_stenosis | LDL_1 (mmol/L) | MYOCARDIUM_NADPH_STIM_O2_PLATEAU | NITRITE_L-HEP_uM | AMI(I210-2, I214, I219)_TIME |
| Aortic_Regurgitation | HDL_1 (mmol/L) | MYOCARDIUM_VAS2870_INHIBITABLE_O2_10MIN | H2S_(L-HEP)_uM | I210 |
| Mitral_Stenosis | Triglycerides_1 (mmol/l) | MYOCARDIUM_VAS2870_INHIBITABLE_O2_PLATEAU | METHYLENEBLUE_CITRATE_H2S_uM | I210_TIME |
| Mitral_regurgitation | SGPT_1 | MYOCARDIUM_VAS2870_PERCENT_INHIBITION_10MIN | | I211 |
| ASPIRIN | SGOT_1 | MYOCARDIUM_VAS2870_PERCENT_INHIBITION_PLATEAU | | I211_TIME |
| CLOPIDOGREL | yGT_1 | MYOCARDIUM_VAS2870_INHIBITABLE_O2_REST_10MIN | | I214 |
| WARFARIN | ALP_1 | MYOCARDIUM_VAS2870_PERCENT_INHIBITION_AT_REST | | I214_TIME |
| HEPARIN | CK_1 | MYOCARDIUM_LNAME_DELTA_O2 | | I219 |
| BETAbLOCKER | CK-MB_1 | MYOCARDIUM_ROTENONE_DELTA_O2 | | I219_TIME |
| CCB | INR_1 | MYOCARDIUM_URATE_INHIBITABLE_SIGNAL | | Cerebral_Infarction_I63 |
| NITRATES | PT_1 | MYOCARDIUM_MYXOTHIAZOL_DELTA_O2 | | Cerebral_Infarction_I63_TIME |
| STATINS | CK_24H | MYOCARDIUM_ALLOPURINOL_DELTA_O2 | | Intracerebral_Haemorrhage_I61 |
| ACEI | CK_MB_24H | | | Intracerebral_Haemorrhage_I61_TIME |
| ARB | CREATININE_24H | | | |
| DIURETICS | CREATININE_48H | | | |
| DIGOXIN | CREATININE_5D | | | |

## Timing and Venue of Research

The work in this thesis was carried out between October 2018 and April 2023 under the supervision of Dr Mark Crabtree and Prof Keith Channon at the British Heart Foundation Molecular Cardiology and Functional Genetics Facility, Division of Cardiovascular Medicine, Radcliffe Department of Medicine, Wellcome Centre for Human Genetics, University of Oxford, UK.


## Research Funding

Research conducted was funded by a non-clinical PhD studentship as part of the British Heart Foundation 4-year PhD programme at the University of Oxford. The laboratory of Mark Crabtree was supported by the British Heart Foundation Intermediate Fellowship (FS/14/56/31049) whilst Keith Channon was supported by programme grants (RG/17/10/32859 and RG/F/22/110085) from the British Heart Foundation.


## Publications

Diotallevi, M., **Ayaz, F**., Nicol, T., & Crabtree, M. J. (2021). Itaconate as an inflammatory mediator and therapeutic target in cardiovascular medicine. *Biochem Soc Trans*, *49*(5), 2189-2198

Diotallevi, M., Nicol, T., **Ayaz, F.,** Bailey, J., Shaw, A., McNeill, E., Davies, B., Channon, K. M., Crabtree, M. J. Isolation and *In vitro* Culture of Bone Marrow-Derived Macrophages for the Study of NO-Redox Biology. *J. Vis. Exp.* (183), e62834, doi:10.3791/62834 (2022)

## Presentations

**Ayaz, F**., Diotallevi, M., Nicol, T, Channon, K. M., Crabtree, M. J. The role of nitric oxide in macrophage metabolism and function. *Gordon Research Conference on Immunometabolism in Health and disease: Basic and Translational Cellular Metabolism in Immunity, Rhode Island, USA,* June 2022 (Poster presentation)

**Ayaz, F**., Diotallevi, M., Nicol, T, Channon, K. M., Crabtree, M. J. The role of nitric oxide in macrophage metabolism and function. *Fuelling the Immune response II: UK immunometabolism meeting 2022, Newcastle, UK,* May 2022 (Poster presentation)